Graduate School of the Southampton Oceanography Centre

This PhD dissertation by

Robin Stuart Smith

has been produced under the supervision of the following persons:

Supervisor:

Prof. Jochem Marotzke

Chair of Advisory Panel:

Prof. John Shepherd

Member/s of Advisory Panel:

Dr. Paul Wilson

UNIVERSITY OF SOUTHAMPTON
FACULTY OF ENGINEERING, SCIENCE AND MATHEMATICS
School of Ocean and Earth Science

Ocean circulation and climate dynamics under idealised continental configurations in a coupled ocean-atmosphere model

by
Robin Stuart Smith

Thesis for the degree of Doctor of Philosophy

January 2004

UNIVERSITY OF SOUTHAMPTON

ABSTRACT

SCHOOL OF OCEAN AND EARTH SCIENCE

Doctor of Philosophy

OCEAN CIRCULATION AND CLIMATE DYNAMICS UNDER IDEALISED CONTINENTAL CONFIGURATIONS IN A COUPLED OCEAN-ATMOSPHERE MODEL

by Robin Stuart Smith

A low resolution coupled ocean-atmosphere general circulation model has been developed for studying the characteristics and impact of the large scale oceanic circulation on the climate in a range of theoretical situations. The model is run with land-shapes significantly different from those present today; the relatively realistic nature of the component models provides simulations of these theoretical climates and their component feedbacks with a greater degree of confidence than the results of less sophisticated models previously applied to similar cases. The model is applied to a series of highly idealised configurations: an aquaplanet with no land at all, a single global basin, a basin with a narrow gap in the lower southern hemisphere allowing throughflow and two scenarios with a Pangea-scale supercontinent - one with a similar gap for zonal flow in the southern hemisphere and one without.

In the first three cases the model develops very warm climates in accordance with the reduced albedo and high abundance of water in the atmosphere. The last two cases produce cooler, highly seasonal climates dominated by the response to the land-sea contrast.

Changes in the ocean heat transport are shown to impact both the meridional temperature gradient and the global mean climate produced. Interactions with the overlying atmosphere result in changes in the system's radiative properties which significantly alter the mean climate simulated.

When a simple radiative model is fitted to the atmosphere obtained in each case, the characteristic parameters are indicative of qualitatively different behaviours for each. These would not be have been reproduced by an EBM-type atmosphere tuned to an *a priori* state and intuitively scaled by the changed surface characteristics of the scenarios, suggesting that such simpler studies may need to be initially guided by more complete GCM results on a case by case basis.

Significant non-advective heat transport is also found in some cases in the ocean, which compensates for changes in the advective transport. The strength of these non-advective fluxes and the degree of compensation is dependent on the strength of the greenhouse forcing.

CONTENTS

Acknowledgements

I would very much like to acknowledge the encouragement, advice and support of Prof. Jochem Marotzke, who has been my supervisor throughout my time as a PhD student. Thanks also go to Dr. Bablu Sinha, with whom I collaborated to produce the model, and who provided training in the ways of coupled models and invaluable advice on every subject, Dr. Joel Hirschi who helped to explain some of the more baffling results and helped with the production of this thesis, and John Stark who worked on the ocean model and provided computing support throughout.

I must thank Prof. John Shepherd and Dr. Paul Wilson who acted as my advisory panel, and Prof. Peter Killworth for helpful comments on the nature of Water-World. I would also like to thank Vicki Robertson and Claire Brown for their help during their short visits to SOC, and Clotilde Dubois, some of whose early results are presented here in support of the model.

Thanks also to Dr. Andy Hogg, Dr. Mark Siddall, Dr. Craig Speed and Adam Blaker for their friendship and competitive spirit over the last few years and lastly, and most importantly, I would like to thank my parents, without whom none of this would have happened (in so many ways) and Jo, who was foolish enough to marry me in the middle of it all and has lived bravely with the consequences ever since.

CHAPTER

ONE

Introduction

1.1 Background

1.1.1 Fundamental Climate Dynamics

The earth's climate is a highly complex non-linear system (Tsonis, 1989; Ghil, 1987), an intricate web of processes and feedbacks that contrives to produce the living environment we take for granted. The dynamics, physics and chemistry of the sun, atmosphere and ocean, not to mention the biosphere, cryosphere and lithosphere all greatly influence the conditions for life on earth on timescales ranging from minutes to many millennia (figs 2.4, 2.7 in Peixoto and Oort (1992)). It is thus important to understand how this system works; not just to explain the conditions we find today but also to understand how they might change and how this has affected life both in the past and the future.

The ocean and atmosphere play crucial roles in regulating the climate on earth. The fast motions of the atmosphere distribute heat around the globe, from equator to pole, in response to the uneven solar heating that results from the curvature of the earth and its rotation (pg14, Peixoto and Oort (1992)). The slow moving, slow warming oceans store heat and act as buffers, smoothing the daily and seasonal temperature swings caused by the lower heat capacity of the solid and atmospheric parts of the system (pg.15, Wells (1997)); although the oceans are slower

they also have a vital part to play in the heat transport process (Broecker et al., 1985; Trenberth and Caron, 2001). The presence of the atmosphere also results in the so-called 'greenhouse effect' (pg.74, Wells (1997)) which, with the clouds, allows in shortwave solar energy but traps the longwave radiation re-emitted by the earth, raising the surface temperature. On a day to day basis then, the oceans, atmosphere and their motions play vital roles in keeping our environment as we see it today.

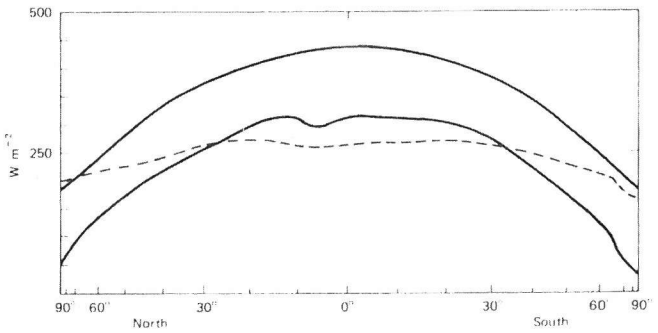

Figure 1.1: *The radiation balance of the earth, from chapter 1 of Gill (1982). The upper solid curve shows the average flux of solar energy reaching the outer atmosphere, the lower solid curve the average amount of this energy absorbed. The dashed curve shows the average amount of outgoing longwave radiation.*

The amount of solar radiation received, averaged over 4 years, as a function of latitude is pictured above (*fig:1.1*). This latitudinal gradient in insolation drives much of the apparent large-scale motion of the ocean-atmosphere system which transports heat from the equator to the cooler poles. As can be seen, the amount of longwave energy emitted follows a much flatter distribution than the shortwave received, less at the equator and more at the poles. The energy budget balances globally, but not locally - energy is being transported from equator to pole.

The atmosphere is largely transparent to incoming solar radiation, absorbing only 20% of the incident shortwave (pg.10, Gill (1982)); most of the heating thus caused happens at the earth's surface. One might therefore expect the atmosphere to act as a large convective cell, with strong heating at the equator causing the air there to rise, to be replaced by the equatorward motion of colder surface air from higher latitudes and poleward heat transport effected that way - indeed, this

regime was proposed more than 400 years ago (Halley, 1686). To a certain extent this does occur and these cells, called Hadley cells after Hadley (1735), do indeed occur. Their poleward motion is however limited by a propensity for atmospheric instability in the mid-latitudes, caused by the rotation of the earth, but there is a similar overturning cell found above the unstable midlatitudes, called the polar cell (Henderson-Sellers and Robinson, 1986). Pressure anomalies associated with the patterns of heating, along with winds induced by these meridional cells, induce surface winds that, because of the earth's rotation, are largely zonal. Easterly winds are induced toward the upward branch of the overturning cells at the equator and westerlies occur further poleward under the descending branch (pg.160, Peixoto and Oort (1992)).

The midlatitude region is characterised by baroclinic instability and the development of Rossby waves, leading to strong westerly flows which increase with height up to the tropopause, forming the jet streams. Details of the local surface (e.g. roughness, elevation, heating rate, moisture) are a major influence and the atmosphere's global coverage means that effects are not confined to the locality of the cause (pg.152, Peixoto and Oort (1992)).

Unlike the atmosphere, solar insolation absorbed at the surface tends to make the ocean stable in the vertical (pg.85, Wells (1997)), but it is still provoked into motion as a result of windstresses at the surface - this is known as Ekman transport (chap. 9, Gill (1982)). Deeper, away from the direct influence of the wind, the convergence and divergence of these wind-forced waters create pressure differences that drive deeper geostrophic flow, known as the Sverdrup flow (chap. 11, Gill (1982)). Situations can also arise however where the static stability is broken as intense cooling or salinification of surface waters makes them more dense than the water below (Killworth, 1983). The resulting convection, and, in the case of near-continent convection, entrainment of surrounding water, supplies dense water to the deep ocean where it is exported to other latitudes, diffusing slowly upwards (the actual locations and speeds of this return process are still something of an open question, e.g. Egbert and Ray (2000); Ledwell et al. (2000)). This process allows for a slow, vertical overturning of the global ocean, known as the thermohaline circulation [THC]. This density driven overturning is inextricably

combined with the wind forced motion - thus the observed vertical circulation is more generally known as the Meridional Overturning Circulation [MOC].

The atmosphere and oceans should not be considered entirely separately however - as is readily apparent, the surface motions of the ocean are largely forced by the atmosphere and since the temperature and humidity of the atmosphere are controlled by conditions beneath it is unsurprising that one needs to carefully consider the state of the one fluid when investigating the behaviour of the other. Features of our climate system such as the El Niño/Southern Oscillation (Philander, 1990) that affect world climate so drastically (and possibly North Atlantic Oscillation that influences European weather (Wallace and Gutzler, 1981)) are inherently coupled (Bjerknes, 1969) and only arise because of close interaction and feedbacks between the two systems.

1.1.2 The circulation today

The circulation resulting from the physical processes sketched above is dependent on the spatial and temporal patterns in insolation and surface forcing they are subject to. In our current climate, considering the annual average, the Hadley circulation is characterised by a rising branch just north of the equator at around 5° and descending branches between 10° and 40°, with the ascending branch linked with local convection and rain and the descending branch with dry, desert regions. The midlatitudes are characterised by storm tracks, the result of the midlatitude instability and its interaction with the continental geography, notably the Icelandic lows. The tropical belts in Asia are subject to the seasonal swings of a strong monsoonal circulation caused by the heating differential between ocean and land and cross-equatorial flow promoted by the geography of the Indian Ocean Basin. (Peixoto and Oort, 1992).

Our current ocean circulation can be characterised by two sorts of motion. Firstly, the predominantly zonal windstresses that result from the motion of the atmosphere above force basin wide, shallow horizontal surface recirculations, with characteristically strong and narrow currents found on the western boundaries, known as gyres. They also drive an intense zonal circulation that circles the globe

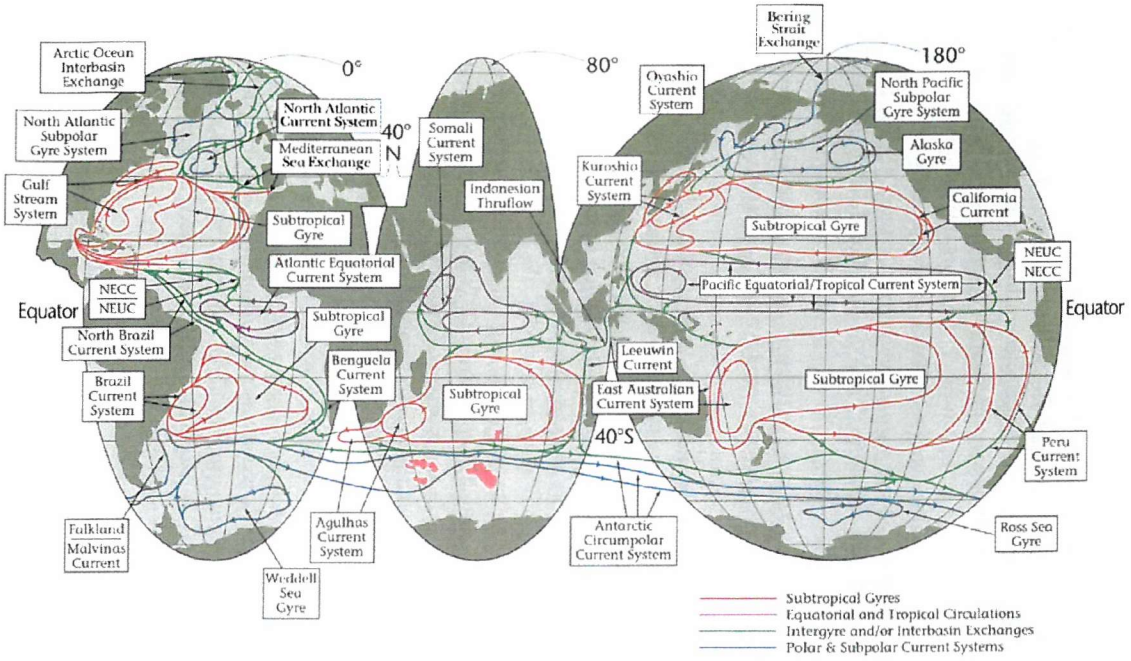

Figure 1.2: *A cartoon of the global surface circulation From Schmitz (1996).*

around Antarctica, known as the Antarctic Circumpolar Current (ACC). A cartoon of this global surface circulation is shown in figure 1.2.

Secondly, there is a much slower vertical overturning that results from the sinking of dense water formed in the north Atlantic. This is transported south as a deep western boundary current and then spreads into the other basins and upwells over the rest of the ocean - this process gives rise to the idea of the ocean conveyor belt, as pictured here (*fig:1.3*). Lower salinities in the Pacific prevent such sinking there, so northern hemisphere deep water formation is confined to the Atlantic, and although dense water is formed in the Southern Hemisphere (Antarctic Bottom Water), it contributes little to the overall heat transport (Weaver et al., 1999). The temperature contrast between the warm surface branch and the much cooler deep return branch means that this overturning carries the bulk of the heat transported by the ocean and is thus important for the regulation of the climate system.

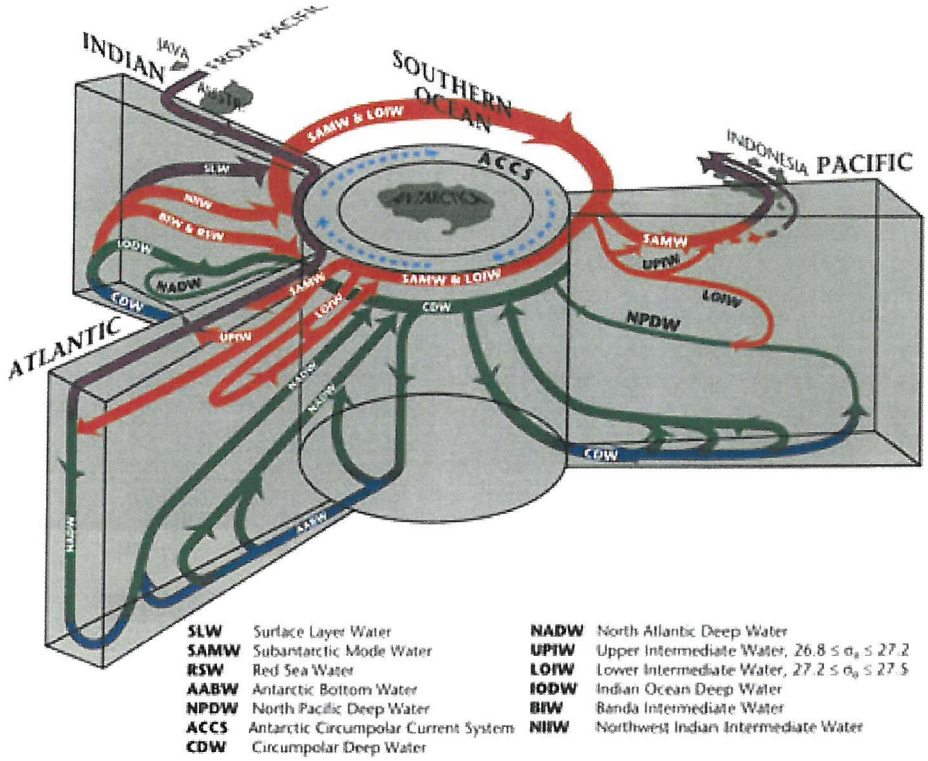

SLW	Surface Layer Water	**NADW**	North Atlantic Deep Water
SAMW	Subantarctic Mode Water	**UPIW**	Upper Intermediate Water, $26.8 \leq \sigma_\theta \leq 27.2$
RSW	Red Sea Water	**LOIW**	Lower Intermediate Water, $27.2 \leq \sigma_\theta \leq 27.5$
AABW	Antarctic Bottom Water	**IODW**	Indian Ocean Deep Water
NPDW	North Pacific Deep Water	**BIW**	Banda Intermediate Water
ACCS	Antarctic Circumpolar Current System	**NIIW**	Northwest Indian Intermediate Water
CDW	Circumpolar Deep Water		

Figure 1.3: *A cartoon of the large scale overturning of the global ocean and the watermasses that play a part in it. From Schmitz (1996).*

1.1.3 Other possible circulation patterns

Paleoclimate proxy records provide evidence that suggests that at various times the earth's climate has been significantly different from today's. There is evidence for both largely frozen (Hoffman et al., 1998) and ice-free (Goloneva, 2000) worlds, with many in between (Scotese, 2002). Concurrent with these is evidence for changes in the atmosphere, both physical (i.e. dust content) and chemical (gas composition) (Raynaud et al., 1993; Taylor et al., 1993; Petit et al., 1999), that are thought to have altered the amount of solar insolation received at the surface.

There is also evidence for changes in deep water production rates (Hughen et al., 1998) and the strength and extent of the circulation (Heinrich, 1988; Lynch-Stieglitz et al., 1999), although the proxy data is sparse and allows many interpretations even where it does exist; as today, the ocean circulation would undoubtedly have played a significant role in the climates of the time (Crowley and North, 1991).

Until fairly recently, the ocean was not considered to be an active part of the climate system, more an inert, high capacity heat sink that mitigated the higher frequency variation of the atmosphere. Whilst the concept of a thermohaline circulation and oceanic transport of heat is not new - it has long been thought that the coldness of deep water in the tropics might be due to the sinking and subsequent spreading of waters cooled at the poles (Rumford, 1798) - the notion that changes in the ocean circulation could seriously affect the global climate is quite recent. The first attribution of actual climate variability from a dynamic change in the ocean came only in 1964 with a suggestion by Bjerknes (1964) that the climatic extremes around 1800, and thus possibly other climate variations, were maintained by changes in the heat transport in the North Atlantic current. Only a few years earlier Stommel (1961) had published a thought experiment that posited the possibility of a buoyancy flow system - with equatorial heating and evaporation and polar cooling and freshening - having more than one stable circulation state, but the two concepts were not connected. Although Stommel's neglected idea was expanded by Rooth (1982) twenty years later it was not until the influential study of Broecker et al. (1985) three years later that the idea found a wider audience. Broecker proposed that changes in North Atlantic deepwater production rates would produce a pattern of regional climate change matching that

derived from ice-core and pollen data, and Stommel's idealised thought experiment was suggested as a means whereby this deepwater production change might have occurred and been maintained. Bryan (1986) and many later studies looking at the THC (e.g. Manabe and Stouffer (1988); Marotzke and Willebrand (1991); Weaver et al. (1993)) recreated different stable overturning modes in more sophisticated ocean models and the climatic influence of the THC mode-switching gained popular acceptance.

The modal nature of the THC has been cited to provide mechanisms to help explain climate oscillations found in the paleodata (Johnson et al., 1992; Petit et al., 1999) - both the 'abrupt' Dansgaard-Oeschger events such as occurred at the end of the last glacial period (Sakai and Peltier, 1997; Ganopolski and Brovkin, 2003) and also the longer period signal of the ice-age cycle itself (Gildor and Tziperman, 2001). The THC is often used here as part of a mechanism that involves other parts of the earth system (e.g. the cryosphere), either as an amplifier for the small amplitude orbital forcing that is proposed as being the root cause for the ice-age cycle (Milankovitch, 1941; Hays et al., 1976), or independently of this. These oscillations often propose a large surface freshwater anomaly as the cause of the shutdown of the polar sinking, and it is thought that the increase in the hydrological cycle expected to occur under current climate change scenarios might have a similar effect, leading to a reduction or shutdown of the THC in the North Atlantic and possible concomitant changes in climate, especially over Europe (Houghton et al., 2001).

Continued investigation into the THC has raised as many questions as it has answered however, and none of the above mechanisms are without some degree of doubt; whilst the existence of multiple stable states, flushing events and commensurate large-scale changes in global temperature, vegetation, ice sheets and the like (in those models that can show them) are common to models of every complexity and type (Marotzke and Willebrand, 1991; Stocker et al., 1992; Manabe and Stouffer, 1993; Higgins et al., 2003), there is less agreement as to the actual sensitivity of these events, their trigger points or the likelihood of their occurrence in the real world.

These model-result inconsistencies stem from a lack of robust knowledge as to the

climate system characteristics and feedbacks that are fundamental to the behaviour of the THC. The behaviour that results from complex climate models is too variable and affected by too many factors to obtain a clear picture, and attempts to produce simple models that retain only the bare bones of the system still produce inconsistent results, depending on which features are retained and in what form. Major issues such as the nature, extent and effect of vertical mixing in the oceans (Marotzke, 1997) and the fundamental atmospheric feedbacks which need to be considered are still unclear. Different representations of these variables in different models can produce different thermohaline flows and sensitivities (Houghton et al., 2001) and we do not have enough theoretical or observational knowledge to separate these into those forms which are possible and those that are unlikely or unphysical. It is thus clear that there are fundamental questions about the mechanisms that drive the THC and their consequent effect on the large-scale climate that remain unanswered.

1.2 This Study

This study aims to investigate the global climatic effects of changing the ocean circulation by changing the basin geometry that confines it. As has been discussed, the ocean circulation is a climate influence that may have significantly different modes of operation and a major impact on climate, so we might expect that any changes in ocean circulation that result from changing the basin geometry will have a significant effect. The physical constraints of basin geometry on the ocean circulation are clear - although the atmosphere forms a continuous field over the earth, the ocean can only flow and transport where the basin topography allows it to go. The form of the THC we see today, with Atlantic and not Pacific high latitude-sinking, and the dominant influence of a northern-hemisphere cell which extends well into the southern hemisphere (Weaver et al., 1999) (and the other possible modes inferred from experiments) are clearly closely linked to the basin geometry. For instance, if there were clear midlatitude northern hemisphere links between the Atlantic and Pacific there would be less difference in the characteristics of their waters and thus possibly a different overturning solu-

tion (Maier-Reimer et al., 1990). The difference between the four possible modes found in the idealised study of Marotzke and Willebrand (1991) as opposed to the two of Rooth (1982) can be seen as a function of the geometry of the experiments and the degrees of freedom implied by the number of basins.

Geographic influences on the ocean circulation range from the subtle: simple application of the geostrophic relation suggests that steady flow should be along contours of f/H , where f is the coriolis parameter and H the depth of the ocean floor (this effect is often small however, given the presence of stratification (Anderson and Killworth, 1977)); to the extreme: continental boundaries block the flow entirely. Aspects such as the separation from the coast of western boundary currents like the Gulf Stream (Tansley and Marshall, 2001) to the possibility of much enhanced vertical mixing over rough bottom topography (Ledwell et al., 2000) are all linked to the physical specifications of the basin, so it is clearly an influence worth studying.

There have been a number of studies looking at the effects of basin geometry and connecting channels on the wider ocean circulation, often based on one of the most recent changes that has occurred in the geologic past: the opening of the Drake Passage. This is a tradition starting with Gill and Bryan (1971), and includes work by Cox (1989) and England (1993) who show effects on water mass properties involved in the global overturning from the opening of the passage, and Bjornsson and Toggweiler (2001) and Mikolajewicz and Maier-Reimer (1993) who investigated the suggestion that the opening of the Drake Passage might be linked with the onset of Antarctic glaciation 35 million years ago. Maier-Reimer et al. (1990), Haug and Tiedemann (1998) and Murdock et al. (1997) also look at the effect of the closing of the Isthmus of Panama, an event to which some have ascribed an increase in Atlantic salinity and the onset of the current THC 'conveyor' as fresh Pacific water was prevented from passing into the Atlantic - this is currently refuted however by Nof and Van Gorder (2003).

Paleoceanographic studies are also sources of information about global circulations under altered physical boundaries (Kutzbach and Guetter, 1990; Fawcett and Barron, 1998), and the warm late Cretaceous has been the focus of a number of studies since the suggestion that intense tropical evaporation may have led

to a haline-dominated 'reverse' THC with equatorial downwelling of warm deep waters (Brass et al., 1982). This idea has not been supported by recent studies however, among which Bice and Marotzke (2001) claim the presence of rough bottom topography - another geographical influence - as a crucial factor.

As well as providing further theoretical knowledge of the possibilities of the multi-modal THC and its interplay with parts of the climate system then, geographical effects are relevant when considering real past climates, when the earth's continental geography was very different from that seen today, and potential future ones when continental drift may once more create a supercontinent (Scotese, 2002). All of the above studies deal with individual, specific circumstances however and the variety of approaches, models and setups means that the different circulations and their climatic impacts cannot easily be compared across experiments to draw out a more general picture of how the ocean circulation might change in an arbitrary scenario. A more general picture of the behaviour of the ocean overturning and resultant climate influences, with a series of experiments carried out in a consistent fashion to enable certain cross-comparison, is thus the aim of this project.

1.2.1 Experimental Philosophy

The remit of investigating geographical influence of ocean circulation, its transport and their consequent effects on climate is clearly a broad one, so care must be taken in the design of the experiments so that the appropriate factors are highlighted and can be pursued easily. To aid the deconstruction of the experiments into readily identifiable feedbacks and thus analyse and explain them, the geographical forcing in each has been kept to a very simple, exaggerated form. The exact forms and more detailed motivations of the individual experiments will be taken up later (see Chapter 3).

Simplified, idealised experiments were once a necessity which led from the limited computing power available (Phillips, 1956; Manabe and Bryan, 1969). Whilst still a limited resource, current facilities allow considerably more calculations to be done in a realistic time-frame, and thus allow for more 'realism' than presented in the scenarios here. The idealised approach is justified however by its very sim-

plicity: in a field where much of the basic behaviour and drivers of a system are unclear, it helps to highlight the effect of the factor under investigation by cutting out other influences. These effects can also easily be amplified by exaggerating the desired forcing without fear of creating unwanted interactions with other features that would be present in a more complete simulation.

Such experiments - which attempt to explain the theoretical underpinnings of a process without attempting to produce a faithfully realistic simulation - are not unknown. For example, Marotzke and Willebrand (1991) and Fanning and Weaver (1997b) feature 'global' models displaying deliberately unrealistic geometries for their global oceans, and single basin models (Cox, 1989; Marotzke, 1997) are often used for simpler proof-of-concept tests.

The general impact of the geometry of the system on the ocean transport has not however been systematically investigated in such a manner. Specific features of the circulation such as the flow along sloping shelves and the separation of western boundary currents have been taken up in highly idealised form, and although more global, geographically influenced studies such as Bjornsson and Toggweiler (2001) and Mikolajewicz and Maier-Reimer (1993) do use idealised basins, they are still predicated around individual, specific situations and do not apply themselves to the more general questions investigated here.

1.2.2 The Model

Basic Requirements

As stated above, the environments to which the model was to be applied are idealised and are deliberately 'non-realistic' in many ways. We are not setting out to recreate, as an end product, distributions of certain fields (e.g. surface temperature, rainfall patterns etc.) to represent current climate, but rather to deconstruct some of the processes and feedbacks that work together to produce the final climate. It is thus more important to work with a model grounded in the pure physics of the system than one that is purposely re-engineered - through data assimilation, climatological fields or convenient approximation - to give the 'right'

answer. Long timescale integrations are required to reach equilibria of the climate system which, even neglecting the lithospheric and cryospheric components, can take several thousands of years to equilibrate as the deep ocean exchanges heat with the surface, limited by slow diffusive processes.

A perfect simulation of the complete earth system is currently well beyond our computational abilities, and our best attempts at such are expensive and hardly suitable for many centuries of integration on affordable equipment. For example, current Earth Simulator (the most powerful computer on the planet devoted to climate simulation) coupled runs (the CFES model) at T319 resolution require ~2 days of run time per year on 80 of the 64 GFlop NEC SX-6 nodes (Takahashi et al., 2003) and the rather more modest ~3° atmosphere, 1.25° ocean HadCM3 model needs 24 hours per year on 8 500 MFlop Cray T3E CPUs (*Sinha, pers. comm.*). A 1000 year run of HadCM3 on such hardware (still too costly for this project) would take the best part of 3 years. A suitable level of simplification and reduction must therefore be found if we are to proceed with a flexible model that allows one to do multiple such runs.

An approach often used when studying coupled problems where long spinups, impractical in a state of the art climate model, are required is to employ a reduced complexity coupled model. These attempt to simulate the responses and feedbacks of the entire climate system, but reduce computational overhead by attempting to reproduce the system in less detail, retaining only what is thought to be essential to the question at hand. There is a class of models, known as EMICs (Earth System Model of Intermediate Complexity) (Claussen et al. (2002), also Marsh et al. (2002)) that are designed to fulfil this role, generally comprising models of reduced physical dimensionality or with one component very much more parametrized than the others. In this project however, another approach has been taken: that of using a coupled General Circulation Model [GCM] that has been made more affordable by employing a low (compared to the state of the art) resolution. Whilst not as fast as the EMICs cited above, the model used here has a higher resolution and explicit representations of more processes have been retained. The use of component models that have been analysed previously and shown to produce reasonable climate simulations (Forster et al., 2000; Webb,

1998) also allows any model-specific issues from those previous studies to be considered here and engenders more faith in the results as compared to those from a model with totally untested components.

Coupled ocean-atmosphere GCMs [OAGCM] are generally not employed for idealised or long-spinup experiments, so currently there exists something of a gap in the literature between models that simplify the interactions of the two components (often ocean GCMs with simple 1D energy-balance atmospheres, or atmosphere GCMs with mixed layer oceans (e.g. Bjornsson and Toggweiler (2001); Sellwood et al. (2000)) used for such studies and the more complex models used for short term current climate experiments (e.g. Gordon et al. (2000); Boville and Gent (1998)). In this case we are bringing the advantages of the explicit process representation of the complex model to the fundamentalist philosophy of the idealised experiment.

A low-resolution OAGCM is ideal for this sort of study: a fully 3D ocean can represent flow around geographical features with latitudinal and longitudinal extent that a 2D or basin averaged model cannot; a 3D dynamical atmosphere is better suited to representing the effect of the changing distribution of surface heat fluxes that will result from changing the ocean circulation than a 1D or 2D one; the low resolution allows a far longer integration time to be completed than would otherwise be possible. The vertical resolution used here, higher than that in any EMIC is also significant: as will be seen, the response of the hydrological cycle, including the different cloud types, plays an important role in determining the climates seen. The results from such a model employed in this way could therefore be expected to be richer in interactions between the systems and resulting climatic behaviour than those from an EMIC or other tuned, simple model and will thus be more illuminating in showing the possibilities for physically consistent states that the system could theoretically produce.

At the start of this project, no such low resolution GCM was available. Previous iterations of the current state of the art, expensive coupled models had lower resolutions but have since ceased active use and have no support. A proposal was however in place for the development of a low resolution GCM under the National Environment Research Council's 'Coupled Ocean Atmosphere Processes and Eu-

ropean Climate' [COAPEC] project at the Southampton Oceanography Centre [SOC] and initial work by Bablu Sinha of the James Rennell Division was already underway. A major part of the work undertaken for this project involved the development and testing of this model, named FORTE (Fast Ocean, Rapid Troposphere Experiment), and as such this is presented here along with the results of the actual climate experiments.

Model Resolution

FORTE has a modular nature which allows it to take advantage of the different model resolutions permitted by each component. The atmosphere can run at T21 or T42 resolution (roughly 5.625° and 2.8° respectively) with 22 vertical levels, whilst the ocean is very flexible and can be run at practically any grid resolution desired. The requirement here of completing several runs on the the order of a thousand years each places a strict limit on the resources that the model can use however. All runs presented here have thus been run with a T21, 22 level atmosphere and at 4°x 4°x15 vertical levels in the ocean. This allows approximately 50 model years to be simulated per day on readily available hardware (see Appendix for hardware details).

This makes for quite a coarse resolution climate model by current standards, where HadCM3 (a commonly used, but more computationally expensive model) runs at ~3° in the atmosphere and 1.25° in the ocean. FORTE's errors in the reproduction of the current climate (see section 2.5.1) can largely be ascribed to this coarse resolution which can have significant impact on the representation of heat transports and, at this resolution in the atmosphere, important momentum transports as well (Boyles, 1993). Compared to the EMICs however, which often use only two-dimensional components, FORTE's resolution, although low by state of the art standards, is rather higher. Along with its basis in the primitive equations, with the idealised nature of the simulations and the fact that mostly qualitative results were required, it was felt that this level of resolution was adequate.

CHAPTER

TWO

The Model

Creating a coupled model does not require one to start completely from scratch; a large number of ocean, atmosphere and other component models already exist. If suitable, one of these can be selected from this wide range of individual models and then linked to others so that they can communicate. Software to enable this communication also exists, so in theory it can be a simple matter of bolting together pre-existing parts. In practice however there are many pitfalls to avoid; the individual implementations found in each component and the need to fill in gaps in models' representations of the climate system that their now-unused boundary conditions may have included implicitly (i.e. land runoff or sea ice) makes the technical task of coupling two arbitrary component models non-trivial.

The choice of component model is a complex one, based on the degree of complexity required in the final model, computing resources and the level of expert help available to aid in development and interpretation of results. For this project integration speed was at a premium, but not at the expense of being unable to use primitive equation models that have a good pedigree as standalone models in their own right. There is an obvious trade-off to be made here: the speed and convenience of using something that has already been programmed, versus the 'ideal suitability' of starting from scratch and designing something to one's own agenda. By and large, no model already available will match the desired criteria perfectly.

2.1 Components

2.1.1 MOMA

The ocean model is MOMA (Webb, 1996), an array version of the widely distributed MOM (Modular Ocean Model), based on the GFDL (Geophysical Fluid Dynamics Laboratory) code which is derived from a model originally designed by Kirk Bryan (Bryan, 1969) and revised by Semtner (1974), Cox (1984), and Pacanowski et al. (1990). The version actually used has been repackaged by John Stark at SOC, who has also made a number of improvements and optimisations. The current version is highly flexible, and has been used widely in applications ranging from state of the art climate change simulations to paleoclimate and idealised models.

There are many reasons why MOMA was chosen for use here. The MOM code and its derivatives are amongst the most widely used and tested ocean codes today, having been used in studies ranging from the most idealistic to the most realistic possible (CFES, a coupled model developed for use on the Earth Simulator (Takahashi et al., 2003)) - it is certainly flexible enough for an idealised study like this. It is also highly configurable, so a suitable level of complexity is easy to specify as required and there is more than enough in-house support at SOC for help in case of problems - a very real consideration when selecting a suitable model.

It is a primitive equation model: this means that the time evolution of the ocean state is based on the Navier-Stokes equation for fluid flow with only a few very general approximations:

1. mass conservation is implied by $\nabla \cdot u + \frac{\partial w}{\partial z} = 0$
2. vertical velocities are expected to be far smaller than horizontal ones so terms that involve vertical accelerations can generally be neglected, due to the small aspect ratio
3. small changes in density can safely be neglected, except where they affect the buoyancy - the Boussinesq approximation

The use of these assumptions in creating a numerical ocean model comes from Bryan (1969). The equations for momentum and tracer evolution integrated are thus:

$$\frac{\partial u}{\partial t} + (u \cdot \nabla)u + w\frac{\partial u}{\partial z} + f \times u = -(\frac{1}{\rho_0})\nabla p + D_u + F_u \tag{2.1}$$

$$\frac{\partial Tr}{\partial t} + (u \cdot \nabla)Tr + w\frac{\partial Tr}{\partial z} = D_{Tr} + F_{Tr} \tag{2.2}$$

where u is horizontal velocity, w vertical velocity, f the coriolis parameter, Tr tracer concentration, t time, D a diffusion term and F the forcing.

The model domain is split into cells along lines of constant longitude, latitude and depth, with the prognostic variables of u, v, T, S placed on these lines according to the Arakawa B grid scheme (Arakawa, 1966; Mesinger and Arakawa, 1976). This is often used in coarse resolution ocean models due to its dispersion relation resulting in an improved representation of Rossby wave propagation compared to other grids when the grid resolution is not fine enough to resolve the Rossby radius (Griffies et al., 2000). The solution is then formulated by a finite difference 'leap-frog' integration of the above equations for each grid point, with occasional Euler steps to remove the even/odd-timestep splitting of the solution.

Older versions used a rigid-lid formulation at the surface to filter out the fast gravity wave modes to allow the timestep to be increased; here an explicit free surface scheme is used which involves fewer dynamics-distorting assumptions and, although requiring short timesteps able to resolve the gravity waves, has computational advantages over rigid-lid and implicit schemes in its ease of parallelisation and avoidance of elliptic equation solvers (Griffies et al., 2000).

The choice of coordinate scheme means that mixing is most naturally implemented along the horizontal/vertical directions - this can lead to significant unphysical mixing across isopycnals, which are not generally horizontal. The Gent and McWilliams [GM] (Gent and McWilliams, 1990; Gent et al., 1995) formulation of isopycnic mixing is implemented in the model, but not generally used in these experiments due to its computational cost. A short, expensive run of one scenario with GM mixing turned on showed qualitatively similar behaviour to

that found in the case with simple vertical mixing (see section: 4.2.2) and it was concluded that the more affordable simple vertical mixing scheme would suffice for general use in this project. Tracer advection, often a source of numerical dispersion or conservation errors dependent on whether a centred (conservative) or dissipative scheme used, is achieved through the hybrid MSQ (Webb et al., 1998) scheme.

The adjustment of the water column toward static stability uses the simple Cox scheme (Cox, 1984): a number of iterative passes through the water column where adjacent boxes are homogenised if found to be unstable. The column can however never be completely stabilised by this method (Marotzke, 1991), so the number of passes is usually set *a priori* to some average, computationally affordable value - here 1. Alternative schemes exist (Marotzke, 1991; Klinger et al., 1996) which completely stabilise the column in one pass; the instant, sometimes full depth mixing this can produce is unphysical though.

When run in standalone mode, surface forcings of heat, fresh water and momentum must be provided. These first two are specified as climatological fields of sea surface temperature [SST] and salinity [SSS] to be 'restored' to: the difference between the model surface and these ideals is taken and a flux calculated that will nudge the model toward the ideal. For the momentum, climatological windstreses are provided and used to calculate the forcing. Originally supplied with zonally and annually averaged fields for these boundaries, monthly varying full-fields have been calculated (Levitus, 1998) in the course of the project and implemented for restoring to in MOMA. When coupled to the atmosphere, these static boundary conditions are completely replaced by the fields provided interactively by the atmosphere model.

2.1.2 IGCM3

Version 3 of the Intermediate General Circulation Model [IGCM3] is a primitive equation spectral atmosphere model from Reading University, incorporating realistic coastlines and orography. Derived from the original dynamical core of Hoskins and Simmons (1975), its current incarnation is much advanced (Forster

et al., 2000). It has a multi-band radiation scheme including effects of water, carbon dioxide and ozone and a cloud scheme with 4 distinct layers. The model includes a land surface scheme able to hold moisture and track soil temperature and surfaces can also be assigned a vegetation index which determines roughness length and albedo. For standalone use there is also a mixed layer ocean model with a prescribed heat transport. It has 22 vertical levels, 7 of which are in the stratosphere.

As a spectral model it is a good choice for use in a coarse resolution coupled model and, whilst somewhat slower than models with less vertical resolution that are sometimes used in intermediate models (e.g. Opsteegh et al. (1998); Molteni (2003)), its degree of sophistication allows the model to be largely free of links to climatological data sometimes used to substitute certain processes. This resolution also allows a more accurate representation of radiative transfer and a complex cloud parametrization - all of this makes IGCM3 suitable for use in the more idealised situations envisioned here. The proximity of the original model developers in Reading for support purposes also makes it a good choice.

IGCM3 is a spectral model, meaning that rather than using a mesh of discrete points to approximate the prognostic fields as MOMA does, the fields in each horizontal layer are represented as a series of suitably combined orthogonal base functions - in this case spherical harmonics (Legendre functions). The resolution of such a model is then determined by the number of terms in the base function expansion, i.e. the smallest wavelength the model can resolve is equal to the smallest wavelength function in its spectral representation. For linear equations this is, computationally, a very efficient way of dealing with numerical approximation: numerical problems due to the aliasing of wavelengths too short to be represented on the grid do not occur since the truncation in wavelength space completely removes them. The issue of convergence of grid lines towards the poles (that leads to a need for ever shorter timesteps in order to satisfy stability criteria in these regions) found with geographically-gridded models is also sidestepped as the Legendre functions used here to describe the latitudinal variation of the fields smoothly approach zero at the poles for the short wavelength components. The avoidance of the aliasing problem means that spectral models are far preferable to

gridpoint models at low (>2°) resolution, but this method is unsuitable for use in ocean models due to issues to do with the inhomogeneity of the ocean fields, i.e. completely separate ocean basins and sharp, localised features such as western boundary currents.

Spectral model resolutions are specified in an XM form, where M denotes the largest wavenumber mode to appear in the representation (wavenumbers from $-M$ to M will be used) and X is the truncation scheme used to determine which meridional modes will be used with each zonal one. Two truncation schemes are popular: Rhomboidal (R) and Triangular (T). In the R scheme, Legendre polynomials of degree $l = |m|$ (m is the zonal wavenumber of the mode under consideration) to $l = M + |m|$ are used, whilst the T scheme uses only $l = |m|$ to $l = M$. The degree is equivalent to the total 2D wavenumber, i.e. the meridional wavenumber is $l - m$; thus the R truncation has the same meridional resolution for every zonal wavenumber and the T provides the same resolution in zonal and meridional directions. Whilst the R truncation is thought to provide better resolution of zonal mean and planetary scale waves and is thus useful in low resolution models, the more uniform resolution over the sphere provided by the T scheme has become increasingly popular in recent years.

The equations of motion are not linear and dealing with the non-linear advective terms would require a large number of relations to describe the interactions between the various modes, were a purely spectral approach to be taken. Instead, the spectral solution is transformed into grid-point space (Orszag, 1970) where the products are worked out before the fields are transformed back into spectral space and timestepped forward. The grid onto which the transform is done must be carefully formulated to avoid the aliasing problems mentioned above that are associated with wave representations on a discrete set of points. It has been found that a uniform zonal resolution of $3M + 1$ points, with a Gaussian distribution of at least $(4M+1)/2$ meridional cells is sufficient (although $(3M+1)/2$ meridional points will avoid aliasing in nearly all terms and errors in the remainder have been found to be negligible in this case). This provides an easy way to compare the resolutions of grid and spectral models; the equivalent grid for this T21 model has 64x32 points, each ~5.625° square.

Common in spectral models, the dynamic equations are formulated here in terms of the vorticity and divergence of the fluid, as this lends itself more readily to the transform method than a u, v formulation; the necessary derivatives are obtained automatically via the transform process and do not have to be calculated explicitly. The vorticity, ζ and divergence D are related to the vector velocity components by:

$$\zeta = \frac{1}{a\cos\phi}\left[\frac{\partial v}{\partial \lambda} - \frac{\partial}{\partial \phi}(u\cos\phi)\right] \tag{2.3}$$

$$D = \frac{1}{a\cos\phi}\left[\frac{\partial u}{\partial \lambda} + \frac{\partial}{\partial \phi}(v\cos\phi)\right] \tag{2.4}$$

where a is the radius of the earth, ϕ latitude, λ is longitude and u and v are zonal and meridional components of the velocity vector respectively.

The standard primitive motion equations are set up with these new variables, non-dimensionalised and cast into a spectral form as above, following the method outlined in Hoskins and Simmons (1975).

As with the ocean model, static instability is dealt with through an explicit convective adjustment scheme (Betts, 1986). There are two forms: dry and moist adjustment, where the dry process sees the entire column adjusted to neutrality in a single timestep and the moist scheme has the column adjusted over a number of timesteps to the ideal profile, as defined by the thermodynamic characteristics of the column. The choice of convection depends on cloud location and relative humidity over the column.

The complex issue of cloud formation and effect is dealt with in a simplified version of the Slingo (1987) scheme, where 5 cloud types are identified: low ($\sigma > 0.7$), middle ($0.7 > \sigma > 0.35$), high ($0.35 > \sigma > 0.12$) and two convective types, shallow and deep. The abundance of these first three depends on the relative humidity, and that of the last two on the amount of precipitation formed in a level. In this simplified scheme the fraction of shallow cloud, where present, is set to an average value of 0.3. The cloud particle size is also set at a constant, average value. In the real atmosphere, different cloud types at different levels have differ-

ing effects when passed to the radiation scheme: low clouds tend to have a cooling effect due to their greater reflectance of the incoming shortwave radiation whilst high clouds warm by absorbing proportionally more of the outgoing longwave - the model has been found to have qualitatively similar behaviour.

Radiative transmittance is affected by the presence of water and ozone in the model: water is a fully diagnostic variable, but the distribution of ozone is based on a monthly varying climatology. The longwave scheme is based on a series of lookup tables in various spectral ranges whilst the radiative scheme has only 2 bands, based on Morcrette (1990).

Comparable to the ocean's requirement of surface fluxes, some account must be provided of the earth's surface influence on the atmosphere. For standalone operation the IGCM3 is equipped with a 'mixed layer' ocean: each box on the transform grid is equipped with a a fixed depth, fixed heat capacity, perfectly mixed bucket of water with which to exchange fluxes, depending on the relative temperatures of air and bucket. A mechanism is provided for specifying a pre-calculated, monthly varying grid of additional fluxes that acts as a parametrization of ocean heat transports. This field is calculated as that which would be required to maintain climatological SSTs, using the surface fluxes obtained from a model run with fixed SSTs. This diagnosed transport field is then added to every later run, where the SSTs are allowed to vary. If temperatures fall below freezing, the buckets are replaced by elements with the heat capacity of a 2m layer of ice.

Whereas the ocean boundary conditions are completely provided by the atmosphere, the solid land boundary formulation remains part of the model when all is coupled together. It consists of two levels of soil, with an average climatological heat capacity. Heat is allowed to diffuse between the two, with the conductivity chosen to reproduce an idealised observed curve for soil temperature. Soil moisture is represented by a simple bucket model that fills or empties according to precipitation and evaporation and affects the surface humidity accordingly; any overflow from the bucket is ignored under the assumption that it finds its way to the sea by some means (this process had to be specified once coupled - see section 2.3.2). Each surface box is assigned a temporally constant vegetation type: this affects the albedo and roughness length over the surface. The albedo can however

be temporarily changed by the presence of snow or ice.

2.2 Coupling

2.2.1 Theory

When running as standalone models, each of the components needs boundary conditions (in this case the atmosphere needs to know SSTs and the ocean needs heat and freshwater fluxes and winds), which are usually provided in each by static files of data (usually climatological) and simple parametrizations. When the two are coupled these static data are replaced with information from the other model. All that is required is to equip the models with some communication method and run them so that when model A requires boundary values, instead of looking to its climatological files it looks to model B, and vice versa.

Each model has scalar fields (i.e. temperature) at the boundary and the boundary condition required therefore takes the form of a flux. There is no salinity/rain- or ocean current/wind speed- feedback between the ocean and atmosphere here (i.e. SSS in MOMA does not affect the freshwater flux from IGCM3 and the momentum transferred depends purely on IGCM3's winds, MOMA's surface u and v are irrelevant) but the necessary heat flux is calculated from the difference between the two boundary temperature fields.

There is an important subtlety here in deciding in which model the fluxes are calculated, which arises from the finite time gap between steps where the models communicate - i.e. the temperature-flux feedback is not instant (*Guilyardi, pers. comm.*). This delay allows the models to evolve independently for periods of time and oscillatory instabilities can arise that are purely numerical.

Consider two models containing fluids of arbitrary depth h_i, density ρ_i and heat capacity c_{p_i}. They each have temperatures $T_{i,n}$, where n is the timestep, and are to be coupled together with an interval Δt. One might expect that boundary fluxes, Q_n, would be calculated at the time of coupling, from the instantaneous temperatures of the two components at that point:

$$\rho_1 c_{p_1} h_1 \frac{(T_{1,n+1} - T_{1,n})}{\Delta t} = Q_n \tag{2.5}$$

$$\rho_2 c_{p_2} h_2 \frac{(T_{2,n+1} - T_{2,n})}{\Delta t} = -Q_n \tag{2.6}$$

$$Q_n = K(T_{2,n} - T_{1,n}) \tag{2.7}$$

where K is the conductivity. We need to find the stability criteria for the coupled system. Eliminating Q these can be recast as

$$T_{1,n+1} = \alpha_1 \left[T_{2,n} - T_{1,n}\right] + T_{1,n} \tag{2.8}$$

$$T_{2,n+1} = \alpha_2 \left[T_{1,n} - T_{2,n}\right] + T_{2,n} \tag{2.9}$$

where $\alpha_1 = \frac{K\Delta t}{\rho_1 c_{p_1} h_1}$ and $\alpha_2 = \frac{K\Delta t}{\rho_2 c_{p_2} h_2}$

This is an eigenvalue problem, i.e.

$\begin{bmatrix} T_{1,n+1} \\ T_{2,n+1} \end{bmatrix} = \delta \begin{bmatrix} T_{1,n} \\ T_{2,n} \end{bmatrix}$, so that $\begin{bmatrix} T_{1,n+1} \\ T_{2,n+1} \end{bmatrix} = \delta^n \begin{bmatrix} T_{1,0} \\ T_{2,0} \end{bmatrix}$

Thus, a substitution can be made, $T_{i,n+1} = \delta^n T_{i,0}$, which can be normalised by the ratio (λ) of T_1 and T_2 to give

$$\begin{bmatrix} T_{1,n+1} \\ T_{2,n+1} \end{bmatrix} = \delta^n \begin{bmatrix} \lambda \\ 1 \end{bmatrix} \tag{2.10}$$

which substitutes into our system:

$$\lambda\delta^{n+1} = \alpha_1\delta^n + \lambda\delta^n(1 - \alpha_1) \tag{2.11}$$

$$\delta^{n+1} = \lambda\alpha_2\delta^n + \delta^n(1 - \alpha_2) \tag{2.12}$$

If the magnitude of any of the eigenvalues, δ, is greater than 1 then that mode will grow and the solution will be unstable. To find the magnitude of δ, we can rearrange this to

$$\delta = \frac{\alpha_1 \alpha_2}{\delta - 1 - \alpha_1} + 1 - \alpha_2 \tag{2.13}$$

$$\delta^2 + \delta(\alpha_1 + \alpha_2 - 2) + (1 - \alpha_1 - \alpha_2) = 0 \tag{2.14}$$

$\delta = 1$ is a solution of this, so can be taken out as a factor:

$$(\delta - 1)(\delta + \alpha_1 + \alpha_2 - 1) = 0 \tag{2.15}$$

The solutions are $\delta = 1$, a stable mode, and $\delta = 1 - \alpha_1 - \alpha_2$, which requires

$$|1 - \alpha_1 - \alpha_2| < 1 \tag{2.16}$$

for stability. Expressed in terms of the original variables, this is

$$\left|1 - K\Delta t(\frac{1}{\rho_1 c_{p_1} h_1} + \frac{1}{\rho_2 c_{p_2} h_2})\right| < 1 \tag{2.17}$$

For a low heat capacity fluid like the atmosphere this explicit flux calculation is very impractical: even a short coupling interval can cause large temperature jumps and unstable oscillations are easily excited. Using values typical of the surface layer in our model a coupling interval of less than 2 hours would be required for this scheme to be stable.

The problem is avoided by making the flux calculation implicit in one of the models. The downside here is that if the models are to be run simultaneously, the other model does not have access to this latest flux until after the next coupling; it uses the flux calculated during the previous interval. The temperature evolutions of the two models are thus out of step and at any given instant energy is not conserved - the energy causing the change in model 1 is only accounted for in model 2 one interval later. If the flux is calculated implicitly in model 1, we have

$$\rho_1 c_{p_1} h_1 \frac{(T_{1,n+1} - T_{1,n})}{\Delta t} = Q_{n+1} = K(T_{2,n} - T_{1,n+1}) \tag{2.18}$$

$$\rho_2 c_{p_2} h_2 \frac{(T_{2,n+1} - T_{2,n})}{\Delta t} = -Q_n = -K(T_{2,n-1} - T_{1,n}) \tag{2.19}$$

As above, we can eliminate Q_n to form

$$T_{1,n+1} = (1 - \beta)T_{1,n} + \beta T_{2,n} \tag{2.20}$$

$$T_{2,n+1} = T_{2,n} - \alpha_2 T_{2,n-1} + \alpha_2 T_{1,n} \tag{2.21}$$

where $\alpha_2 = \frac{K\Delta t}{\rho_2 c_{p_2} h_2}$ again and $\beta = \frac{1}{1+\frac{\rho_1 c_{p_1} h_1}{K\Delta t}}$

and make an eigen- value/vector problem as before:

$$\lambda\delta^{n+1} = (1 - \beta)\lambda\delta^n + \beta\delta^n \tag{2.22}$$

$$\delta^{n+1} = \delta^n - \alpha_2\delta^{n-1} + \alpha_2\lambda\delta^n \tag{2.23}$$

eliminating λ,

$\Rightarrow \lambda\left[\delta - 1 + \beta\right] = \beta$, $\lambda = \frac{\beta}{\delta - 1 + \beta}$

$\Rightarrow \delta^2 = \delta - \alpha_2 + \frac{\alpha_2\beta\delta}{\delta - 1 + \beta}$

and multiplying out gives

$$\delta^3 + \delta^2(\beta - 2) + \delta(1 - \beta + \alpha_2 - \alpha_2\beta) + \alpha_2(\beta - 1) \tag{2.24}$$

$\delta = 1$ is also a solution of this, but now the inclusion of the extra time step means that we are still left with a quadratic for the other values:

$$(\delta - 1)(\delta^2 + \delta(\beta - 1) + \alpha_2(1 - \beta)) = 0 \tag{2.25}$$

$\Rightarrow \delta = \frac{(1-\beta)\pm\left[(\beta-1)^2-4\alpha_2(1-\beta)\right]^{\frac{1}{2}}}{2}$

This can have real or imaginary roots.

real roots: $\alpha_2 < \frac{1-\beta}{4}$

$$2\delta = (1-\beta) \pm (1-\beta)\left[1 - \frac{4\alpha_2}{1-\beta}\right]^{\frac{1}{2}} \tag{2.26}$$

where the fraction in the brackets has been kept small in order to keep the root positive - this allows us to approximate:

$2\delta \sim (1-\beta) \pm (1-\beta)\left[1 - \frac{2\alpha_2}{1-\beta}\right]$

This gives

$\delta \sim 1 - \beta - \alpha_2$ and $\delta \sim \alpha_2$

Using physical values of K, t, ρ etc. implies

$0 \leq \beta \leq 1$,

$0 \leq \alpha_2$

so for $|\delta| > 1$ here we need $|\alpha_2|$ >1. Since in keeping the root positive we have kept $\alpha_2 < 1/4$, these roots are always stable.

imaginary roots: $\alpha_2 > \frac{1-\beta}{4}$

$$2\delta = (1-\beta) \pm i\left[4\alpha_2(1-\beta) - (1-\beta)^2\right]^{\frac{1}{2}} \tag{2.27}$$

Taking the magnitude of delta, we get

$2\,|\delta| = \left[(1-\beta)^2 + \left\langle[4\alpha_2(1-\beta) - (1-\beta)^2]^{0.5}\right\rangle^2\right]^{\frac{1}{2}}$

$\Rightarrow 4\,|\delta|^2 = 4\alpha_2(1-\beta)$

Again, instability requires $|\delta| \leq 1$, here implying $|\alpha_2(1-\beta)| > 1$. Unlike the positive root case, this *can* occur for physical values of α_2 and β and there is the possibility for instability based purely on the coupling interval chosen.

Written in terms of the original variables, this is

$$\left| \frac{\frac{1}{\rho_2 c_{p_2} h_2}}{\frac{1}{\rho_1 c_{p_1} h_1} + \frac{1}{K\Delta t}} \right| < 1 \tag{2.28}$$

Provided $\rho_1 c_{p_1} h_1 < \rho_2 c_{p_2} h_2$, which is generally satisfied in climate models by having the implicit calculation done in the atmosphere, the scheme is stable, however long the timestep. For the other case, with implicit fluxes calculated in the larger heat capacity fluid, the scheme will be unstable for anything other than a rather short coupling interval - less than 50 minutes for the same values as used for the explicit scheme above. This implicit scheme is the one commonly employed in coupled ocean-atmosphere models: fluxes are calculated implicitly in the atmosphere and passed down to the ocean, which thus uses fluxes lagged by one coupling interval from the atmosphere. Free from stability concerns, the coupling interval can then be chosen in order to capture the level of climate variability required.

2.2.2 Actual Coupling

The fundamentals of the coupling mechanism run thus. During integration, each model accumulates average values of certain fields: MOMA accumulates its average SST for that day, and IGCM3 accumulates values of the radiative, sensible and latent heat fluxes directed downwards from the bottom of the atmosphere, a freshwater flux comprising precipitation plus runoff minus evaporation and zonal and meridional components of wind stress. The models communicate at the end of every model day. The model that reaches the end of the day first is made to wait until the other model reaches the same point; data is then exchanged and the models start integrating the next day. MOMA thus uses the previous day's flux forcings as its boundary conditions and IGCM3 uses the previous day's SSTs to calculate the next set of boundary fluxes.

2.3 Necessary Additions

Once the basic boundary conditions for each component have been replaced by the other model as described above, there are still a number of vital features - provided implicitly by the standalone configuration but not replaced in the new coupled system - needed for a realistic climate simulation to be obtained.

2.3.1 Sea Ice

Usually run with a climatological, constant surface restoring, MOMA has no built in sea-ice model - its effects can all be accounted for within the fixed boundary conditions. On coupling to the atmosphere however it was found that the polar oceans were very quickly super-cooled to unphysically low temperatures by the cold atmosphere above (*fig:2.2*). Some freezing mechanism or parametrization was required to keep realistic polar air and sea temperatures. Accurate sea-ice simulation is an active research topic taken alone, and many climate models are coupled to a separate sea-ice component but in this case it was felt that keeping the model fast and simple and providing some insulation for the ocean would be enough. The ice/surface-albedo feedback, often cited as an important factor in climate evolution, was also an important candidate for inclusion in the parametrization.

IGCM3's mixed layer ocean model provides a very basic sea-ice scheme whereby, when cold enough, the gridbox assumes the albedo and heat capacity of a 2 metre thick layer of ice. Heat fluxes and temperature changes are then calculated accordingly until the box temperature is greater than freezing again. This was adapted for the coupled model so that once the ocean temperature dips below -1.96°C (an average freezing temperature for sea water), IGCM3 sees its 2m thick layer of ice instead of the sea surface temperature. All heat fluxes for this gridbox now go into changing the temperature of the ice, so the ocean receives no heat flux and becomes perfectly insulated from the air while the ice is present. When the ice temperature rises above this freezing point, heat exchange between atmosphere and ocean resumes. The latent heat of fusion released from this freez-

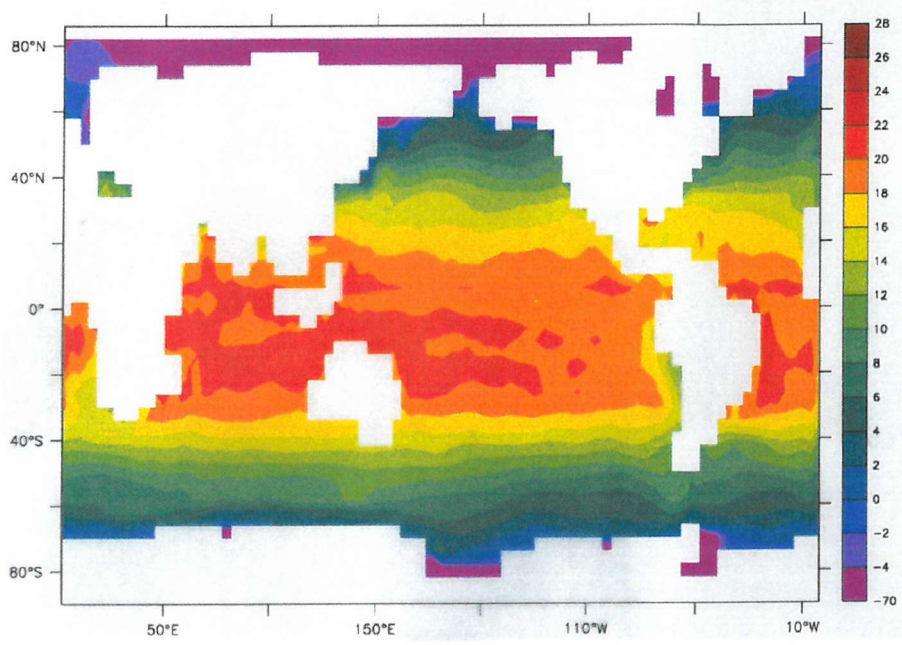

Figure 2.1: *A sample SST (°C) field from before FORTE had a sea-ice parametrization. SSTs as low as -70°C were observed.*

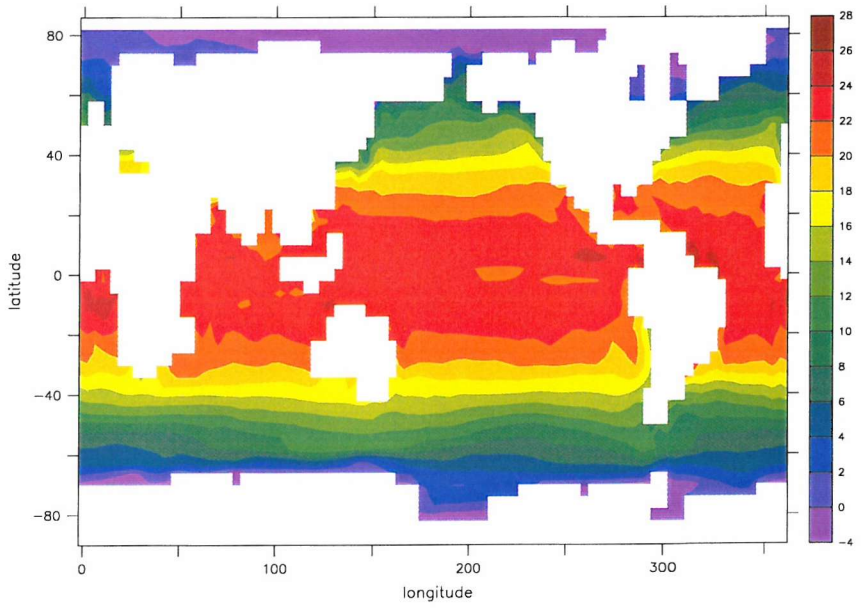

Figure 2.2: *Sample SST (°C) immediately after the introduction of a basic insulating layer under <-1.96°C air.*

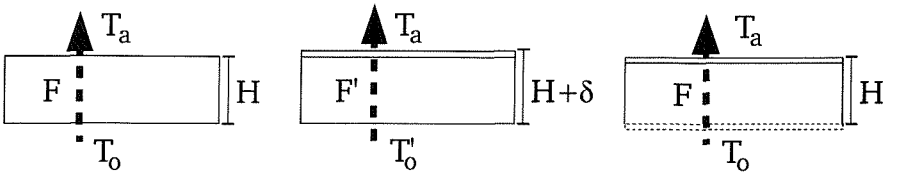

Figure 2.3: *Illustrating the physical justification for the passing of freshwater flux 'through' ice. If a small amount of precipitation falls on the ice, increasing its thickness by δ, the flux F through the ice would be reduced to F' and T_o would increase accordingly. Since the water in contact with the ice must be at the freezing point in order to be in thermal equilibrium with the ice, raising the temperature would bring it above the temperature of the ice. This would cause some of the ice to melt, until the thickness of the ice has decreased to the point where the equilibrium flux F can get out again and T_o can cool again. H is thus left unchanged.*

ing is neglected, as is that required to melt it later, temporarily disturbing energy conservation.

Although insulated from heat exchange and winds, the ocean under the ice still receives freshwater forcing from the atmosphere, passed through the ice. This is a scheme used by others before in simple ice parametrizations (Zhang et al., 1995), and can be physically motivated as compensating the accumulation of ice from precipitation at the surface with melting an equal amount of ice from the bottom of the sheet (*fig:2.3*). This keeps the insulation properties, and hence thickness, of the ice constant; this method also ensures conservation of water, as otherwise any precipitation that falls on top of the ice is not taken account of and is lost from the model.

With this simple scheme it was found that, although insulated from the atmosphere, the ocean temperature under the ice can still drift due to exchange of heat with neighbouring ocean boxes. This can lead to having an ocean which is not in thermal equilibrium with the ice layer above, with the ocean having no means of communication with the atmosphere since the heat flux feedback has been blocked. These anomalies are not large (<5°C), but to remedy them in our scheme the ocean surface under ice feels a small restoring flux, nudging it towards the correct freezing point temperature. Energy is conserved by adding the

required amount to the ice temperature, allowing warmer waters advected under the ice sheet to help melt it.

Another feature of real ice lacking from this model is the phenomenon of brine rejection. As sea water freezes, the salt ions contained within cannot incorporate themselves into the crystal structure and the as-yet-unfrozen water becomes more and more salty. Small pockets of this brine get trapped in the forming ice structure - this is why sea-ice is not pure, but still has a much lower salinity than seawater, from ~10 p.s.u. for young ice to 1 to 3 p.s.u. for older, multi-year ice. The net result is a layer of negatively buoyant water local to the region of ice formation. This process is important when considering deepwater formation in the polar oceans, as the dense water convects. A very simple parametrization of this local salinification effect has been included in the most recent version of the sea-ice model, but has yet to be fully tested. The effect is absent from all results presented here, but is available in the latest version of FORTE.

2.3.2 Runoff scheme

When run as a standalone atmosphere model, IGCM3 considers the ocean to be an infinite reservoir of water. As a result, it need not worry about the fate of rain that falls on the land; any water that cannot be absorbed by the soil-moisture bucket model used is disregarded under the assumption that it finds its way back to the sea somehow. Thus no account is kept of sea-level or salinity, merely SST. This is no longer a valid shortcut once coupled to an ocean that tracks salinity changes; any water taken out by evaporation needs to be returned in order to stop the ocean becoming ever more salty. The distribution of this freshwater input is also important in recreating realistic near-shore water-masses near major river outflows.

To this end a runoff scheme had to be incorporated into the model to collect the excess water rejected from the land scheme and ferry it back to an appropriate location on the coast. This was implemented as a routine in IGCM3 which keeps track of this excess water, then adds it to certain boxes in the precipitation field that is passed to MOMA. These coastal dump boxes are intended to represent the

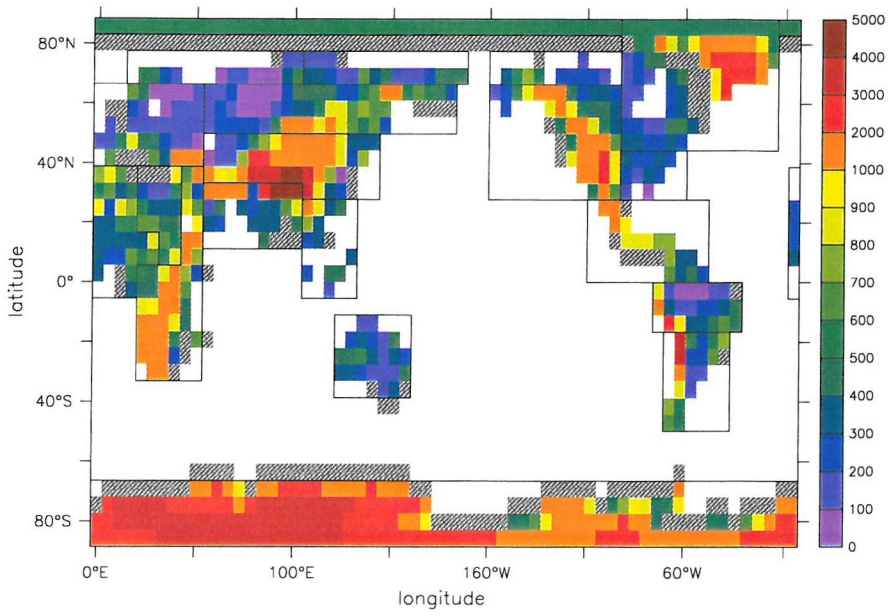

Figure 2.4: *Map showing the IGCM3 orography (colours, in metres) runoff catchment areas (black boxes) and the dump zones for each catchment (grey shaded).*

major land freshwater inputs to the oceans; each dump has a catchment area and all the runoff from that area is instantly transported to the relevant dump point, split equally between the number of boxes in that particular dump.

For the simple, idealised geographies that comprise the majority of this experiment these schemes are simple to implement, with the runoff usually being pushed to the nearest ocean point. For the more realistic geography however, a more sophisticated design was required. This was derived from Fanning and Weaver (1997a) and then fine-tuned by Vicki Robertson (a student in SOC's summer-school) to give suitable magnitudes of freshwater inputs to the correct areas wherever possible (*fig:2.4*).

2.3.3 Coastal Tiling

As has been mentioned, MOMA and IGCM3 are on grids of differing resolution: 4° and ~5.6°. Any section of coastline is therefore not going to look the same on

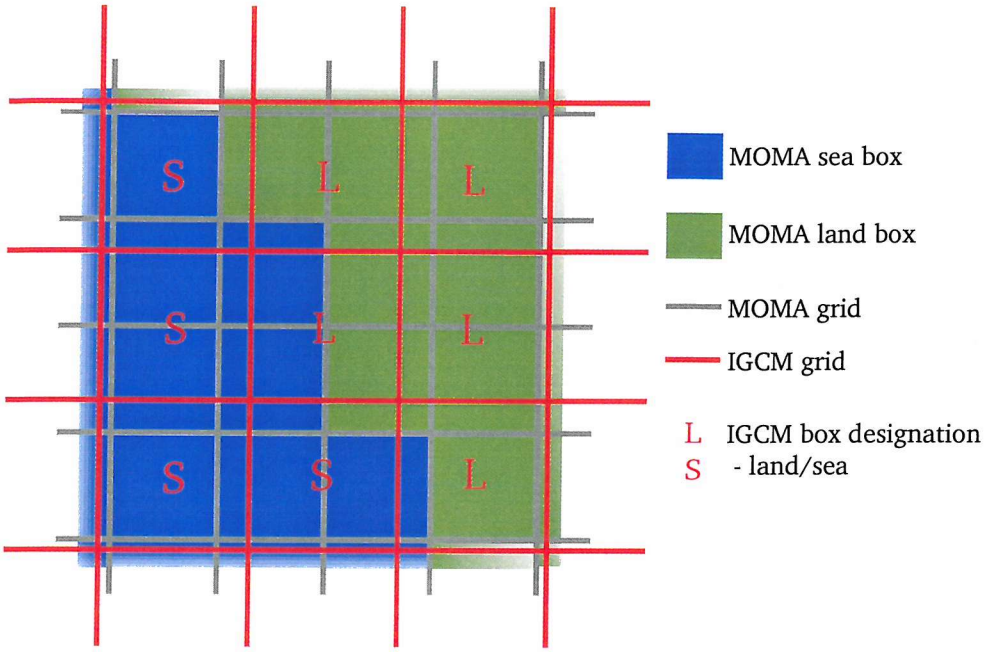

Figure 2.5: *Mismatch between model coastlines due to different model grid resolutions.*

both grids, since each grid box must normally be assigned, as a body, as either an ocean or land one (see figure 2.5). This can lead to complications when coupling the models together, both in ensuring that the global land/sea ratio is the same in each model, thus conserving energy as the fluxes are passed from atmosphere to ocean, and locally at mismatching coastlines to ensure that only valid data is passed. If a MOMA ocean box straddles the boundary between IGCM3 ocean and land boxes, MOMA needs to see only the ocean data and cope with the area with no valid data.

There are a number of methods for overcoming this issue. One used early in the development process involved merely screening out all land values from either model during the communication part of the coupling and extrapolating from the remaining valid data into other areas as necessary. This works well (i.e. produces a reasonable looking climate) but does not conserve energy, as fluxes are created or ignored as is convenient.

A far more satisfactory method is that of 'coastal tiling', which essentially allows

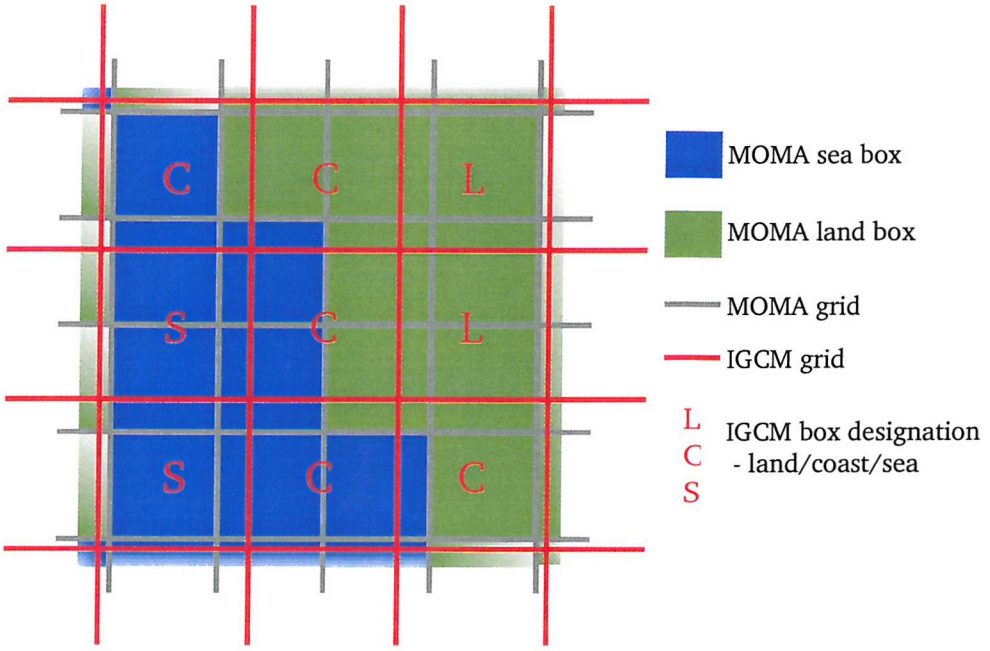

Figure 2.6: *The introduction of a third surface type allows the coarser grid to provide a fully energy-conserving representation of the finer grid.*

the use of partial gridboxes - instead of being wholly land or sea, boxes can be, say, 70% sea and 30% land, or any ratio required. The two model grids are laid over each other, and for each point in MOMA that is below IGCM3 land *and* sea boxes, the overlying boxes on the IGCM3 grid are redesignated to a new category - 'coast' - with the relevant ratio of land/sea area dependent on how much of the box is over the ocean (*fig:2.6*). When the boundary layer routines are called to work out the fluxes for these points, each of these coastal points is assigned two sets of fluxes, one associated with its land characteristics, and one with the ocean ones. The 'ocean' fluxes are passed down into the ocean, the 'land' fluxes into the land surface scheme and an average of the two (weighted by the land/sea ratio of the point) passed upwards into the atmosphere. Thus the scheme conserves energy exactly, both in the global average and also on a local gridbox scale.

The introduction of this scheme was indeed shown to conserve energy correctly and a spurious source of ~4W/m^2 was found to be eliminated.

2.4 Additional Features

2.4.1 Periodic Coupling

Theory

In the current model setup (T21 atmosphere resolution, 4° ocean), the atmosphere model is the most computationally expensive part of the system, requiring ~4 times more integration time per step than the ocean, and thus is a bottleneck in the system. This is a common problem, as atmosphere models need relatively short timesteps due to the shorter adjustment time of the atmosphere system, compared to the ocean. Running the model with a straightforward synchronous timestepping scheme on the available hardware gives an integration speed of ~12 model years per day. To do a 1000 year run would then take the best part of 3 months, which is unaffordable within the scope of this project.

The difference in equilibration time between the two systems can be used to alleviate the problem somewhat. The ocean adjustment time is slow and over a period of a few years the surface conditions, and thus the influence on the atmosphere, will not change very much. A periodically synchronous time stepping scheme, developed by Sausen and Voss (1996), takes advantage of this to allow portions of the integration to be run without the atmosphere model at all, thus removing the bottleneck and allowing periods of much faster integration.

The basic scheme is illustrated in figure 2.7. To begin with, the two components are run synchronously. During this period, the boundary conditions provided by the atmosphere are stored in a data array. When a year's worth of values are stored the atmosphere model is 'switched off' and the ocean integrated on, recycling these stored conditions - since the ocean is slow to change, this method assumes that atmospheric conditions will not change very much over a few years and the initial boundary conditions can simply be recycled, rather than recomputed. After a period of time when it is judged that the ocean will have changed enough for the stored boundary conditions to be significantly wrong, the atmosphere model is brought back in as a fully interactive component again. The faster atmospheric equilibration time means that it will not take very long for the atmosphere to adjust

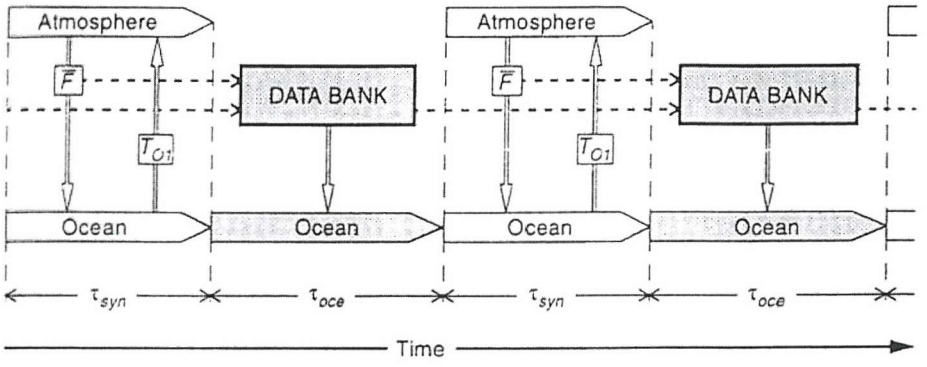

Figure 2.7: *Schematic of the basic periodic coupling scheme (taken from Sausen and Voss (1996)).*

to the new ocean state, and after a few months, the new boundary conditions are ready to be archived for reuse during another 'ocean-only' period.

This is the method in its simplest form. A refinement to this, also developed by Sausen and Voss (1996) involves extracting the seasonal variations from the most recent synchronous period and creating the boundary conditions by combining them with an annual average constructed from the long term trend in the model. Each annual mean (F_{oce}) is constructed from the mean of the boundary conditions from this year (F_{syn}) and those from previous years ($F_{oce(old)}$), with a weighting so designed to create some memory of the long term trend, not just that of that particular year:

$$F_{oce} = \frac{g \cdot F_{oce(old)} + F_{syn}}{g + 1} \tag{2.29}$$

Following Voss et al. (1998), a weighting value (g) of 2 was used. The full forcing field to be used for the ocean-only period (f_{oce}) is then constructed by removing the mean (F_{syn}) from the most recent year's full field (f_{syn}) and adding in this new running mean:

$$f_{oce} = f_{syn} - F_{syn} + F_{oce} \tag{2.30}$$

Voss et al. (1998) found that this produced a smoother, more faithful reproduction

of the climate state obtained from a conventionally coupled model.

Periodic Ratios

The degree of error involved in the periodic coupling depends on the ratio of recomputation to recycling time. In the limit of no recycling one regains a normally coupled model and, at the other extreme where the initial conditions are recycled forever, a standard uncoupled ocean model. Voss et al. (1998) implemented periodic coupling in a quasi-geostrophic model of similar resolution to FORTE, with a ratio of ~1:4 years (recompute:recycle). They suggested that their choice had proved quite conservative and that higher ratios would be acceptably accurate. Kim et al. (2003) used it in a more complex coupled model and used a higher ratio of 1:5 years during a single 1000 year run to simulate the Last Glacial Maximum. All of the runs documented here were done with 5 years of recycle time and 19 months of synchronous run in between; thus the model has 7 months to recover from any small coupling shock (a jump in climate characteristics produced by coupling two models that have been spun up independently) in each cycle before the new boundary conditions are stored. In choosing the ratio it is important not to make each cycle (recompute time + recycle time) a multiple of 6 months: in tests on an energy balance coupled model Sausen and Voss (1996) found that these multiples caused the greatest Root Mean Squared [RMS] error when synchronous and periodically synchronous runs were compared.

Figures 2.8 and 2.9 show the global average difference in SST and SSS between a fully synchronous idealised run and one done with this 1:5 year periodic ratio. After approximately 80 years the two runs have essentially converged - the average SST difference is 0.035°C, 0.00208 p.s.u. for SSS. The RMS differences between the two runs are 0.44°C and 0.18 p.s.u.. The discrepancy can be ascribed to the two runs having different 'weather' but the same 'climate' - the error is comparable to that obtained by comparing 2 different years from one of the runs during a later, stable period which would also represent different realisations of the same mean climate state. The initial deviation between the two runs can be ascribed to coupling shock. As the periodic coupling reduces the feedback between the two models, it might be expected that using it would cause the models to take longer

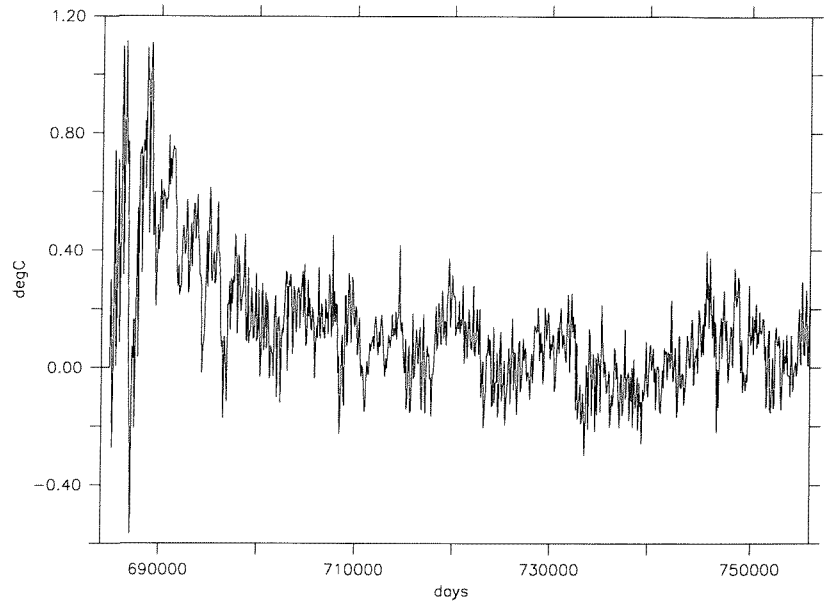

Figure 2.8: *SST difference (°C) between synchronously and periodically coupled WaterWorld runs over 200 years.*

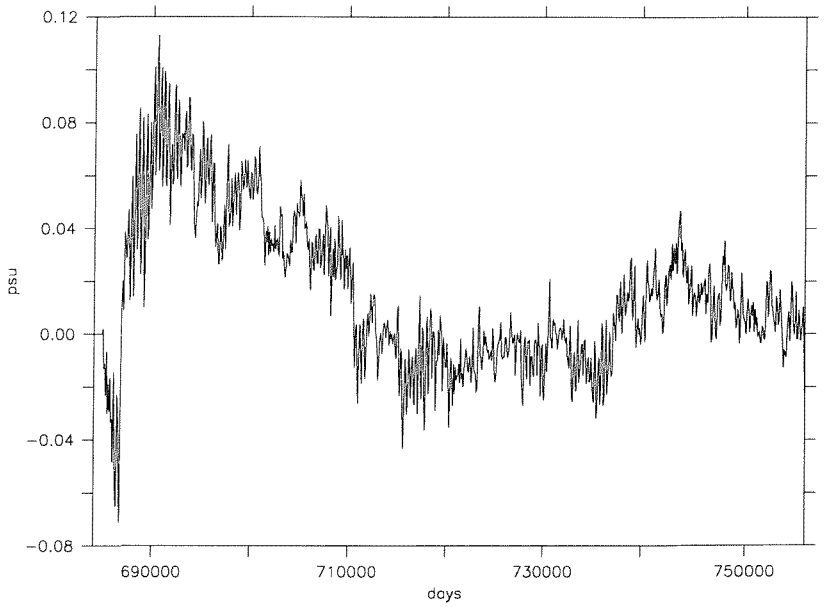

Figure 2.9: *SSS difference (p.s.u.) between synchronously and periodically coupled WaterWorld runs over 200 years.*

to adjust to each other's state. Kim et al. (2003) adopted a policy of starting their runs with a 100 year period of synchronous integration to avoid this phenomenon, but as can be seen here, our model still converges on the same state as for the synchronous case. For the run shown, only a two year initial synchronous period was used. Most of the runs in this project were done by running on from the end of the previous coupled scenario, so the models are already well adjusted to each other.

It might be expected that a scheme such as this might introduce spurious frequencies, forced by the turning on and off of the atmosphere, into the climate forcing. A frequency-power plot of northern hemisphere SST variation (which one would expect to be sensitive to this, since it is so directly affected by the imposed fluxes) during the above two runs (*fig:2.10*) shows a generally noisy signal with a strong annual signal (at 0.00278 cycles/day). There is some suggestion of power in lower frequencies in the periodic runs, apart from the general drift at 0Hz, but this is small and generally not distinguishable from the noise. A variable such as the overturning rate does not show any signal above the noise level at these low frequencies.

The RMS error tests above show that both synchronous and periodically forced simulations follow very similar evolutions toward an equilibrium state, so we conclude that the periodic coupling spinup method does not introduce any spurious features to the final state. To avoid any signal biassing in the results shown here however, a synchronously coupled period of 100 years was nevertheless appended to the end of every simulation - the small low frequency spikes in the power spectrum disappear completely during this period.

2.5 RealWorld Tests

2.5.1 Control Integration

Constructed during the course of this project, FORTE required a fair degree of testing, both to ensure that it was functioning as intended and to acquire a control profile of its behaviour against which the experiments could be compared to see

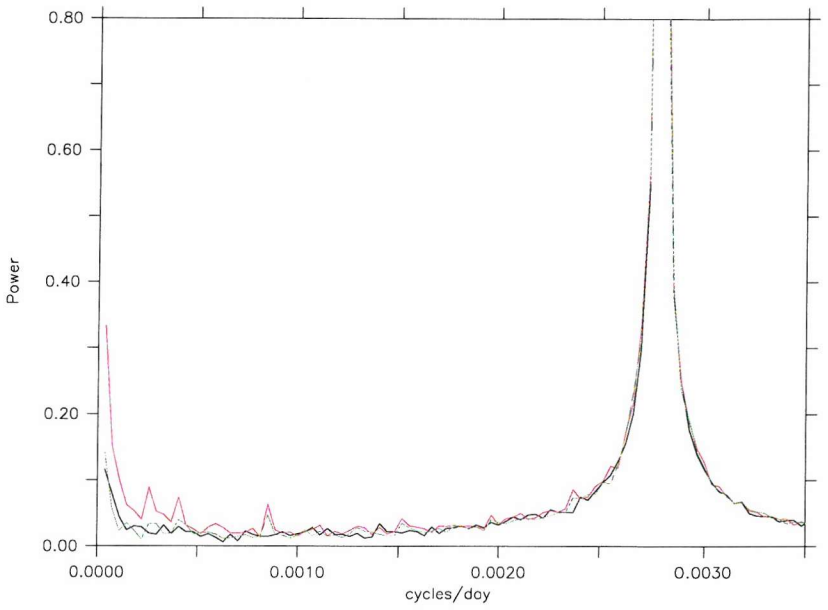

Figure 2.10: *Power frequency diagram for northern hemisphere SST for 100 sample years of WaterWorld run.* Black*: synchronous coupling;* Red*: asynchronous sample 1;* Green*: asynchronous sample 2. The asynchronous runs show small amounts of power at 0.00028 cycles/day (~10 years), 0.0004 cycles/day (~6.8 years) and 0.00085 cycles/day (~3 years). The peak at 6.8 years could correspond to the periodic coupling ratio of 570 days synchronously coupled plus 1800 days of ocean only run.*

which scenario changes were significant. The easiest scenario in which to test the model is that of the current climate, as this is the only one for which reliable observations of all relevant factors are easily obtainable and is also the one that the individual components were designed to model - the first model runs were therefore based on a 'real' configuration (experiment 'RealWorld'). Any model behaviour that deviates from observations can readily be spotted and flagged as either a coding error or a weakness in the model design. Coding errors can be fixed, but inaccuracies in the representation caused by some over-approximation present a greater problem. Since the model is deliberately simplified, in most cases little could be done about these sources of error except note them and take account of them in the analysis stage. Given the idealised nature of this project such errors do not invalidate the model, rather they indicate areas of the climate where more care may have to be taken in interpreting the results.

It is naturally difficult to validate that a model is accurately simulating the effects of an arbitrary, idealised climate configuration, as there are no observations against which to check. This is an unavoidable concern when attempting to make climate predictions: how to ensure that a model designed to simulate one situation (i.e. the current climate) will provide accurate predictions when applied to another (i.e. a world with increased CO_2) for which no observations exist. In our case it must be enough, having tested the model under current, observable conditions, to hope that the primitive-equation nature of the two models - that they are not overly parametrized and tuned to one particular state - is sufficient for the same fundamental physics that guide the 'real' climate simulation (that we *can* verify) to accurately reproduce the new scenarios. If we can analyse the resultant new climates and explain them in the analytical terms of the physics that we understand, independently from the model then there is a good chance that we are seeing a valid result.

Most climate models undergo a tuning process (e.g. Jones et al. (2003); Gordon et al. (2000)) under which climatologically sensitive parameters are tweaked to improve representation of the top/bottom of atmosphere fluxes or ocean transports once the basic model setup has been achieved. This has not yet been done for FORTE, and all parameters are set at default 'sensible' values (see the archived

code for details). FORTE's RealWorld representation would no doubt benefit from this process, but the process would be somewhat arbitrary for the idealised scenarios as the 'correct' fluxes for such imaginary configurations are unknown - all model runs, real and idealised, are thus presented 'untuned'. The sensitivity of the model to various climate forcings may not therefore be 'correct', but the processes and feedbacks that result will still be qualitatively valid, if not quantitatively.

Given here is a brief overview intended to demonstrate that, whilst not up to the standards of a state of the art coupled model, FORTE's climate profile for a situation able to be tested against modern observations suggest that the various processes present in the model are likely to be functioning in the manner intended to produce a 'sensible' climate. Data here is from a simulation conducted by Clotilde Dubois, also at SOC. The 'untuned' model has been run here for 700 years, with no form of flux adjustment or climatological restoring. The model is not yet at full thermal equilibrium - deep ocean temperatures are still drifting downwards at a rate of ~0.1°C per century. Unlike most of the idealised runs, Gent-McWilliams isopycnal mixing has been used here - this improves representation of the North Atlantic MOC, which is otherwise too strong.

As can be seen from figures 2.11 and 2.12, FORTE captures the basic features of the global surface ocean reasonably. The maximum average temperature at the equator is about 30°C, dropping to freezing at the poles, with some sign of a warm pool in the west Pacific. The model also reproduces a marked asymmetry between the salinities of the Atlantic and Pacific, with a very salty Mediterranean and a fresh Arctic ocean.

The too-cool equator is a result of the coarse resolution exaggerating upwelling there, and the polar oceans, especially the Southern Ocean, are rather too warm. The salinity field shows some unrealistic (and in some cases, unphysical) extremes around the coasts, with the riverine dump points having some very low values (negative in areas of the Hudson bay!) and other areas being too high.

Surface air temperatures (*figs:2.13,2.14*) show a reasonable pattern, with polar temperatures reaching -40/-60°C at the N/S pole and inland high temperatures of up to 50°C in summer - this range is quite wide, but not unreasonable. Reflecting the too warm Southern Ocean, southern hemisphere winter freezing is restricted

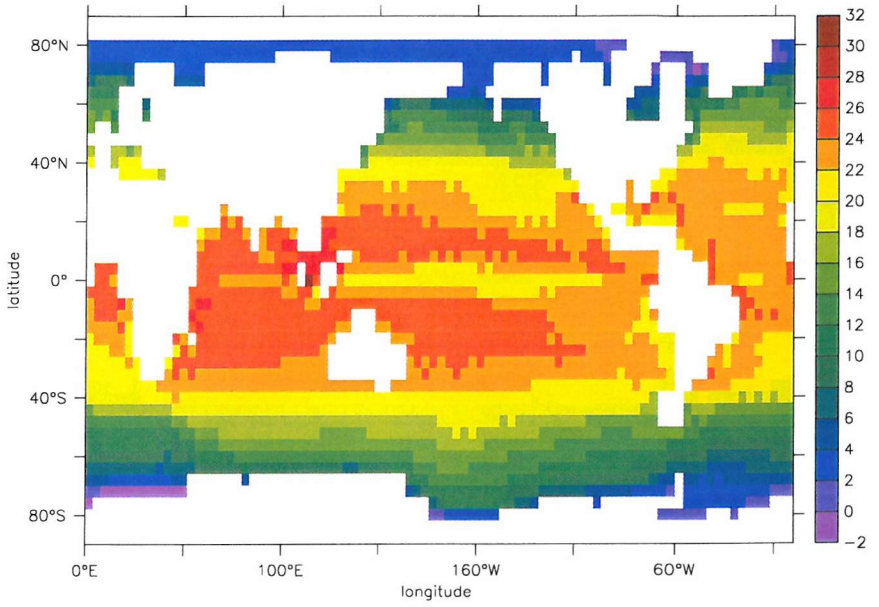

Figure 2.11: *Annual average SST (°C) after ~700 years of periodic model integration.*

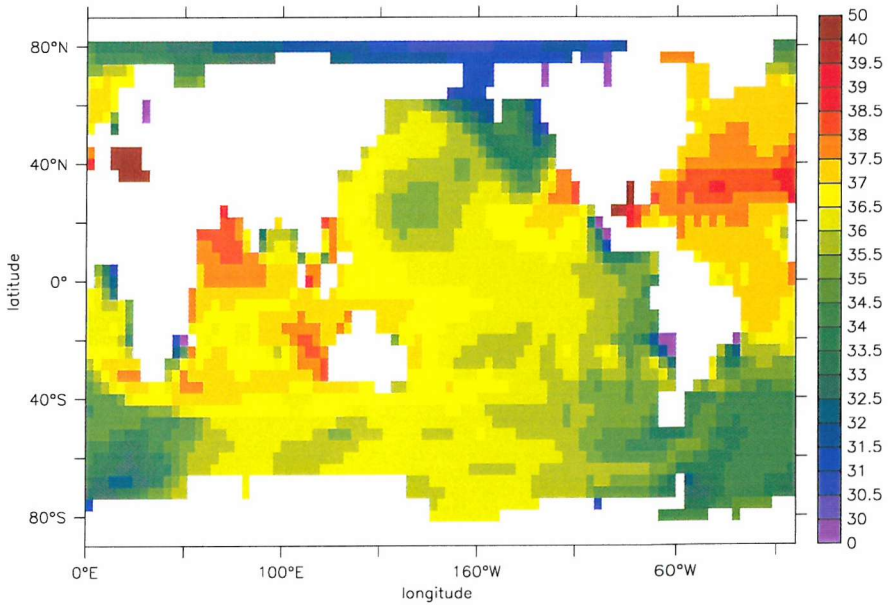

Figure 2.12: *Annual average SSS (p.s.u.) after ~700 years of periodic model integration.*

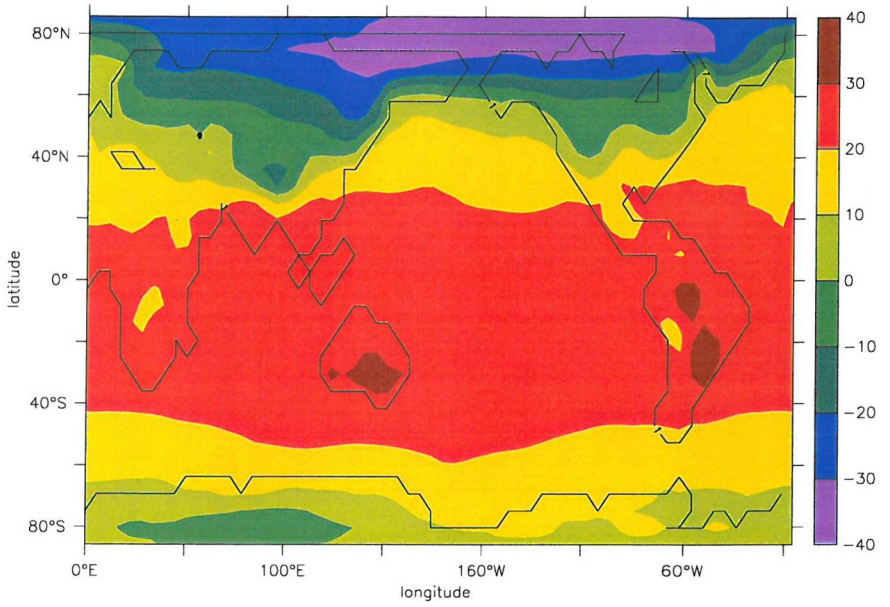

Figure 2.13: *December, January, Februrary average [DJF] surface air temperatures (°C) after 700 years of coupled run. The landmask is outlined in black.*

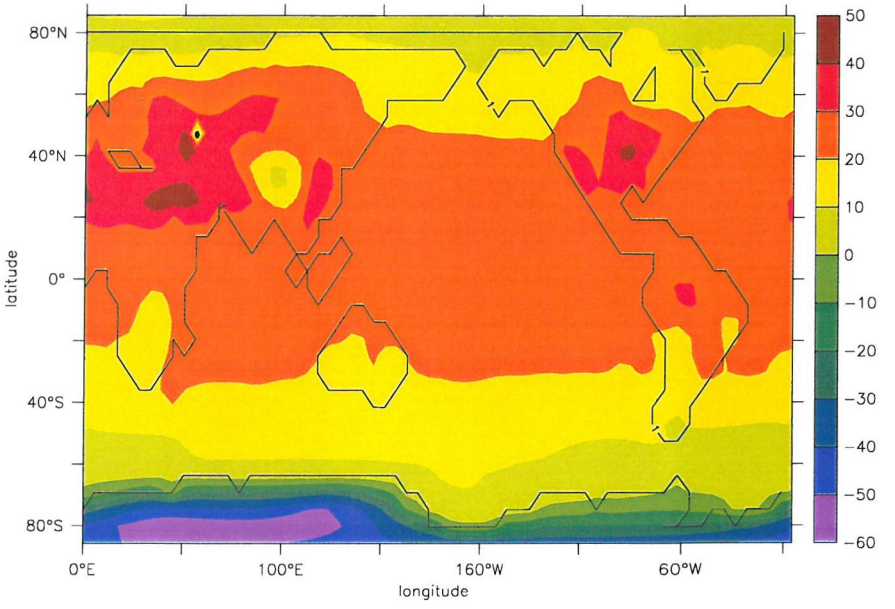

Figure 2.14: *June, July, August average [JJA] surface air temperatures (°C) after 700 years of coupled run. The landmask is outlined in black.*

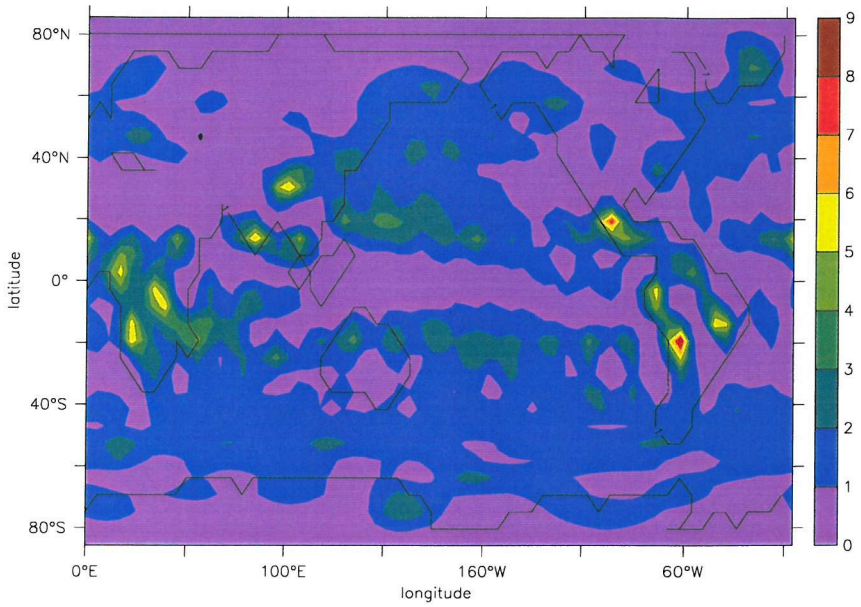

Figure 2.15: *Annual average rainfall (mm/day) after ~700 years of periodic model integration. The landmask is outlined in black.*

to Antarctica.

The rainfall figure (*fig:2.15*) for the coupled run shows a similar pattern to that obtained from a control run of the atmosphere (*fig:2.16*), although the lower tropical SSTs result in a reduction in precipitation in this region, with the loss of the maxima over the ocean around 10°N/S.

A plot of the Atlantic overturning streamfunction (*fig:2.17*) shows a strong cell with a maximum transport of 22 Sv at around 1000m depth with significant cross-equatorial transport. The cell extends almost to the bottom of the ocean - there does not seem to be any indication of the intrusion of Antarctic Bottom water into the Atlantic.

Unfortunately the model also displays a significant overturning cell in the Pacific (*fig:2.18*), not observed in the real world. This has a maximum around 30Sv, with little cross-equatorial transport. The reasons for the existence of this cell in the model are currently unknown; it is somewhat surprising, given the reasonable representation of surface salinity in the basin and the fact that high latitude SST

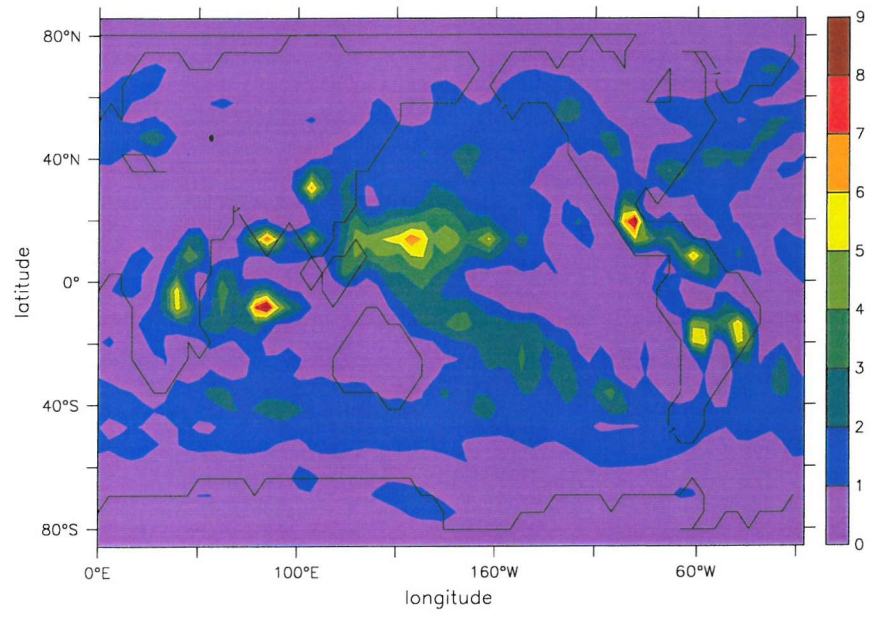

Figure 2.16: *Annual average rainfall (mm/day) from an IGCM3 run with specified climatological SSTs. The landmask is outlined in black.*

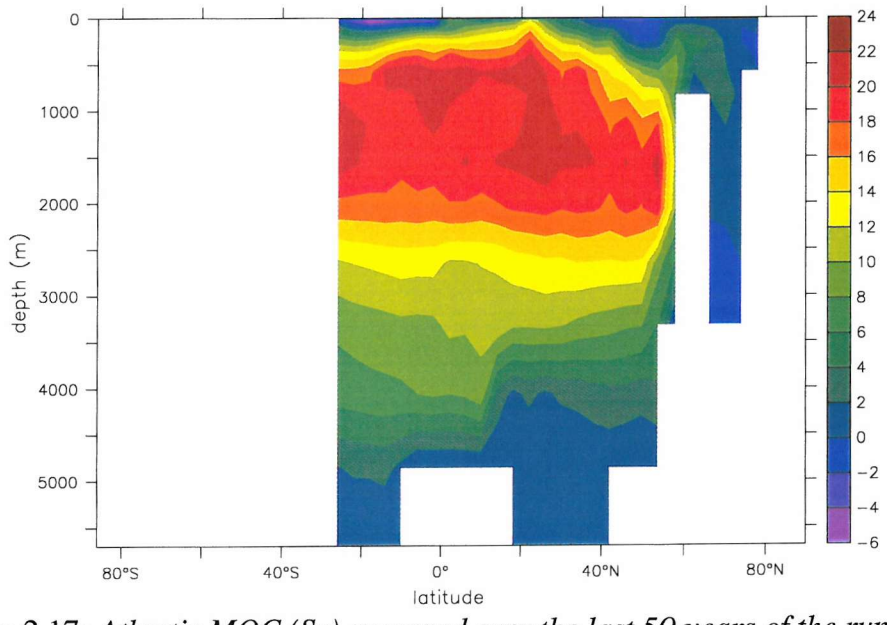

Figure 2.17: *Atlantic MOC (Sv) averaged over the last 50 years of the run.*

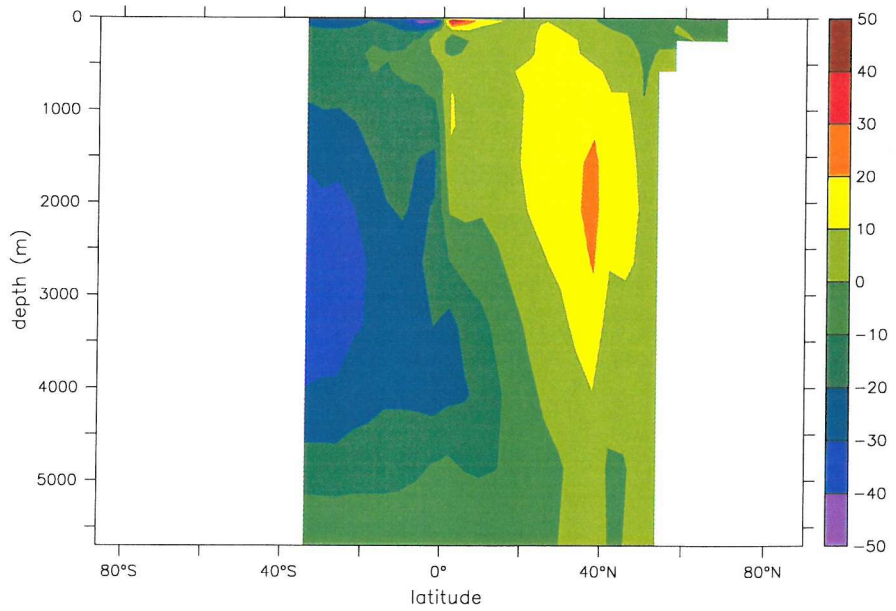

Figure 2.18: *Pacific MOC (Sv) averaged over the last 50 years of the run.*

is generally too warm, both factors that would tend to stablise the stratification and inhibit overturning. Limited tests with flux adjustments (see section 2.5.2) do however remove this cell.

2.5.2 Flux Adjustments

As was mentioned in the introduction, FORTE was originally developed for use as part of the COAPEC project, to look at variability in current climate using a coupled system. It is therefore desirable for the model to produce a faithful simulation of this current climate. A problem long associated with coupled models, especially those of coarser resolution, has been that of climate drift when spun up to modern day conditions (e.g. Gregory and Mitchell (1997)). When the models are run with non-interactive climatological boundary conditions, the fluxes they receive will force the model into the observed state - they act as a brake on how far the model's representation can drift from observations. Separated from their static boundary conditions and coupled together, this limitation is removed. A faithful representation of the real system will only be achieved if the transports

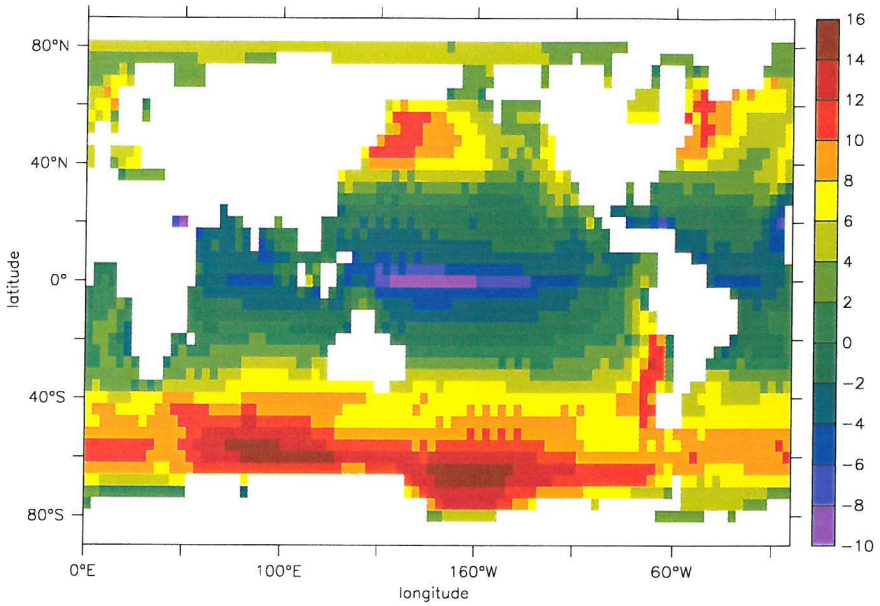

Figure 2.19: *Difference of figure 2.11 from the Levitus (1998) climatology (°C).*

and processes in the models are good enough not to need this brake to stop them drifting away from the desired state. Coarse resolution models often have trouble producing realistic transports; in ocean models this is often associated with poor resolution of relatively narrow western boundary currents, poor representation of sub-gridscale eddy processes and the significant numerical diffusion that is required for stability, in the atmosphere with the representation of storm tracks and sharp fronts. Unsurprisingly, a coupled model made of such components will tend to drift. For short runs of a few years this can sometimes be accepted, dependent on the rate of drift, but this can be a major issue for longer runs (*fig:2.19*).

A common method of cancelling this drift is that of 'flux adjustment' (Sausen et al., 1998). Essentially a sandwich layer is put in between the models that adds or subtracts some constant value from each gridpoint before the fluxes are passed, so that each model sees fluxes that imply that the other model has a compatible transport - compatible in that, when they are combined, the model state does not drift.

The theoretical rationale behind this seemingly arbitrary forcing of the solution

toward the one desired is that, because the changes in the fields are constants, perturbations in one model will still be passed as such to the other model which will then respond accordingly, unaffected by the constant offset. Indeed, because the offset ensures that the perturbations occur around a realistic mean, a *more* accurate response should be obtained. Unfortunately the climate system does not work in such a linear way: the transport errors that were the reason for the adjustment in the first place are expressed once more (Marotzke and Stone, 1995) as soon as there is any perturbation from the adjusted-to mean state.

This warping of the perturbation response clearly reduces the credibility of climate model predictions and some of today's state of the art climate models have progressed to the point where a stable mean climate, comparable with that observed, can be achieved without them (e.g. Gordon et al. (2000); Boville and Gent (1998)). Given that some climate models do show significant drift from the observed mean climate state however, (e.g. Gregory and Mitchell (1997); Furevik et al. (2003)) and that not starting from the same equilibrium state as the current climate may result in an incorrect response of the system under a climate change scenario, flux adjustments can help make the best of the situation. Since the causes of errors in the climate without flux adjustment contribute to the errors of the perturbed adjusted system as well, it may be more accurate to use flux adjustments to at least start from the correct mean state when doing a climate change experiment, rather than start from an unrealistic state of a non-adjusted system and still have those errors expressed in the response. Half of the models cited in the IPCC Climate Change 2001 report (Houghton et al., 2001) used flux adjustments in calculating the response of their climate systems, and no systematic difference was observed in their responses as compared to the non-adjusted models. Whilst not ideal then, flux adjustments are still required in many models of higher complexity than used here and it is not surprising that FORTE suffers from similar symptoms as some of these models (e.g. warming in the Southern Ocean and underestimation of sea-ice extent) when attempting to reproduce the observed climate. For this reason, a method for calculating and using flux adjustment fields has been implemented for use in FORTE.

FORTE does not, however, drift to completely unphysical climate states or fail

catastrophically when run unadjusted, as can be seen from the unadjusted Real-World tests previous (see section 2.5.1). This is fortunate, as the flux adjustment method cannot be used in idealised configurations, since one needs to know the 'correct' climatology from which you do not want to drift and these are unknown for the imaginary situations used here. The idealised runs are thus all done *without* flux adjustments and the model is left to come to a state where the different components are 'naturally' balanced. The flux adjustment framework presented here has only been used in the following, rather limited tests of the RealWorld climate and is here purely as part of the documentation of the model development work.

The adjustment fields are calculated thus: the component models are run, communicating as normal, but MOMA does not use the IGCM3 fields, instead it is forced by monthly climatological fields (a daily restoring field is calculated from the nearest two monthly fields, based on the day of the year). These climatological values are also passed up, through OASIS, to act as boundary conditions for IGCM3. Both the heat and freshwater fluxes used by MOMA to restore to these fields, and the fluxes IGCM3 produces in response to them are archived on a daily basis throughout the calculation run. After the run, these fields are averaged over a suitable time period and subtracted from one another to produce an annual climatology of monthly average flux-difference fields. These are the flux adjustments which are then added to the fields passed through to MOMA before they are used to force the ocean.

The fields shown here are from a proof-of-concept run where the adjustments were calculated over a ten year period following the spin up of the coupled model with monthly fields from Levitus (1998) and the European Centre for Midrange Weather Forecasting. The adjustments were then applied over the following 5 year run. The lack of real ocean-atmosphere feedback under sea-ice, due to the rather basic nature of the scheme used, occasionally produced some extremely high adjustment fluxes in ice-bound areas that, when used, produced very inaccurate results - for these test runs all fluxes in the Southern Ocean were thus ignored and the drift errors seen previously are still apparent in these regions. For a production run, flux adjustments would need to be calculated as averages over a much

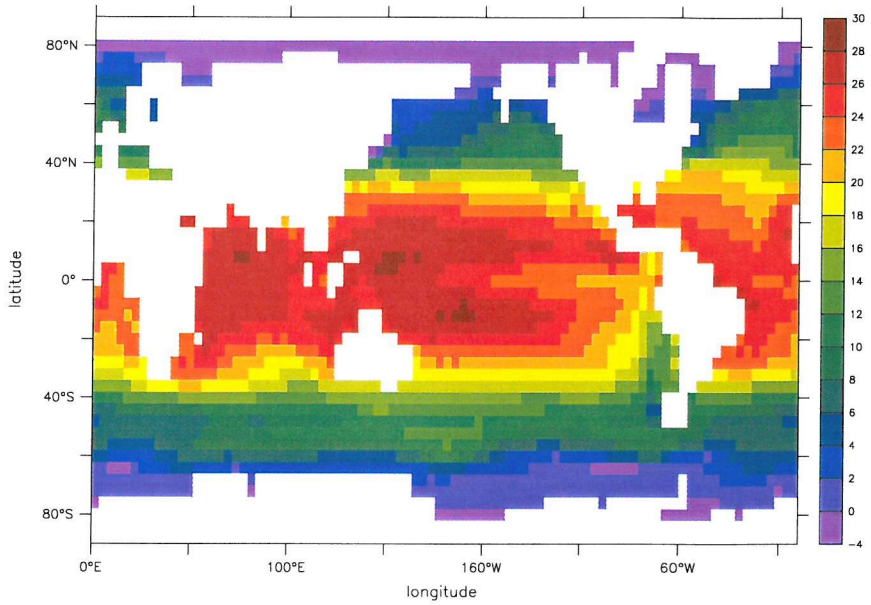

Figure 2.20: *Flux adjusted SST (°C) field after ~5 years.*

longer period to be certain of avoiding model drift: Furevik et al. (2003), with a more complex and expensive coupled model use a 10 year calculation period and still find some drift that they ascribe to their adjustments not averaging over the timescales of interdecadal variability.

The 'adjusted' MOMA fields (*fig:2.20*) are, unsurprisingly, far closer to the observed climatology than before. Much of the freshwater adjustment (*fig:2.22*) is quite small, with significant amounts of water only required around the Arctic and in some of the river drainage areas. The heat field (*fig:2.23*) shows more error in the model, with some large values required over the Southern Ocean and in some western boundary current regions where FORTE's resolution is likely to underestimate the flow and associated heat transport.

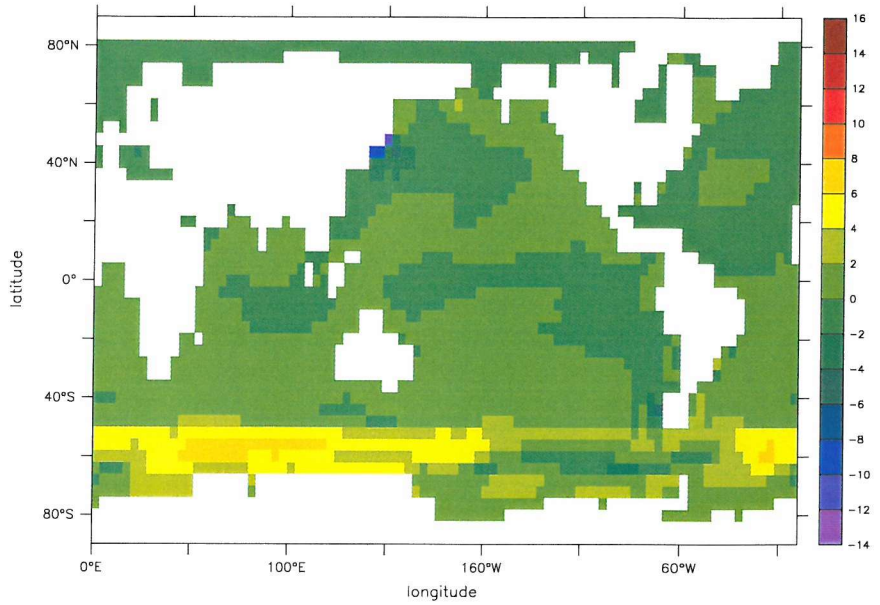

Figure 2.21: *Difference of the flux adjusted SST (°C) field from Levitus - c.f. figure 2.19.*

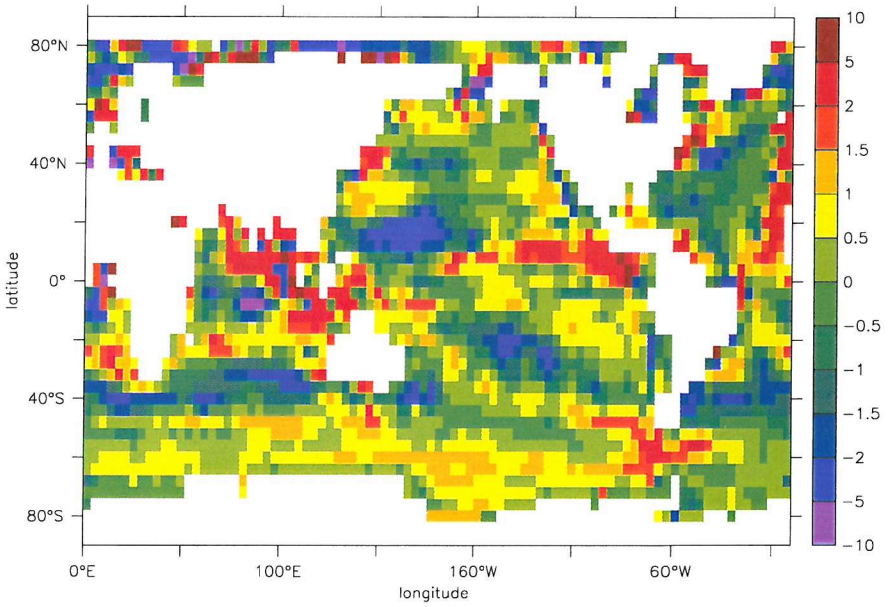

Figure 2.22: *Annual average flux adjustment field for the freshwater forcing (m/year).*

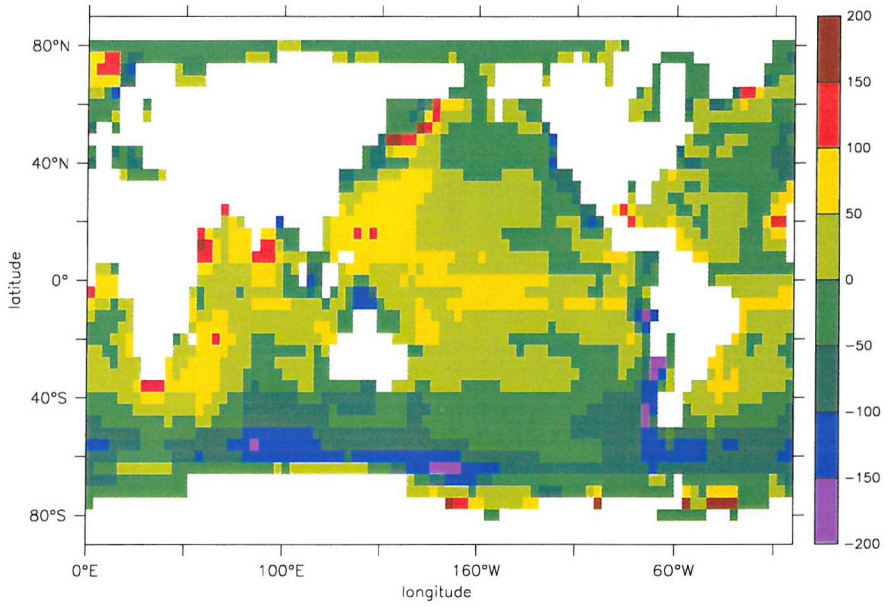

Figure 2.23: *The annual average flux adjustment for the heat forcing (W/m^2).*

CHAPTER

THREE

Experiments

3.1 Experimental Setup

Model development aside, the aim of this project is to isolate and study the effects of changing the ocean circulation by geographical forcing on climate and the mechanisms whereby these changes occur. To this end, a set of idealised geometries were designed. These fall roughly into two categories: aquaplanets with virtually no land at all, and basin planets which have a more substantial amount of land.

3.1.1 Aquaplanets

To maximise the effect of the ocean and reduce the presence of non-ocean effects, these first experiments were done with global setups that contain as much ocean and as little land surface as possible. Each case differs from the others only by a low ridge of land one grid box wide that stretches the whole depth of the ocean, blocking ocean flow completely but having relatively little direct impact on the overlying atmosphere. The three cases are designed to cover a (highly idealised) spectrum of ocean circulation regimes (*fig:3.1*). The first, WaterWorld [WW], lacks any form of barrier to zonal flow in the ocean, so is unable to support any form of meridional flow by geostrophy as it is unable to build up the

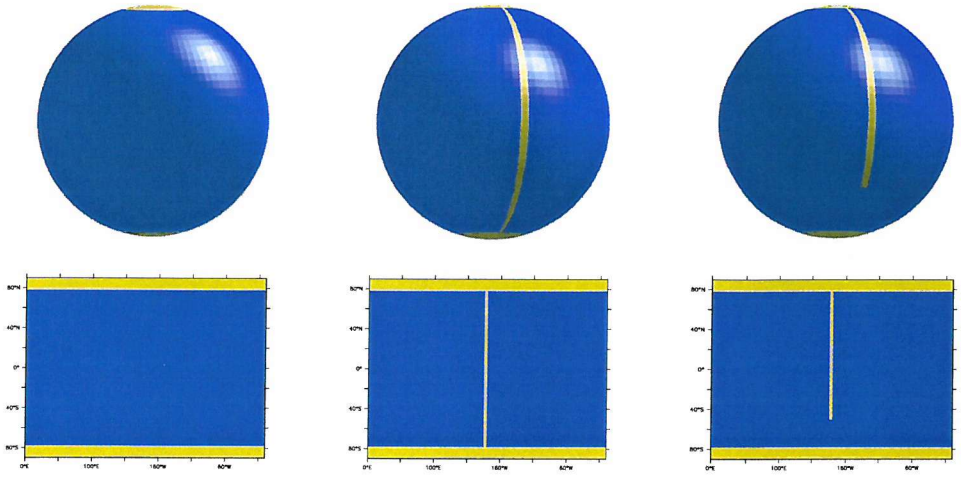

Figure 3.1: *The geometries of the first three idealised scenarios, 3D and plan views - all later results will be presented in the plan view format. Experiments WaterWorld, RidgeWorld and DrakeWorld.*

zonal pressure gradient that supports normal meridional flow (see section 4.5.2). The second, RidgeWorld [RW] represents a standard ocean basin that can support a normal Sverdrup circulation as it does now have a meridional barrier, so might be expected to form a more 'normal' MOC of a form similar to those found in other two-hemisphere single-basin studies, e.g. (Bryan, 1986; Marotzke and Klinger, 2000). The third, DrakeWorld [DW], named for the gap between South America and Antarctica that is the narrowest restriction to circumpolar flow in today's Southern Ocean, is intended to emulate the currently observed flow regime as forced by the geography. It can support geostrophic gradients and basin type flow in the landed northern hemisphere but has a gap in the barrier in the southern hemisphere allowing for circumglobal flow there, an idealised analog of the Antarctic Circumpolar Current [ACC].

Pure aquaplanet experiments are not unknown; it is a scenario often used to test the dynamics of atmospheric GCMs without worrying about the complicating effects of topography and changing surface characteristics (Alexeev, 2003; Neale and Hoskins, 2000), but they are less common in oceanographic studies due to the 'unrealistic', totally zonal nature of the flow. Such a configuration has been the subject of thought experiments (Warren, 1981) but this is however the first time

that a coupled GCM, or anything with so many degrees of freedom and little tuning to current climate parameters has been applied to the scenario - presumably due to the expensive nature of most coupled model simulations.

DrakeWorld is somewhat of a misnomer for this last case: in the RealWorld geography the Drake Passage extends from 50°S to 66°S, whilst here the narrowness of the polar island, relative to the representation of Antarctica, means that the gap extends further south to 78°S. The gap is therefore much wider, and, as a result of the lack of bottom topography, also far deeper than the actual Drake Passage. The rationale here was more to combine the two previous cases and produce an idealisation of the basic flow regime than produce a realistic simulation of flow through the Drake Passage, and it was felt that retaining a smooth southern boundary and keeping the floor of the ocean flat rather than adjusting to a sill depth was more in keeping with the philosophy of an idealised experiment.

Comparing the DrakeWorld and RidgeWorld experiments directly will obviously highlight the impact of opening a passage in the Southern hemisphere to allow circumglobal flow. This is a scenario that has received a fair amount of attention in the literature (Gill and Bryan, 1971; Cox, 1989; England, 1993; Nong et al., 2000; Bjornsson and Toggweiler, 2001), in part due to the hypothesis of Kennett (1977) that the opening of a Southern hemisphere passage (probably actually the separation of Australia and Antarctica, rather than the actual opening of the Drake Passage, which was already open to some depth (Lawver and Gahagan, 1998)) about 35 Ma was linked to an abrupt cooling of the ocean's deep water and the accumulation of glacial ice on Antarctica. Although the experimental setups here are highly idealised and not intended as paleo-climate simulations, the above experiments, conducted in a variety of models, have not yet been done in a full, coupled GCM as here.

3.1.2 Basin Planets

Whilst the aquaplanet experiments are designed to show the fundamental effect of the change in circulation, their lack of any significant land area is something of a handicap. The presence of land surface, which plays a fundamentally different

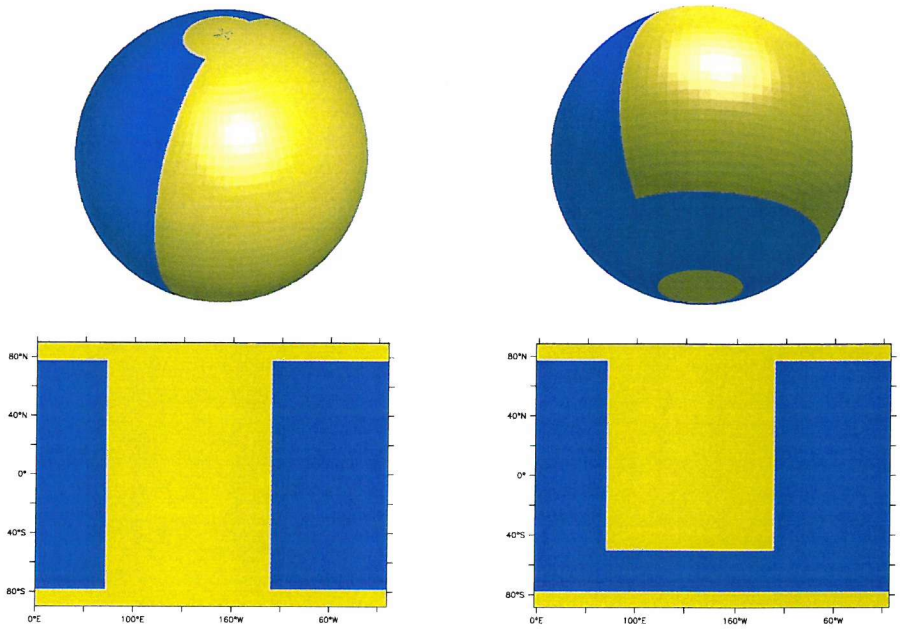

Figure 3.2: *3D and plan views of the two other idealised scenarios - experiments PangeaWorld and PangDrakWorld.*

role in the climate system to the ocean, with its lower heat and moisture capacities and inability to transport heat, is obviously of prime importance to the climate system so it is important to see to what extent the conclusions of the first three basic simulations still apply when land is included. In keeping with the highly idealised nature of the study the land is kept as one single, rectangular mass (*fig:3.2*).

For PangeaWorld [PW], the land/sea ratio is approximately 50/50, leaving an ocean basin 192° wide. The second of the two scenarios, PangDrakWorld [PDW], has a channel of the same width as that in the DrakeWorld simulation above cut into the continent to allow the same ocean circulation change as from RW to DW to occur. The width of the ocean basin in both is based on that of the main ocean basin (outside the partially enclosed Tethys ocean) found around 250 Ma, when the supercontinent of Pangea existed (*fig:3.3*), during and after the Triassic period.

As with the 'Drake Passage' case, Pangean climate has received a fair share of attention in the modelling literature (e.g. Kutzbach and Gallimore (1989); Valdes and Sellwood (1992); Sellwood et al. (2000)). The presence of such a large, contiguous landmass cutting across every latitude would be expected to

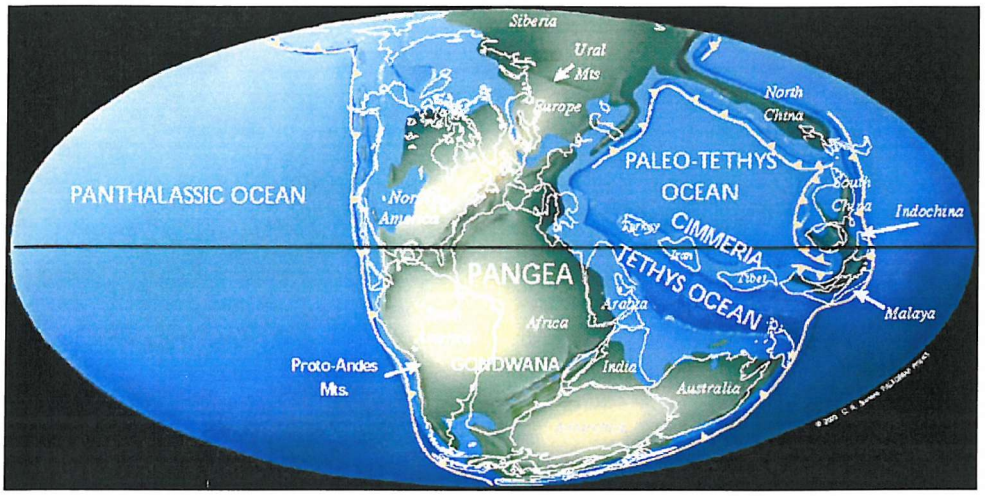

Figure 3.3: *A reconstruction of Triassic geography, from Scotese (2001).*

have an extreme impact on the climate, and proxy evidence of 'red-beds' (e.g. Glennie (1987); Enos (1993)) suggests a highly seasonal climate (Bárdossy and Aleva, 1990), first suggested as 'monsoonal' by Robinson (1973), and then 'mega-monsoonal' by (Kutzbach and Gallimore, 1989). This is predicted to arise from the geographical configuration - a large single landmass with a low latitude seaway to provide moisture - with possible high altitude heat sources provided by various topographical features on the continent. Again, although the highly idealised nature of the setup here, in particular the lack of the cross-equatorial land/sea contrast that results from missing the Tethys ocean, means that the experiment here cannot be taken as an attempt to simulate the details of the actual paleoclimate during these times, no Pangean-time simulation has been conducted with a coupled GCM before and as such the results here are interesting, especially with respect to the extent of the continental seasonal cycle that results from allowing the ocean and atmosphere to interact freely unlike previous studies. The results may also allow the ocean heat transports to be specified accurately in higher resolution AGCM studies of the climate.

3.1.3 General specification

In these theoretical geographies the choice of the height of land orography and ocean bottom topography is entirely arbitrary. Here, both have been set completely flat. Studies suggest that the presence or absence of bottom topography can qualitatively change the circulation system shown in the ocean (Bice and Marotzke, 2001), and the presence of mountains and other blocking features in the atmosphere are crucial for creating a realistic representation (Manabe and Terpstra, 1974). The decision here to exclude these is in no way an indication of their lack of importance, rather a reflection of the lack of data available and the inability of applying any solution other than 'flat' in a consistent manner, given the changing shape and area of the land masses/basins.

The ocean floor is thus set at a constant 5.8km everywhere, and the land height to a constant 50m. The land height was selected as one that allowed the atmosphere model to be nudged from its current climate representation toward those consistent with the idealised geometries without causing large transient anomalies that caused the model to crash, and was left at this value once the idealised states had been achieved.

There is also the question of land surface type - roughly corresponding to an assessment of vegetal cover - which controls both the albedo and surface roughness seen by the atmosphere. Although in some sense as arbitrary as the topographical question, it is possible to derive a 'potential vegetation' surface type distribution by using the climate state to iteratively find a distribution that is consistent with the temperature, rainfall etc. distributions. This was thought to be unnecessary - in keeping with the idealised nature of the experiments and the focus on dynamical factors it is sensible to keep other influences constant, although it is a possible avenue for future work. The surface type was somewhat arbitrarily picked as a constant 'desert' value, with an albedo for each land square close to the current earth average at 0.35. The ocean albedo value is 0.1. These can only change during a model run by the presence of snow or ice. Runoff is arbitrarily specified by transferring excess water to the nearest coastal point.

It was decided to keep the solar insolation parameters at the top of the atmosphere

unchanged from the present day values. This includes a small asymmetry between the northern and southern hemispheres which derives from the eccentricity of the earth's orbit. Although aiming for idealised, theoretical results it was felt best to keep this basic connection to the earth's current state constant so as not to be completely disconnected from reality. For this reason the climatological ozone distribution and CO_2 amount was also kept as for the model's current-day simulation at 358 ppmv.

Grid-based models formulated on regular latitude-longitude grids suffer from problems due to the convergence of latitude lines towards the poles. There are a number of ways to avoid this problem, using various different grid formulations or so-called 'polar-patches' (NCAR, 2000) that pass fields across the poles without explicitly calculating them, extrapolated from the nearest valid grid value. A simpler solution was used here, also applied to the RealWorld simulation as seen above: thin land islands are placed over the poles to remove the need to calculate ocean values. These were used throughout as it was felt that, since they do not obstruct the ocean circulation very much, the gross qualities of the solutions would remain unaffected and as long as they were used consistently all model results would still be comparable.

3.1.4 Spin-up

As shown from figure 3.4, the simulations were not spun up independently from each other. Initially, the component models were run separately with the WW geography using zonally averaged fields from a current climatology (Levitus, 1982; Hellerman and Rosenstein, 1983). On coupling it was found that the temperature profile of the restored-to fields was far from the model's equilibrium point as there was a large and rapid shift in the surface temperature. Another standalone spinup to fields nearer to where the coupled model seemed to be heading was thus carried out, so once this initial surface temperature adjustment had slowed somewhat the surface fields from this coupled run were used for a further standalone (the components uncoupled) spinup with surface restoring to these fields. The ocean component was run for 2000 years, the atmosphere for 10.

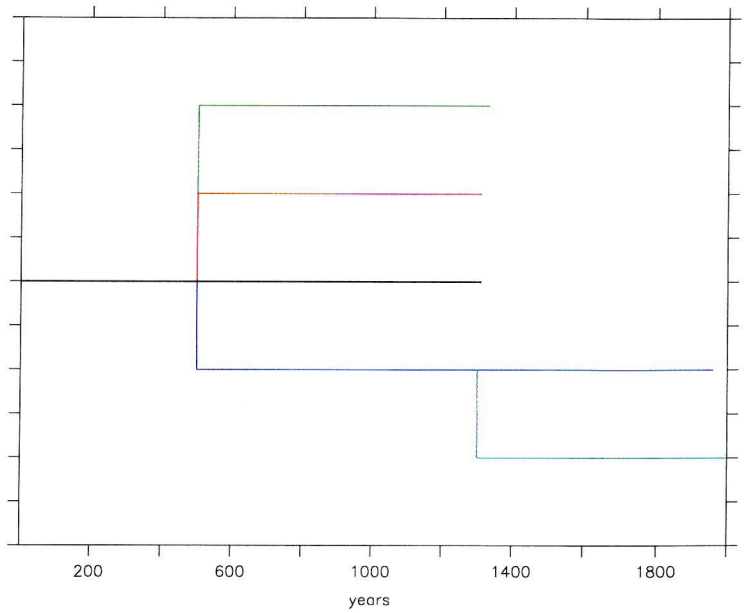

Figure 3.4: *Illustrating the integrations times and how the various scenarios were initialised.* Black*: WW;* Red*: RW;* Green*: DW;* Blue*: PW;* Cyan*: PDW.*

The components were then recoupled and run on for 500 years with the WW geography. This state was then used to initialise the RW, DW and PW runs, the landmasks for each scenario changing instantaneously in both atmosphere and ocean. The PDW run was initialised in a similar manner from a state 800 years further on in the PW simulation, after the initial adjustment had slowed. In all cases the periodic coupling method was used, with a ratio of 19 months synchronous run to 60 months ocean only. 100 years of non-periodic, totally synchronous run was appended to all these cases at the end; this period is where all the results presented here are from. It is worth reiterating that all of these model runs were done without flux adjustments of any kind and that the climates produced are thus 'natural' states of the model.

Due to the slow processes of diffusion and overturning in the ocean, the equilibration timescale for the coupled ocean-atmosphere system is on the order of thousands of years. Although FORTE was designed to be able to produce long timescale runs with the idea of being able to integrate configurations to equilibrium, the efficiency improvements achieved do not allow many runs of this

timescale to be performed. None of the simulations shown here have thus reached a true equilibrium yet - see table 3.3. There are also figures for total salinity drift in the ocean; these arise from the fact that spectral atmosphere codes do not conserve mass, leading to a long-term drift in the water content of the system. Although these are long timescale runs, such a slow, general drift in salinity should not affect the qualitative behaviour of the model studied here.

	WaterWorld	**RidgeWorld**	**DrakeWorld**
Total Runtime (years)	1310	810	830
ocean ΔT per 100 years (°C)	0.019	-0.088	-0.067
ocean ΔS per 100 years (p.s.u.)	0.009	0.003	-0.005

	PangeaWorld	**PangDrakWorld**
Total Runtime (years)	1460	695
ocean ΔT per 100 years (°C)	-0.246	-0.127
ocean ΔS per 100 years (p.s.u.)	0.073	0.054

Table 3.3: *Total integration times and ocean heating/cooling rates and salinity drift for each run.*

However, this study only aims to show the qualitative possibilities that are consistent with the scenarios. It is suggested that each of the scenarios has been integrated long enough that it is at a stage of slow asymptotic adjustment towards the precise values that would be found in equilibrium and thus has achieved a circulation that is qualitatively the same as that of the true equilibrium. Klinger (2000) uses the concept of this slow decreasing exponential in values to accelerate the adjustment of a model, again on the assumption that no major circulation differences are to be expected after a long enough period of time. In addition, results for WW, RW and DW have all been run on for the same period of time from the same state (there is also data from PW from the end of this same period, but not PDW as it had not been started); the slow vertical diffusion processes acting to equilibrate the ocean will have been acting for the same period of time in each

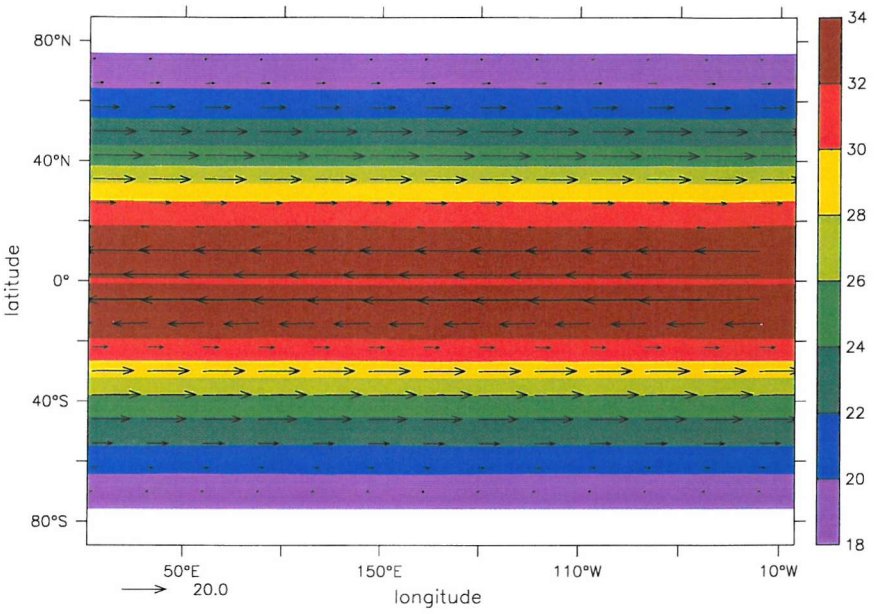

Figure 3.5: *Annual average SST (°C) and surface currents (cm/s, averaged over the top 250 metres) on WaterWorld, averaged over the last 30 years.*

case, so it should be valid to draw direct comparisons between these runs.

An overview of the main climate features in each scenario will be presented here. Such idealised climates have not been run before in a model of this complexity, so the general results are of interest from a purely 'observational' point of view as well as for the details of the areas of interest. References to RealWorld values are taken from an IGCM3 run with fixed climatological surface values.

3.2 AquaPlanets

3.2.1 WaterWorld

Surface conditions

The most striking thing in a plot (*fig:3.5*) of surface conditions on WaterWorld is how warm it is. In the annual average, SSTs range from a maximum of 33.0°C

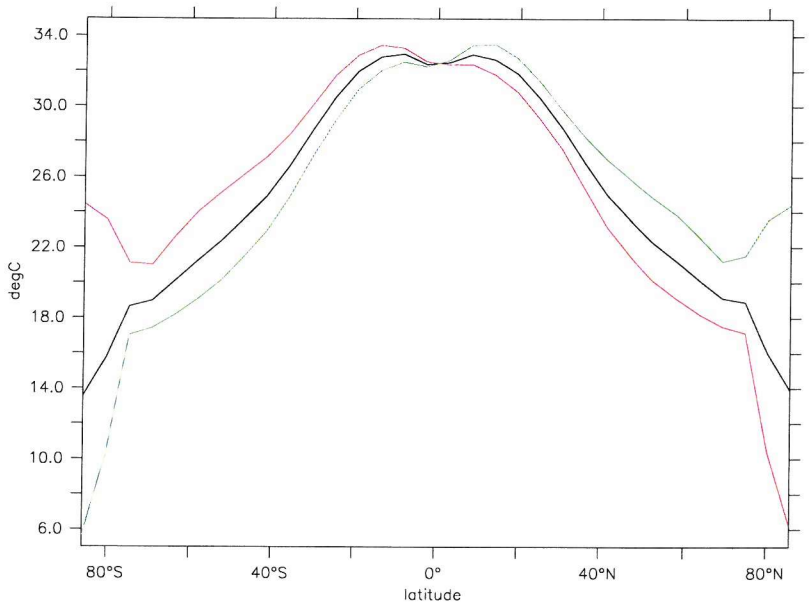

Figure 3.6: *Zonally averaged air surface temperatures on WaterWorld from a climatology of the last 30 years.* Black*: annual average;* Red*: DJF average;* Green*: JJA average.*

just off the cooler upwelling region at the equator to a minimum of 18.6°C at the poles. Even right at the poles the minimum annual average air surface temperature is only 12°C.

Looking at seasonal variation (*fig:3.6*), the air temperature rarely drops below freezing anywhere in winter, even on the polar islands (there are occasional patches of land where the air temperature dips below 0°C) the minimum reached in the last 30 years is -1.78°C, but these do not show up as below freezing in the zonal average or the averaged climatology of the last 30 years. The SST variation at the poles is 5.23°C, reaching a maximum of 22.4°C, whereas on the polar islands the average seasonal air surface temperature variation is 21.1°C. The warmest SSTs achieved in the climatology are around 34°C off the equator at 12°N/S. There is a small degree of asymmetry in the latitudinal temperature profile - this stems from the current eccentricity of the earth's orbit which is retained when calculating the seasonal insolation and results in a small warm bias to northern hemisphere winters.

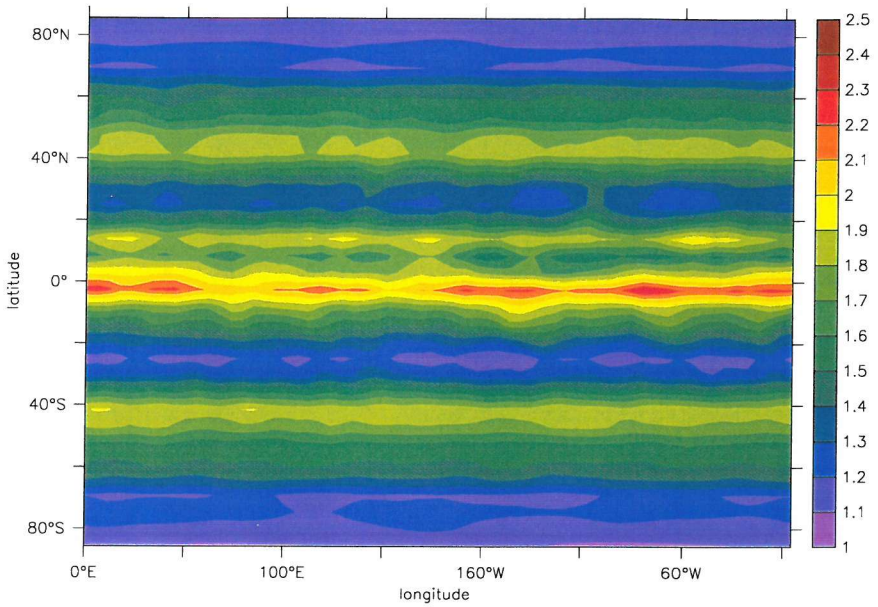

Figure 3.7: *Annually averaged rainfall field for WaterWorld (m/year).*

The rainfall distribution on WaterWorld shows a very even, zonally constant, banded structure, and although lacking in localised extreme maxima, at an average of 1.57 m/year (*fig:3.7*) the amount of rainfall on WaterWorld has increased by 29% from that found in the RealWorld configuration. Seasonally (*fig:3.8*) the central maxima shifts off the equator into the summer hemisphere and the mid-latitude maxima around 40° in the winter hemisphere gains in amplitude, from an average of 1.5 m/year in summer to 2.3 m/year in winter, whilst that in the summer hemisphere weakens.

Surface winds (*fig:3.9*) have a hemispherically symmetric pattern with the annual average maxima roughly the same as that for RealWorld, with a westerly at 3.7 m/s at 40°S and a 3.2 m/s easterly at around 15°S. Seasonally, the 40° westerly maximum in the winter hemisphere increases to 4.9 m/s and the easterly to 6.7 m/s whilst in the summer hemisphere the westerly maximum broadens and moves slightly equatorward; all these changes are slightly more exaggerated than in the RealWorld case, with the maxima ~1 m/s greater. There is a small global net torque on the earth surface found in all the runs on the order of 0.001 N/m^2

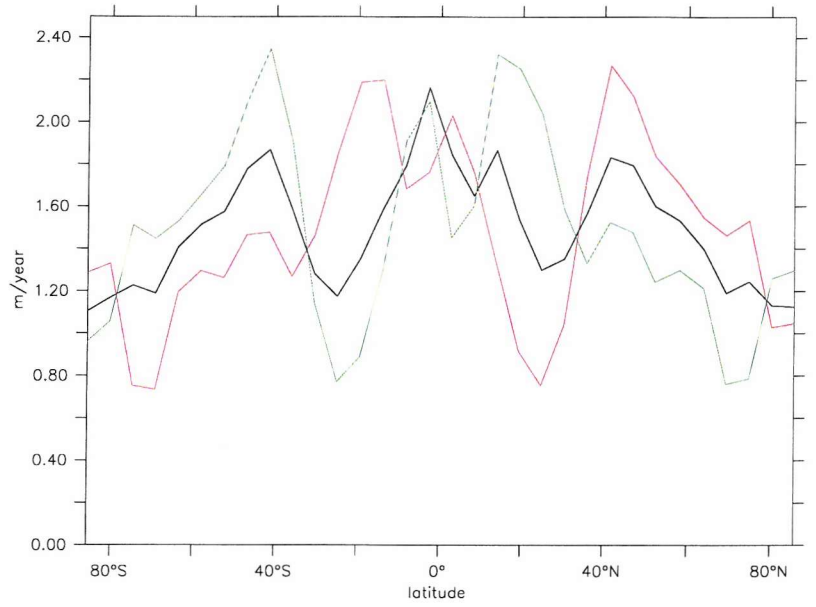

Figure 3.8: *The zonally averaged rainfall distribution on WaterWorld.* Black*: annual average;* Red*: DJF average;* Green*: JJA average.*

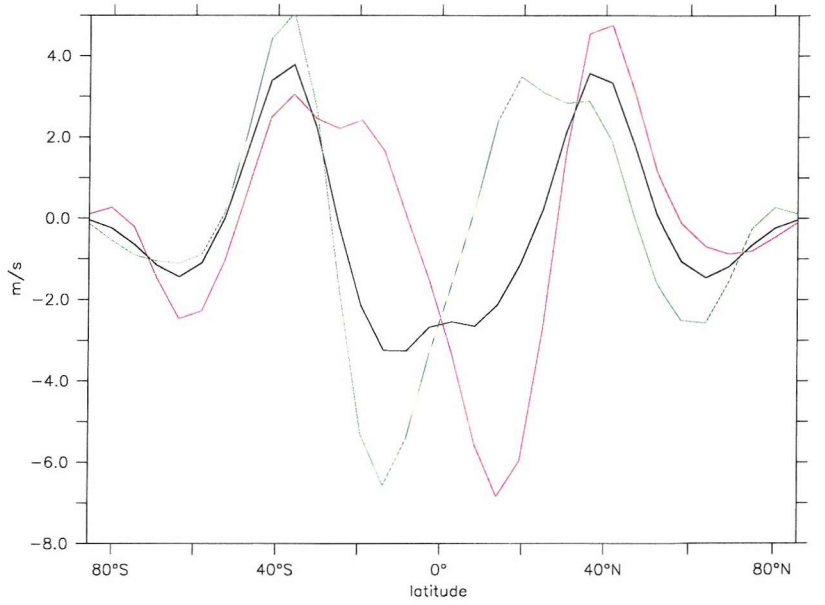

Figure 3.9: *Zonally averaged zonal wind (m/s) on WaterWorld.* Black*: annual average;* Red*: DJF average;* Green*: JJA average for the last 30 years.*

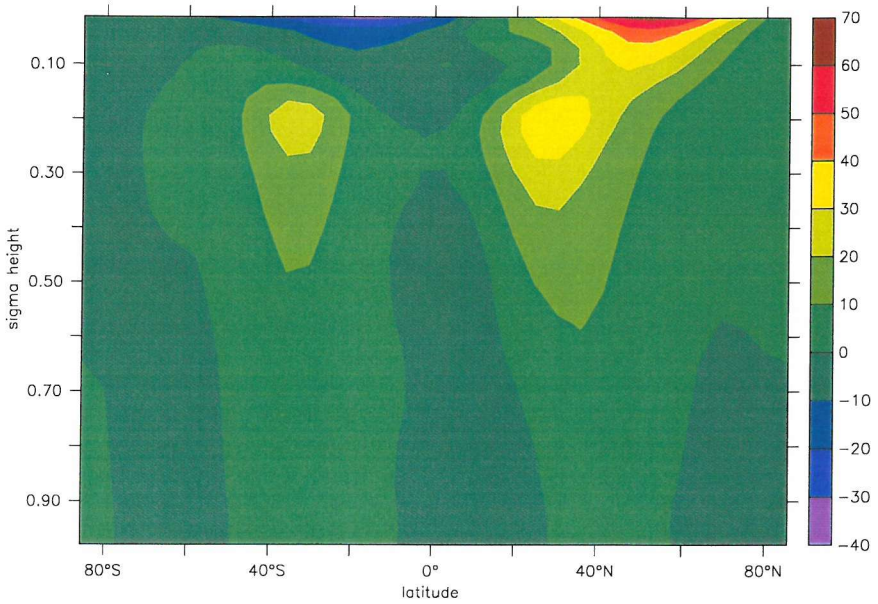

Figure 3.10: *Zonally averaged zonal wind (m/s) on WaterWorld, DJF average for the last 30 years.*

(0.0019 for RealWorld, 0.0011 for WaterWorld, 0.0062 for PangeaWorld), between 1% and 3% of the maximum seasonal windstress. The direction of this torque is not systematic, comparing runs. There does not appear to be any trend in the kinetic energy content of the atmosphere, and since there is no feedback to change the day length in the atmosphere model, this must be considered a source of error in the model.

Atmosphere

The zonal wind structure higher up in the atmosphere (*fig:3.10*) also shows a similar structure to the RealWorld pattern, with jet-stream maxima around 200 mbar at 30° latitude. The maxima are slightly higher up than those found in the RealWorld control run and the jet streams stronger, up to 10 m/s for the subtropical jet and 20 m/s for the polar.

WaterWorld also has a well defined Hadley circulation (*fig:3.11*) with the Intertropical Convergence Zone [ITCZ] right on the equator in the annual average

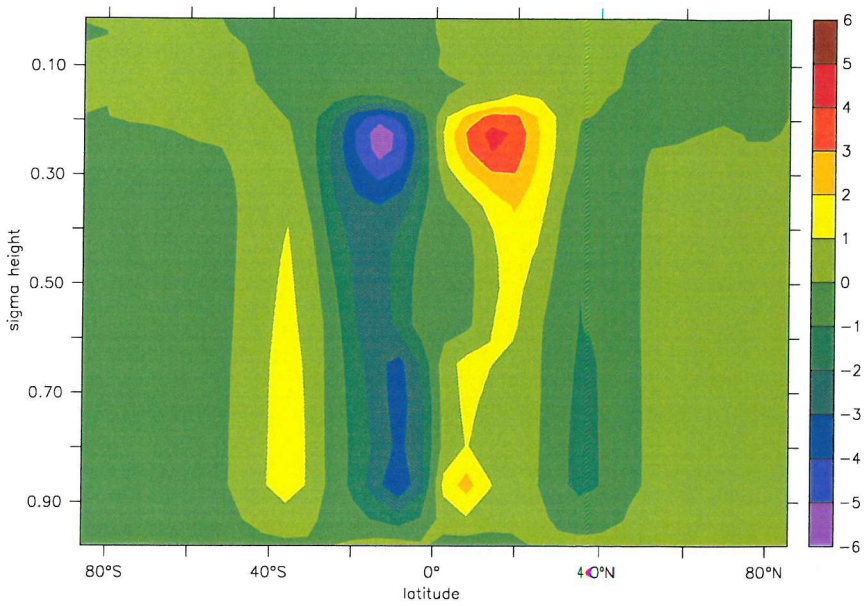

Figure 3.11: *Annual average atmospheric overturning streamfunction on WaterWorld for the last 30 years* ($10^{-4} kgm/s^3$).

and the main equatorial cells extending over about 30° latitude. The northern hemisphere winter-time picture (*fig:3.12*) shows the dominance of the summer-hemisphere cell as the rising branch moves into the summer hemisphere, with a maximum twice the strength of the annual average and about twice the width.

As with the rain, the cloud distribution (*fig:3.13*) displays zonally constant bands. There is a large amount of low cloud (see section 2.1.2), especially over the poles and WaterWorld also displays a higher amount of convective cloud over the entire domain than the RealWorld run.

Oceanic Regime

Surface currents (*fig:3.5*) are almost entirely zonal, producing surface westward currents up to 50 cm/s in the tropics and eastward currents up to 25 cm/s in the extratropics. A plot of the horizontal streamfunction (*fig:3.14*) highlights the lack of the usual gyre features that cannot be supported without some barrier to the overall zonal flow.

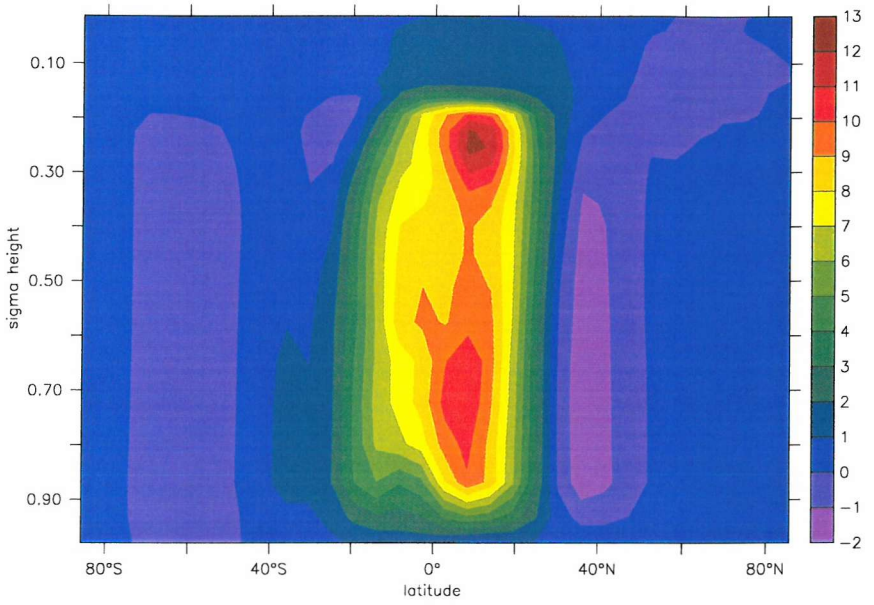

Figure 3.12: *DJF average atmospheric overturning streamfunction on WaterWorld for the last 30 years* ($10^{-4} kgm/s^3$).

The oceanic overturning is very different (*fig:3.15*) from that observed today, consisting of 6 individual cells, each about 30° wide that extend from the surface down to the ocean floor, with the equatorial cells being stronger than the polar ones. The maximum overturning is about 100 Sv. The deviation from hemispherical symmetry arises from the northern hemisphere warm bias in insolation which comes from the earth's orbital eccentricity.

The pattern of the meridional overturning circulation [MOC] is very seasonal - the nicely symmetric pattern seen in the long-term annual average is exactly this, a product of the averaging process. The seasonal variation of this pattern mirrors that of the Hadley cells and their associated wind patterns, the ocean MOC moving with the main equatorial cell of the winter time hemisphere, extending across the equator from 30°N to 40°S instead of from 30°N to the equator as seen in the global average. The maximum strength of this cell can be up to ~140 Sv.

WaterWorld has a well stirred/mixed ocean, as figure 3.16 shows - the warm bottom waters reflect the relatively warm polar waters. The model does not display

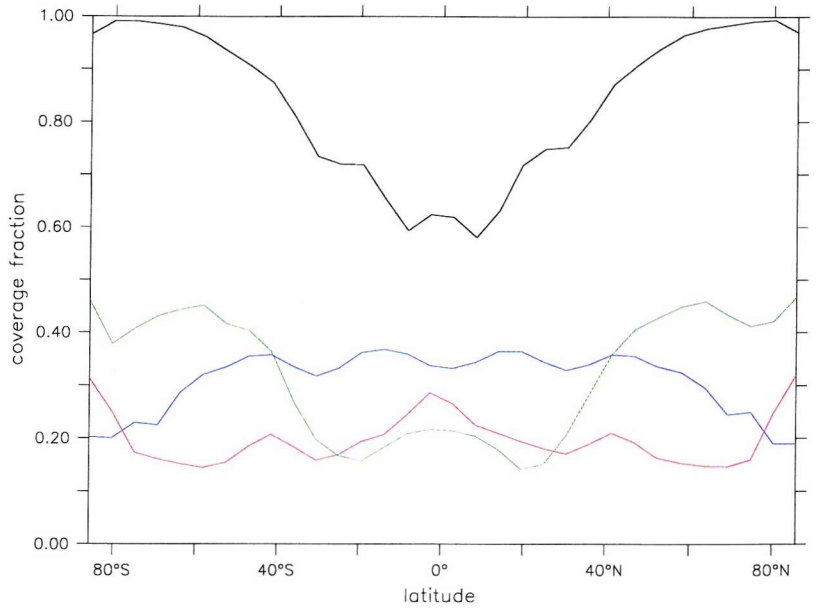

Figure 3.13: *Annual average cloud area-cover fractions for WaterWorld (0=grid box completely free of cloud, 1=box totally covered).* Black*: low cloud;* Red*: mid-level cloud;* Green*: high cloud;* Blue*: convective cloud.*

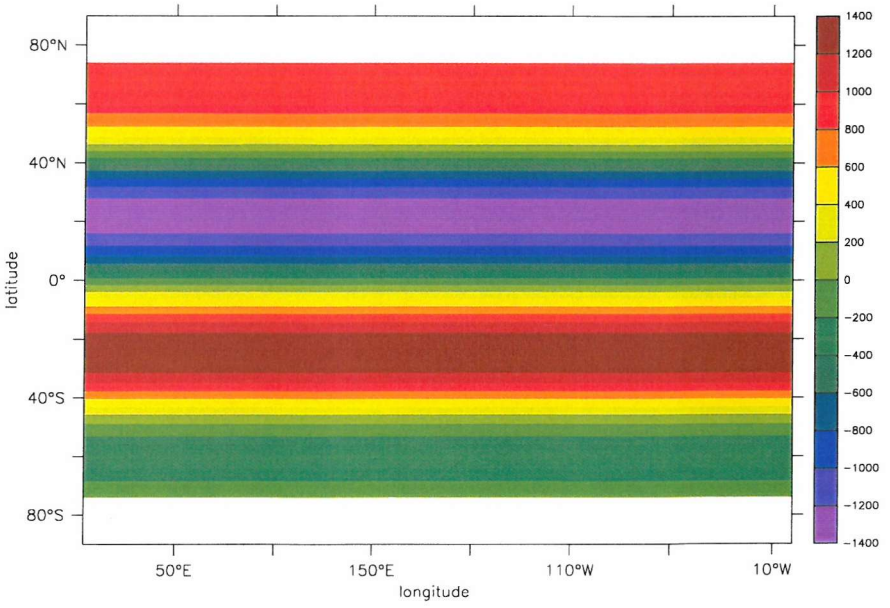

Figure 3.14: *Global ocean horizontal streamfunction for WaterWorld (Sv).*

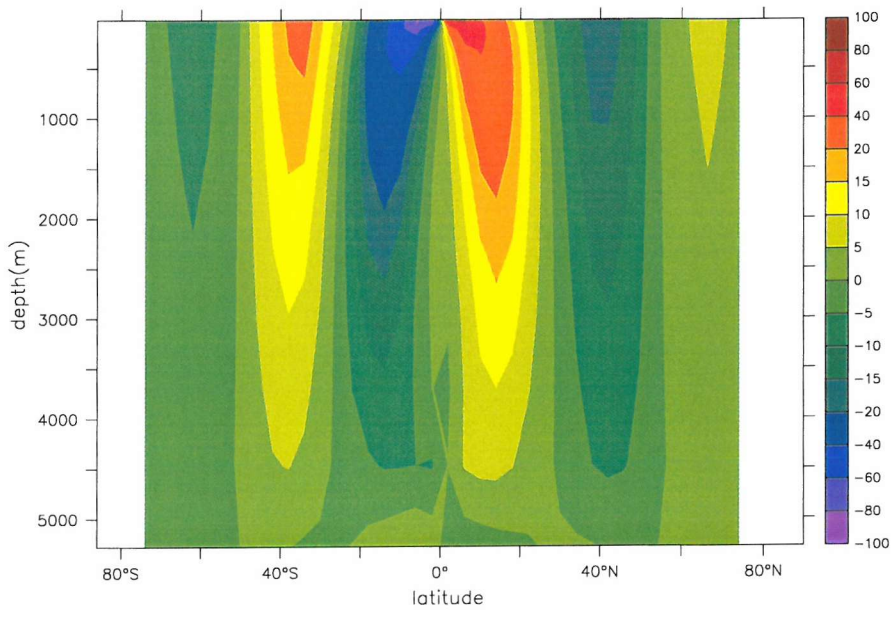

Figure 3.15: *Global ocean meridional overturning on WaterWorld (Sv).*

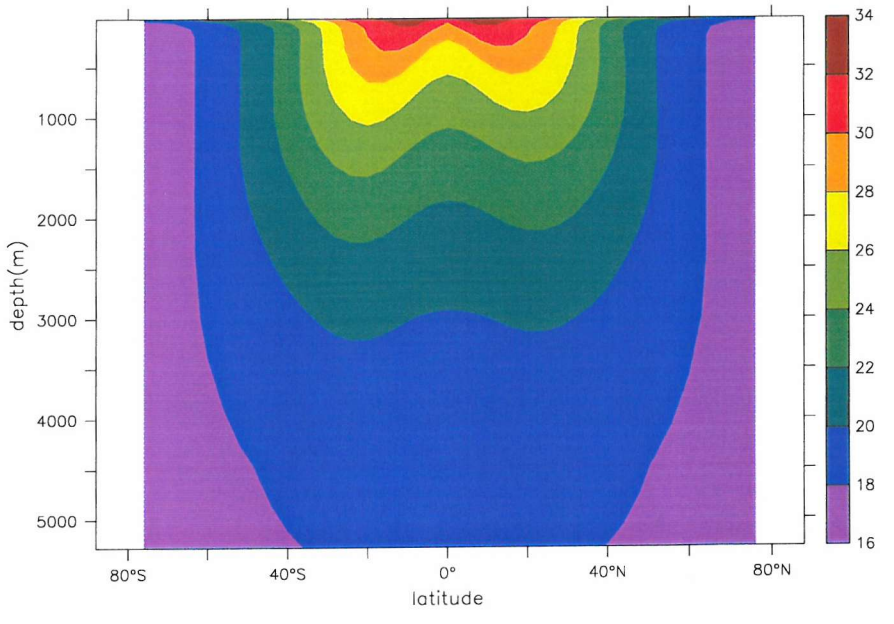

Figure 3.16: *Zonally, annually averaged temperature on WaterWorld (°C), latitude versus depth.*

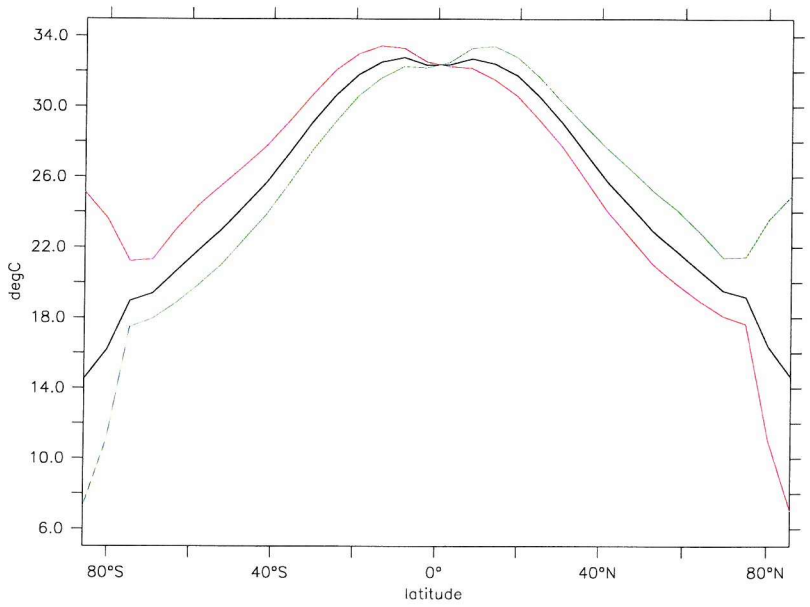

Figure 3.17: *Zonally averaged air surface temperatures on RidgeWorld from a climatology of the last 30 years.* Black*: annual average;* Red*: DJF average;* Green*: JJA average.*

anything like the traditional thermocline structure, displaying a much smoother change in temperature from the surface to the ocean floor. However, there appears to be absolutely no convective activity present at any time of year.

3.2.2 RidgeWorld

RidgeWorld's basic climate is little different from WaterWorld's in form. It has WaterWorld's general warmth, with a very similar symmetric equator to pole temperature profile (*fig:3.17*) and seasonal variation. There are some differences in this field though, with tropical SSTs on average half a degree lower and polar SSTs a degree higher than on WaterWorld.

The rainfall pattern (*fig:3.18*) shows a similar banded background structure to WaterWorld, but with the addition of several maxima and minima around the location of the ridge. The dry minima are found on the ridge around 30° in the winter hemisphere and the maxima occur just to the east of the ridge, on the equator and at 40°

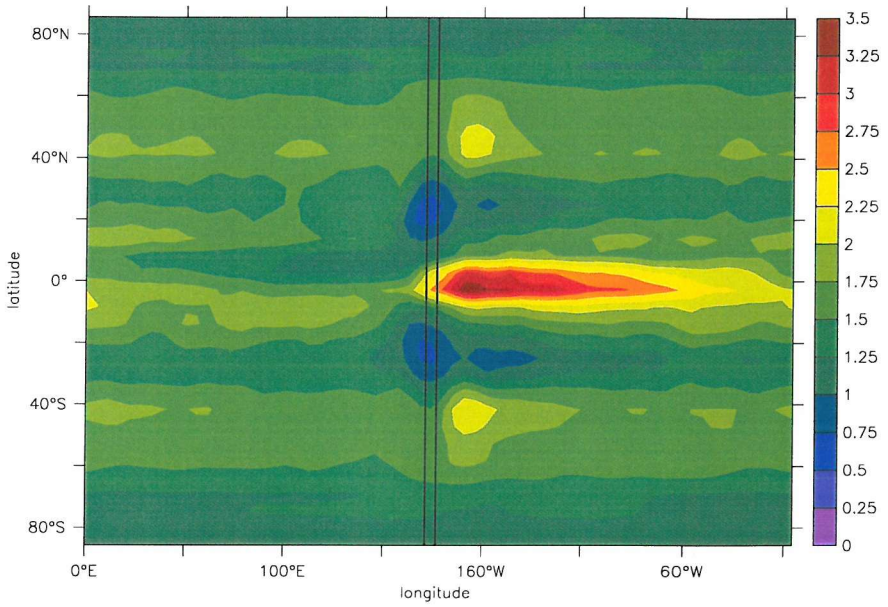

Figure 3.18: *RidgeWorld annual average rainfall m/year. The edges of the ridge are marked by the overlaid black lines.*

in the winter hemisphere. At 1.57 m/year the global average amount of rainfall is the same as for WaterWorld.

Zonal winds have a similar pattern to, but are in general about 0.5 m/s slower than those on WaterWorld. The Hadley cell structure is also very similar, as is the cloud distribution - see section 3.2.1.

Ocean Circulation

Where the two scenarios differ most is in their oceanic circulation. The addition of a barrier creates one large closed basin out of the global ocean and adds an important new factor into the force balance controlling the ocean. The barrier allows the familiar ocean gyres to form (*fig:3.20*), along with strong western boundary currents (*fig:3.19*) with surface speeds of up to 57.9 cm/s.

The overturning pattern (*fig:3.21*) now looks more familiar. The narrow cells that formed the entire part of the WaterWorld circulation are still present, but on the

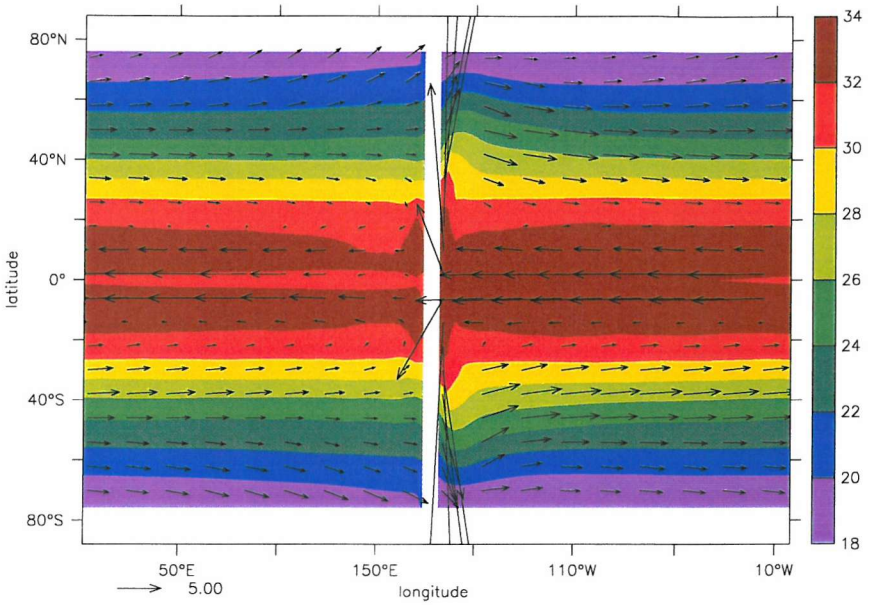

Figure 3.19: *SST (°C and currents (m/s, averaged over the top 250m) on RidgeWorld, annual average from the last 30 years of run.*

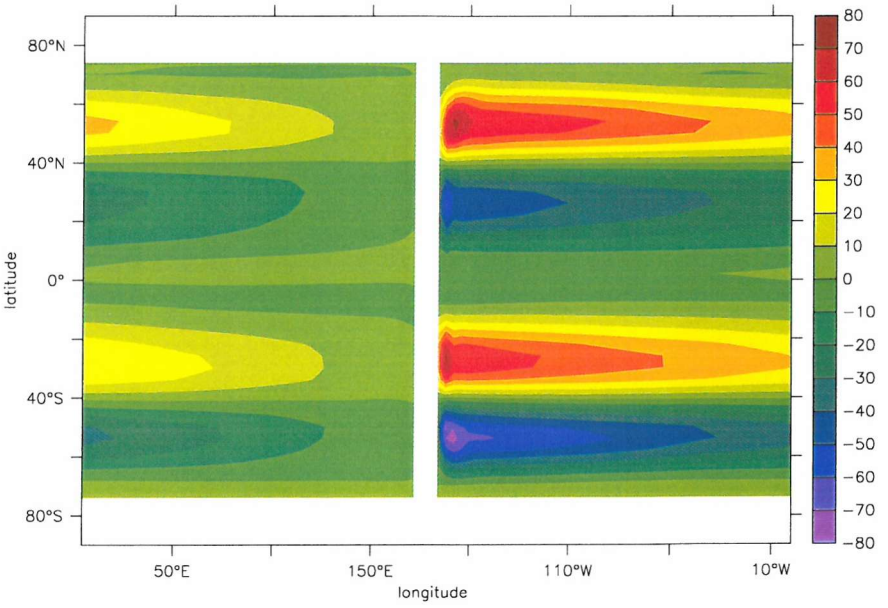

Figure 3.20: *Horizontal streamfunction (Sv) for RidgeWorld averaged over the last 30 years of the simulation.*

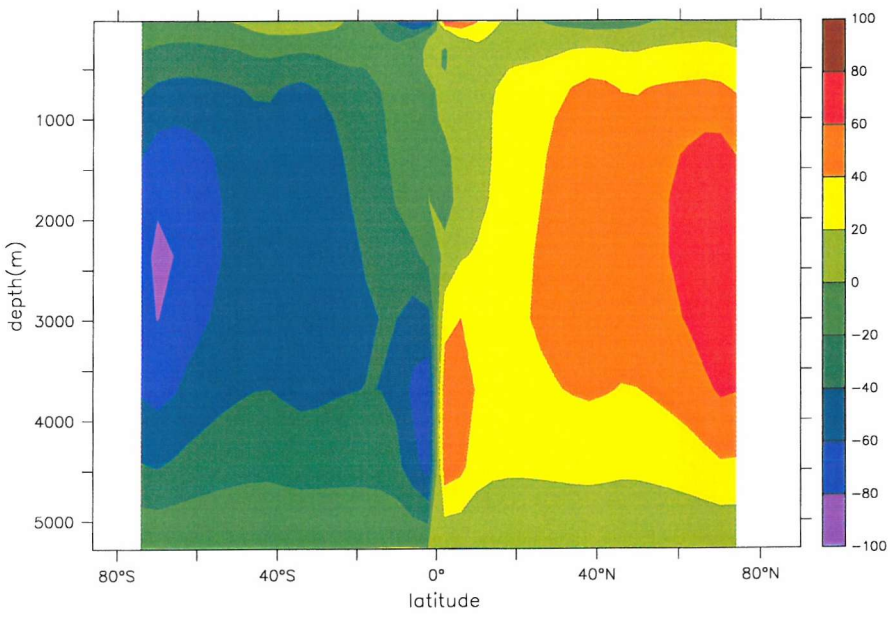

Figure 3.21: *RidgeWorld ocean meridional overturning (Sv), averaged over the last 30 years.*

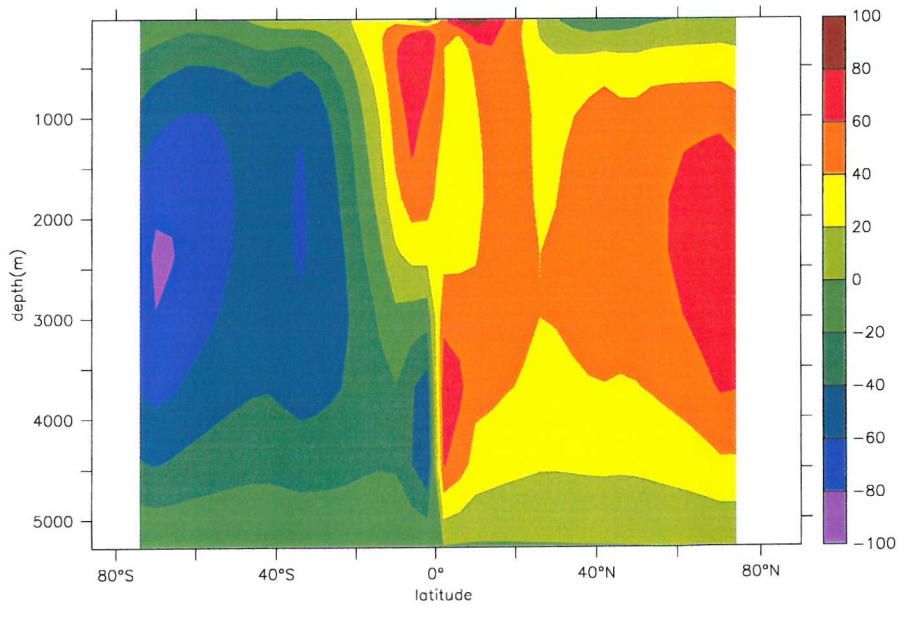

Figure 3.22: *RidgeWorld ocean meridional overturning (Sv), DJF averages.*

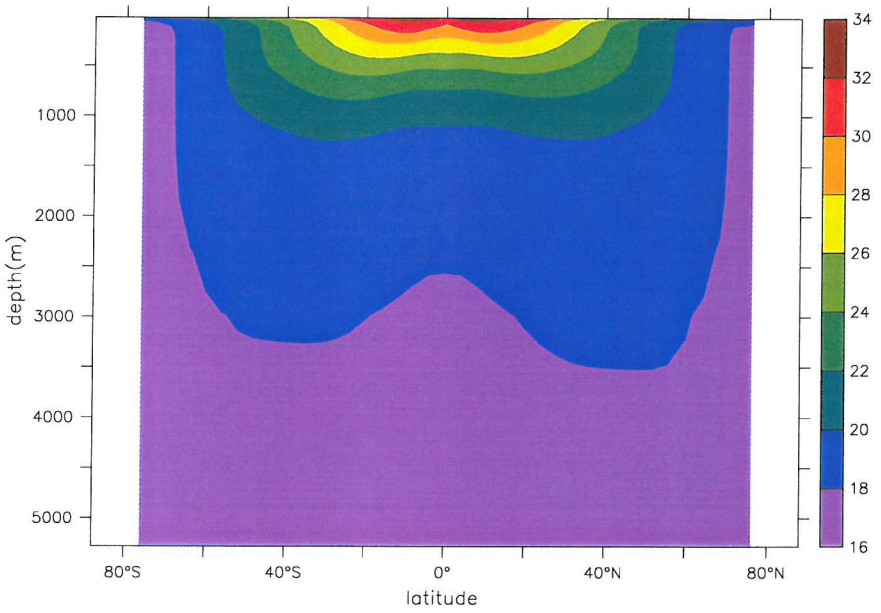

Figure 3.23: *RidgeWorld temperature (°C) / depth profile.*

long-term mean they are confined to the top 500 m or so. Comprising the main part of the picture are two hemispherically symmetric cells, dominated by high latitude sinking bringing warm equatorial water out to the poles at the top and returning at depth. The maxima of the pattern are located right up against the polar islands, with the main part of the upwelling at the equator - there is also some around 60°N/S. This pattern is far less seasonally variable than the WaterWorld one, with the DJF average for the same time period (*fig:3.22*) showing some changes around the equator but little in the overturning at higher latitudes and little change in the polar sinking. These polar cells are slightly stronger in the summer hemisphere.

The zonally averaged temperature depth profile (*fig:3.23*) shows differences from WaterWorld as well, with a sharper change between warmer surface waters and isothermal bottom waters. The coolest bottom water spreads right from the poles into the equator.

Unlike WaterWorld there is plenty of convective activity on RidgeWorld, shown in figure 3.24. It is concentrated around the polar island in the winter hemisphere, although some still occurs during the summer months right up against the island.

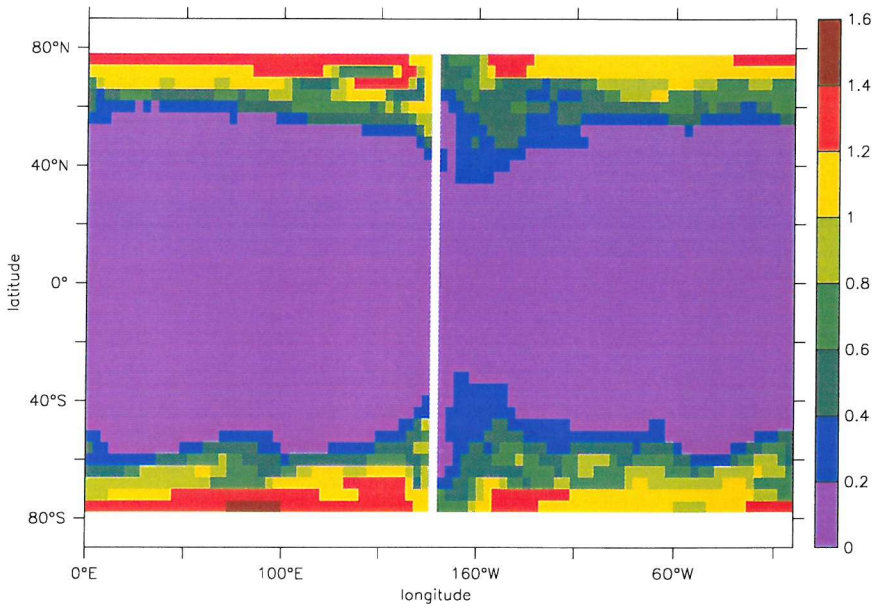

Figure 3.24: *Surface (top 500m) convection frequency (per timestep) on RidgeWorld. Counting convection with the cell above and the one below separately, each box can convect twice per timestep.*

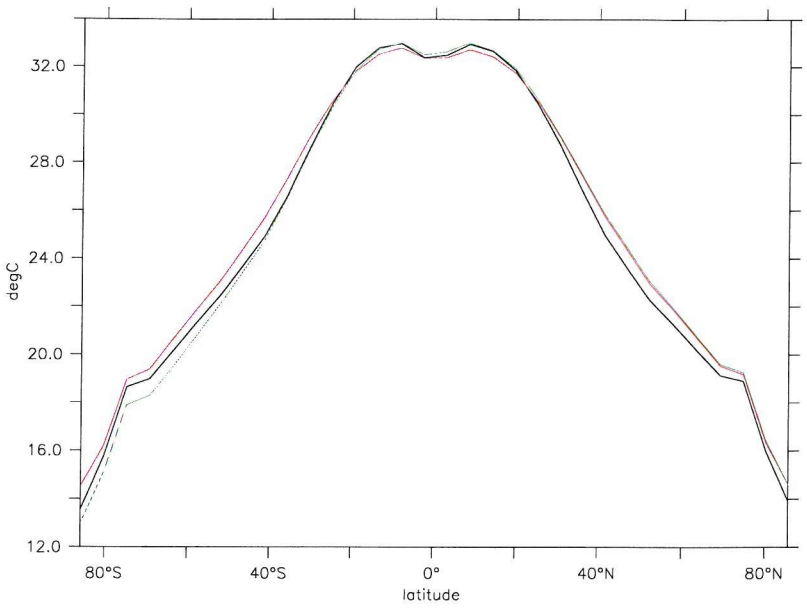

Figure 3.25: *Average surface air temperature for the idealised runs.* Black*: WaterWorld;* Red*: RidgeWorld;* Green*: DrakeWorld.*

3.2.3 DrakeWorld

DrakeWorld has the same general warm, shallow latitudinal surface temperature profile as the previous two idealised runs (*fig:3.25*) and very similar atmospheric characteristics. As with RidgeWorld though, there are a number of small notable differences in the atmospheric profile, and a different ocean circulation.

The surface temperature profile (*fig:3.25*) is not as neatly symmetric now: the northern hemisphere side follows that of RidgeWorld, whilst the southern hemisphere has the slightly sharper WaterWorld profile down to about 40°S where it sharpens more to end up about a degree and a half cooler than RidgeWorld. This change is reflected in the zonal wind profile (*fig:3.26*) with the northern hemisphere winds matching RidgeWorld's slightly weaker pattern and the southern hemisphere winds matching WaterWorld's, strengthening a little more towards the poles.

Rainfall patterns are similar to those on RidgeWorld, with the central maxima to the east of the ridge and the same globally averaged amount. Again, little change

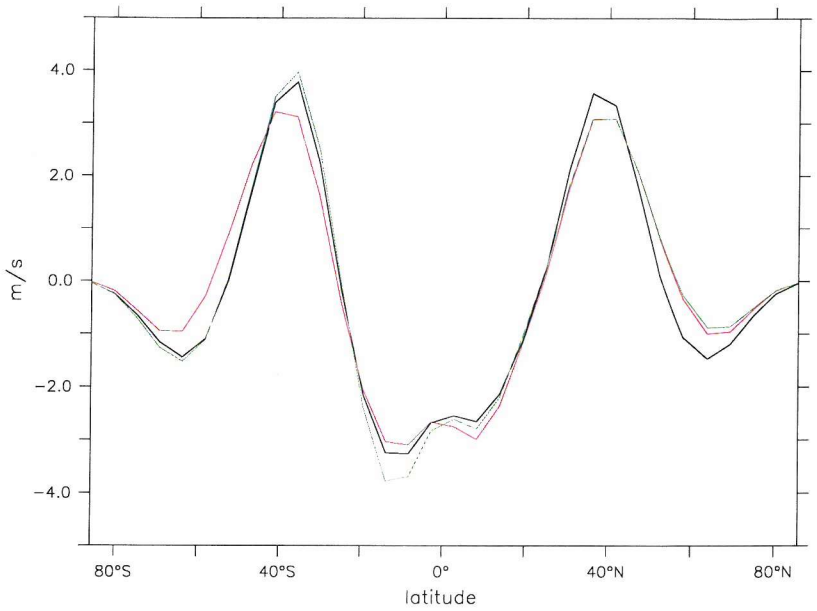

Figure 3.26: *Annually averaged zonal surface wind for:* Black*: WaterWorld;* Red*:RidgeWorld;* Green*: DrakeWorld.*

is seen in the strength and extent of the Hadley cells between this and the other idealised simulations.

Ocean circulation

Whilst the northern hemisphere circulation appears very similar to that in RidgeWorld, the southern hemisphere is an interesting mix of the RidgeWorld and WaterWorld cases. Notable is a strong ACC-analog around the south polar island, going in the opposite direction to the ACC seen today (*fig:3.27*) with westward motion extending right to the bottom.

The oceanic overturning (*fig:3.28*) also shows a combination of features of the RidgeWorld and WaterWorld cases, with a strong, deep overturning cell in the north fed by downwelling right up against the polar island. The strong south polar cell found with RidgeWorld has disappeared, replaced by a weak, narrow cell at the south pole like the ones on WaterWorld. There is some evidence of an extra cell in the southern hemisphere, fed by downwelling around 50°S near the end of

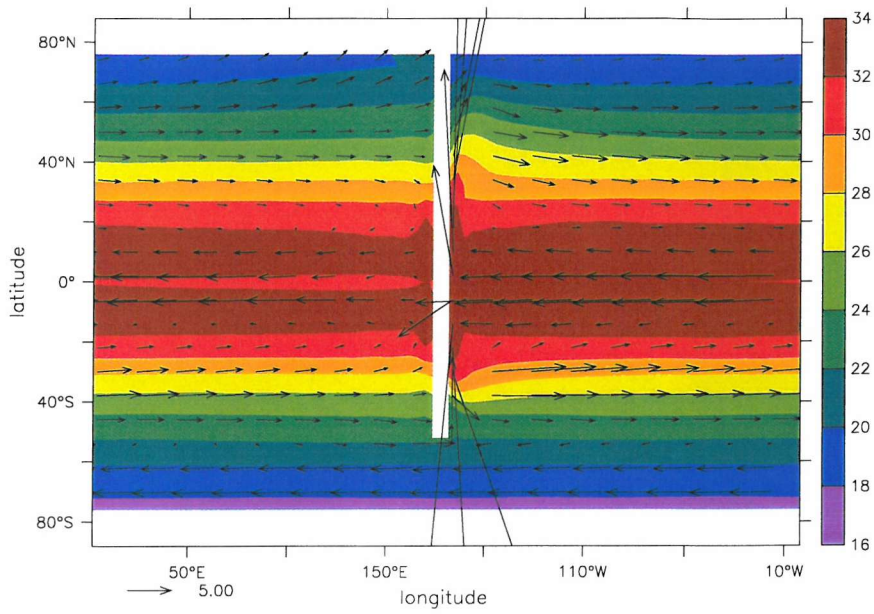

Figure 3.27: *Average SST (m/s) and surface currents (cm/s, averaged over the top 250m) for DrakeWorld.*

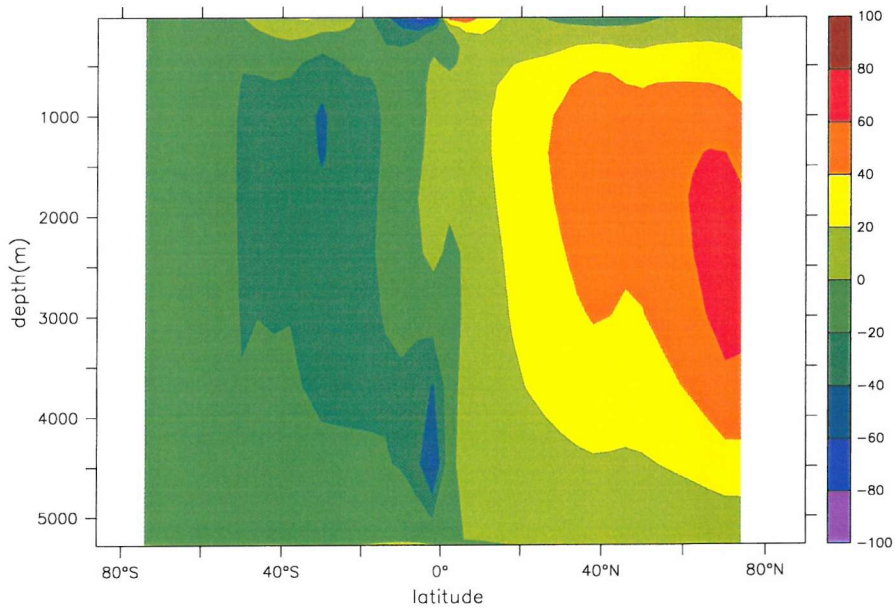

Figure 3.28: *DrakeWorld ocean meridional overturning (Sv).*

the ridge. As with RidgeWorld, the strong northern cell shows little variability, a few Sverdrups stronger in summer (JJA) than in winter. The extra southern cell is also more marked in (DJF) summer than winter.

3.3 Basin Planets

3.3.1 PangeaWorld

The introduction of a large amount of land into the model set up radically changes the climate observed. For one thing, the global mean air surface temperature drops by 6.5°C. This is to be expected: the surface albedo has been substantially increased by the addition of so much land, and the patterns of surface heating and moisture availability will also have changed, forcing a significant response from the atmosphere that may change its radiative properties. As suggested above, the effect of the differential heating of land and sea should produce a highly seasonal climate dominated by a monsoon-like response.

In our current climate, monsoonal climates prevail over parts of Asia around the Indian ocean, controlled by the thermal contrast between land and ocean, a supply of moist air and the particular geography of the region, with a cross-equatorial land/sea contrast and a high altitude heating source on the Tibetan Plateau. In summer when the land surface of Asia begins to warm, the surface air there rises and is replaced by cooler, moist air drawn north from the Indian ocean in the thermally direct overturning cell that results from the weak coriolis force at the equator. As the air ascends, the latent heat released when this rains out strongly reinforces the circulation, as does the high altitude warming provided by the surface of the Tibetan Plateau in the north. The monsoon is thus characterised by torrential summer rain over land and the seasonal reversal of the low/high pressure system and the equatorial winds as the easterlies are diverted towards the summer hemisphere.

PangeaWorld lacks a cross-equatorial land/sea contrast and high altitude heating, but the low heat-capacity nature of the landmass will still allow for a highly seasonal response to the annual heating cycle, and where moisture is brought on-

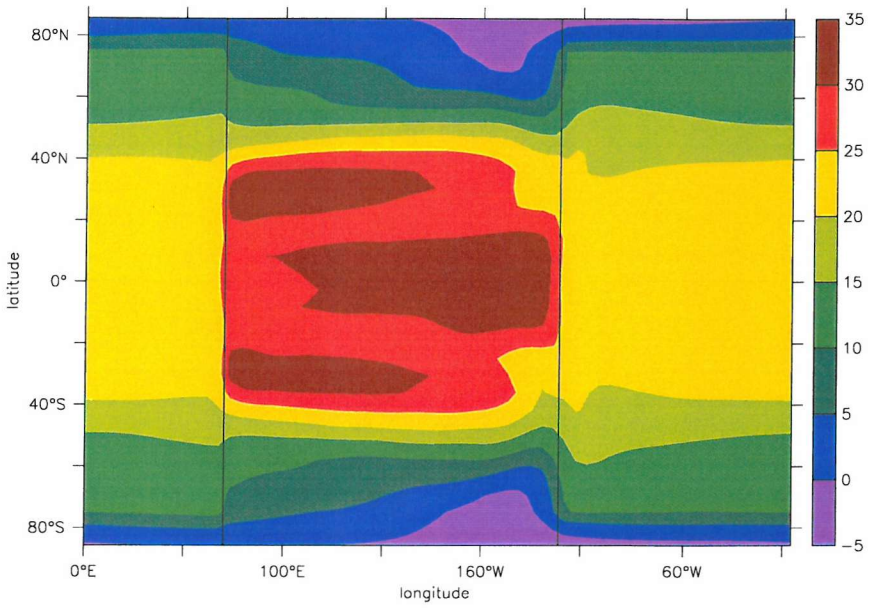

Figure 3.29: *Annual average air surface temperature (°C) on PangeaWorld from a climatology of the last 30 years.*

shore the latent heat released in the ascending air should provide for rainfall maxima in the summer hemisphere and reinforce the cycle.

Surface temperature

Figure 3.29 shows the annual average air surface temperature on PangeaWorld, and figure 3.30 the northern hemisphere winter. The seasonal picture shows extremely high temperatures in the middle of the land mass around 40°, with the coldest temperatures at the poles in the winter hemisphere, also over land. The maximum temperature reached in the climatology is 53.3°C and the minimum is -28.1°C.

In contrast, RidgeWorld's highest temperature (also over land, on the ridge) was 34°C, with the coolest at 7°C. PangeaWorld's land mass clearly allows for a far greater range of surface temperatures to be achieved. As a result, PangeaWorld is the only one of the idealised scenarios with the potential for any ice sheet formation during winter, although the warm polar SSTs mean that sea ice is still absent

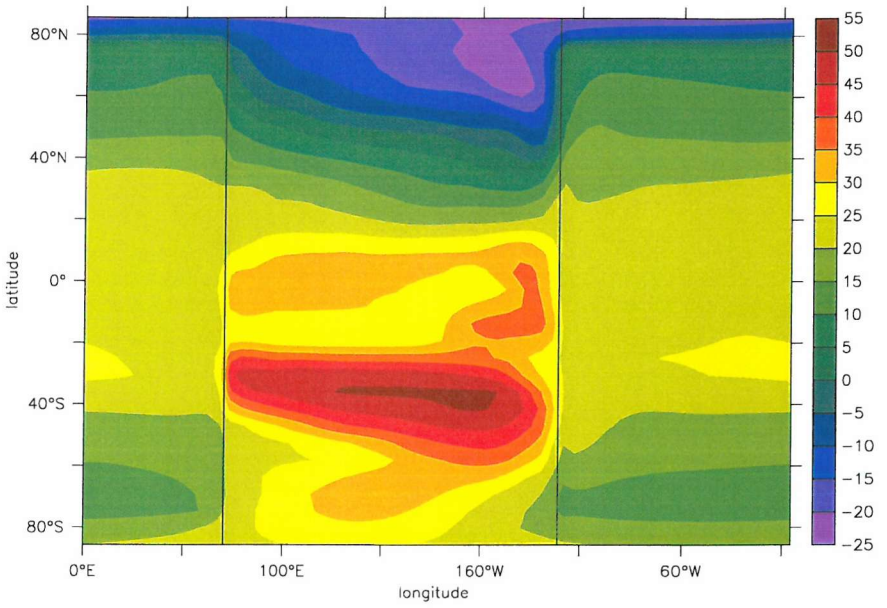

Figure 3.30: *DJF air surface temperature (°C) on PangeaWorld from a climatology of the last 30 years.*

year round (*fig:3.31*).

Winds

Averaged annually, the surface winds (*fig:3.32*) are of similar magnitude to those on RidgeWorld, but the zonal wind distribution is more spread out. The polar easterlies found in the other idealised runs, although weaker on RidgeWorld, are entirely absent here. Seasonal variation in the zonal wind pattern is extreme, showing the characteristic monsoonal reversal with the seasons. The summer hemisphere has high eastward winds around 15°N/S at all longitudes.

A plot of the surface pressure explains the pattern of the surface winds (*fig:3.33*). The continent is the centre of two dominating pressure extremes: a low centred over the land temperature maximum in the summer hemisphere and a high pressure at the same location in the winter hemisphere. This high is spread more longitudinally, not such a bullseye, as there is not a corresponding temperature minimum here. This pattern reverses completely in the other season. It is the

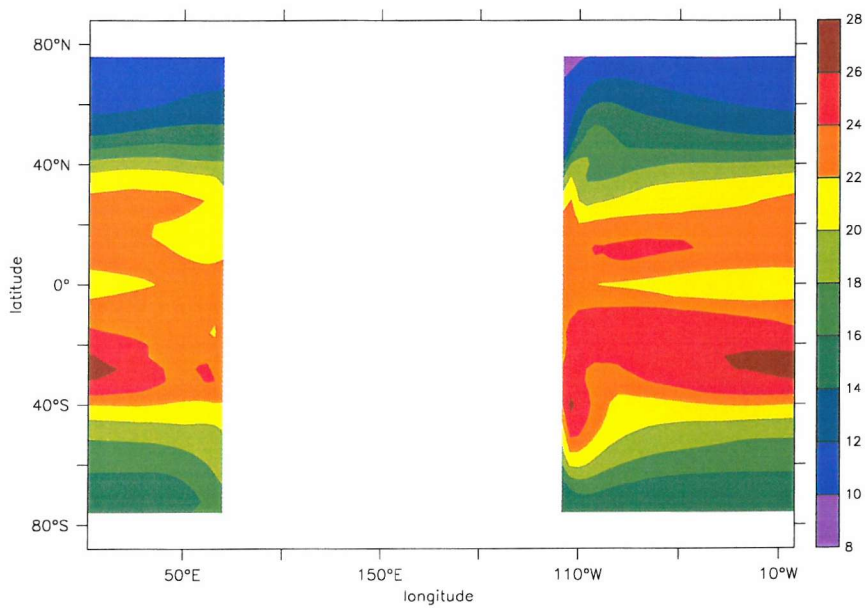

Figure 3.31: *DJF averaged SSTs (°C) for PangeaWorld.*

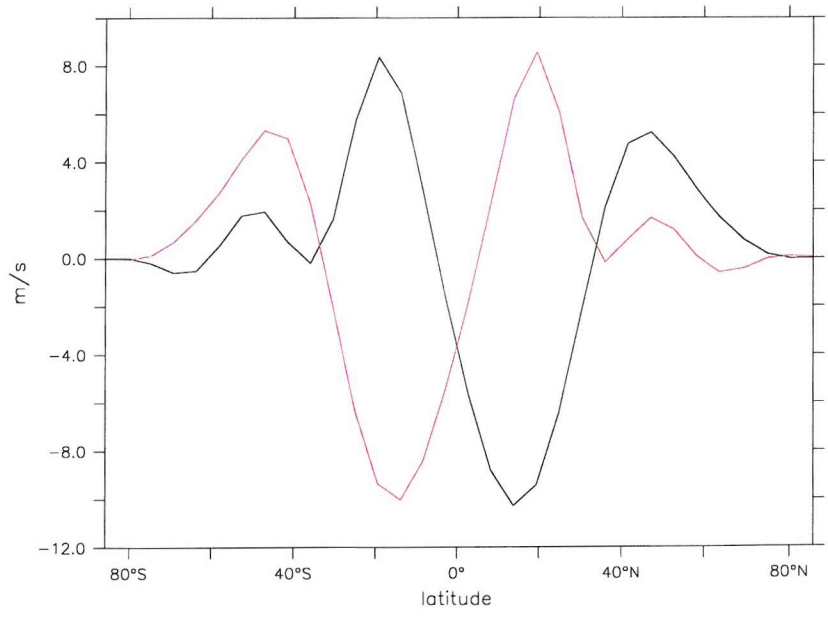

Figure 3.32: *The surface zonal average winds on PangeaWorld.* Black*: DJF;* Red*: JJA.*

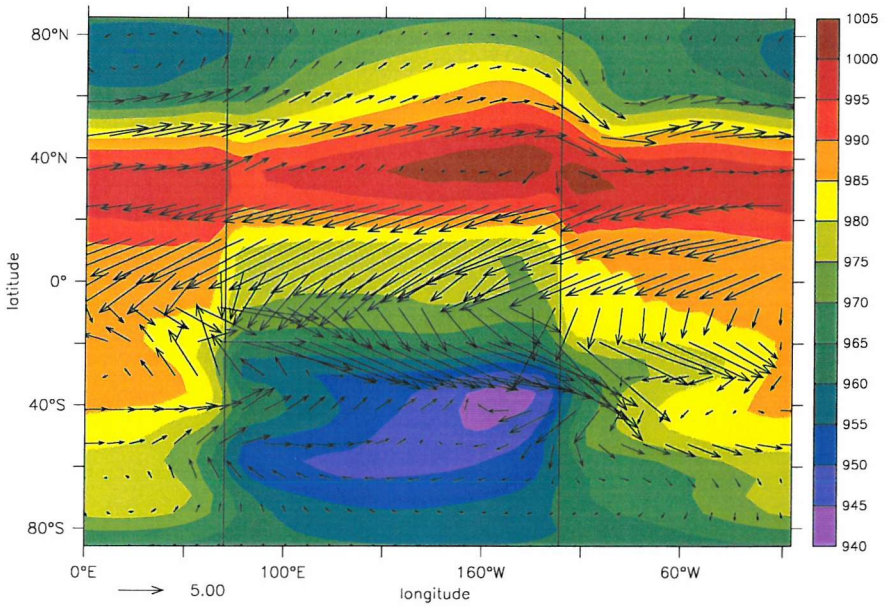

Figure 3.33: *DJF surface pressure (mbar) and surface winds (m/s) on PangeaWorld. The zonal extremes of the continent are outlined in black.*

cause of the tropical summer westerlies as it forms the centre of a strong anticyclone, as shown by the wind vectors. The diversion of the equatorial easterlies towards the summer hemisphere is also clear. The reason for the apparently low mean sea-level pressure [MSP] is the removal of all the high altitude land from the RealWorld configuration; the mass of the atmosphere is invariant so the *surface* pressure remains the same between the runs. Thus the flat PangeaWorld, where everywhere is practically at sea-level has an MSP equivalent, not to RealWorld's MSP, but to RealWorld's total surface pressure that takes into account the high altitude, low pressure areas in that configuration.

Higher up, the zonal jets are rather weak with maxima of only 20 m/s on average and spread quite wide at around 40°N/S compared to 30 m/s at 30°N/S on RidgeWorld. The separation of the westerly jets allows a strong easterly jet to form between them at 300 mbar. This is a consequence of the temperature maximum being so far off the equator in this scenario, around 40° rather than 20° on RidgeWorld. Just as the westerly jet streams are formed from the meridional temperature gradient in the midlatitudes, this tropical easterly jet is formed from the

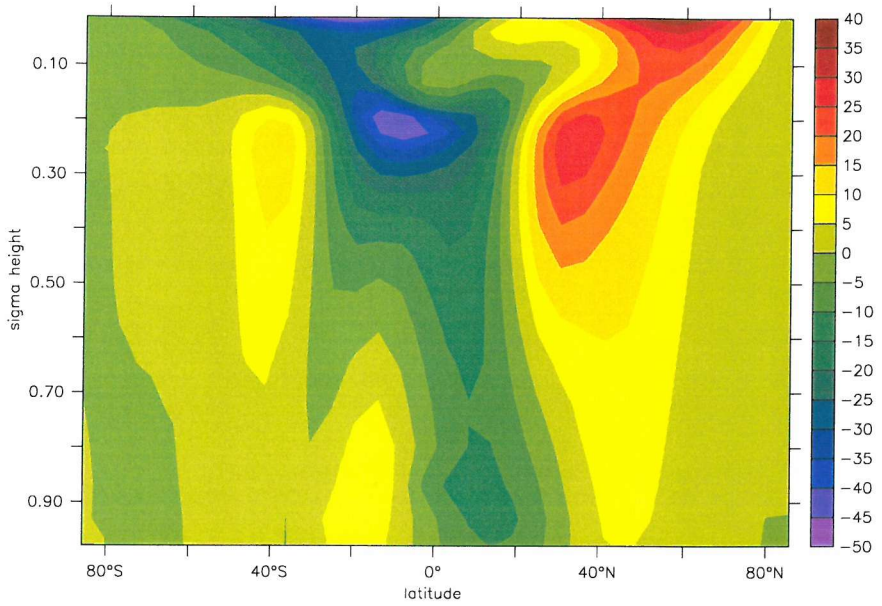

Figure 3.34: *Zonally averaged DJF zonal winds on PangeaWorld (m/s).*

opposite gradient between the 40° temperature high and the equator. The same effect pertains when the seasons reverse, reinforcing the equatorial reverse jet.

The form of the vertical overturning in the atmosphere is also curious. The seasonal picture has a normal form, with a very vigorous overturning (*fig:3.36*) and the clear dominance of the summer hemisphere cell, but the annual average does not show the usual symmetric pattern with an ITCZ, ascent over the equator and one low latitude cell per hemisphere. Instead (*fig:3.37*), the extreme seasonal temperatures that cause the vigorous ascent in the summer hemisphere bias the pattern out to higher latitudes, so that it appears that there is actually *divergence* and subsidence at the equator when the two seasonal extremes are overlaid in the average.

Rain

The total annual average rainfall amount is rather lower, at 1.15 m/year, than for the aquaplanets, back to roughly the same amount as seen on RealWorld. Portions of the continent under the downwelling branches of the Hadley circulation

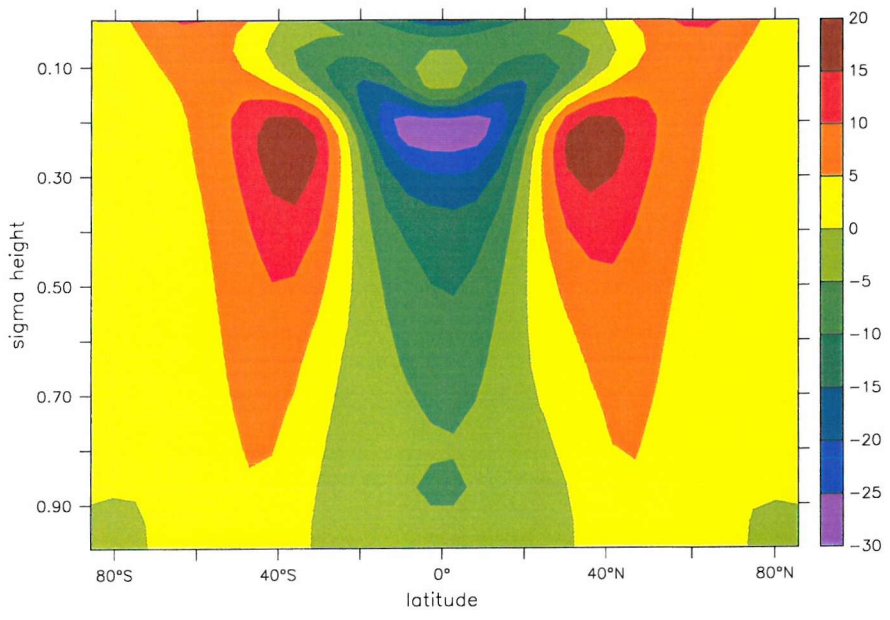

Figure 3.35: *Zonally, annually averaged zonal winds on PangeaWorld (m/s).*

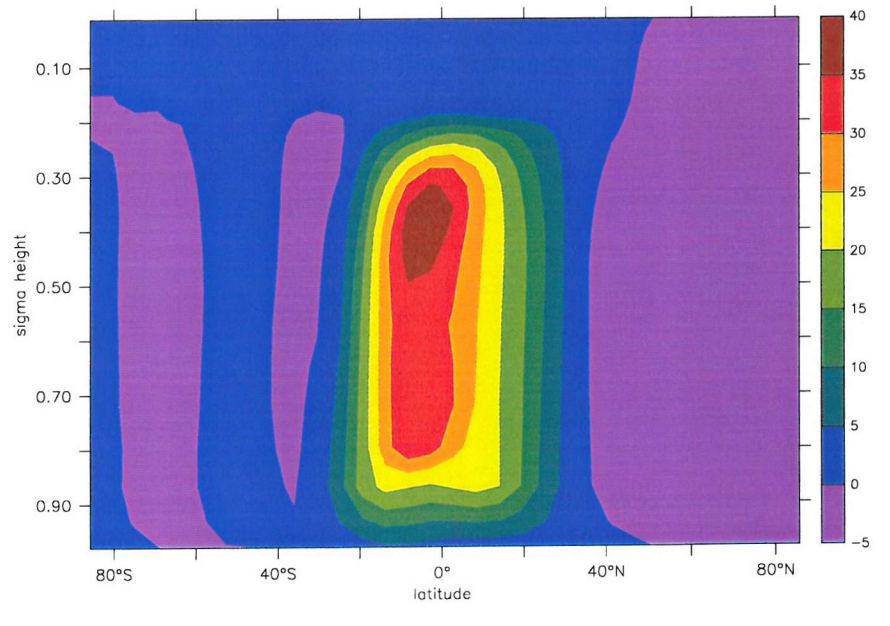

Figure 3.36: *Vertical overturning streamfunction* ($10^{-4} kgm/s^3$) *in the atmosphere for PangeaWorld, DJF.*

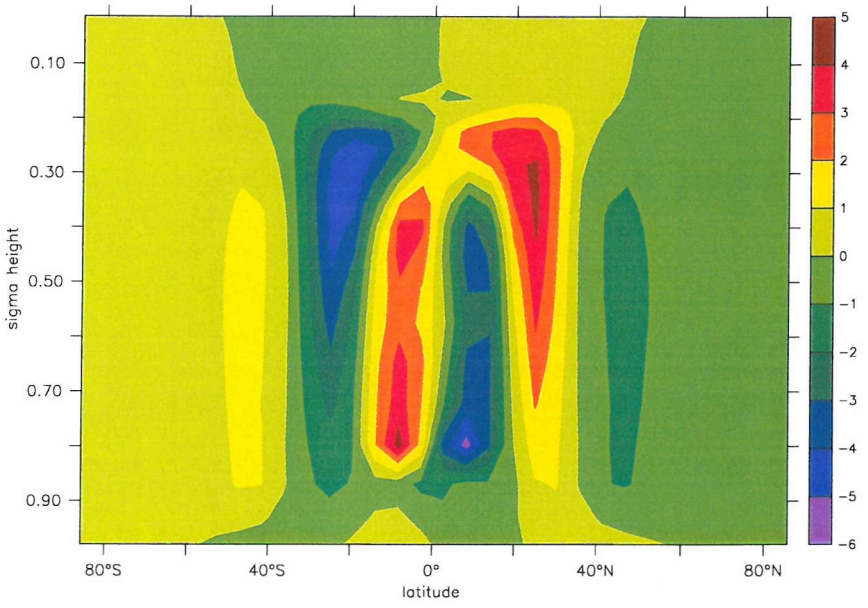

Figure 3.37: *Vertical overturning streamfunction* ($10^{-4} kgm/s^3$) *in the atmosphere for PangeaWorld, annual average.*

between 30-40° have low rainfall amounts year round (*fig:3.38*), and a large part of the continent receives only 0.7 m/year of rain, whilst in the wetter bands it is as high as 2 m/year.

The highest areas of rainfall are found in a band between 15° and 30° in the summer hemisphere (*fig:3.39*), with maxima in this band found over the western coast at 30°, a little off the western coast at 20° and inland off the eastern coast at the same latitude. This strong reinforcement of the summer rainfall maximum, as compared to the RW case, is also indicative of the switch to a monsoonal climate. Taking a climatology of an inland location in the rain belt (*fig:3.40*), it can be seen that most of the rain comes between June and September (northern hemisphere). The equatorial region is far drier than observed in the RidgeWorld case and, consistent with the monsoon concept, the winter hemisphere is generally dry, especially over land.

A plot of the soil moisture levels (*fig:3.41*) shows that no part of the continent is permanently arid, with coastal regions at high latitudes being saturated (hold-

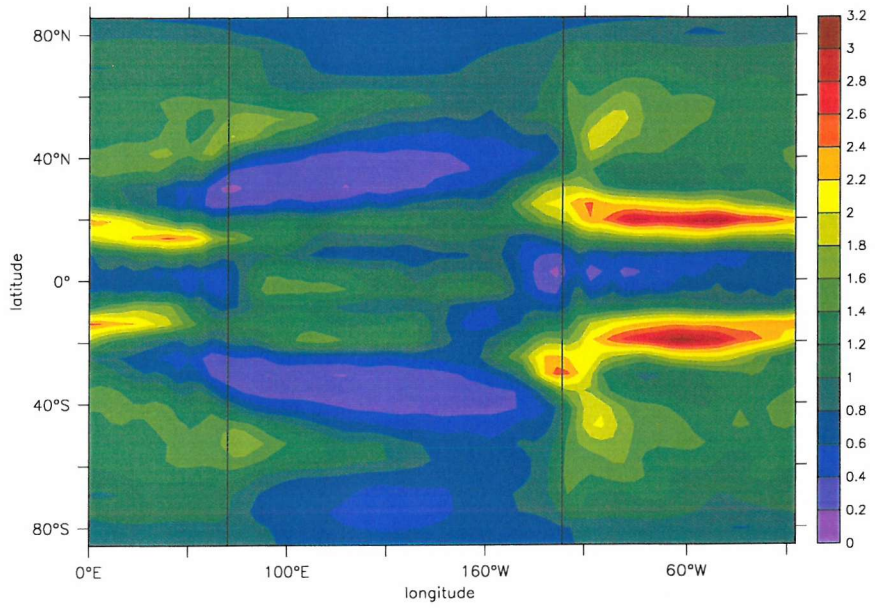

Figure 3.38: *Annual average rainfall on PangeaWorld (m/year).*

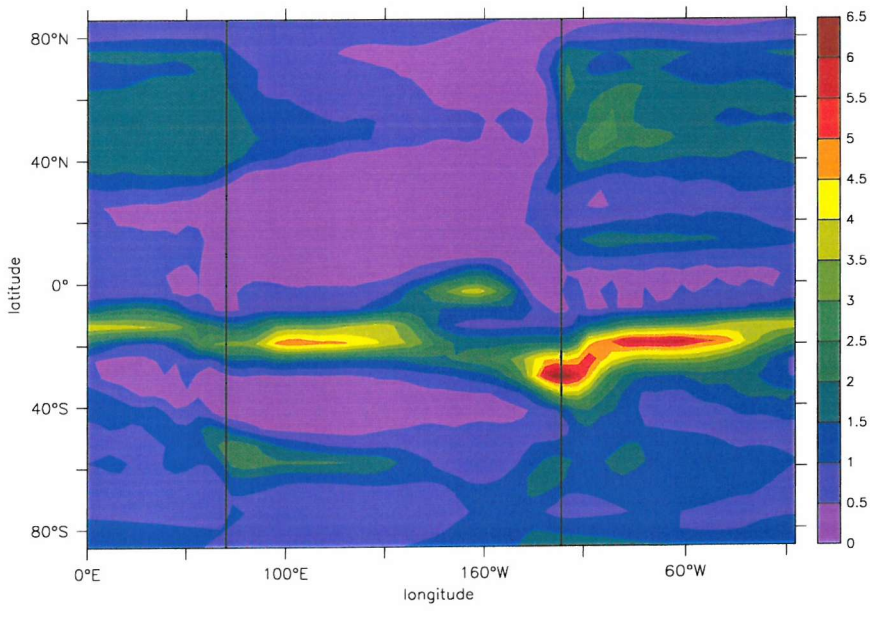

Figure 3.39: *DJF rainfall on PangeaWorld (m/year).*

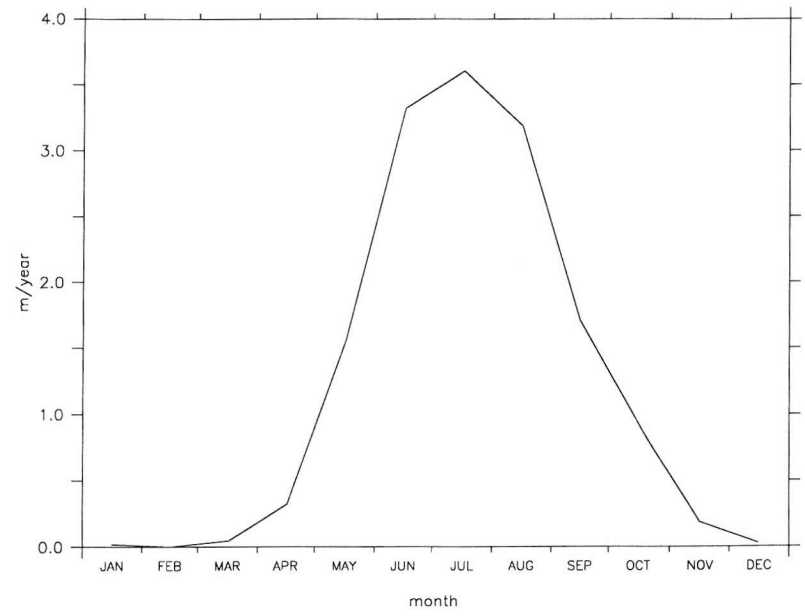

Figure 3.40: *Precipitation amount (m/year) for 100°E, 18°N, in the rain belt on the PangeaWorld continent.*

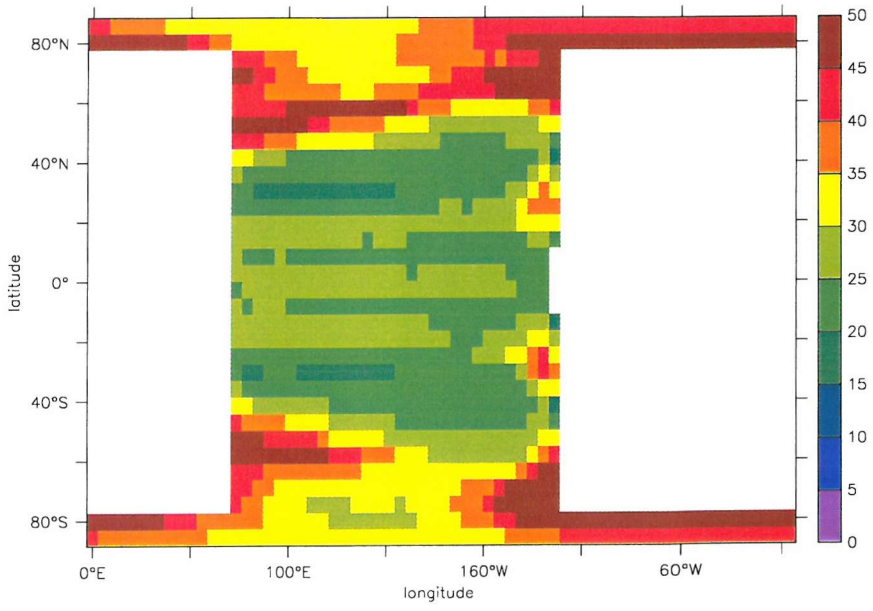

Figure 3.41: *Annual average soil moisture (cm) on PangeaWorld, annual average (50cm is saturated).*

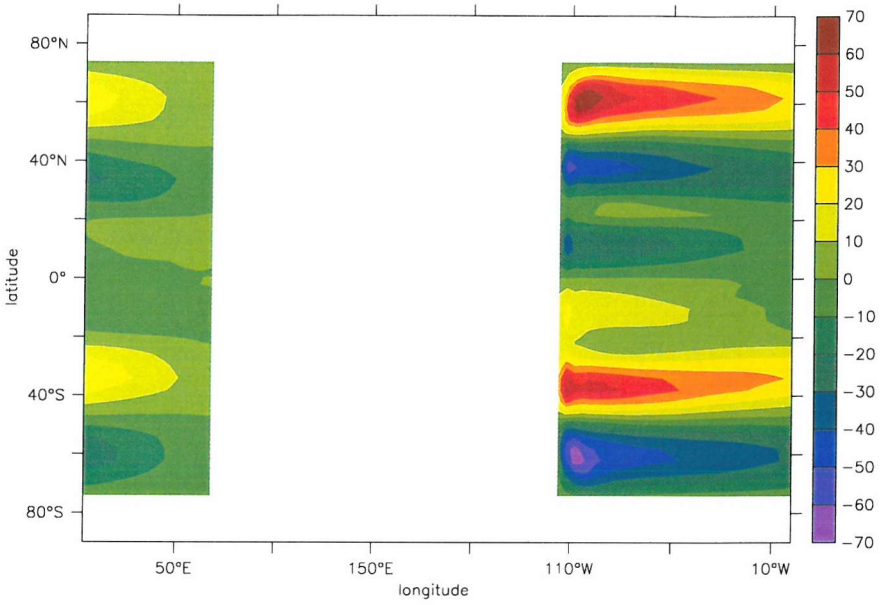

Figure 3.42: *Horizontal streamfunction (Sv) for the PangeaWorld ocean.*

ing 50cm of water) and the driest regions corresponding to those regions of low rainfall in the midlatitudes.

Ocean Circulation

The general ocean circulation, unsurprisingly, follows a similar form to that on RidgeWorld: both are single, rectangular ocean basins, so the usual gyre transports (*fig:3.42*) and western boundary currents obtain. The gyre pattern is slightly more spread out than that on RidgeWorld, a result of the wider spread of the surface zonal wind maxima. The maxima in the polar gyres is weaker than on RidgeWorld, a result of the weaker winds. Conversely, the stronger tropical winds give rise to current speeds up to a third stronger than on RidgeWorld, with surface speeds of up to 96.3 cm/s against the western boundary.

The MOC (*fig:3.43*) is also of the same form as that on RidgeWorld and still has no cross-meridional transport. It is a little stronger than on RW though, with transports of up to 102 Sv in the main deep polar overturning maximum, an increase of 18 Sv, and increases of up to 40 Sv in other parts of the cell. This stronger

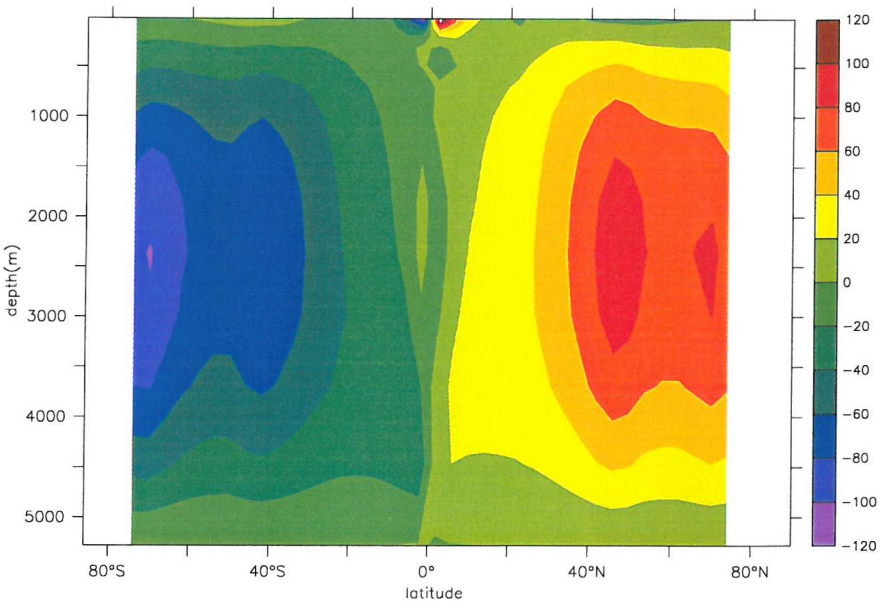

Figure 3.43: *Overturning streamfunction (Sv) for the PangeaWorld ocean.*

overturning is in agreement with a plot of convection on PangeaWorld (*fig:3.44*), which shows more activity than for RidgeWorld, especially up against the cooler poles.

3.3.2 PangDrakWorld

PangDrakeWorld shows a similar surface temperature distribution to PangeaWorld. The seasonal maximum temperatures are found in bullseye patterns over the land, centred around 40°, and, for the southern hemisphere summer case, there is a similar temperature contrast between summer and winter hemispheres, a range of about 70°C. The northern hemisphere summer temperature maximum shows a curious slanted pattern, starting at 30° on the western coast and stretching to 50° on the eastern side, and the loss of the southern hemisphere land means that winter there is less severe, lacking the low temperatures seen on PangeaWorld. In general the mean temperature is slightly warmer than for PangeaWorld, about 0.6°C. Despite the sub-zero temperatures observed on the PangeaWorld landmass at high latitudes, when replaced by ocean these temperatures are not reproduced

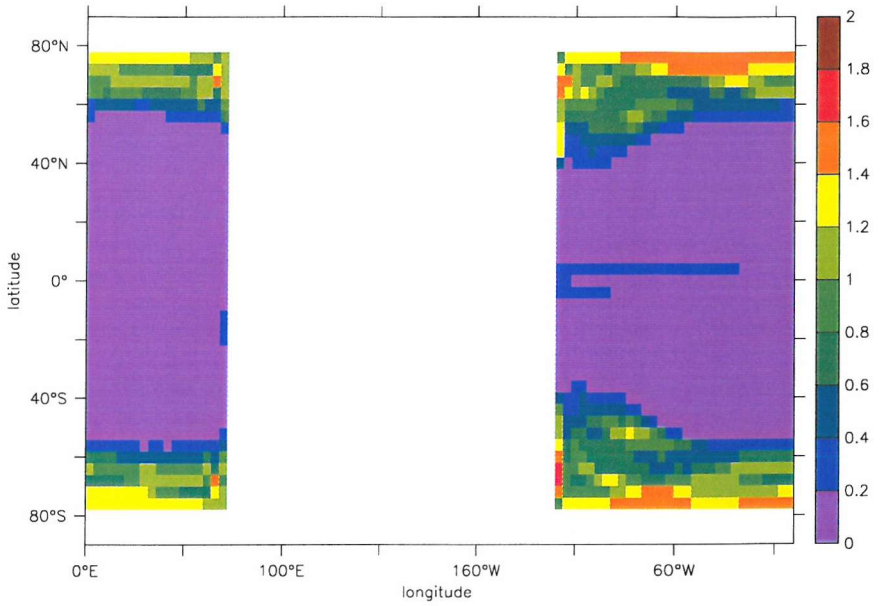

Figure 3.44: *Annual average convective frequency for PangeaWorld (per timestep, averaged over the top 500m).*

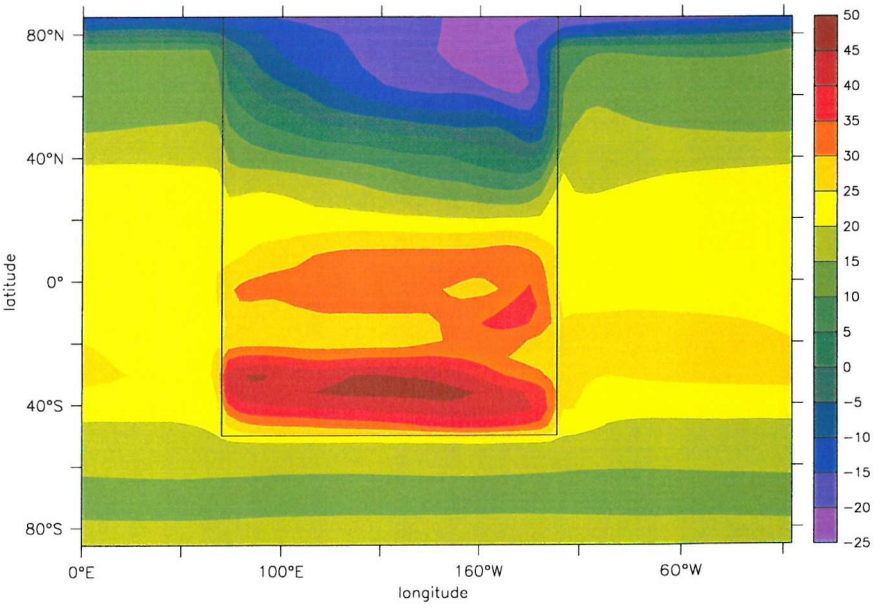

Figure 3.45: *Surface air temperature (°C), DJF, PangDrakWorld.*

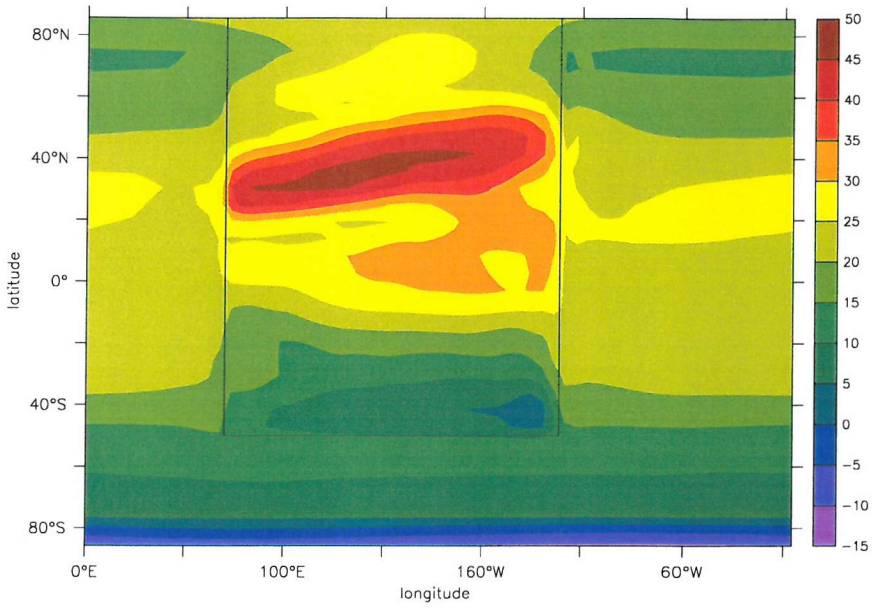

Figure 3.46: *Surface air temperature (°C). JJA, PangDrakWorld.*

so there is still no sea ice formed in this scenario.

Surface pressure pictures (*figs:3.47,3.48*) show a repeat of the bipolar pressure system over land, with the low pressure centred over the land in the summer. The opening of the gap in the southern and consequent temperature response, as seen above, reduces the strength and extent of the southern hemisphere summer low.

The rainfall picture is similar to that on PangeaWorld, although the southern hemisphere east coast maximum has shifted about 10° back towards the equator, a response to the weakened influence of the summer pressure system.

SSTs show a similar pattern to the AST differences PangeaWorld, slightly warmer (0.8°C) and obviously more zonal in the southern hemisphere through the gap. On the annual average, the north pole is 1.2°C warmer than the south. Particularly notable here though, in comparison to the DrakeWorld run, is the direction of the flow through the gap: this is now eastward, as for the current day Antarctic Circumpolar Current (the DrakeWorld run has the circumpolar flow going westward).

The meridional overturning here (*fig:3.50*) shows a similar difference from PangeaWorld as DrakeWorld does from RidgeWorld: the strength of the northern over-

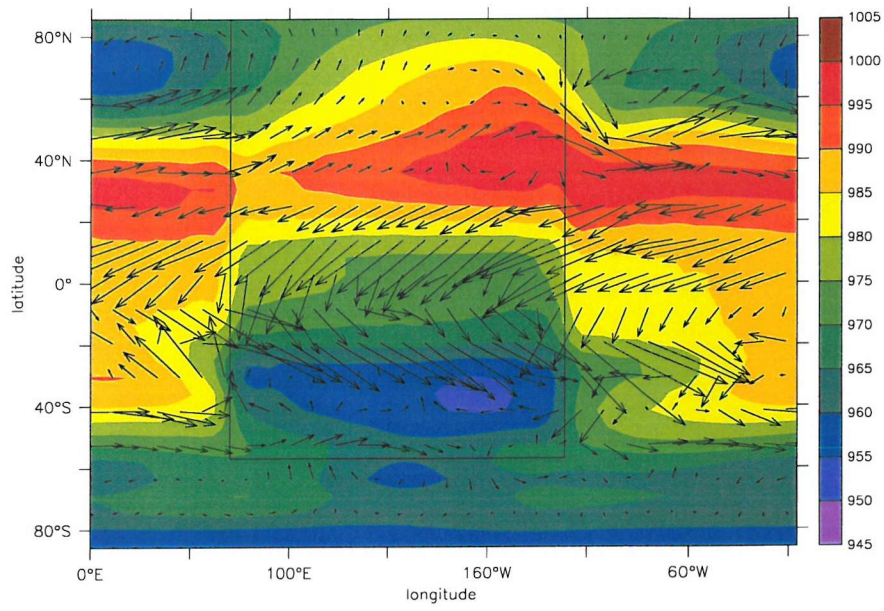

Figure 3.47: *Surface pressure (mbar) and winds (m/s) for DJF, PangDrakWorld.*

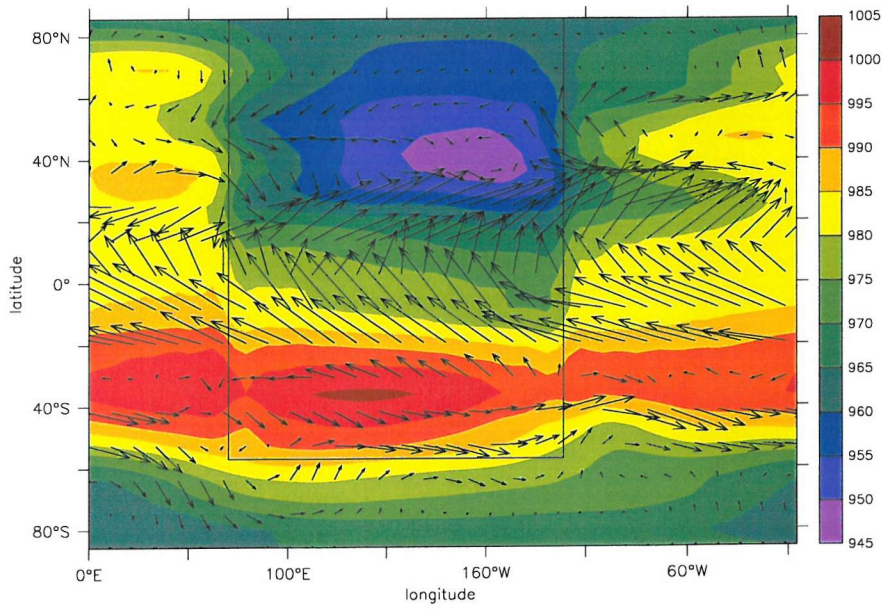

Figure 3.48: *Surface pressure (mbar) and winds (m/s) for JJA, PangDrakWorld.*

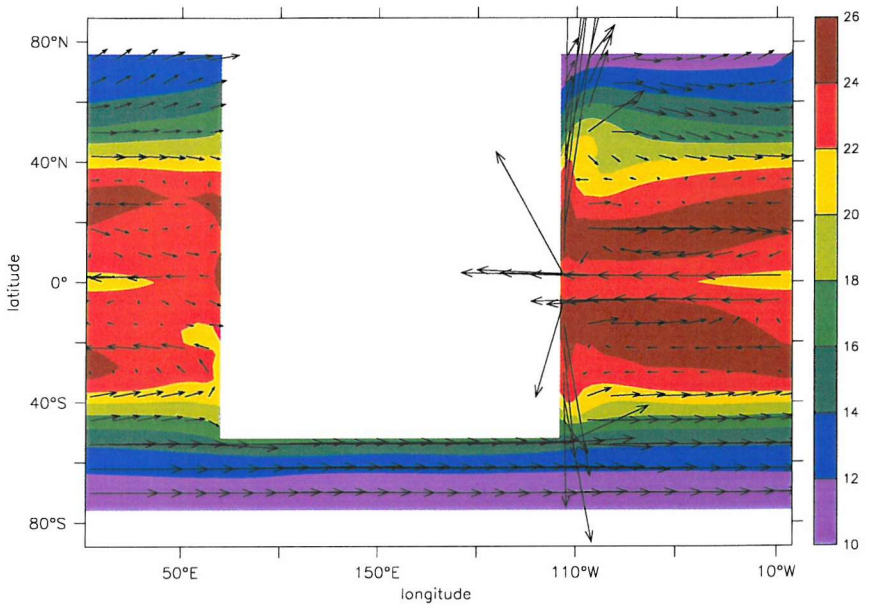

Figure 3.49: *Annual average SST (°C) and surface currents (averaged over the top 250m) for PangDrakWorld.*

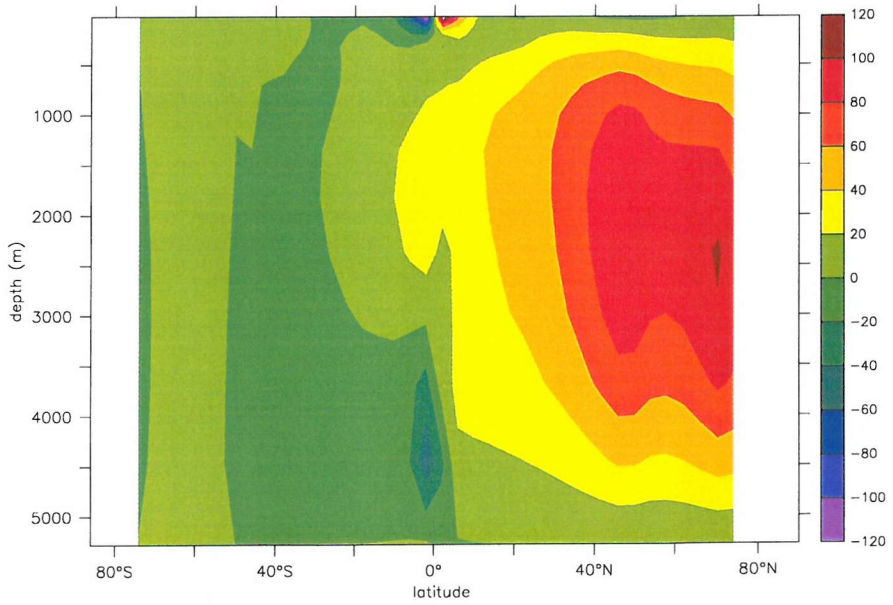

Figure 3.50: *Meridional overturning for PangDrakWorld (Sv), averaged over the last 30 years.*

turning remains the same and the major overturning cell in the southern hemisphere disappears. In this case though there is evidence of some cross equatorial transport as water is drawn north across the equator, the influence of the northern cell which extends as far south as 30°S.

CHAPTER

FOUR

Analysis

In this chapter, notable features of the first three idealised runs will be drawn out, analysed and discussed. Except where stated, all comparisons with 'current climate' or RealWorld data is drawn from a 10 year control run of FORTE with specified (the models essentially uncoupled as a result) climatological SST and SSS from the European Centre for Medium-Range Weather Forecasting data set and ocean wind forcing from a thus-forced previous IGCM3 run. This run is used to provide an idea of how the model behaves when being forced to simulate the current observed climate.

4.1 Global Average Warmth

4.1.1 RealWorld vs. Idealised Experiments

The mean surface air temperature of the 3 mostly-water simulations is much higher than that of the RealWorld: ~12°C averaged annually over the globe. Apart from the flattening of the land surface resulting in the loss of high altitude cold-air areas in the idealised runs, high average temperatures in these runs would seem to stem from two readily identifiable side effects of having replaced the entire planet's surface with water. Water has a lower albedo than most land surface

types so an aquaplanet might be expected to absorb more of the incoming solar radiation and, assuming no other changes in the system, consequently heat up. Since atmospheric water vapour is a strong absorber of (longwave) radiative energy, increasing its availability would also be expected to have an impact on global mean temperatures. Taking the basic WaterWorld as typical of the response of the idealised simulations, we can investigate these effects.

Albedo effect

Comparing the FORTE's RealWorld configuration with the idealised runs, the average surface albedo value α_s has changed from 0.152 to 0.102. The canonical simple radiative equilibrium model for surface temperature of

$$(1 - \alpha_p) \cdot S_o = \varepsilon \sigma T^4 \tag{4.1}$$

(where α_p is the planetary albedo (incoming shortwave at the top of the atmosphere divided by outgoing shortwave, the albedo for the whole surface/atmosphere system), S_o is the average solar insolation, ~344 W/m^2, ε is the average longwave emissivity of the atmosphere (longwave escaping the top of the atmosphere divided by the total emitted by the earth), σ is the Stefan-Boltzmann constant and T is the average surface temperature of the earth)

implies, assuming no consequent change in emissivity, a WaterWorld temperature given by

$$T_W = T_R \cdot \sqrt[4]{\frac{1 - \alpha_{p,W}}{1 - \alpha_{p,R}}} = T_R \cdot \sqrt[4]{1 + \frac{\alpha_{p,R} - \alpha_{p,W}}{1 - \alpha_{p,R}}} \tag{4.2}$$

(T_W is the average surface temperature of WaterWorld, T_R the temperature of the RealWorld and $\alpha_{p,W}, \alpha_{p,R}$ are the planetary albedoes of WaterWorld and RealWorld respectively).

Assuming no change in atmospheric albedo, so that $\alpha_{p,R} - \alpha_{p,W} = \alpha_{s,R} - \alpha_{s,W}$ the change in surface temperature purely due to the extra shortwave absorption at ground from this surface albedo would be roughly

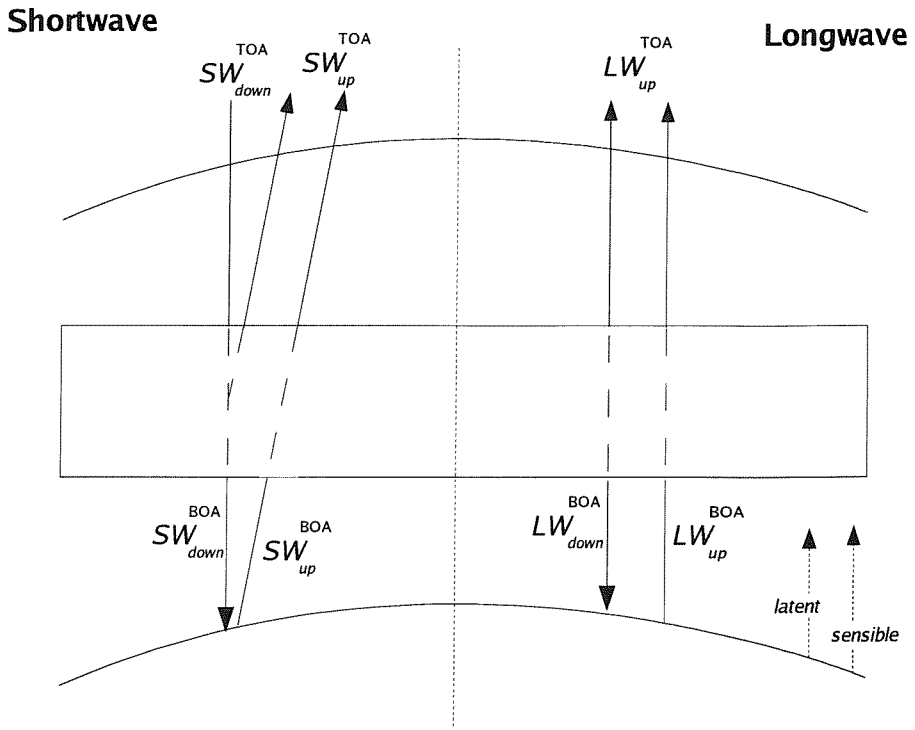

Figure 4.1: *Definitions of various terms in the energy balance model.*

$$T_W = 288 \cdot \sqrt[4]{1 + \frac{0.05}{1 - 0.32}} \tag{4.3}$$

- only 5°C higher. So the surface albedo change on its own cannot be responsible for the full increase.

Energy Balance

Comparing the surface, bottom of atmosphere [BOA] and top of atmosphere [TOA] energy balances on WaterWorld with the values that the model sees for the Real-World climate is instructive.

Evidenced by imbalances in the TOA net radiative fluxes (*figs:4.1,4.2*), neither of

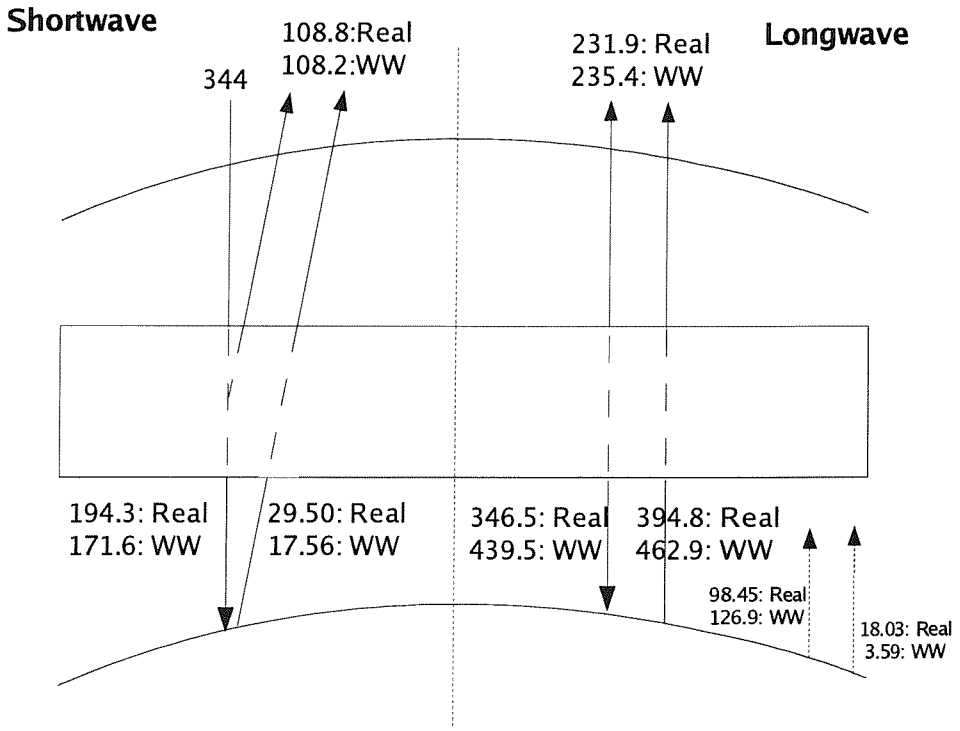

Figure 4.2: *Energy balances for WaterWorld and RealWorld simulations (all numbers are W/m^2). See figure 4.1 for definitions of each flux, and equations 4.4 to 4.7 for their use in the simple radiative model.*

these two sample states is at equilibrium, with the RealWorld system absorbing 3.2 W/m^2 and the WaterWorld 0.37 W/m^2 - WaterWorld is evidently closer to equilibrium. Not all of this excess energy goes into warming the ocean, as both systems lose energy through friction, but RealWorld coupled runs show significant warming in the ocean when started from this state and the WaterWorld ocean is also not yet at full thermal equilibrium, warming at a rate of 0.018°C per century (see table 3.3).

In light of the above discussion of surface albedo, it is interesting to note that the net shortwave at the top of the atmosphere is almost unchanged between the RealWorld and WaterWorld runs - WaterWorld's lower surface albedo should have resulted in an decrease in the amount of shortwave energy escaping. The WaterWorld atmosphere has undergone changes such that the amount of shortwave reaching the ground is reduced and the surface albedo effect is cancelled out of the total shortwave budget.

The simple model (equation: 4.1) specified above can be broken down somewhat to yield more insight into the radiative characteristics of the systems involved.

The planetary albedo, α_p, which is characteristic of the system as a whole can be derived from diagnostics as presented above as:

$$\alpha_p = \frac{SW_{up}^{TOA}}{SW_{down}^{TOA}} \tag{4.4}$$

since nothing in the system is warm enough to emit shortwave radiation. The amount of shortwave escaping can be deconstructed into its dependence on 3 different parameters: the shortwave reflectance of the atmosphere, α_a; the shortwave transmissivity of the atmosphere, ε_S; and the shortwave reflectance of the earth, α_e, where

$$\alpha_e = \frac{SW_{up}^{BOA}}{SW_{down}^{BOA}} \tag{4.5}$$

$$SW_{up}^{TOA} \sim \varepsilon_S \cdot SW_{up}^{BOA} + \alpha_a \cdot SW_{down}^{TOA} \tag{4.6}$$

and

$$SW_{down}^{BOA} \sim SW_{down}^{TOA} \cdot (\varepsilon_S - \alpha_a) \tag{4.7}$$

These last two are approximated from assuming that reflectance from and absorption in the atmosphere both happen throughout its entire depth.

Comparing the two cases, we have:

	α_p	α_a	ε_S	α_e
RealWorld	0.316	0.247	0.812	0.152
WaterWorld	0.315	0.275	0.774	0.102

Table 4.1: *RealWorld and WaterWorld parameters for the simple radiative model, equations 4.4 to 4.7.* α_p *- planetary albedo;* α_a *- atmospheric albedo;* ε_S *- shortwave transmissivity of atmosphere;* α_e *- surface albedo.*

As expected, the surface albedo implied by the fluxes is lower than that in the RealWorld simulation but the overall reflectance of the system, the planetary albedo, does *not* reflect this change - the two cases are almost identical. Although both the shortwave absorbancy of the atmosphere and the surface are higher on WaterWorld, this is balanced by an increase in reflectivity, so the amount of shortwave absorbed by the two systems is equal. The use of WaterWorld as typical of the idealised simulation response is borne out here: numbers for Ridge- and DrakeWorlds are almost identical to WaterWorld.

WaterWorld's higher temperatures are thus not directly caused by the lowering of surface albedo and higher absorption of shortwave radiation. This leaves the effect of the extra availability of water and its insulating effect in the atmosphere. Taking the longwave emissivity as

$$\varepsilon_L = \frac{LW_{up}^{TOA}}{LW_{up}^{BOA}} \tag{4.8}$$

we find that WaterWorld has a value of $\frac{235.4}{462.9} = 0.508$ whilst RealWorld is higher at $\frac{231.9}{394.8} = 0.587$. RealWorld has a greenhouse that lets through 59% of the surface-emitted longwave, whilst WaterWorld's lets only 51% out - WaterWorld's surface

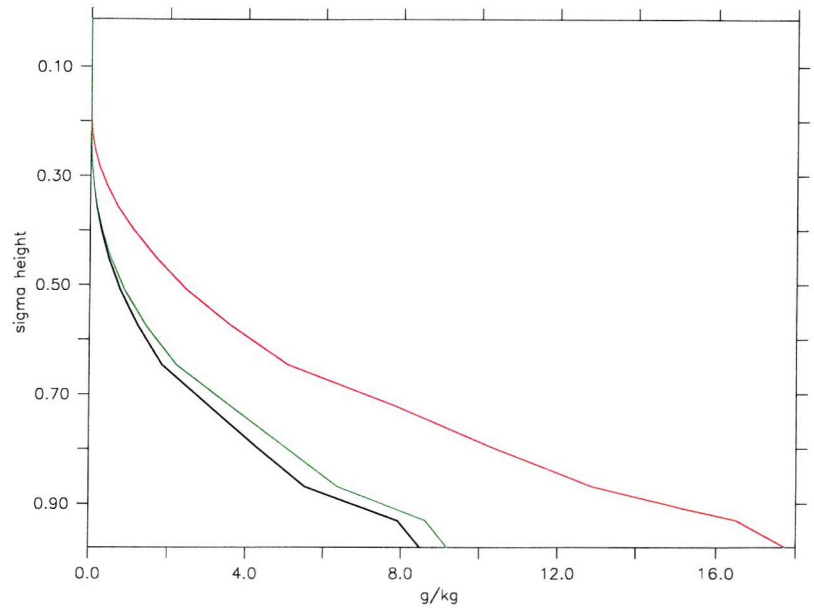

Figure 4.3: *Global average specific humidity for the RealWorld and an idealised atmosphere.* Black*: RealWorld;* Red*: WaterWorld;* Green*: PangeaWorld.*

therefore needs to be at a higher temperature in order to get enough longwave out of the top of the atmosphere to balance the shortwave energy absorbed. The radiative fluxes presented here are quite in agreement with the average surface temperatures observed in the two cases.

Water vapour is the principal gas that contributes to our atmosphere's greenhouse effect, but the atmosphere above continental interiors will only have substantial amounts of water if it is brought there through transport processes - the distribution of water vapour is therefore uneven and often much less than saturated. On a WaterWorld there is an abundant supply of water everywhere, with an average surface relative humidity of over 80%. Very important here is a positive feedback associated with water vapour: the saturation pressure of water vapour in air increases with temperature, so the warmer the atmosphere, the more water vapour it can hold and the warmer it gets. It might be expected that an initial warming due to the reduced surface albedo of WaterWorld might help start such a process, that then becomes limited by, for instance, increased shortwave reflection from clouds.

A graph of the humidities (*fig:4.3*), of the two cases indicates that a large water vapour forcing will be acting throughout the troposphere on WaterWorld - this water vapour will clearly have a major effect on the radiative absorption profiles, increasing both long- and short-wave absorption as seen in the analysis above.

Although less important for shortwave absorption but also linked to water vapour, the changing cloud profile between the two scenarios is also important in explaining these general properties of the atmosphere. Levels of low cloud (*fig:3.13*), which has the highest shortwave reflectivity, are higher on WaterWorld than RealWorld (with an average coverage fraction of 0.78 as opposed to 0.66), tallying with the higher atmospheric reflectivity noted above. Levels of mid- and high-level clouds are slightly lower.

As the basin planets have a significantly cooler climate than the aquaplanets - about 6°C on average - it is worth repeating the calculation. Comparing WaterWorld and PangeaWorld:

	α_p	α_a	ε_S	α_e	ε_L
RealWorld	0.316	0.247	0.812	0.15	0.587
WaterWorld	0.315	0.275	0.774	0.10	0.508
PangeaWorld	0.311	0.234	0.808	0.17	0.549

Table 4.2: *Comparison of parameters for RealWorld, WaterWorld and PangeaWorld for the simple radiative model, equations 4.4 to 4.8.* α_p *- planetary albedo;* α_a *- atmospheric albedo;* ε_S *- shortwave transmissivity of atmosphere;* α_e *- surface albedo;* ε_L *- longwave transmissivity.*

The desert covered surface of the continent has significantly elevated the surface albedo value, so would be expected to absorb rather less of the incoming shortwave on these grounds. This is not, however, reflected in the overall planetary albedo value which shows PangeaWorld, through a low atmospheric reflectivity value, absorbing *more* of the sun's radiation overall than the other two cases.

The fact that the atmosphere absorbs less (has higher ε_S and ε_L) than WaterWorld is what makes it actually cooler, despite absorbing more of the incoming shortwave. Both values are still smaller than the RealWorld case, indicating that temperatures will still be, on average, higher on PangeaWorld. Figure 4.3 shows that there is still more water vapour in PangeaWorld's atmosphere than for the

RealWorld configuration, and so it is again the water vapour greenhouse that is responsible for the longwave absorption that keeps the climate warm.

4.1.2 Atmosphere-Only Global Mean Temperature Experiments

Although for both basin planet and aquaplanet experiments the warmth of the global mean climate is explained by the higher amounts of water in the atmosphere, the warmth of the basin planets, relative to the RealWorld configuration, raises questions about the reasoning applied above to explain the presence of this water. Whilst the aquaplanets have a lower albedo and a higher availability of water vapour due to their lack of land surface, PangeaWorld has both a higher surface albedo (although as for the aquaplanets this is not directly reflected in the planetary albedo) than the RealWorld and a smaller area of ocean surface; judged on only these criteria this should result in less water in the atmosphere and a cooler climate than RealWorld. Unlike other Pangean climate simulations the CO_2 level here is at present day values so the climate should not be warmer on that account. This is not the case - there is clearly more controlling the strength of the water vapour greenhouse here than global mean surface albedo and mean land/sea area ratios.

Further investigation of the effects of the surface albedo and land surface area on the global mean temperature were therefore conducted with a series of short additional runs with varying land characteristics. These were all performed with the atmosphere component of FORTE coupled to a 30m deep swamp ocean so as to come to equilibrium over a much shorter timescale than the full coupled model. As mentioned in the model section, IGCM3 has a mixed-layer ocean option that provides each surface gridbox with a fixed depth bucket of water with which to exchange heat fluxes to simulate the thermal inertia of the ocean's upper layer. Transport of any kind in this ocean is achieved through the specification of additional fluxes, derived from climatologically forced runs, which simulate a divergence/convergence of heat for each box. Given that a number of further geographies were to be tested in this series, for which the climatologies and thus appropriate transports were unknown, this additional transport flux was not spec-

ified for these experiments, leaving an ocean with no heat transport whatsoever - this transportless ocean is the 'swamp' ocean. This allows the effect of the change of land-surface on the atmosphere to be unbiassed by changing ocean influences.

Total Ocean Heat Transport Effects on Global Climate

The first of these experiments was a test to see what systematic differences would be induced in a basic model climatology through the use of this much reduced ocean system. This experiment also makes for a good comparison with the full WaterWorld experiment: what is the effect on the climate of forcing the biggest possible change in the ocean circulation/heat transport - shutting it down completely? In the absence of any further climate feedbacks, one might expect the primary effect to be on the distribution of heat at the surface: the equator-pole temperature gradient would be increased as the reduced transports restrict the amount of heat that can be taken from the tropical regions of net warming to those of net cooling at the pole, but that the mean amount of heat absorbed, and thus the average surface temperature, would not change.

This, surprisingly, is not what happens (*fig:4.4*). There is some change to the surface temperature gradient, becoming steeper poleward of 40° as predicted, but the most notable effect is that the mean surface temperature has dropped by 7.9°C. Clearly there is a substantial feedback to the atmosphere that results in a change to its radiative properties and the resultant energy balance. The radiative model parameters for this new case can be seen in table 4.3:

	α_p	α_a	ε_S	α_e	ε_L
RealWorld	0.316	0.247	0.812	0.15	0.587
WaterWorld - coupled	0.315	0.275	0.774	0.10	0.508
WaterWorld - swamp	0.342	0.302	0.790	0.10	0.541

Table 4.3: *Comparison of parameters for RealWorld and WaterWorlds -coupled and -swamp for the simple radiative model, equations 4.4 to 4.8.* α_p *- planetary albedo;* α_a *- atmospheric albedo;* ε_S *- shortwave transmissivity of atmosphere;* α_e *- surface albedo;* ε_L *- longwave transmissivity.*

As for the cooler PangeaWorld case, WaterWorld swamp has less of a greenhouse than the coupled WaterWorld and there is an additional cooling feature: the total

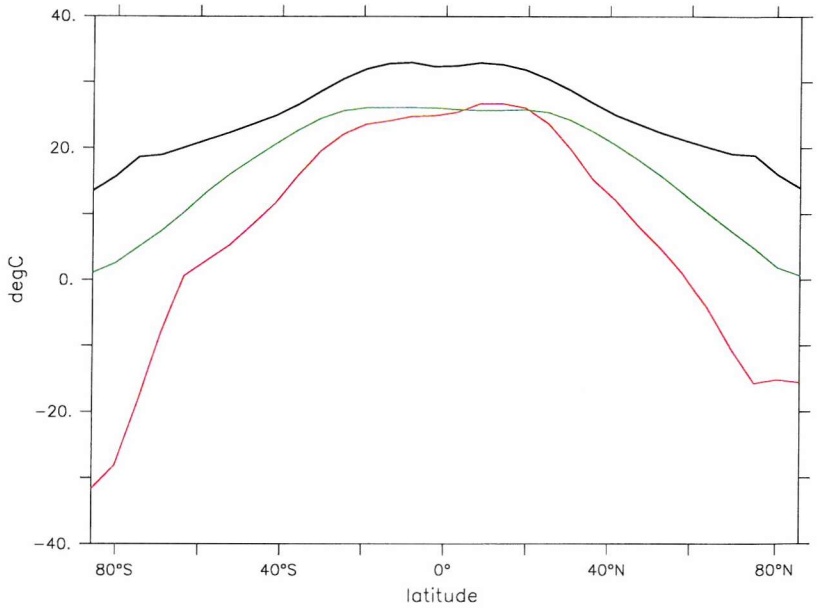

Figure 4.4: *Annual, zonal average air surface temperature profiles.* Black*: Coupled WaterWorld;* Red*: RealWorld;* Green*: Swamp WaterWorld.*

planetary albedo, which has only changed by at most 1.6% between any of the other runs despite changes of up to 70% in surface albedo, has here increased by 9% from the coupled WaterWorld case, despite no change at all in the surface value.

Plotting the difference in TOA shortwave between the two WaterWorld runs (*fig:4.5*) shows that the main difference here is in the tropics, which see a reduction of up to 30 W/m^2 in the swamp case. This is accompanied by an increase in the low cloud coverage fraction in exactly the same region. The increased cloud levels result in a higher reflection of the incoming shortwave and contribute to the net cooling of the swamp WaterWorld.

Swamp WaterWorld is cooler than the coupled case, and this state is maintained by reduced levels of water vapour in the atmosphere and a higher tropical atmospheric reflectivity. The question then arises of how this state evolved: did it become cooler because there was less water vapour in the atmosphere, or is the reduced greenhouse just a consequence of the cooling, rather than the initial

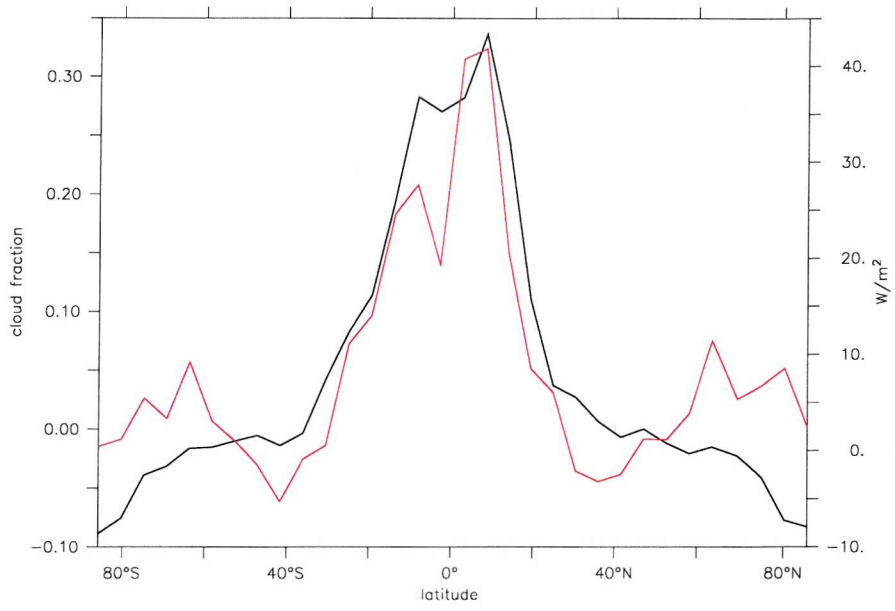

Figure 4.5: *Difference between the coupled and swamp WaterWorld runs.* Black, left axis*: Low cloud profile (swamp-coupled);* Red, right axis*: Net shortwave downward at the TOA (coupled-swamp). Both are annual, zonal averages.*

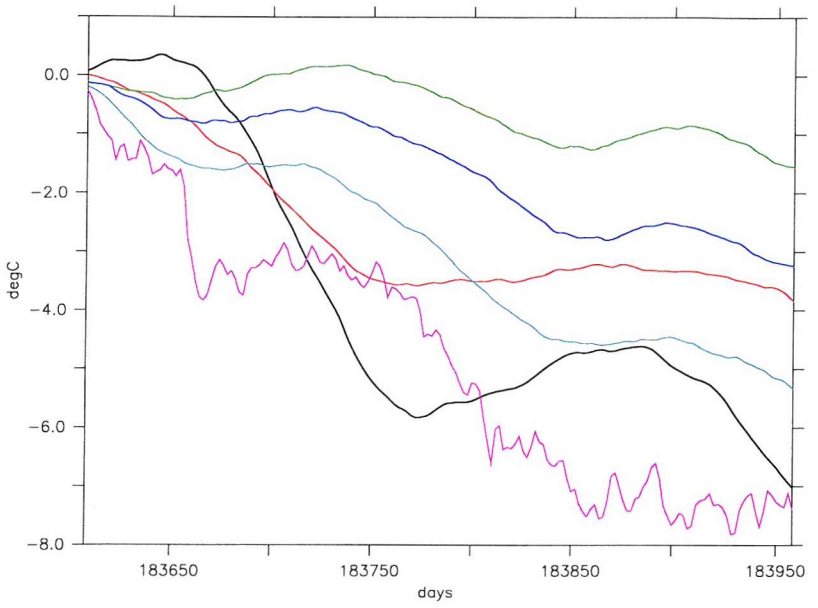

Figure 4.6: *Difference between the coupled and swamp WaterWorld runs - surface temperature evolution at different latitudes over the first year after switching off the ocean.* Black:*0-10°;* Red:*10-20°;* Green:*40-50°;* Dark Blue:*50-60°;* Light Blue:*60-70°;* Pink:*70-80°.*

cause. Low SSTs have been shown to correlate with increased lower atmosphere stability, which increases the strength of the inversion at 700 mbar, resulting in more low level cloud (Philander et al., 1996), but which came first, the shortwave reduction and cooling from the increased cloud or the cooler SSTs?

The changes observed are rapid - the global average surface temperature drop in the first year is 3.8°C - so the following analysis looks at the changes in the first year, averaging northern and southern latitudes together to eliminate the seasonal signal. The effect expected initially from shutting down the ocean heat transport must play an initial role: this is the first thing to change and everything else must react to it. From this, we would expect to see an initial increase in tropical temperatures and a decrease of those at higher latitudes as the ocean can no longer move the excess heat to the cooler poles.

Figure 4.6 shows the difference in air surface temperature from the coupled WaterWorld, where both have been averaged over the specified latitude band in both

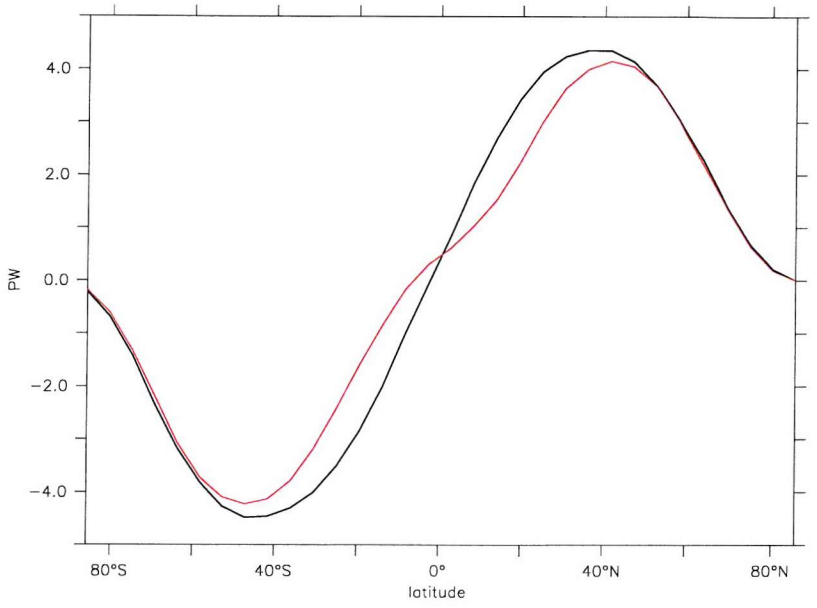

Figure 4.7: *Total system heat transports derived from TOA fluxes. Both curves show a small net imbalance, which has been removed for this plot via a constant correction from each gridpoint.* Black*: coupled WaterWorld;* Red*: swamp WaterWorld.*

northern and southern hemispheres. As expected, the equatorial temperatures do not immediately drop, whereas all other latitudes show an immediate reduction as they are affected by the lack of heat transported to them by the ocean. Between 20° and 50° the lines are much the same, so for clarity only one of the three has been plotted. The final profile of surface temperature, with greater cooling at the equator and pole and less in the midlatitudes is reflected in the final position of the lines in this picture.

Assuming that the atmospheric poleward heat transport will not immediately compensate for the loss of the oceanic, temperature drops at high latitudes are thus to be expected, resulting in a reduction in latent heat flux and local availability of water vapour to insulate the surface and even more surface cooling. The evolution in the tropics is less clear cut. Atmospheric transport does not compensate for the loss of the ocean heat transport (*fig:4.7*) which shows a drop in the total climate system heat transport in the same regions where the ocean transport normally

dominates the picture, yet despite the loss of a transport mechanism to remove excess heat from the tropics, temperatures here do not increase by the same amount as the higher latitudes' decrease.

The regulation of equatorial SSTs in our current climate and the processes that prevent the positive water vapour feedback from creating a runaway greenhouse is an open research question, and some of the possibilities arising from it may be applied here. Pierrehumbert (1996) suggests that excess heat is transported away from the saturated equatorial region to areas of subsidence where the air is drier and radiated through these 'windows' of dry air. We would not expect this mechanism to operate here as we are reducing the amount of transport away from the equator, but a plot of the TOA longwave (*fig:4.9*) which shows high emission regions at around 30° for the coupled case suggests that this mechanism is probably at work there and may well, along with the generally elevated levels of reflective cloud be responsible for the relatively small increase in coupled WaterWorld tropical SSTs relative to the poles. The mechanism clearly does not apply when a swamp ocean is present: instead, the lack of ocean transport to these radiative windows results in the loss of the excess longwave emission in these regions and so the radiative profile depends more linearly on latitude, with a lower average amount due to the lower average surface temperature.

Another suggestion is that of Ramanathan and Collins (1991), who predict that greater SSTs lead to greater convection and the formation of reflective high cirrus clouds that reduce the shortwave insolation and cool the sea surface again. Whilst a plot of convective cloud activity for the swamp case shows only a small relative increase in this region, followed by a swift drop as the tropical SSTs fall, figure 4.8 shows the temperature change in the tropical band *following* the change in low cloud fraction that is responsible for the reduced shortwave in the final equilibrium state, suggesting that a form of cloud feedback is limiting equatorial temperatures in the swamp case.

We thus conclude that suppressing the ocean heat transport in this scenario leads to a mean global cooling via a reduction in the strength of the water vapour greenhouse, caused by decreased latent heat flux from the immediately cooled higher latitudes and an increase in the low latitude low cloud amount that limits initial

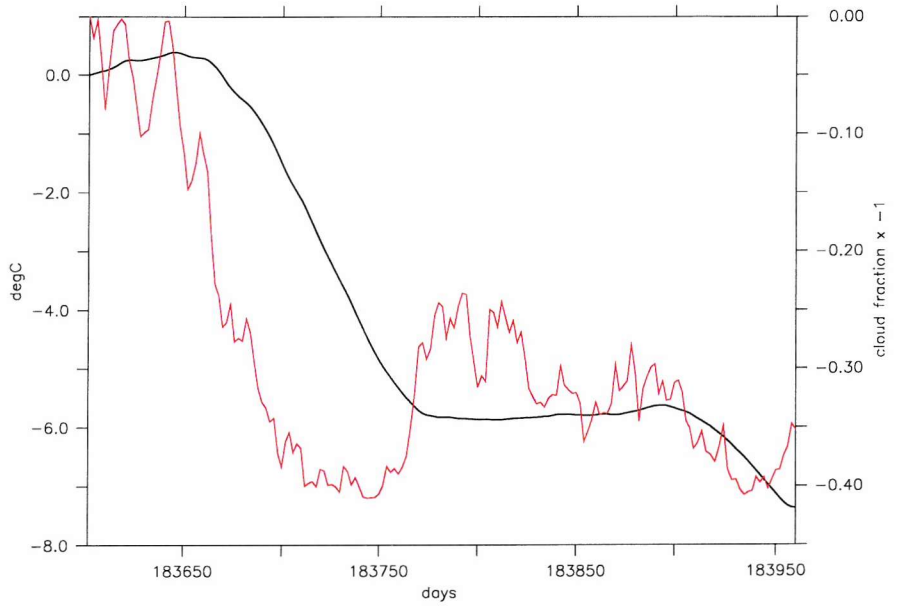

Figure 4.8: *Evolution of equatorial temperature (*Black, left axis*) and low cloud amount (*Red, right axis*, has been inverted for comparison) for the swamp WaterWorld.*

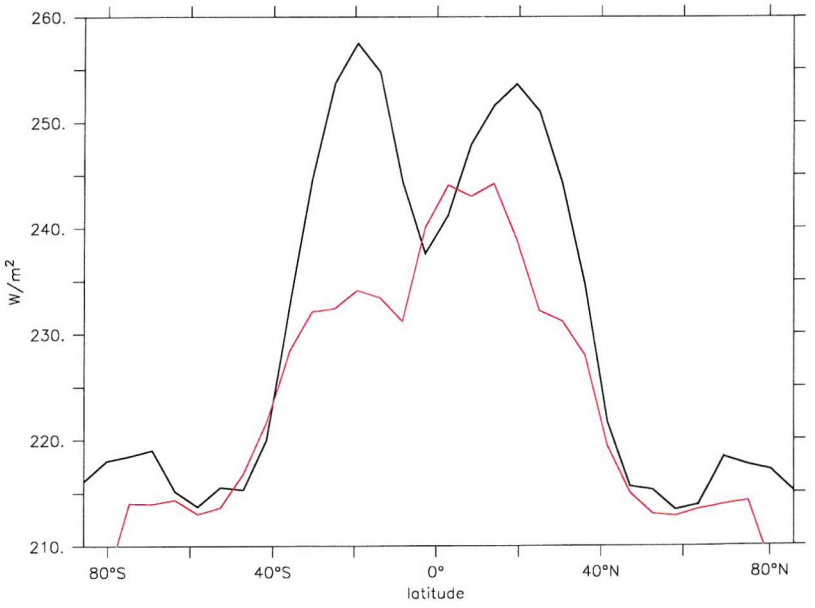

Figure 4.9: *Zonal, annual average TOA longwave emission for coupled and swamp WaterWorlds.* Black*: coupled;* Red*: swamp.*

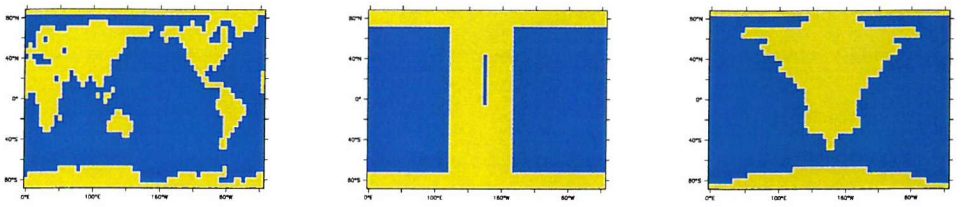

Figure 4.10: *Further test geographies with the same global mean land surface area and albedo. Left: RealWorld; Middle: RTRW; Right; RTRW-lat.*

equatorial warming and reduces the amount of solar insolation received by the planet as a whole. This dramatically demonstrates the possible effects on global climate of changes in the ocean heat transport that extend far beyond the simple redistribution of the heat in the system.

Land Surface Specification

It has been seen that the mean surface temperature, although controlled by the strength of the atmospheric greenhouse which is influenced by the availability of water, does not depend simply on the global mean surface area of land - Pangea-World is still warmer than WaterWorld despite having a greater surface of land. Aside from the sensitivity of the global greenhouse on the ocean heat transport demonstrated above, a series of short experiments was carried out to determine whether the distribution of the land surface, not just the amount, was a factor influencing the mean climate.

Figure 4.10 shows the first three maps used. These all have the same land surface area and global mean surface albedo. The inland lake in the second is to preserve the perfectly rectangular coastline whilst keep the correct total amount of land. All the land is set to a constant albedo value of 0.23 to give the same global average surface albedo in each case of 0.135, that of the initial RealWorld map used here. The first map has the same land distribution as the RealWorld run, but has the swamp ocean as used above and a globally uniform land surface albedo. This was run twice, once with realistic surface topography and once without, with the land everywhere at a constant 50 metres height. The second is a RidgeWorld analog 'ReallyThickRidgeWorld [RTRW]' which is also flat, and the third has the

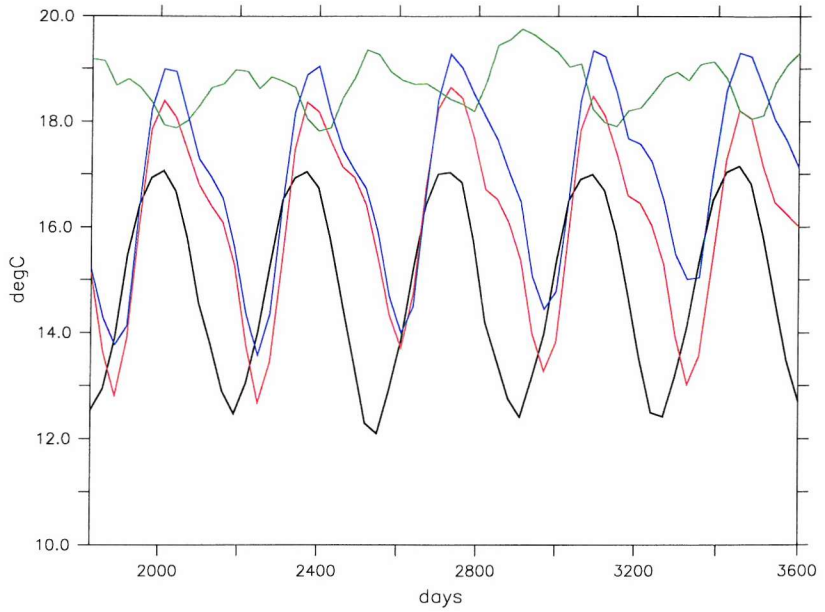

Figure 4.11: *Global average land surface temperatures for the first three land-distribution experiments.* Black*: RealWorld (topography);* Red*: RealWorld (flat);* Green*: RTRW;* Blue*: RTRW-lat.*

	RealWorld(topog)	RealWorld(flat)	RTRW	RTRW-Lat
Mean AST, °C	14.88	16.11	18.70	16.98

Table 4.4: *Comparison of global mean air surface temperature for the IGCM3-only geographies shown in figure 4.10.*

ridge altered so as to have the same latitudinal land distribution as the RealWorld [RTRW-lat]. These were run for just 10 years each, by which time the interannual trend in the globally averaged surface temperature had levelled out.

The distribution of the land surface does make a significant difference to the global mean temperature here (*fig:4.11*). The mean values of global air surface temperature are given in table 4.4.

Flattening the land surface down to sea-level unsurprisingly increases the average surface temperature by removing cold, high elevation areas from the average, so the real comparison here is between the three 'flat' runs. As shown in figure 4.11, redistributing the land to be hemispherically asymmetrical allows the seasonal cy-

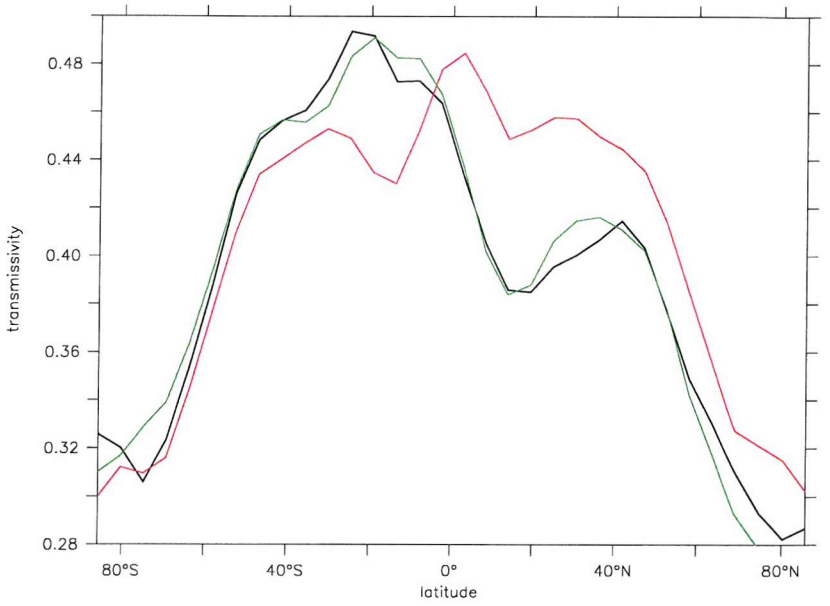

Figure 4.12: *Zonal, annual average longwave transmissivity for the first three land-distribution experiments.* Black*: RealWorld (flat), mean 0.417;* Red*: RTRW, mean 0.430;* Green*: RTRW-lat, mean 0.418.*

cle to be observed in the global mean average, as now the temperature responses of northern and southern hemispheres to the changing seasons are no longer equal. However, it also lowers the global mean. Looking at the longwave transmissivity of the three runs (*fig:4.12*) shows that the two hemispherically asymmetrical runs with more land in the northern hemisphere have reduced greenhouse forcing over the northern hemisphere. Whilst they have more than the RTRW run over their southern hemisphere oceans, this does not fully compensate for the reduction in the north, leaving them with lower global average greenhouses and lower temperatures.

The above runs suggest that it is the greenhouse response over the different surface types that controls the surface temperature, and that different distributions of land produce different mean effects. As the global mean of this last RTRW-lat run is still higher than that of the RealWorld simulation, a further series of tests was carried out to investigate how the detailed distribution of land might be causing these differences in atmospheric response. It was thought that the size of individ-

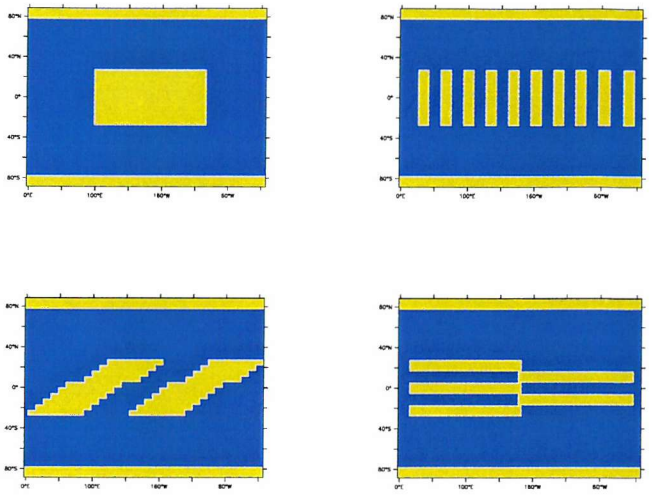

Figure 4.13: *Test geographies to investigate the effects of changing coastline length. Top left: TOG; top right: VERT; bottom left: DIAG; bottom right; HORZ.*

	TOG	VERT	DIAG	HORZ
Mean AST, °C	20.34	20.36	19.67	20.78

Table 4.5: *Comparison of global mean air surface temperature for the IGCM3-only geographies shown in figure 4.13.*

ual landmasses might be an important factor in determining this - the smaller the landmasses the nearer any given land point will be to the ocean and the easier it will be to transport moisture to them and keep global coverage of the water vapour greenhouse. This is especially likely to be true in an atmosphere model of this resolution where inland moisture transports are thought to be underestimated (Valdes and Blackburn, 1989). In keeping with the philosophy of the rest of this project a more idealised approach was taken here than in the above 4 experiments and these integrations were done with a simple block of land, cut up so as to give different land mass sizes and different lengths and orientations of coastline (*fig:4.13*). The experiments are 'Together' [TOG] 'Vertical Split' [VERT], 'Diagonal Split' [DIAG] and 'Horizontal Split' [HORZ].

The results of these experiments - and a number of further geographies not shown - were inconclusive, suggesting that the atmospheric response and resulting surface temperature was linked more to the degree of hemispherical asymmetry than

the individual land mass size. The issue was also complicated by differing temperature responses in the upper atmosphere, where some of the runs with cooler surface showed a compensating warming at higher altitudes, and some did not. Together with the previous results that suggest a strong dependence on the latitudinal placement of the land, this short series of experiments shows that atmospheric feedback and global mean surface temperature response of the model to an arbitrary landmap is complex and highly dependent on the mean size and placement of the land, not just the total surface area. Given that this study is aimed at looking at the effect of changing the ocean circulation on the climate, and that the landmap stays very nearly constant between the runs being compared (the global mean temperature difference between PangeaWorld and RidgeWorld is not being looked at as a function of the ocean circulation) it was felt that the details of the complex picture emerging from the above line of study were something of a diversion from the main focus of the project and were not investigated further due to time limitations.

We can therefore conclude that the previous summary is valid, and that high mean temperature of the idealised configurations as compared to current climate observations is a result of the longwave water vapour greenhouse, a feature that is dependent on the amount of ocean surface. The global average strength of this greenhouse is, however, also dependent on the heat transport in the ocean and the size and placement of the land masses as well, explaining why the PangeaWorld simulation is still warmer than the RealWorld despite its smaller total ocean area.

4.2 Temperature Gradient and Heat Transports

4.2.1 Total Transports

Another notable feature in the averaged surface climate for the idealised runs is the shallowness of the meridional temperature gradient - the annually, zonally averaged extremes for the RealWorld are -30°C at the pole to +27°C at the equator (*fig:3.25*), whilst on WaterWorld they are +14°C to +33°C. Clearly the average temperature increase investigated in the previous section does not apply equally at

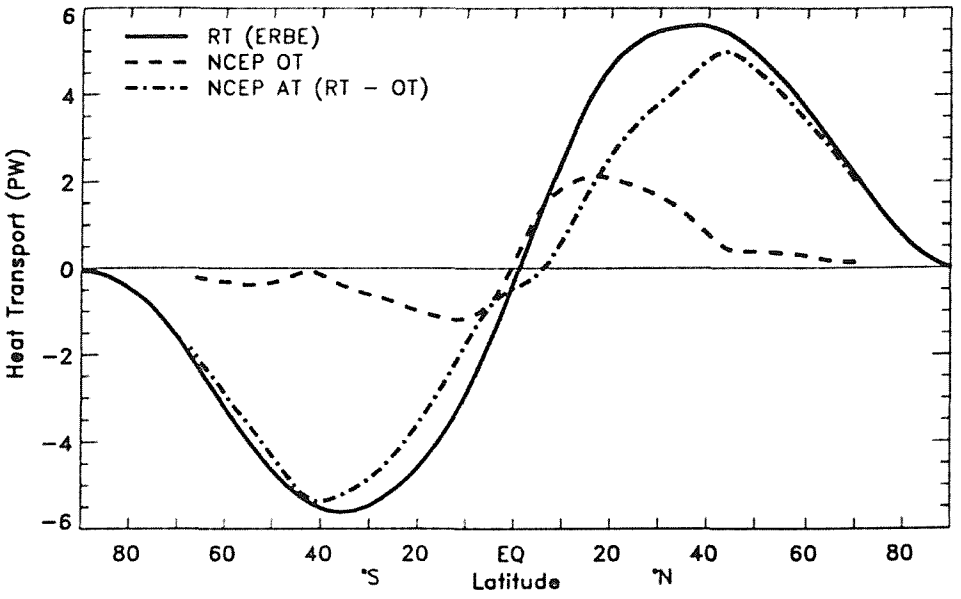

Figure 4.14: *Current estimates of global meridional heat transport (PW), from Trenberth and Caron (2001).* Solid*: Total transport;* Dashed*: Ocean contribution;* Dot-Dashed*: Atmospheric contribution.*

all latitudes for the idealised runs - the poles have a greater than average change and the equator a lesser.

As described in the introduction, the difference between the incoming shortwave and outgoing longwave TOA curves, and the associated latitudinal temperature profile observed in today's climate, is due to the heat transports found in the ocean and atmosphere. It might therefore be thought that the further changes in latitudinal distribution of temperature might be due to an increase in equator-pole transport activity somewhere in the system. Observations of current heat transports produce figures like figure 4.14. As can be seen, the northern hemisphere heat transport has an oceanic peak ~2PW at ~20°N, with the total peak ~5.5PW at 50°N.

The WaterWorld equivalent (*fig:4.15*) is not too dissimilar in form but is certainly not significantly stronger, as required by this hypothesis. As with current observations, the ocean transport is only stronger than the atmosphere in the tropics. The implied ocean heat transport has a peak around 1PW, although broader and more hemispherically symmetrical than observed today - this breadth may contribute

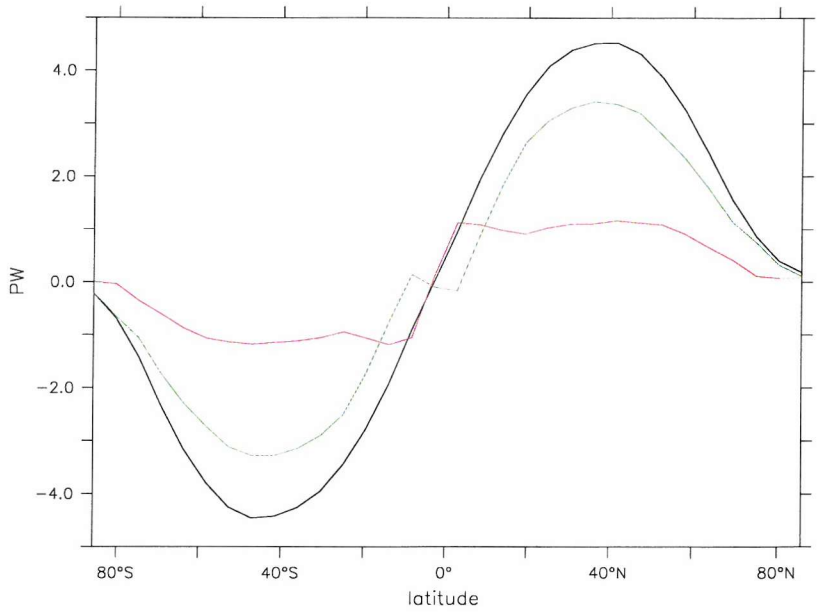

Figure 4.15: *WaterWorld heat transports (PW) derived from atmospheric fluxes.* Black*: Total;* Red*: implied ocean transport from BOA fluxes;* Green*: atmospheric transport derived as the residual of the two above.*

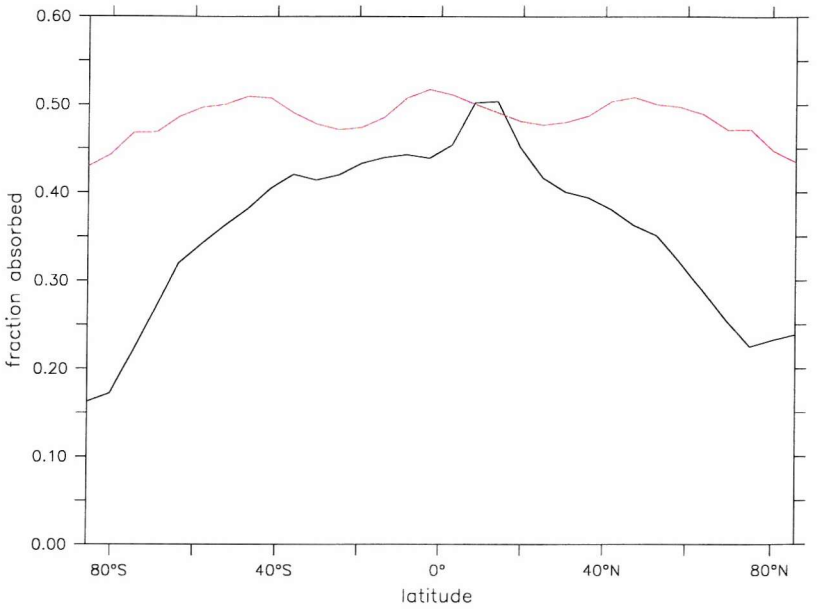

Figure 4.16: *Average longwave absorption as a function of latitude for the RealWorld (*Black*) and WaterWorld (*Red*) atmospheres. As can be seen, the WaterWorld atmospheres absorb proportionately more at higher latitudes.*

to the polar warmth, but the total transport peaks just above 4PW, lower than the current amount. Increased heat transport cannot be the answer to the reduced gradient. Indeed, the total transport picture seems to suggest that *less* transport is occurring - all else being equal the temperature gradients observed should be sharper, not weaker on WaterWorld.

A plot of the longwave emissivity (*fig:4.16*) provides the requisite forcing: as one approaches the poles on WaterWorld the longwave greenhouse strength does not reduce as fast as for the RealWorld, in fact it remains almost constant. Thus whilst the equatorial temperatures are largely unchanged, the relative warming at the poles will be much greater. The latitudinal evaporation profiles also show this bias toward greater polar forcing. The cloud profile is not so clear - only low and convective cloud show any marked increase in coverage in these regions between the two runs. This absorption profile is mirrored in the other idealised runs, as are the magnitudes and forms of the heat transports implied by the TOA and BOA fluxes.

4.2.2 Ocean Heat Transports

As has been seen (*fig:3.25*), the other two 'water' simulations have the same average warm climate as WaterWorld, and a similar gradient of shallow surface temperature profile. Although the same arguments apply as to the high moisture content of the atmosphere, they all clearly have different oceanic overturnings, and thus would be expected to have a very different advective ocean heat transport. For this reason, we might expect that the temperature profile might be significantly different. Although the smooth equator-pole temperature profile and the implied ocean heat transport for all these cases shows a constant poleward transport in both hemispheres, whilst this tallies with the general two-cell overturnings form seen on RidgeWorld and DrakeWorld, it is rather at odds with the multi-cell form on WaterWorld where warmer, top waters are drawn pole- or equator-ward alternately. The case of the swamp WaterWorld (section: 4.1.2) above also suggests a strong dependence of the atmospheric radiative properties on the ocean transport (impacting on the surface SST distribution) that is not compensated for by atmospheric transport, so it is not clear *a priori* that the same climate should result in these idealised cases when different ocean overturnings are present.

Aquaplanets

As figures 4.17, 4.18, 4.19 and 4.20 show, although each case has a different advective transport as intended by the applied geographical forcing, a significant diffusive contribution in each case means that the overall oceanic transport effect is that of an always-poleward transport in each hemisphere, whatever the overturning circulation.

This diffusive transport is somewhat unusual, as the current ocean heat transport shows little significant contribution from this effect. The controlling factor in this case appears to be the imposition of the temperature gradient by the atmospheric greenhouse, which results in a diffusive flux in each scenario which makes the total ocean heat transports, to first order, the same. This is especially notable in the light of the run with a swamp ocean, where an inhibited ocean heat transport *did* produce a significant mean surface temperature difference (see section: 4.1.2). In

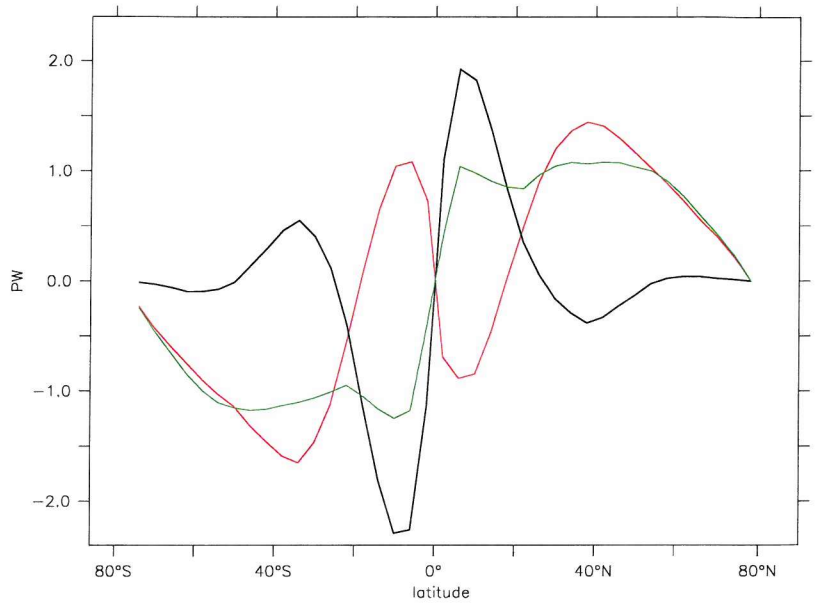

Figure 4.17: *Heat transport for the WaterWorld ocean, calculated explicitly from ocean fluxes.* Black*: advective transport;* Red*: diffusive transport;* Green*: total.*

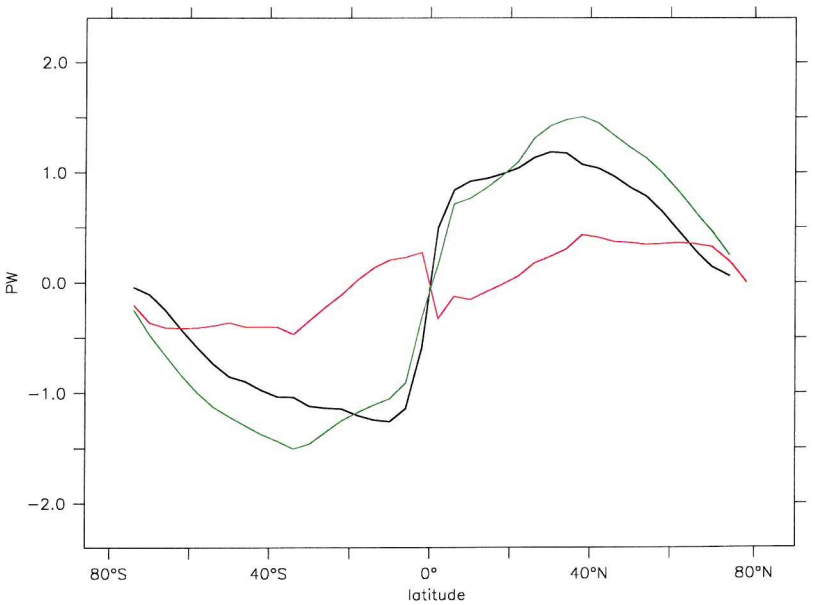

Figure 4.18: *Heat transport for the RidgeWorld ocean, calculated explicitly from ocean fluxes.* Black*: advective transport;* Red*: diffusive transport;* Green*: total.*

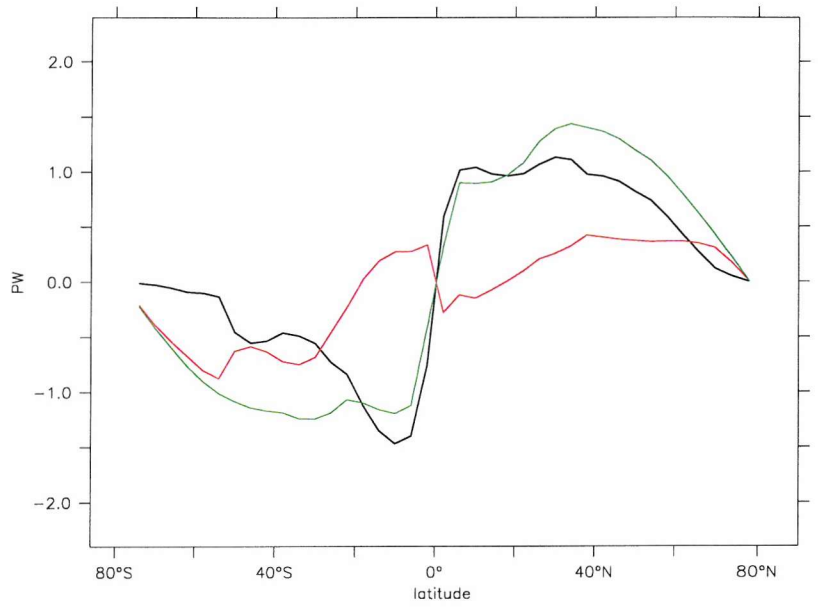

Figure 4.19: *Heat transport for the DrakeWorld ocean, calculated explicitly from ocean fluxes.* Black*: advective transport;* Red*: diffusive transport;* Green*: total.*

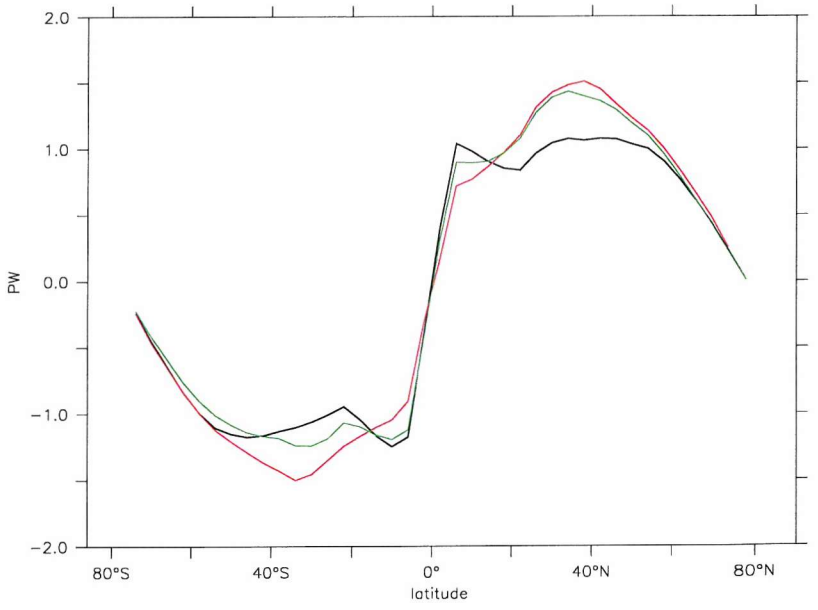

Figure 4.20: *Total ocean transport for the 3 cases* Black*: WaterWorld;* Red*: RidgeWorld;* Green*: DrakeWorld.*

that case however, all forms of ocean heat transport, including diffusive, were restricted so it was a question of ocean versus atmospheric transport compensation. Here it is only intra-ocean compensation being considered, the question of oceanic atmospheric compensation does not play a primary role. The difference then is the presence of a medium beneath the atmosphere capable of transporting heat. In the coupled cases, that medium can respond to the surface temperature gradient with a non-advective heat flux as well as an advective one, and here that response is such that the non-advective part is efficient enough to be of similar magnitude to the advective part. In the uncoupled case, neither of these transports is an option and a fundamentally different regime results, highlighting that atmospheric-oceanic compensation here is less efficient than the intra-ocean compensation that arises from the non-advective flux in the ocean. The surface temperature here is not so much dependent on the form of the ocean circulation as on the mere presence of a fluid ocean.

The vertical/horizontal diffusion mixing scheme employed in these runs is a somewhat crude approximation of real ocean mixing (which tends to occur along isopycnals which are not always horizontal) and the effect of eddy transports (which are hugely sub-gridscale at this resolution). A model of this resolution also has a significant degree of diffusion built in for numerical stability, so the prominence of the diffusive transport here is concerning - is it a reasonable approximation under this regime and would the real ocean behave like this under this forcing? Whilst we cannot definitively answer this, more confidence might be gained by using a model that represents eddies and mixing more realistically. As a first step towards this, a relatively short run of the WaterWorld scenario was done using the Gent-McWilliams (Gent and McWilliams, 1990; Gent et al., 1995) isopycnal mixing scheme which also includes some explicit parametrization of eddy transports. This scheme makes the ocean model approximately four times more expensive to run and also impacts the effectiveness of the periodic coupling scheme, so for this reason only 100 years have been integrated.

Although the scenario is far from equilibrium - it begins to warm further - and the heat transports are larger than for the vertical mixing case, the same qualitative response can be seen in the isopycnal flux that was approximated in the previ-

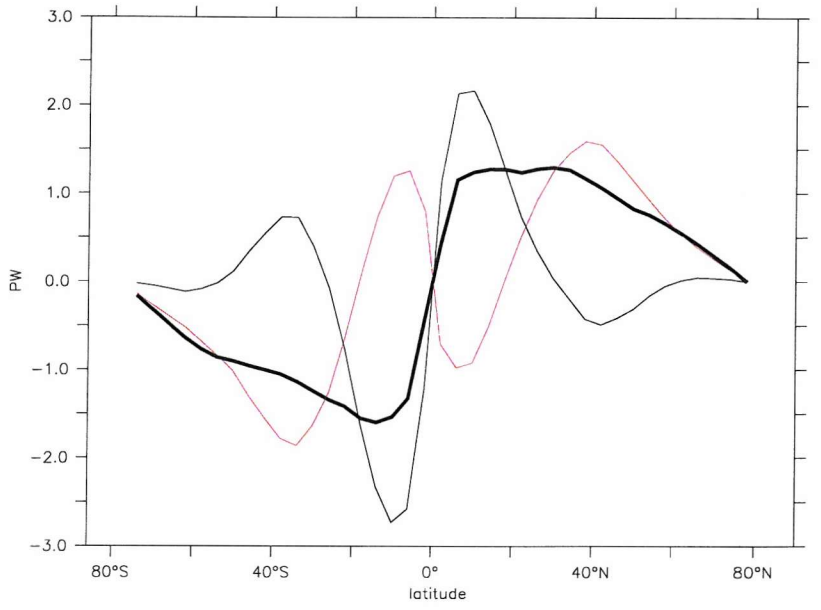

Figure 4.21: *Ocean heat transport components for the WaterWorld - GM run.* Thin black*: Advective;* Red*: Isopycnal flux;* Thick Black*: Total.*

ous run by the horizonatal mixing scheme. This result gives us some confidence that the diffusive transport effect observed above is not just an artefact of a model approximation. This diffusive transport has also been observed in a higher resolution run. A RidgeWorld integration by Bablu Sinha with a 2°x4° resolution ocean produced a more vigorous advective transport due to the higher resolution of the strong boundary currents along the ridge, but the mean temperature gradient was not much altered as the diffusive component grew equally.

Basin Planets

Given that the high non-advective ocean heat fluxes that are seen in the aquaplanet experiments are not seen in our current climate, or indeed FORTE's simulation of it, and that they seem to be induced by the greenhouse-controlled surface temperature profile, the question arises as to whether, or to what extent, this feature may be seen in the basin planet experiments. They have been shown to have a reduced greenhouse, as compared to the aquaplanets (but still stronger than the RealWorld

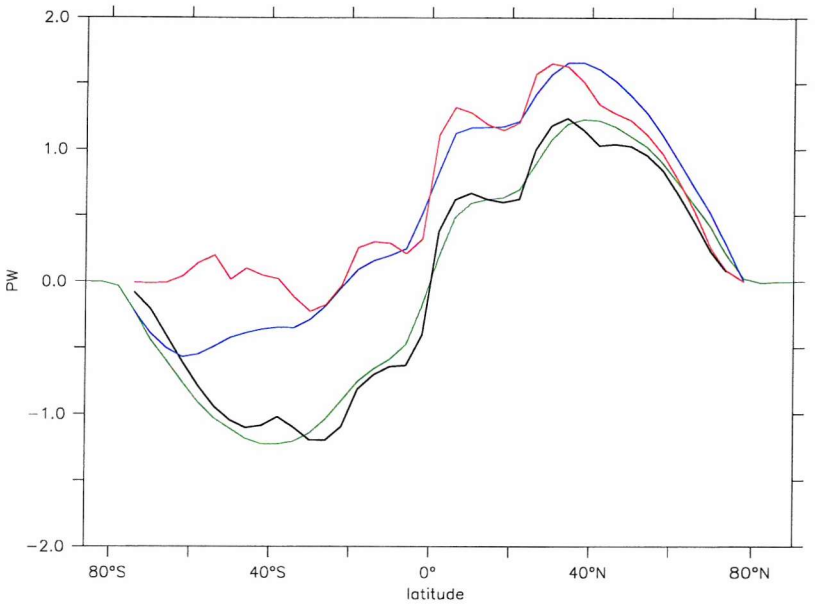

Figure 4.22: *Comparison of ocean heat transports for the two basin planets.* Black*: PangeaWorld - advective;* Red*: PangDrakWorld - advective;* Green*: PW - total (advective+diffusive);* Blue*: PDW - total.*

one) and with the aquaplanets' shallower temperature profile. The two scenarios run here provide a direct comparison to the increase in southern hemisphere diffusive transport seen above between RidgeWorld and DrakeWorld.

Figure 4.22 shows the result. For the PangeaWorld simulation the advective and total transports agree well, indicating virtually no diffusive input. As expected, there is a sharp drop in the advective transport for PangDrakWorld in the southern hemisphere past the gap around 60°S. To this extent the pattern seen for and Ridge- Drake- Worlds is reproduced. But the PDW run has a total heat transport that is very different from the PW total, with only a 0.4 PW increase in transport amplitude in the southern hemisphere. In this case the non-advective transport in the ocean does not provide the necessary compensation to make up the difference in the advective part, resulting in a different total heat transport.

Also notable here is that PDW is the only case to display any cross-equatorial transport at all - this is also suggested by the slight dominance of the northern overturning cell that can be seen in figure 3.50. This trait is also not compensated

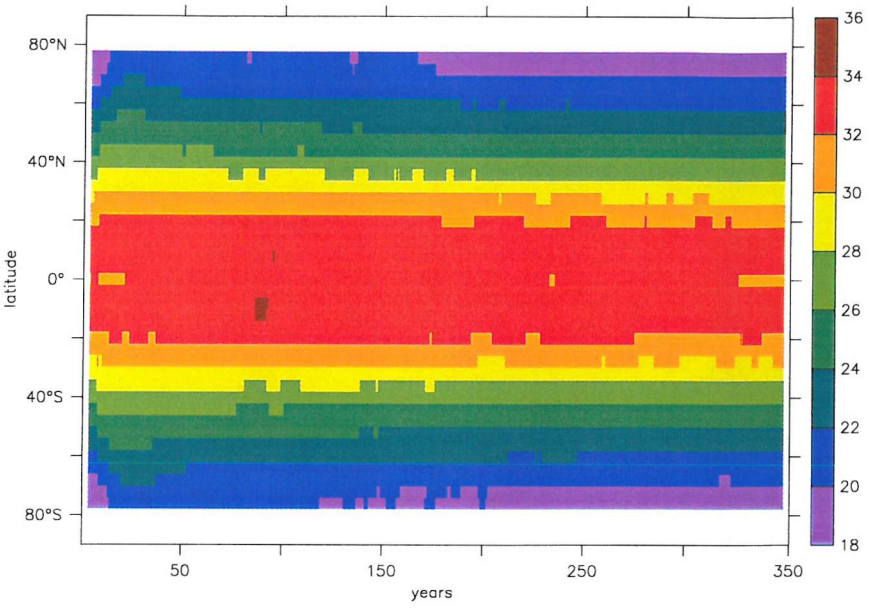

Figure 4.23: *Evolution of the zonal average SST (°C) over the first 350 years following the transition from WaterWorld to RidgeWorld. The series has been smoothed to remove seasonal variation.*

for by the diffusive transport, and results in a net heat transport for the southern to northern hemispheres.

Timescales

All the above look at data from the near-steady states at the ends of the runs, nearly a thousand years after the initial change in the ocean circulation has been forced. The question arises as to the evolution of the compensating non-advective fluxes, where present - how fast does the compensation occur, and what would be observed in a system undergoing the transition to the new state?

The above plots (*figs:4.23,4.24*) show the evolution of the zonal average SST following the introduction of the ridge barrier into WaterWorld which produces the RidgeWorld scenario. As can be seen, the equator to pole difference initially decreases, then starts to adjust back to its previous value after 100 years or so. After 350 years the profile is almost the same as it was in the original WaterWorld case.

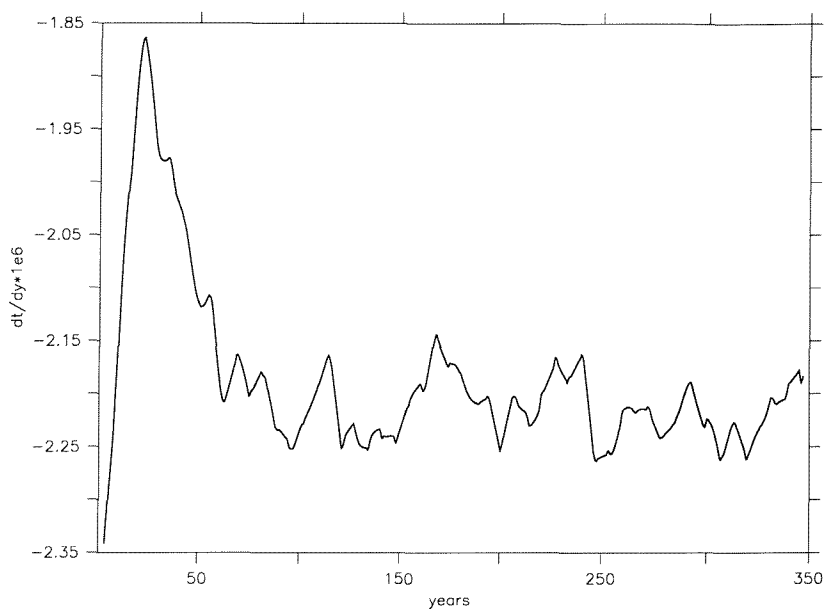

Figure 4.24: *Time series of the mean SST meridional gradient between 20 °N and 60°N following the transition from WaterWorld to RidgeWorld. The series has been smoothed to remove the seasonal signal.*

The change made primarily affects the ocean circulation; the introduction of a geostrophic meridional transport should initially increase the poleward heat transport as compared to a WaterWorld scenario, in the absence of other changes - this is the cause of the initial reduction in meridional SST gradient. That there is a change in the global mean temperature (there is not a decrease in equatorial SST to compensate for the polar increase) suggests that there is also some mean radiative response in the atmosphere to the changed ocean heat transport. The increase in gradient back to the original value is evidence of a compensating mechanism at work. These results suggest that a timescale suitable for investigating this mechanism is on the order of a few hundred years - this is a reasonable timescale for considering changes in the large-scale geostrophic circulation of the world ocean. Unfortunately, the data collected here is not well suited to an analysis of this as the asynchronous coupling scheme used here distorts climate data collected during its use, and there are also gaps in the data from the periods where the atmosphere was switched off. What is required for a reasonable investigation of this phenomenon is a synchronously coupled run of several centuries, an additional computational expense beyond the scope of this project.

4.2.3 Heat Transport Effects

The main effect expected from a change in ocean heat transport [OHT] is a change in the distribution of heat over the earth's surface, and although the radiative properties of the atmosphere have been shown to be the primary factor in determining the equator to pole temperature profile, the changes in OHT that are present do have some impact. Although the non-advective transport works to compensate for the heat transport differences in the aquaplanet cases, differences of up to 0.5PW remain in some places and the lack of compensation on the basin planets provides a more substantial discrepancy.

For the aquaplanets, regions with a lack of geostrophic meridional transport - all of WaterWorld and the southern part of DrakeWorld - have a somewhat lower amount of total ocean heat transport. Here, figures 4.20 and 3.25 tally well, with RidgeWorld's higher transport resulting in a slightly cooler equator and warmer

poles than WaterWorld. DrakeWorld's altered surface temperature gradient can also be ascribed to the effect of the heat transport, the collapse of the RidgeWorld-like cell in the south below the barrier reducing the advective heat transport here. As can be seen, the diffusive transport on DrakeWorld is highest here, although it does not compensate entirely for the reduced advective transport.

These small meridional temperature gradient changes are also reflected in the surface zonal wind profile (*fig:3.26*), with WaterWorld's higher gradient producing stronger winds (a consequence of geostrophy) than on RidgeWorld, and DrakeWorld following the RidgeWorld pattern in the north and the WaterWorld one in the south. The cooler temperatures at the south pole on DrakeWorld force slightly stronger winds than found on RidgeWorld, which has a significant impact on the barotropic flow through the gap there (see section: 4.4.3). Even though the surface temperature gradient is far lower than that found in the RealWorld run, these zonal wind strengths are comparable. This is most likely due to the reduced temperature forcing being compensated for by the lowered surface friction that results from the lack of orography, a factor cited by Neale and Hoskins (2000) in explaining higher zonal wind strengths in an atmosphere GCM aquaplanet.

For the basin planets, the climatic differences observed are harder to attribute to the change in ocean circulation as the opening of the passage removes a large area of land and so makes a substantial change to the overall global surface characteristics which did not occur for the DrakeWorld case. The radiative properties of the atmosphere have already been shown to have a sensitive response to the presence or absence of water, so the mean temperature change observed between the two basin planet scenarios is as much a response to these surface changes as to the ocean circulation change. The removal of land also changes the characteristic surface pressure response that drives the monsoonal climate - the equatorward shift of the southern hemisphere rain maximum is likely a result of this.

Figure 4.25 shows the SST changes associated with the circulation changes when the gap is opened in each case. For the aquaplanet case there is no great change in the northern hemisphere: a slight rise of up to 0.3°C in the tropics and a cooling of 1.2°C in the surface waters at the south pole. This qualitatively agrees with the ocean heat transport differences shown in figure 4.26, where the northern hemi-

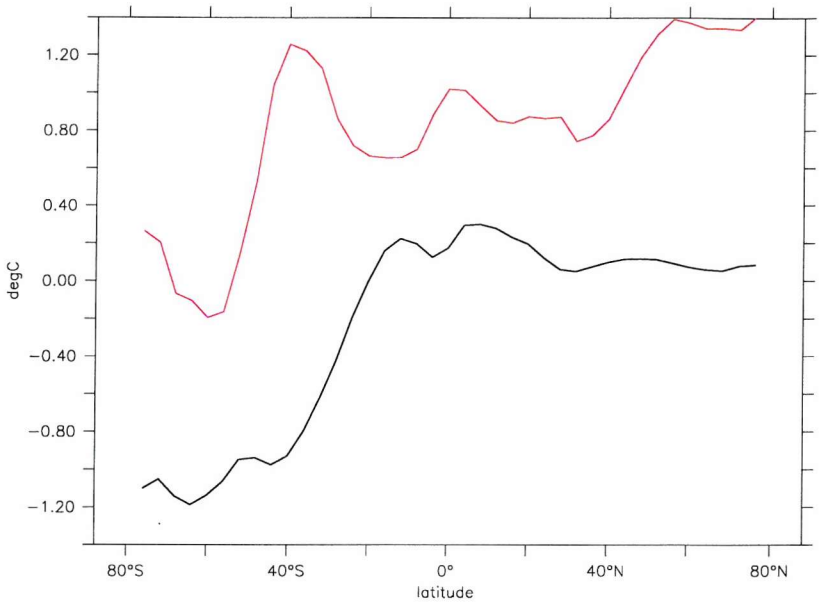

Figure 4.25: *Annual average SST differences on allowing circumpolar flow.* Black*: DW-RW;* Red*: PDW-PW.*

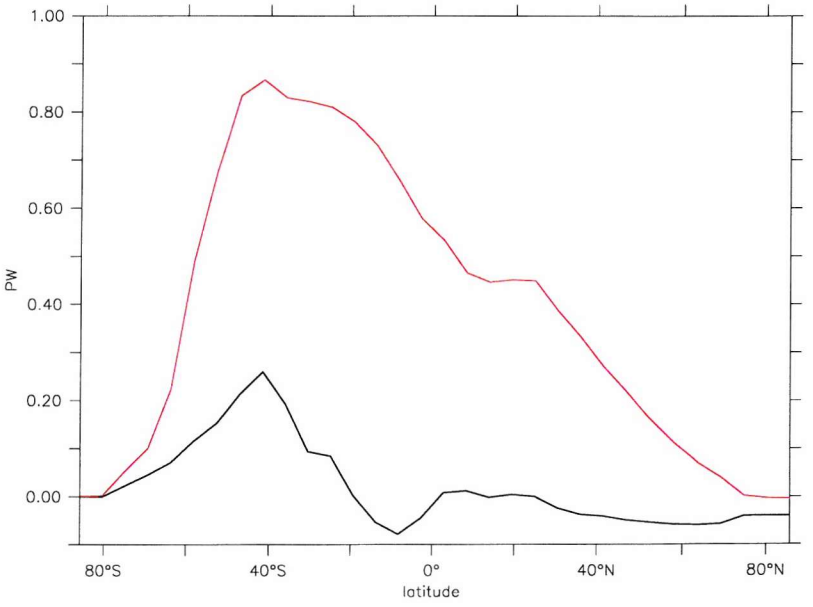

Figure 4.26: *Annual average total ocean heat transport difference between the 'Drake Passage' runs.* Black*: DW-RW;* Red*: PDW-PW.*

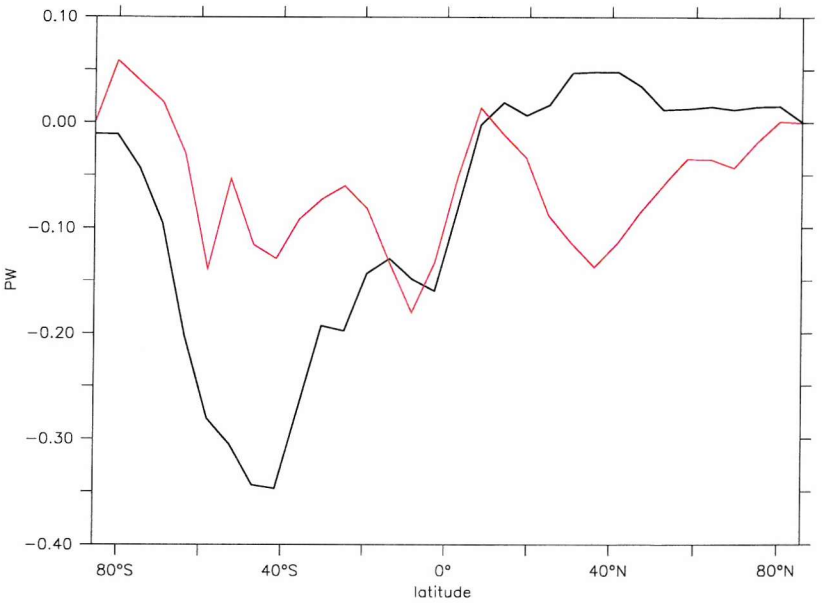

Figure 4.27: *Annual average atmospheric heat transport differences between the 'Drake Passage' runs.* Black*: DW-RW;* Red*: PDW-PW.*

sphere transport is little different and the southern hemisphere one is reduced by 0.3 PW - the non-advective flux here partially compensates for the more significant loss in advective heat transport. The basin planet case is a little more complex as the heat transport picture reflects the lack of compensation by the non-advective flux here with a bigger northward heat flux everywhere, yet the SST picture shows an uneven drop in SST past the gap of equal magnitude to the aquaplanet case, despite the greater difference in heat transport and a rise of 0.5°C in the extreme northern waters.

The atmospheric heat transport picture (*fig:4.27*) does not show greater compensation in the basin planet case, in fact there is less here than for the aquaplanet. The longwave greenhouse is the reason the southern hemisphere does not cool more - in the basin case a significant change has been made to the land surface and water availability in opening the Drake Passage, and the longwave greenhouse in this region has strengthened accordingly (*fig:4.28*). This greenhouse strengthening is thus mainly due to the land surface type change, equivalent to the global strengthening in the greenhouse seen for WaterWorld where the land surface is

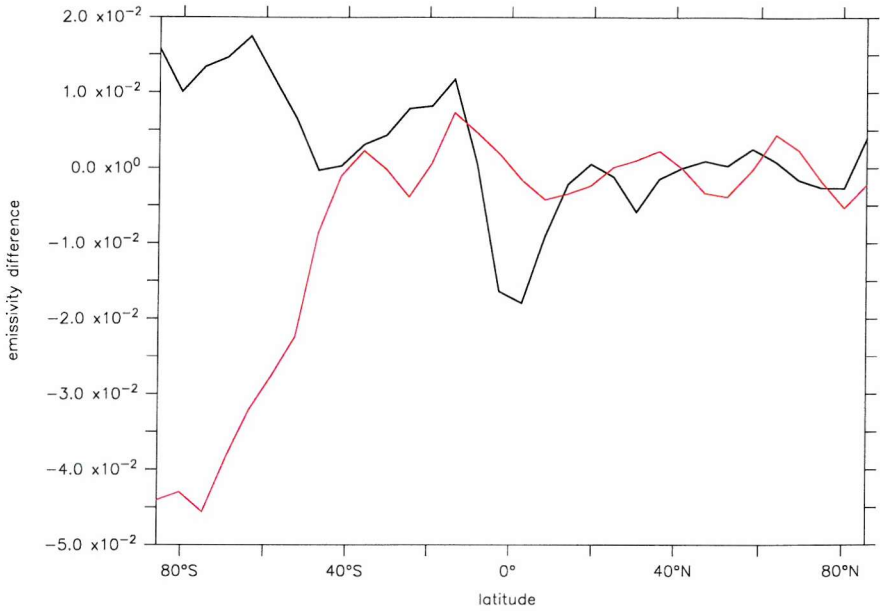

Figure 4.28: *Annual average longwave emissivity differences between the 'Drake Passage' runs.* Black*: DW-RW;* Red*: PDW-PW.*

entirely changed to water. This is also responsible for the mean warming seen here: for the Ridge- to Drake-World case there is little change in total land area so this effect does not apply. In the basin planet case then, the radiative changes in the atmosphere that occur in response to the land surface change are taking precedence over the changes forced by the ocean heat transport.

4.3 Rainfall Distribution

The three aquaplanet runs all show a background distribution characterised by a banded pattern as shown in figure 3.8. This pattern matches well with the seasonal motion of the Hadley cells (see *fig:3.12*) as the ITCZ tracks north and south across the equator: as shown (*fig:4.29*) the rainfall maxima are matched with regions of meridional surface wind convergence (and thus upwelling and convective rain-out) and the minima with regions of divergence (thus downwelling and inhibited rainfall). The absence of any significant orographic forcing means that the atmo-

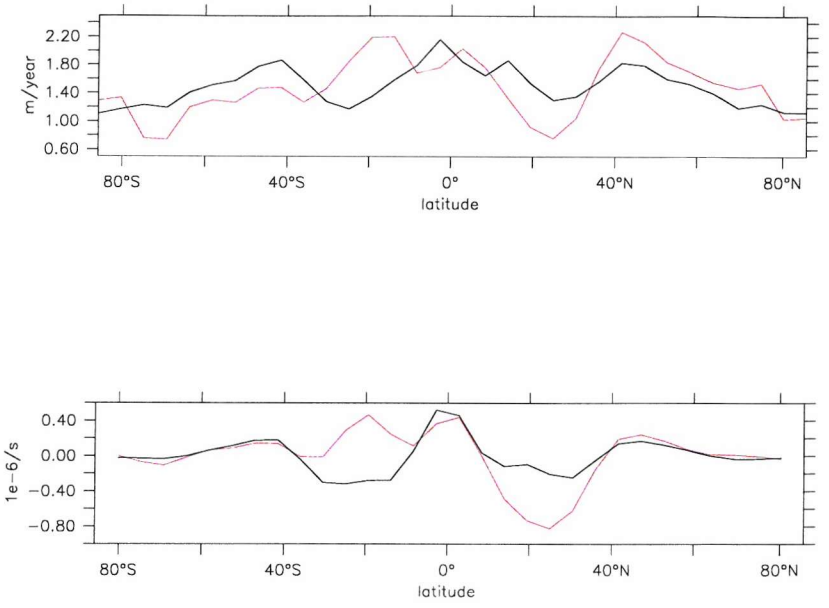

Figure 4.29: *Comparison of zonally averaged rainfall amounts (above) with areas of surface wind (lowest 100mbar) convergence/divergence (below).* Black*: Annual average;* Red*: DJF.*

spheric overturning is also consistently zonally even.

The RidgeWorld and DrakeWorld scenarios also have localised rainfall maxima and minima in the region of the ridge (*fig:3.18*), with a strong maxima on the equator to the east of the ridge and a weaker one further poleward at about 50°; both these maxima are consequences of the altered ocean circulation induced by the ridge. Figure 4.30 shows the differences in the precipitation and BOA flux fields between RidgeWorld and WaterWorld.

The equatorial rainfall maxima shows up directly over a region of increased ocean-atmosphere flux, and there are also high flux patches to the east of the ridge around 50°. The equatorial flux high is a result of the warm pool of water that gathers up against the ridge, brought there by the westward flowing surface waters at the lowest latitudes. This shows up nicely in a plot of the thermocline depth (*fig:4.31*) where the angled RidgeWorld line shows a warm pool in the west of the basin shallowing to the east. The higher latitude flux anomalies are co-located with strong SST anomalies, where the western boundary current in the RidgeWorld scenario

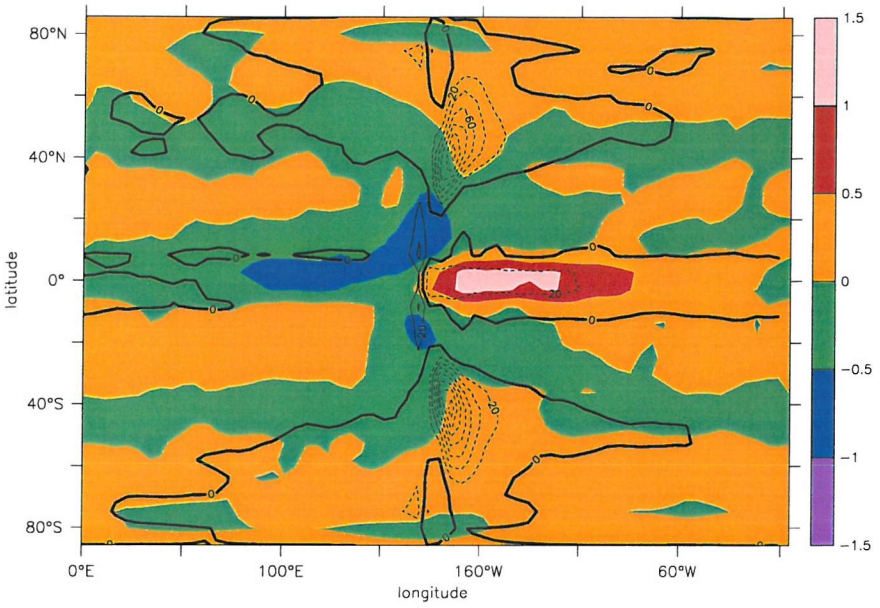

Figure 4.30: *Annual mean precipitation differences (colours, m/year), overlaid with BOA flux differences (contours, W/m^2), RW minus WW.*

that is absent from WaterWorld has brought warm equatorial waters poleward as part of the gyre circulation. The minimum around 25° in the winter hemisphere is co-located with a particularly strong patch in the high pressure zone of the downwelling branch of the Hadley cell, caused by the lower temperature over land in this area, which has a low heat capacity relative to the surrounding ocean.

The situation is rather different for the basin planets, where the presence of the landmass and its impact on the pressure systems and wind patterns has a large effect on the rainfall pattern as well. The equatorial rainfall maxima seen above which is caused by the warm pool disappears, replaced by maxima at higher latitudes (*fig:3.38*). This is a result of the strong low pressure system set up in the summer on the landmass which diverts the equatorial easterlies poleward around them (*fig:3.33*), bringing the rains with them and leaving the eastern equatorial part of the land mass dry, a situation seen today in east Africa as the rains are drawn northward onto Asia in the summer monsoon. These warm, moist winds mix with those brought across the hot landmass in the seasonal westerlies, rise up and rain out over the cooler waters of the eastern coast of the land mass as they en-

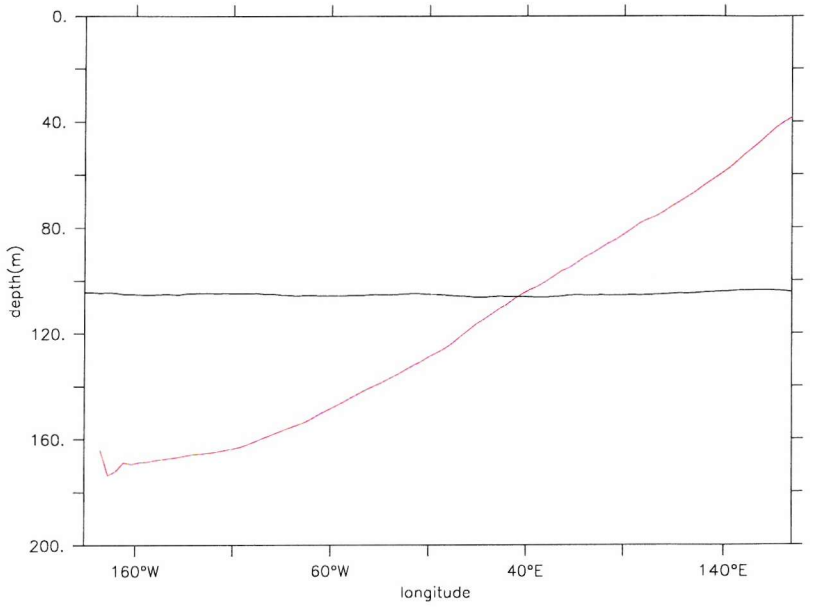

Figure 4.31: *Annual mean depth of the 30°C isotherm on the equator.* Black*: WaterWorld;* Red*: RidgeWorld.*

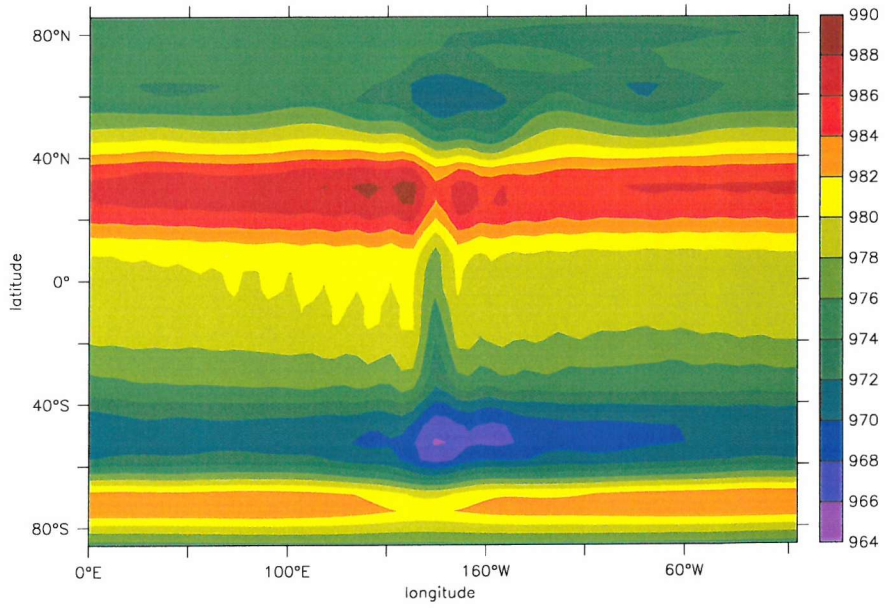

Figure 4.32: *Surface pressure map for RidgeWorld (mbar), DJF.*

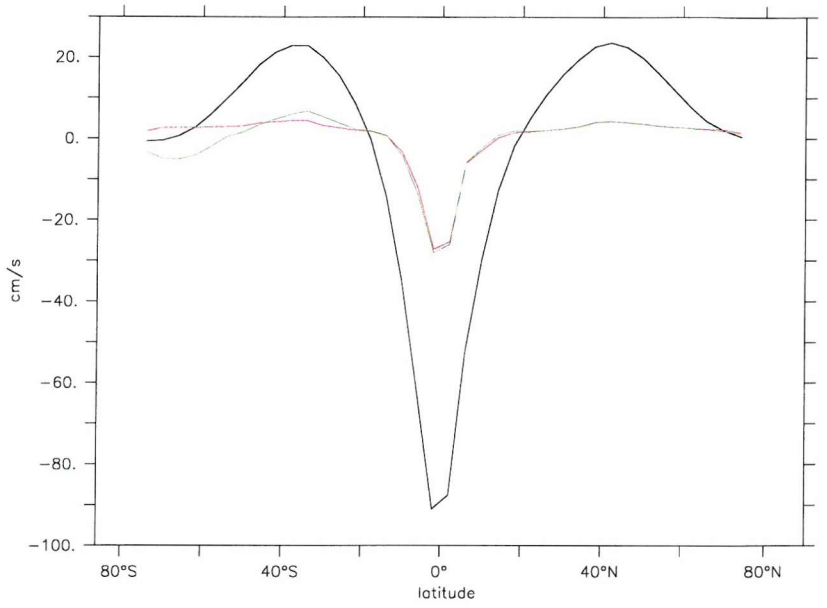

Figure 4.33: *Annually averaged zonal surface currents.* Black*: WaterWorld;* Red*: RidgeWorld;* Green*: DrakeWorld.*

ter the anticyclonic system, giving rise to the rainfall maximum at 30°. The band of rain across from the western coast is caused by the strong westerlies bringing moist air onshore to the warm, summer land.

4.4 Surface Currents

4.4.1 WaterWorld

The surface zonal currents (*fig:4.33*) are in very good agreement with those derived via geostrophy from the free surface height [FSH] (*fig:4.34*). The free surface deviation ranges from +2 metres at the equator to -4 metres at the poles. The tropical reversal from eastward to westward currents comes with the gradient change in FSH approaching the cooler upwelled waters at the equator. Surface meridional currents are in good agreement with those expected from the strong zonal wind stress applied at the surface.

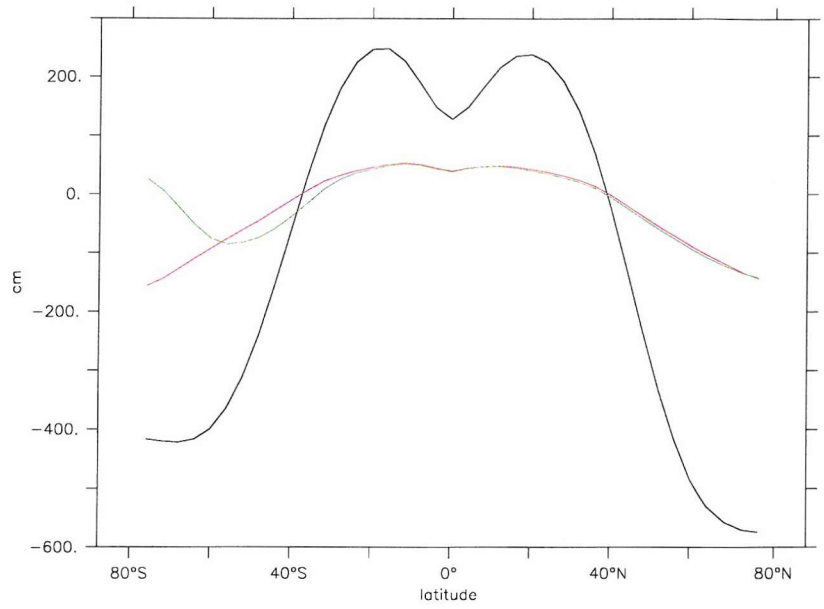

Figure 4.34: *Annually averaged free surface height.* Black*: WaterWorld;* Red*: RidgeWorld;* Green*: DrakeWorld.*

Integration of column densities throughout the ocean reproduces a surface relief similar (*fig:4.36*) to that observed - the zonal currents are mostly geostrophically forced through the latitudinal density gradient that results from the temperature profile. The nature of the overturning cells keeps the lower depths warmer and ensures a shallower temperature gradient with depth; there is virtually no sharp thermocline so there are significant contributions to this density gradient down to ~3000 m at each latitude, leading to the exaggerated surface relief pattern and high zonal velocities.

The main difference between the actual FSH and the density-derived reconstruction occurs near the poles where the barotropic zonal velocity that results purely from the wind forcing dominates, producing a weak easterly current.

4.4.2 RidgeWorld

The closed basin-like nature of RidgeWorld allows a 'normal' Sverdrup circulation to form, with a subtropical gyre and a strong western boundary current one

grid cell wide where currents up to 57 cm/s form (*fig:3.19*).

There is a strong geostrophic forcing from the denser waters at the pole - eastward currents flow right up to the boundaries before turning poleward into the most easterly corner of the basin. These are a consequence of the overturning cell now supported by the ridge: now that water can move meridionally by geostrophy, cold deep polar water moves equatorward, fed by downwelling (*fig:4.35*) at the poles. A classic pattern now emerges: convection occurs at the coldest points (along the polar boundary), resulting in more dense water at the surface. Geostrophic currents are induced along the edge of this region due to the density gradient - these are the eastward boundary currents seen. Downwelling occurs where the flow meets the barrier, feeding the equatorward flow below and transporting the cold water away from the neighbouring convecting columns, allowing them to become unstable again. The lack of this on WaterWorld may be why there is no observable convection there, despite having similar surface temperatures - the column may convect and mix to start with, but as there is no latitudinal transport away from the region, it stays in its well-mixed state and cannot convect any more. The localisation of this downwelling at the poles is the reason for the maxima of the overturning (*fig:3.21*) being so far poleward.

Again, zonal surface currents are in reasonable agreement with the forcing factors as analysed above. This time however the latitudinally averaged FSH only ranges between about +50cm and -150cm, with commensurately lower zonal velocities. As above, a reconstruction (*fig:4.36*) from density anomalies suggests a reason for the reduced FSH - although the surface tracer gradients are very similar in the two runs, RidgeWorld's overturning cells are not as efficient at moving tracers down through the column, but are more efficient horizontally. The meridional density gradients produced by integrating over each column are thus far less than those on WaterWorld and produce weaker currents.

4.4.3 DrakeWorld

DrakeWorld is an interesting mix of the above cases. As most of the basin has a zonal barrier and it displays quite a hemispherically independent flow, the FSH

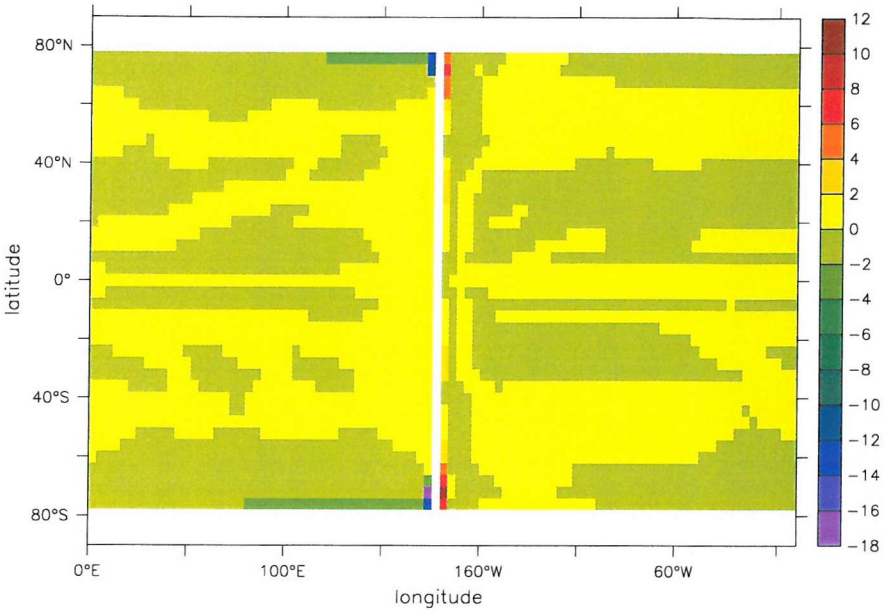

Figure 4.35: *Annual average upwelling (m/day) on RidgeWorld.*

profile over most of the ocean is identical to RidgeWorld's. The FSH derived from density anomalies also looks very similar to RidgeWorld, although cooler in much of the southern hemisphere, so likely to have an exaggerated eastward density-forced current towards the South Pole. This is not the case however - past the end of the ridge the flow is quite strongly *westward*, more so than the WaterWorld case.

The cause for this is the same reason as for the polar currents on WaterWorld: the windstress here is stronger than RidgeWorld, slightly stronger than WaterWorld even, in accordance with the inhibited ocean heat transport and consequent steeper surface temperature gradient. This induces the westward flow. Although the windstress in this region is only slightly greater than for the WaterWorld case, the westward currents are significantly stronger. In this region of zonal flow, as with the whole of WaterWorld, the surface windstress must be balanced by friction within the water column and at the bottom - this is not a linear process, with stress proportional to the square of the velocity, so even a small change in applied wind can produce significant change in the current.

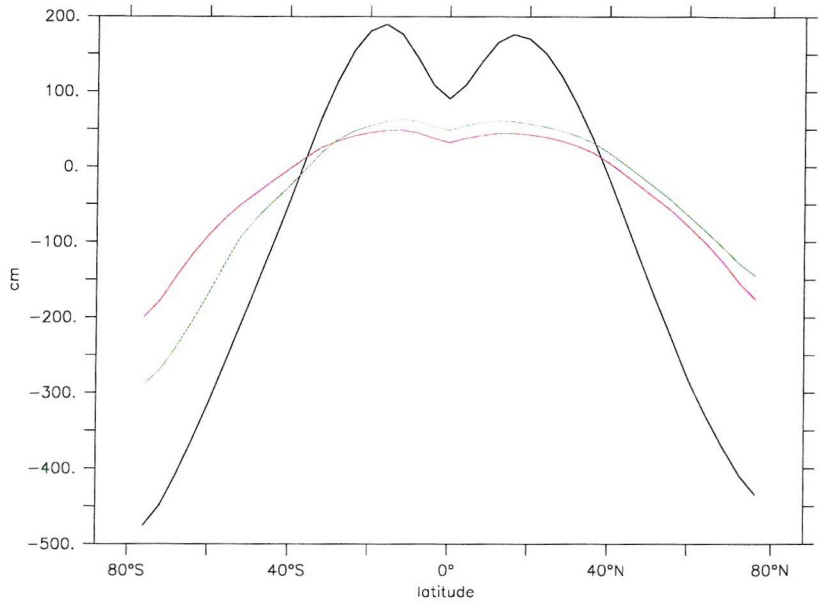

Figure 4.36: *FSH contribution derived from the column density anomalies.* Black*: WaterWorld;* Red*: RidgeWorld;* Green*: DrakeWorld.*

To confirm this diagnosis of the anomalous current/FSH pattern, an attempt was made to separate the buoyancy and wind-forced effects. A 'buoyancy FSH' was derived by integrating the temperature- and salt- induced density anomalies up through each column (*fig:4.36*):

$$fsh_{(y)} = \int_{east}^{west} \int_{floor}^{surface} \left[\rho_{(x,y,z)} - \rho_{0(z)}\right] dzdx \tag{4.9}$$

and a 'wind-forced' pressure gradient was found by applying the zonally, annually averaged wind forcings from each run to an isohaline, isothermal ocean with the requisite landmap and no other surface forcing (*fig:4.37*).

As can be seen, the sharp turn to westward currents below the gap in DrakeWorld can be entirely ascribed to the wind forced part of the pressure gradient. The windstress here is in the opposite direction to that experienced over the ACC today due to the different latitude of the gap in the ridge here, the narrower meridional spread of the wind distribution on the aquaplanets and the fact that there is a more vigorous reversal in wind in these idealised cases too.

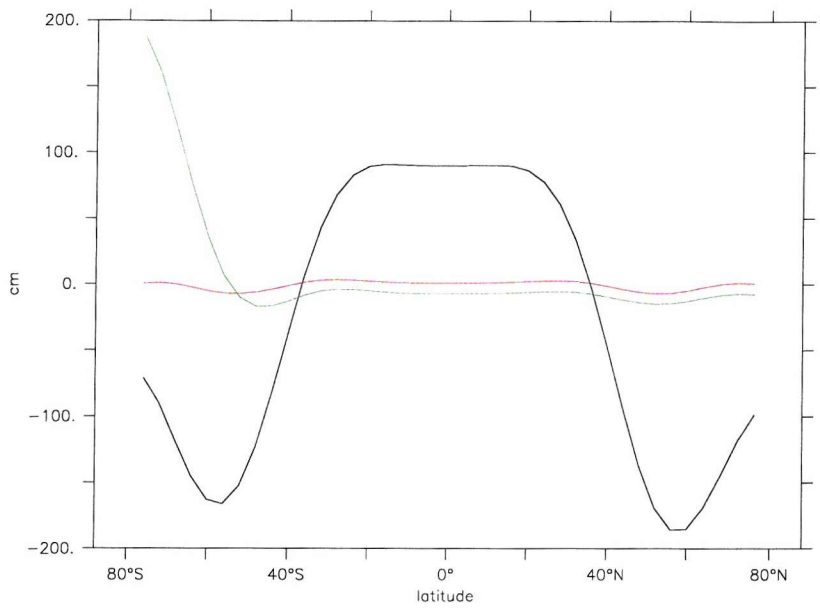

Figure 4.37: *FSH from an isothermal, isohaline model with just zonal wind forcing.* Black*: WaterWorld;* Red*: RidgeWorld;* Green*: DrakeWorld.*

There is however a striking difference in the PangDrakWorld case, where the circumpolar flow, despite a similar shallow temperature gradient, flows eastward not westward. This is readily explained within the same framework as that presented above, as the wider spread of the surface zonal wind pattern here (*fig:3.47*) means that the winds in this region are now eastward, reinforcing the pressure from the temperature gradient rather than opposing it as for DrakeWorld and providing an eastward flow.

The Drake Passage throughflow in this case appears then to be primarily wind driven in this case, opposed by the geostrophic forcing from the temperature gradient. As with WaterWorld, frictional dissipation at the bottom and in the viscous fluid is responsible for removing the energy input by the wind and setting the actual level of transport (see section: 4.5.1). The question of how the real Antarctic Circumpolar Current is controlled is a subject of open debate. The wind is generally considered to provide the dominant forcing, with topographic friction a likely limiting factor, but thermohaline buoyancy forcing has also been considered, and Bryden and Cunningham (2003) argue that the two are in fact inherently coupled

through the mesoscale eddy dynamics of the flow. FORTE has far too coarse a resolution to reproduce the details of these processes and, if the two forcings are coupled, experiments such as those above where the temperature and wind fields are specified and fixed independently are unlikely to be helpful. They do however allow us to say something about this unusual feature in the idealised experiments here.

4.5 Overturning Reconstruction

Although vertical overturnings in both atmosphere and ocean are a robust feature of the current climate, theoretical climates have been posited that do not have any. Held and Hou (1980) hypothesised that Hadley cells only exist if the winds, induced by the temperature gradient at the surface to transport heat, violate the planet's rotational angular momentum conservation - with a shallow enough surface temperature gradient a regime can be formed that does not have the traditional Hadley cell pattern and atmospheric GCM experiments have confirmed this. Neale and Hoskins (2000) in particular have shown this for an atmosphere-only aquaplanet simulation. For the ocean, Warren (1981) suggests the possibility of an aquaplanet in which a low meridional temperature profile allows all the heat transport to occur through diffusion, the seas remaining motionless.

As has been seen, all the idealised scenarios contain Hadley circulations, despite a shallow surface SST meridional profile on a par with those used in Neale and Hoskins (2000). This may be due to differences in the convective scheme used in the model or to the fact that the underestimation of eddy transport - a consequence of the relatively low resolution of our model - results in the direct advective heat transport required being higher, and thus more likely to violate Held and Hou's angular momentum hypothesis.

All the scenarios, including WaterWorld, have very vigorous oceanic overturnings as well. An attempt will now be made to derive and explain these by reconstructing their forms from their basic forcings. The following method is derived from Hirschi et al. (2003).

4.5.1 Ekman forcing

The reason that the overturning on WaterWorld is so different from that seen today lies in the complete lack of zonal boundaries. This means that no zonal pressure gradient can build up from the wind-forced motion of the surface waters, and hence no geostrophic meridional flow. In the absence of this zonal pressure gradient, there is nothing but the convergence/divergence of the water, and the physical barrier of the ocean floor to direct the flow. For a totally inviscid, frictionless ocean the applied wind stress would cause the cells to spin up to ever higher speeds, there being no force to dissipate the energy - this effect has already been mentioned in looking at the wind-forced zonal flow on WaterWorld and in the gap on DrakeWorld. This is of course unphysical, and here there are two forces to oppose the wind: friction at the ocean floor and horizontal viscosity in the fluid. Some of the viscosity present here is numerical, required for stability due to the coarse resolution, so cannot really be taken as a real physical parameter. For the WaterWorld case, the bottom stress is ~9 times smaller than that applied at the surface, so it is clear in this case that most of the force balance occurs within the fluid column.

To help explain this overturning regime, a simple model was created whereby the Ekman motion of the surface waters was derived from the zonal wind forcing, and this motion compensated by a barotropic return flow spread over the whole depth of the basin. Although the significance of the horizontal viscosity in this case suggests that this simple approach to the return flow cannot be fully physically justified, it is a sensible first step in the absence of more detailed knowledge of the viscous friction.

Wind stress at the surface directly forces motion in the ocean beneath, satisfying

$$\frac{\partial u_E}{\partial t} - f v_E = \frac{1}{\rho}\frac{\partial X}{\partial z} \tag{4.10}$$

$$\frac{\partial v_E}{\partial t} + f u_E = \frac{1}{\rho}\frac{\partial Y}{\partial z} \tag{4.11}$$

where u_E, v_E are zonal and meridional components of the wind forced velocity,

t is time, f is the coriolis parameter, ρ the density and X and Y the zonal and meridional wind stresses.

Assuming a constant, purely zonal wind forcing and integrating up from the level where the wind forcing has no effect (over the so-called 'Ekman layer') gives a meridional surface volume transport for the stationary state of

$$V_E = -\frac{1}{f\rho}X \tag{4.12}$$

for V_E the depth integrated meridional velocity - i.e. the meridional transport per unit length.

When integrated over the whole zonal width and depth of the (closed) basin there can be no net meridional transport, so this surface volume flow must all return at some point on the same latitude line. Since the reconstruction involves dividing by f, values at the equator are likely to be invalid as f approaches zero at the equator. For this first step, spreading the return flow evenly over the whole basin depth gives a reconstruction as in figures 4.38 and 4.39.

The overturning obtained bears a striking resemblance in form and magnitude to that seen in the GCM, confirming the hypothesis of a fully wind driven circulation. Thus Warren's idea of a temperature gradient too shallow to force an overturning circulation is unlikely to be possible - even for a case where the Hadley circulation did not exist, as in Neale and Hoskins (2000), the wind field present would still force some surface motion whose return flow response, in the absence of zonal pressure gradients, would fill the whole depth of the basin. The essentially wind-forced nature of the overturning here explains why the variability (see section: 3.2.1) follows that of the overlying atmospheric winds/overturning so closely.

4.5.2 The thermal wind

The differences between the WaterWorld and Ridge- Pangea- World overturnings can be illustrated well with an attempt to reconstruct their MOCs in a similar manner. Using just the Ekman-derived component coming from the surface wind forcing produces a very similar picture to that for WaterWorld - unsurprising, since

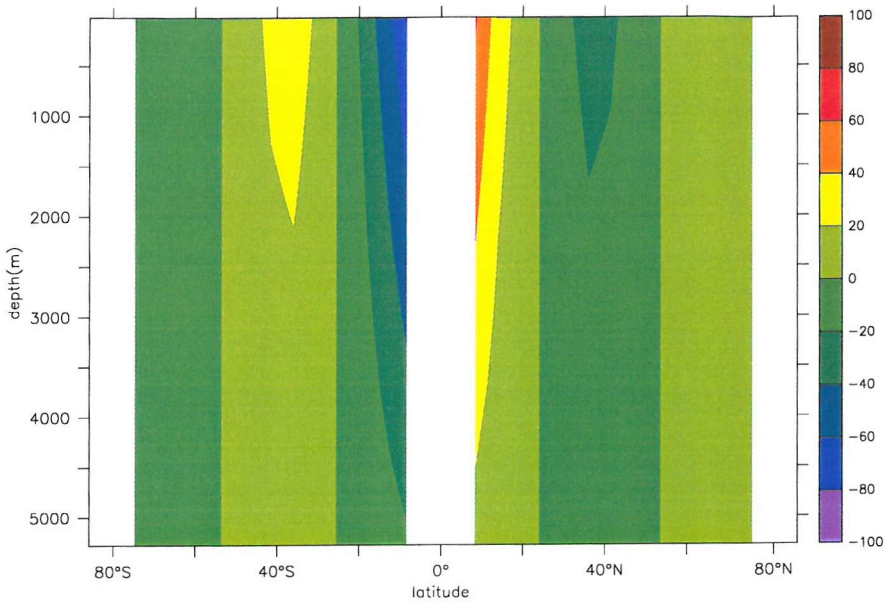

Figure 4.38: *WaterWorld meridional overturning reconstructed from surface Ekman transport compensated by a barotropic return flow (Sv).*

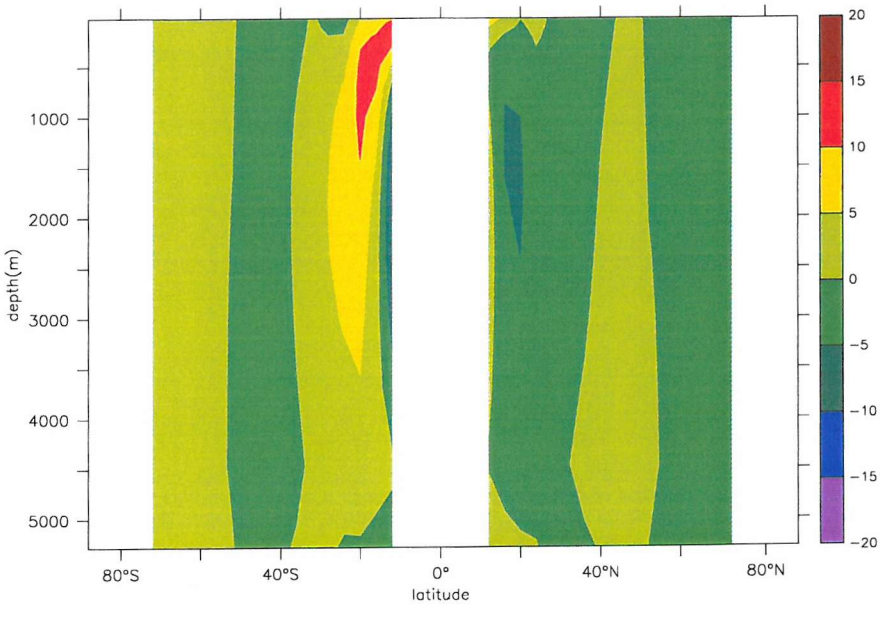

Figure 4.39: *Difference between the reconstruction of WaterWorld overturning and the actual result (Sv).*

the wind forcings are much the same between the two runs, little having changed in the parameters that set these. RidgeWorld's actual overturning looks, however, nothing like the previous reconstruction. The next step is to introduce a second component, dependent on the zonal density variations that are allowed to build up by the presence of the ridge, this being the fundamental change between the two scenarios.

By geostrophy, a zonal density gradient supports meridional flow:

$$fv = \frac{1}{\rho}\frac{\partial p}{\partial x} \tag{4.13}$$

(for v the meridional velocity and p the pressure)

which gives the thermal wind relation relating the vertical shear of the velocity to density differences:

$$f\frac{\partial v}{\partial z} = -\frac{g}{\rho_0}\frac{\partial \rho}{\partial x} \tag{4.14}$$

using ρ_0, an average reference density.

Deriving a density field from the T and S grids of the model and applying this formula between each pair of tracer-grid points gives a velocity shear profile for every v-grid longitude. Integrating up, choosing a bottom velocity such that the profile gives no net column transport gives the final density-induced meridional velocity profile. Combining this with the velocity induced by the wind, derived in the same manner as for WaterWorld, produces a simple reconstruction of the final overturning picture. This thermal wind reconstruction also fails at the equator as f becomes small and geostrophy no longer holds.

The thermal contribution to the reconstruction (*fig:4.40*) clearly shows a similar structure outside of the tropics, similar to the major features of the real overturning. The loss of the two separate maxima lobes at 35° and 70° in the final reconstruction (*fig:4.41*) is attributable to the Ekman contribution, since they are present in the thermal wind part. The barotropic structure of the Ekman return flow is as arbitrary in this case as for WaterWorld, so may be in error. The largest errors in

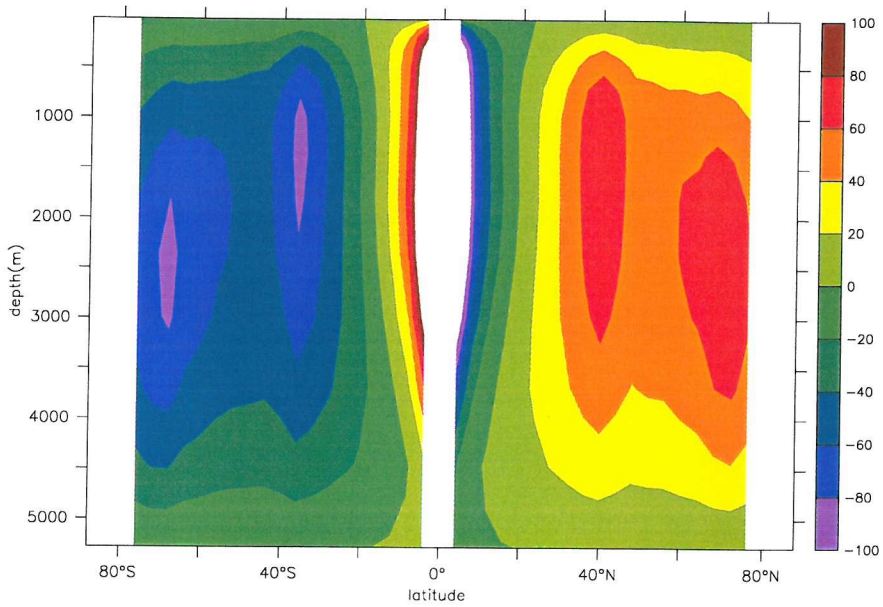

Figure 4.40: *Thermal wind component of the reconstruction of RidgeWorld's meridional overturning (Sv).*

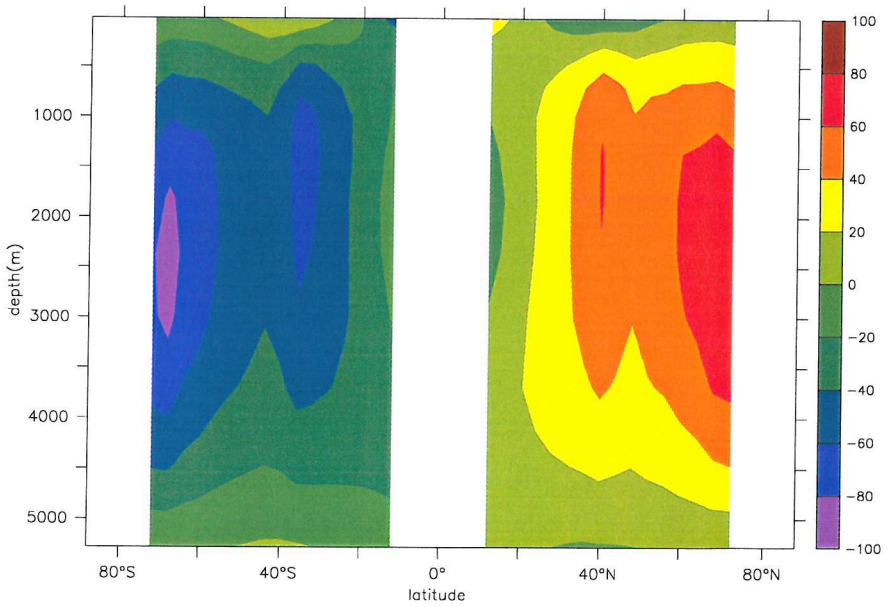

Figure 4.41: *The total (thermal wind + Ekman contribution) reconstruction of the RidgeWorld overturning (Sv).*

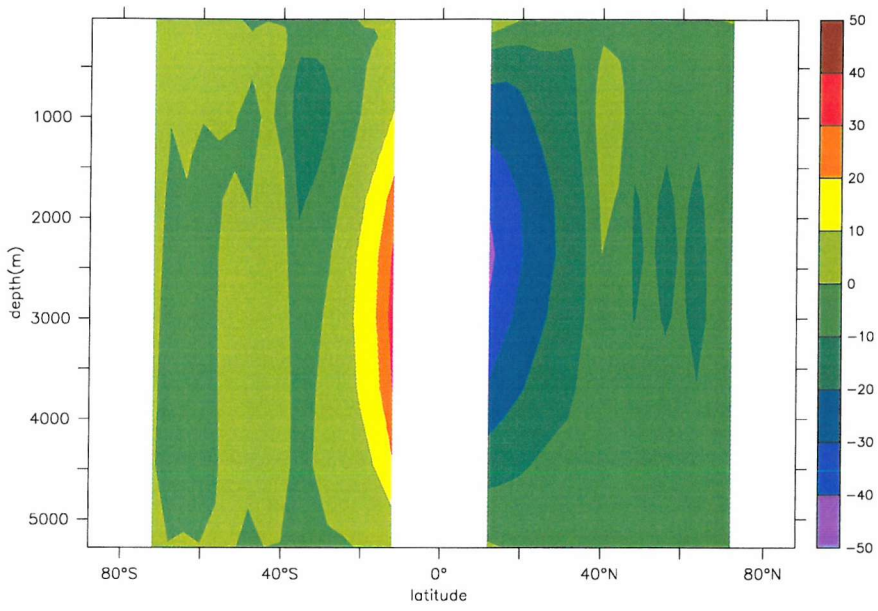

Figure 4.42: *Difference from the total reconstruction and the actual result for the RidgeWorld overturning (Sv).*

the reconstruction occur at the equator (*fig:4.42*), where the method has already been shown to be invalid. The major part of the overturning in the RidgeWorld case can thus be shown to be attributable to simple geostrophic compensation to the density gradients set up by the ridge.

The differences between the two overturnings shown here help explain the temperature/depth (*figs: 3.16, 3.23*) plots for the two scenarios. The strong vertical motion induced on WaterWorld results in a fairly well mixed water column, with warm surface water being taken down most of the way to the ocean floor - this explains why there is a very weak thermocline in this scenario. This reduced stratification and the consequent ease with which the column can overturn may also explain why this scenario (and also the others, as this run was used to initialise them) seems to be in better thermal equilibrium than a large global ocean might be expected to be after only ~1500 years. The RidgeWorld overturning provides less opportunity for warm surface waters to reach the deep ocean, with most of the downwelling filling the deep with cooler polar waters, allowing more of a thermocline to be established.

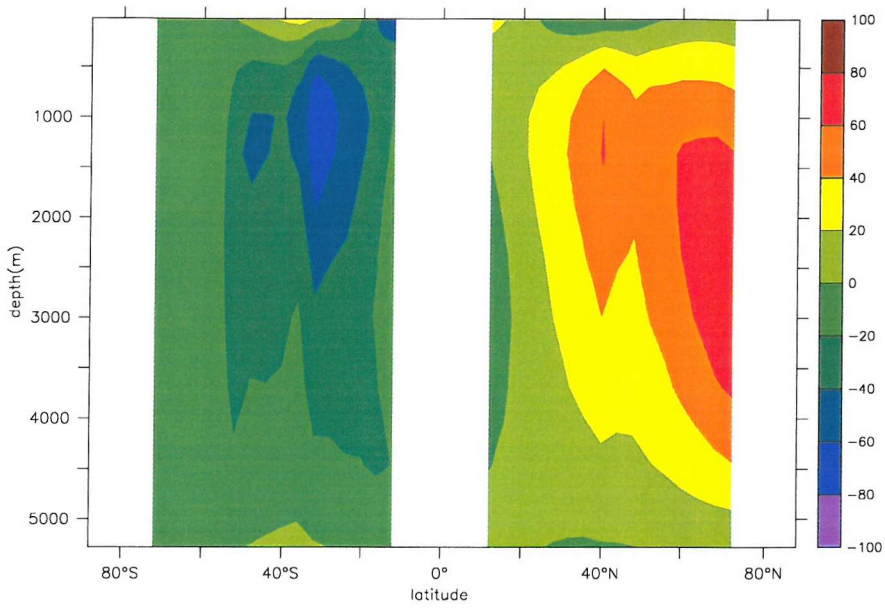

Figure 4.43: *The total (thermal wind + Ekman contribution) reconstruction for DrakeWorld (Sv).*

Following the same procedure for the DrakeWorld case produces equally sensible results (*fig:4.43, 4.44*). The geographically-forced nature of the overturning is highlighted here with the northern part of the basin reflecting the RidgeWorld pattern and the more open southern hemisphere being more reminiscent of WaterWorld's narrow cells, although weaker away from the strong tropical winds. This reconstruction shows similar errors around the equator and also around the reduced southern hemisphere overturning centred further equatorward at 40°S; the reconstruction produces a cell there, but its magnitude is not quite right.

The RidgeWorld overturning pattern shows a high degree of hemispherical symmetry and the DrakeWorld run, although asymmetric in that it lacks a strong southern overturning cell, also shows no signs of cross equatorial transport - the northern hemisphere overturning is confined to that hemisphere. Although the surface forcing is fairly symmetric, this pattern is somewhat surprising. The currently observed MOC shows asymmetry, with the dominance of the northern sinking cell providing for a net export of heat from the southern to northern hemisphere, and studies such as Marotzke and Willebrand (1991) have shown that symmetric solu-

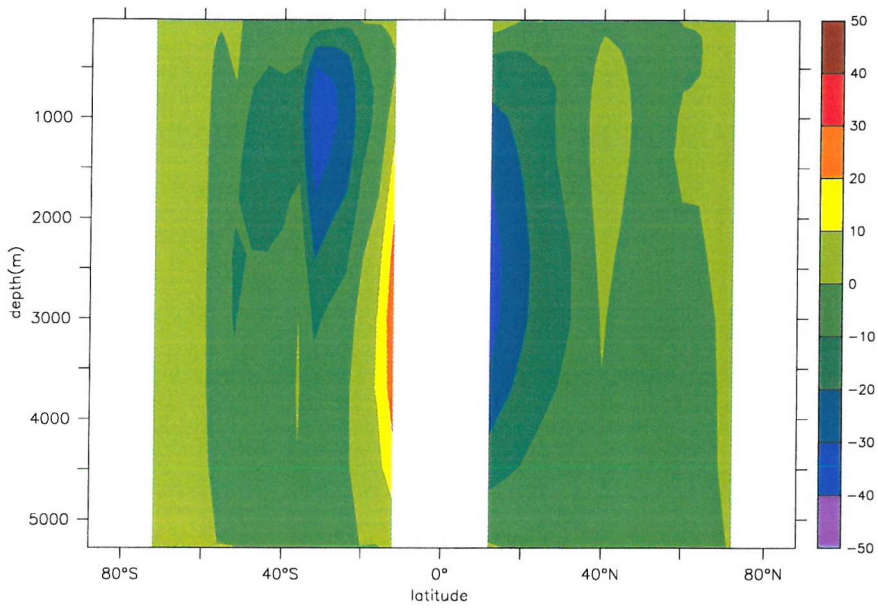

Figure 4.44: *Difference between the reconstruction and the actual overturning for the DrakeWorld overturning (Sv).*

tions, whilst theoretically possible, are unstable and prone to collapse into asymmetric ones with only a small initial asymmetry in their freshwater forcing. This is clearly not the case here, where the RW run has remained symmetric for the entire span of the run, and even the opening of the gap in the southern hemisphere which cuts off the largest portion of southern hemisphere deep water formation does not prompt a switch to another MOC mode.

Deconstructing the thermal wind contributions to the overturnings presented above helps to provide an explanation. As figures 4.45 and 4.46 show, the thermal wind part that dominated the total reconstruction is itself dominated by the thermal contribution to the density field; the contribution to the pressure field coming from salt differences is minimal. The MOCs seen here are thus likely to be little affected by any changes in the freshwater forcing, as this plays only a small role in the formation of the pattern. As has been seen, the temperature gradients and distributions here are hemispherically symmetric and relatively constant from one run to the next. The symmetric nature of these idealised overturnings can thus be seen to be due to the relatively weak nature of the freshwater forcing that occurs.

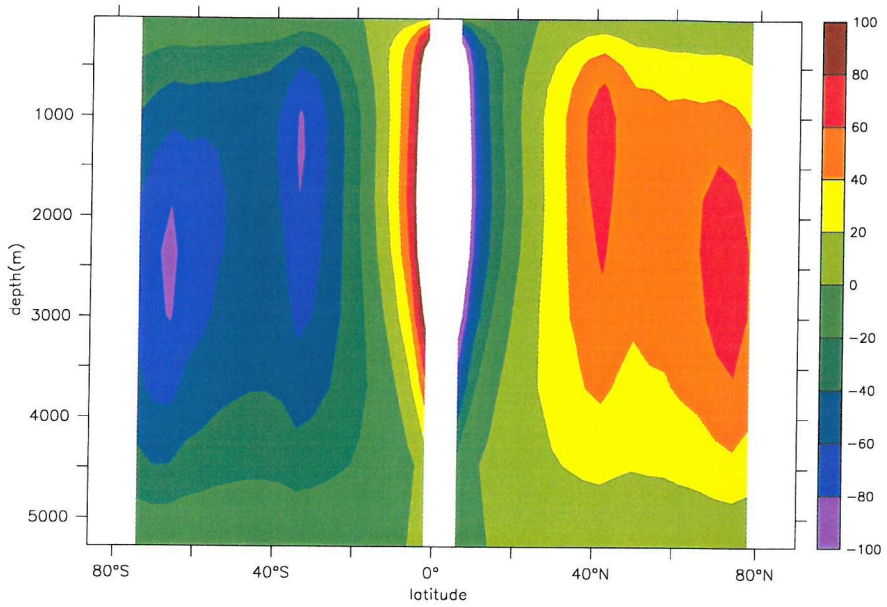

Figure 4.45: *Temperature contribution to the thermal wind reconstruction for RidgeWorld (Sv).*

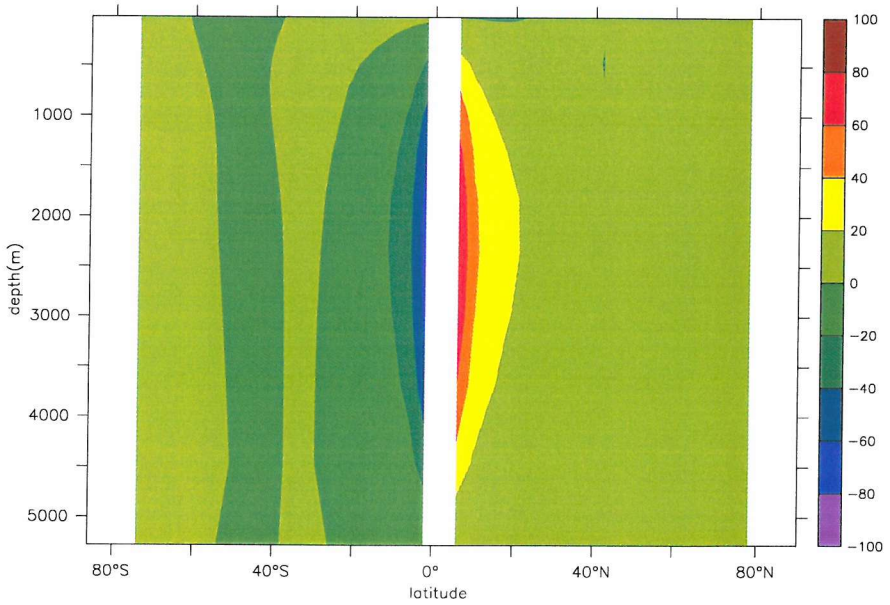

Figure 4.46: *Haline contribution to the thermal wind reconstruction for RidgeWorld (Sv).*

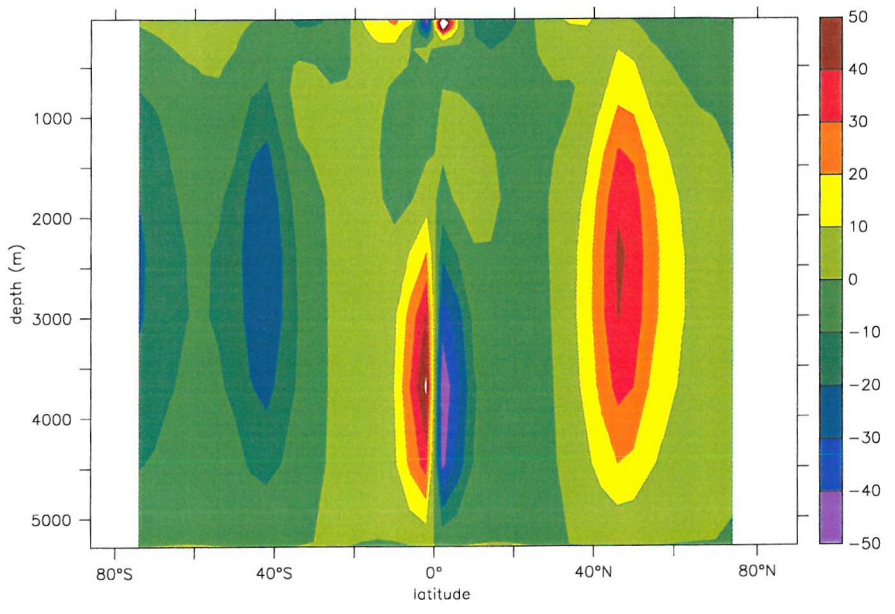

Figure 4.47: *Difference between the observed MOCs on PangeaWorld and RidgeWorld (Sv).*

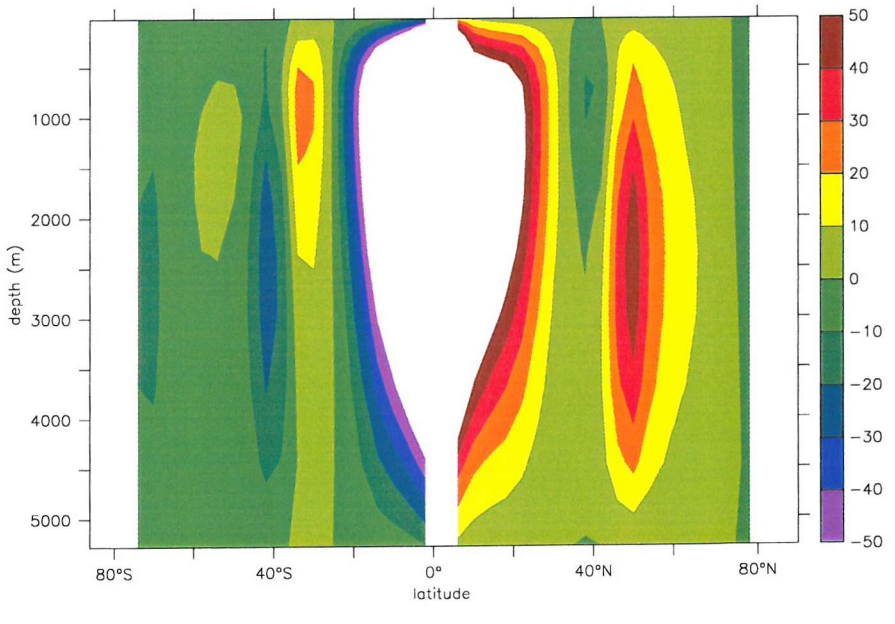

Figure 4.48: *Thermal contribution to the thermal wind part of the reconstruction of the overturning. PangeaWorld-RidgeWorld(Sv).*

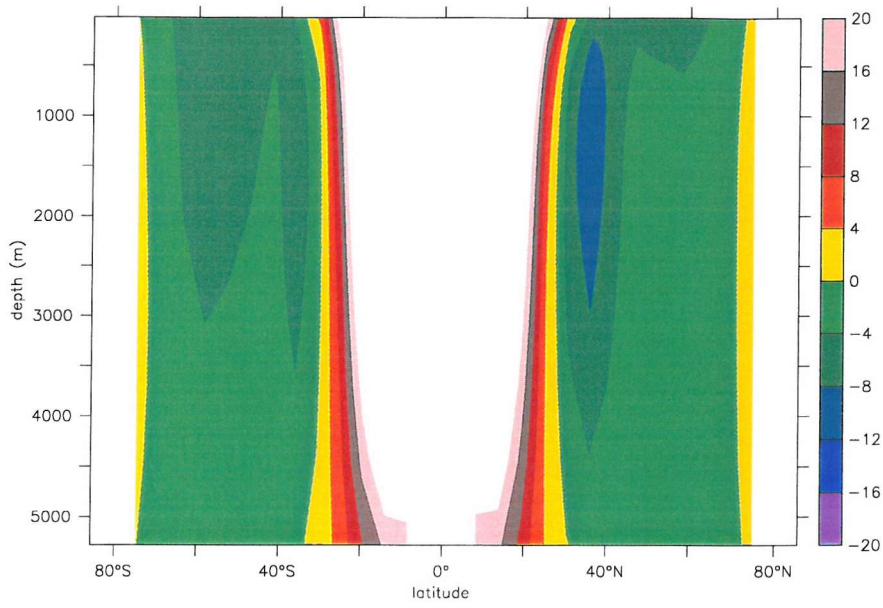

Figure 4.49: *MOC for the RidgeWorld run - DJF anomaly, compared to annual average (Sv).*

This method is also useful for examining other features of the MOCs observed. For instance, the PangeaWorld overturning can be seen to be about 20% stronger than that on RidgeWorld (*fig:4.47*). Examining the three components used here (Ekman, thermal contribution to thermal wind, haline contribution to thermal wind) for the reconstruction of the overturnings, it is clear that the difference lies in the thermal forcing between the runs (*fig:4.48*), rather than a more intense wind forcing or a stronger hydrological influence on the smaller basin of the Pangea scenario.

Figure 4.49 shows the strengthening of the southern hemisphere (anti-clockwise, so negatively signed) cell during its summer, the DJF period. From 30° to 70° in both hemispheres there is a more negative (up to 8 Sv anti-clockwise) overturning, which will both weaken the northern clockwise cell and strengthen the southern cell. This summer strengthening can be explained by deconstructing this into the individual components - figures 4.50 and 4.51 show that the main part of this change is in fact contributed by the wind driven Ekman part of the circulation, whilst the more patchy thermal wind contribution is again dominated by the

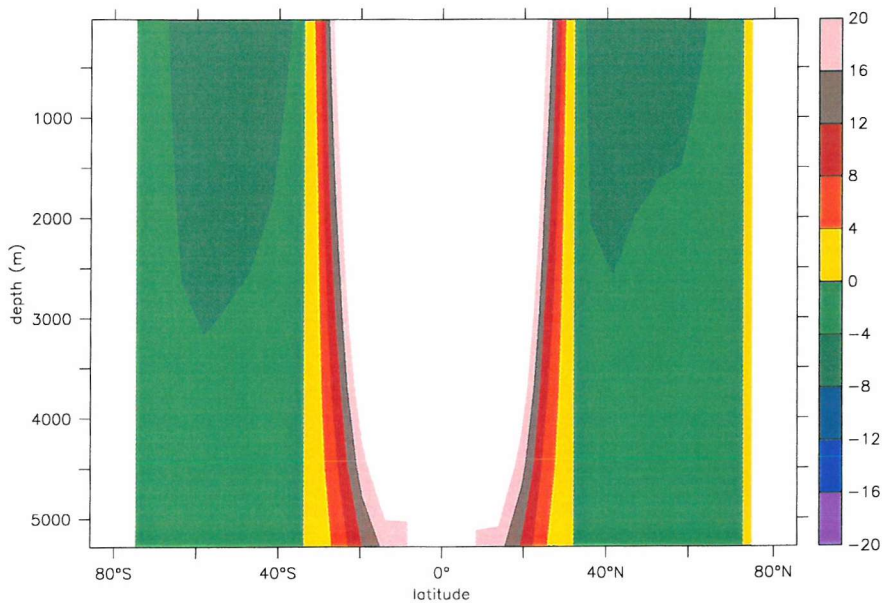

Figure 4.50: *RidgeWorld MOC - contribution of the Ekman component to the DJF overturning anomaly (Sv).*

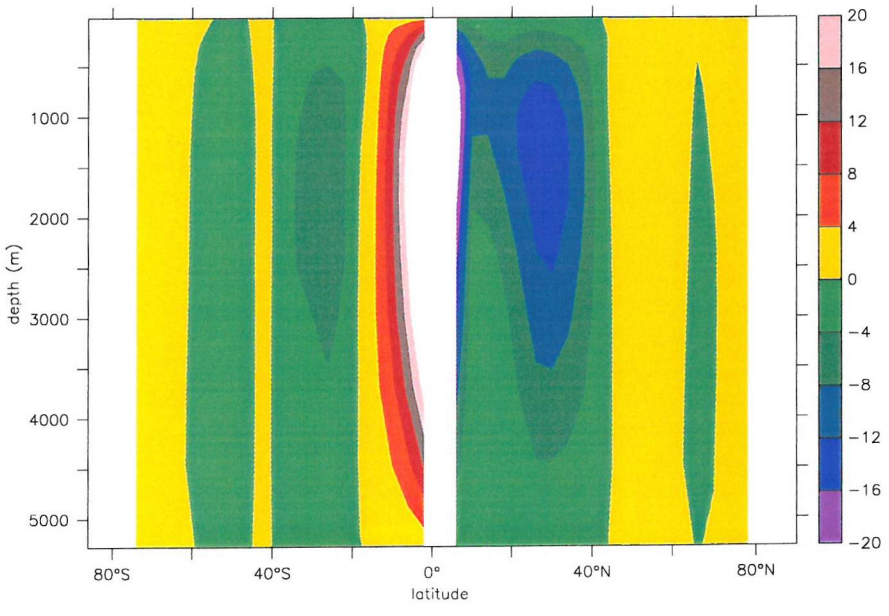

Figure 4.51: *RidgeWorld MOC - contribution of the thermal component of the thermal wind to the DJF overturning anomaly (Sv).*

thermal part and is responsible for the patch of 12 Sv anti-clockwise reduction in the northern hemisphere.

CHAPTER

FIVE

Discussion and Conclusions

5.1 Model

One of the initial goals of this project was to create a new, flexible, coupled OAGCM that was capable of millennial scale integrations. Whilst these theoretical experiments are not the ideal arena in which to evaluate the model, FORTE has been shown to produce stable climates in a number of situations and more than five thousand model years have been integrated over a period of 6 months. Taken with a reasonable initial reproduction of the current climate, we can conclude that the model production phase of the project has been successful. That is not to say that the model should be applied blindly in the state described here to provide quantitative results for, say, modern climate change under a CO_2 increase scenario - the errors shown in section 2.5.1 and the scale of and problems with the flux adjustments in section 2.5.2 suggest that much could be done in the way of improving the model's reproduction of the observable climate - this work is currently being done by others. For idealised use as here, to find qualitatively possible processes and feedbacks between aspects of the climate system in general, the model has shown itself capable. Others plan to use FORTE in work ranging from determining short-term climate variability in the North Atlantic to use in a glacial systems model on truly millennial timescales, demonstrating the flexibility and potential of the model.

Although not available for use at the beginning of this project, there are now two other low resolution GCM models on a similar level to FORTE. There is FAMOUS (Jones et al., 2003), a reduced version of HadCM3 (Gordon et al., 2000) which has undergone systematic tuning of various parameters to produce a similar climate to its more advanced parent, and also FOAM (Poulsen et al., 1999), which has a similar basic specification to the model used here (having slightly less resolution in the atmosphere and more in the ocean) which has been applied to paleo-climate problems. FORTE can thus take its place in an emerging set of models that occupy a middle ground between the EMICS and advanced coupled models which can be used to inform both the very long and short timescale integrations done by these two extreme classes of models, as well as in their own right.

The use of a faster, less complex model to help narrow the parameter space studied in a more expensive, high resolution study has obvious merit, but the use of an intermediate model to guide *less* detailed studies is not so clear. However the results presented here of the response of a complex atmosphere model to somewhat unusual forcings suggests that the application of simple EBM-type atmospheres, which have been tuned to reproduce one particular climate, to such scenarios may be prone to error. These simple atmospheres, often used for long timescale coupled model integrations, rely on the careful choice of parameters to provide their radiative characteristics; results here from the simple analytical radiative model suggest that not only would very different parameters be required in each case to reproduce the behaviour of the RealWorld, WaterWorld coupled, WaterWorld swamp and PangeaWorld atmospheres, but that there is no simple scaling based on the changing 1/2D characteristics of their initial setups that would allow one to find these values. This is especially true of the two WaterWorld cases where one might normally expect to see no great difference in the radiative properties of their atmospheres, as the surface-type specification has not changed at all. The use of a more simple model in cases such as these is obviously desirable as it would allow a true equilibrium to be found for each case and would also allow the parameter space to be effectively explored - here only one run for each scenario has been possible - so the possibility suggests itself of using a model such as FORTE to more accurately define the parameters for the simple atmosphere before a cheaper

model run. This would allow one to take full advantage of all types of model, from the cheapest to most advanced, in exploring a theoretical climate.

5.2 Climates

5.2.1 Aquaplanets and WaterWorld

Aquaplanet experiments are not uncommon for atmosphere only models, usually with a fixed SST profile to keep the general climate in the same regime as that currently observed. What can we conclude from the less restricted study here?

In this case, allowing the model to find its own equilibrium results in a positive water vapour-warmth feedback bringing the model to a very warm, very humid climate where the global climate response is dominated by the availability of so much water and the atmosphere's sensitivity to it. The equator to pole surface temperature gradient becomes much shallower than that currently observed, a fact which is again due to the water vapour content of the near saturated atmosphere rather than any increased poleward heat transport mechanism. Equatorial temperatures do not rise as much as those at higher latitudes, confirming the idea that the climate system has innate feedbacks that regulate tropical SSTs to prevent a runaway water vapour greenhouse - in this case the longwave emission profile and the increase of shortwave-reflective low clouds suggest that the mechanisms of both Pierrehumbert (1996) and Ramanathan and Collins (1991) are at work. Despite the shallow SST profile that results, the climate still has a recognisable Hadley circulation, in contrast to the behaviour of some fixed SST aquaplanet experiments with shallow gradients found by Neale and Hoskins (2000). Precipitation patterns are generally zonal and defined by the areas of vertical motion associated with the atmospheric overturning. The zonally even patterns of rainfall can be substantially disrupted by changes in the zonality of the ocean surface characteristics - here a low barrier with no direct atmospheric effect gives rise to strongly localised rainfall maxima over the equatorial warm pool and western boundary currents.

For WaterWorld, the ocean circulation consists of strong surface zonal flows, forced by both the wind and the geostrophic effect of the applied surface tem-

perature gradient. The magnitude of the zonal flow is limited by bottom friction and energy dissipated through the internal viscosity of the fluid. The Ekman flow forced by the zonal surface winds forces divergence/convergence of surface waters that, in the absence of zonal pressure gradients to provide for geostrophic flow, is compensated for by return flow spread throughout the entire depth of the water column. This gives rise to an oceanic overturning similar in form to the Hadley circulation seen above in the atmosphere and consequently mixing the deep waters efficiently with those at the surface, as compared to the currently observed mixed layer, effectively removing the thermocline from the ocean structure. This overturning pattern gives rise to an advective heat transport that is alternately poleward then equatorward in each hemisphere, but a non-advective transport of similar magnitude also occurs that gives a total ocean heat transport that is continuously poleward.

The addition of a zonal barrier provides for a thermally forced geostrophic meridional overturning which does not settle to a single-hemisphere-dominated asymmetric mode such as often found in THC studies. Instead, strong upwelling at the equator restricts each overturning cell to its own hemisphere. Where the barrier spans the whole globe, the strength of the overturning cell in each hemisphere is the same. These oceans show more of a thermocline than found on WaterWorld due to their more conventional overturning motions, but have a very similar total ocean heat transport.

This is, to my knowledge, the first time that a primitive equation GCM not tied to climatological values has been applied to such idealised circumstances. Whilst these climates are not directly applicable to any particular paleo-configuration or future landmap possibility, they demonstrate some interesting climate dynamics - the nature of the WaterWorld overturning in particular deserves further investigation with a less viscous model - and highlight the importance and potential of the water vapour/warmth greenhouse feedback. The other major feature, the non-advective flux, will be addressed below.

5.2.2 Drake Passage Opening

As mentioned earlier, the possibilities of changes in the ocean circulation and the wider climate on the opening of the Southern Ocean to fully circumpolar flow 30-40 Ma (Lawver and Gahagan, 1998) have been modelled in a number of previous studies. The experiments of Ridge-, Drake-, Pangea- and PangDrak- Worlds however constitute the first time such an experiment has been done with anything approaching the complexity of a coupled GCM, albeit with greatly idealised geographies.

In common with the previous studies, the removal of the zonal pressure gradient that comes with opening the gap results in a significant reduction in the strength of the southern hemisphere overturning cell and evidence of a shift in southern deep water production northward to the start of the gap (e.g. Gill and Bryan (1971); Cox (1989); Mikolajewicz and Maier-Reimer (1993); Bjornsson and Toggweiler (2001); Nong et al. (2000)). Here however the effect on the northern hemisphere cell varies: in the aquaplanet case it reduces by a small amount, less than 10% and in the basin case it increases by around 10% and, the only case here of any hemispherical asymmetry in the overturning, intrudes a short way into the southern hemisphere. Previous studies have generally found an increase in the northern cell and the overall pattern asymmetry, and a corresponding increase in transport from northern to southern hemispheres - such a transport change only occurs in the basin planet case here. This reduced response of the northern hemisphere to the southern overturning cell can be explained through the symmetry of the overturning patterns here that, forced by a stable thermal gradient and insensitive to salt forcing changes, are apparently robust.

Most previous studies were done with standalone ocean models using restoring to climatological temperatures as a surface boundary condition (e.g. Gill and Bryan (1971); Cox (1989)). This dependence on fixed SSTs makes it difficult to determine the temperature effect of the observed change in circulation, and only changes in the circulation of the ocean could be inferred. However Mikolajewicz and Maier-Reimer (1993) took the heat flux anomalies that occurred upon opening the Drake Passage in their model, forced a one-dimensional EBM with them and inferred that there was no systematic temperature change in the southern hemi-

sphere after opening the Drake Passage. They did find temperature changes of up to 5°C in localised areas, but there were both warmings and coolings with no general trend. Nong et al. (2000) use a surface heat flux formulation for their OGCM that is more flexible to ocean changes than pure restoring and find a reduction of 4°C on closing the Drake Passage in a flat bottomed Atlantic sector model and 1.5°C for a global model with realistic bathymetry. Bjornsson and Toggweiler (2001) use an OGCM actually coupled to an EBM to find between 2.8°C and 3.4°C changes in extreme southern SSTs. Compared to these, proxy data from the early Oligocene suggest that changes of up to 4-5°C occurred (Shackleton and Kennett, 1975).

The southern cooling seen here of ~1°C, in the only study with interactive winds and a hydrological cycle, are therefore on the lower end of the scale with respect to the results from previous models and are definitely lower than those suggested by the evidence. The qualitative nature of this study would suggest that the absolute magnitude of the temperature change here be taken with a pinch of salt, but the additional complexity of this model provides for extra feedbacks than those previously applied - that those feedbacks act to reduce both the climate change observed and the heat transport change thought to cause it is an important result. Given that other's studies have generally produced numbers smaller than those suggested by the proxy evidence, and we are proposing feedbacks that would reduce them further, we therefore conclude that ocean circulation and THC change coincident with the glaciation of Antarctica are unlikely to have enough climatic impact to be responsible for the glaciation on their own and that further atmospheric influences must be taken into account. At the very least, this study suggests that further investigation with fully coupled models, preferably in a more realistic paleo-setting, is necessary to determine the full role of the ocean in this question.

5.2.3 Pangean Climate

The basin planet climates are rather different from those of the aquaplanets, mostly due to the influence of the extremely large continental mass. This results in a

change of mean global temperature and creates seasonal pressure systems that drive a monsoonal climate. A number of previous modelling studies have looked at the behaviour of the climate system under a similar geographical forcing, as during the Mesozoic era continental drift is thought to have joined all of the land on earth together into one supercontinent which would have been subject to a similar set of forcings (e.g. Parrish (1982); Kutzbach and Gallimore (1989); Valdes and Sellwood (1992); Sellwood et al. (2000)). The idealised setup used here lacks a number of features crucial to the reproduction of an accurate Pangean climate (for example the lack of a Tethys ocean or a CO_2 concentration change in the atmosphere) but does however include a significant feature missing from these other studies: a fully interactive ocean. Previous studies (except the ocean-only study of Kutzbach and Guetter (1990)) have used atmosphere GCMs of varying levels of complexity, with either fixed, zonally uniform SST profiles derived from modern climatologies or energy balance considerations, or mixed layer models with either no ocean heat transport or a fixed one derived from the above energy balance SSTs. The results found here are thus worth comparing with those of the previous studies in order to see what may be gained from introduction of a more fully interactive ocean.

As has already been addressed, all the idealised experiments here are characterised by an atmospheric greenhouse that keeps them substantially warmer than the global mean temperature observed today; this is achieved through the increased water vapour content of the atmosphere. The Mesozoic was indeed thought to be a period of global warmth, with observed SSTs around 25-30°C in the tropics (Douglas and Woodruff, 1981) and about 10-15°C (Parrish and Spicer, 1988) at high latitudes. This was partly due to elevated levels of CO_2 (Berner, 1990) in the atmosphere which increased the greenhouse effect and partly due to effects arising from the changed land configuration; Barron and Washington (1984) concluded that whilst some of this warming can be attributed purely to the change in land configuration, the changes deduced from proxy evidence could only be reproduced by including the effect of a change in CO_2 concentration of around x4 modern values. It is unclear whether the geological evidence supports CO_2 change as large as required by those studies, and it may be that an increased water vapour greenhouse as seen here may have a role to play in this question.

Aside from the details of atmospheric chemistry then, it can be seen that the warm mean climate, with a shallow equator to pole SST contrast, produced by the simulation here is actually in reasonable agreement with proxy evidence and is also reproduced in the modelling studies. The majority of the data also indicate that the land would be free of ice (Crowley and North, 1991), but all the models have found areas of sub-zero temperatures on land. Previous studies have found temperature minima on land of -40°C (Kutzbach and Gallimore, 1989), -20°C (Valdes and Sellwood, 1992) and -24°C (Sellwood et al., 2000) - all have found the possibility of supporting some degree of snow or ice cover, even if only seasonal in some cases.

As with Barron and Washington (1985), who prescribed a high latitude SST as warm as those found here in an effort to increase land temperatures in that region, warm SSTs here do not result in a zonally equable land temperature and the minimum found here is of a similar degree, -28°C, to those seen previously. The inclusion of a warming CO_2 factor which has not yet been included in this simulation would increase this, but might make the overall climate, already as warm as the others at its maximum, too warm. Accepting Valdes and Blackburn (1989)'s criticism of models with lower than T31 resolution as unable to produce realistic inland penetration of stormtracks and thus having too cool continental interiors, especially considering the greater size of the landmass caused by the lack of a Tethys ocean, the use of an interactive ocean has not greatly changed the outlook on this issue.

The seasonality of the monsoon climate with heavy, localised summer rains and the enormous size of Pangea is thought to have left many inland areas almost completely dry throughout the year, giving rise to large, very arid regions in the tropics that leave telling geologic proxies (Frakes, 1979). This pattern is generally reproduced in other models, although the rainfall pattern is heavily influenced by the Tethys sea, which is of course missing here. The soil moisture pattern found on PangeaWorld however shows no arid regions at all - it may be that the generally more humid atmosphere responsible for the global warmth is also responsible for higher amounts of inland rain.

The ocean circulation is where this study has an advantage over those that have

gone before. Only Kutzbach and Guetter (1990) (hereafter K90) have conducted a paleoceanographic study of the period, and that with an ocean-only model restored to surface conditions found previously with an atmosphere-swamp model. The basin shape used here differs greatly from theirs as well, as they used a completely open Tethys sea. As there is evidence for a number of peninsulas and islands that would have restricted exchange in with the main Panthalassa ocean (Scotese, 2002), there is some merit in the square basin approach taken here. Like K90, the overturning circulation found is hemispherically symmetrical, although it is far more vigorous here, with an 120 Sv maximum rather than 20 Sv. Surface current speeds are also higher here, with average speeds around 5 cm/s, up to 40-50 cm/s along the equator and in the western boundary current. Despite that, the total ocean heat transport, also symmetric, is slightly weaker, with a maximum of 1.2 PW compared to 1.7 PW there. This implies a much weaker surface to bottom temperature contrast between the runs, which is indeed the case, with the previous study failing to reproduce the proxy-suggested bottom water temperature of around 15°C (Stevens and Clayton, 1971). This warm bottom water has sometimes been cited as evidence for the haline-forced sinking of warm equatorial waters (Brass et al., 1982), and indeed, K90 found that although the integrated oceanic MOC was of a similar form to here, they did see substantial sinking of salty surface waters in the inland Tethys sea. The equatorial-sinking concept is less in favour now, as several recent studies have failed to reproduce it (Bice et al., 1998; Bice and Marotzke, 2001) and, although there is no Tethys sea here, there is no evidence of any haline influence or slowdown of the thermally forced overturning here, and none is needed to produce the warm bottom waters found.

Overall then, within the geographical limits of the scenario, a reasonably likely picture of a monsoonal Pangean climate has been simulated. The ocean circulation, not before modelled with this degree of complexity, shows a thermally driven, vigorous, symmetric overturning with no low-latitude deep water formation, that transports about 1.2 PW of heat poleward in both hemispheres. The high latitudes are free of sea-ice year round.

5.3 Overturning and Heat Transports

5.3.1 Effects of OHT

A major aim of this project was to look at the effect of the ocean circulation on the climate dynamics of the scenarios in question. Although certainly not ineffectual, it must be concluded from the data presented here that the direct oceanic influence on the surface climate is largely secondary to that of the atmospheric radiative properties. In each case, the global mean temperature, which changes significantly between runs, is set by these radiative characteristics; little direct effect is seen from the changes to the surface albedo that are made. The equator to pole surface temperature profile is also primarily set by the radiative characteristics, as the generally shallow profile seen in all the idealised runs does not result from any enhanced poleward heat transport of the system, and changes to the transports cause relatively small changes to this gradient.

However, there are some notable effects of changing the ocean circulation, some direct and some where the ocean acts as the primary agent in affecting the atmosphere to produce some change. On the aquaplanets, where the presence of the non-advective flux limits the changes to the temperature field made by the total ocean heat transport, two significant differences can be attributed to the ocean circulation. For one, the difference in rainfall patterns observed between WaterWorld and RidgeWorld is due to the formation of the warm pool and western boundary currents brought about by the introduction of the zonal barrier. Also, the temperature change that is induced by the opening of the southern hemisphere gap to form DrakeWorld increases the surface wind forcing, so is thus responsible for the strengthening of the westward flow of the 'ACC' in this case.

The temperature changes expected however do not, to zero order, follow from a change in the ocean circulation. In the case where a significant atmospheric effect is triggered (sections 4.1.2, 4.2.3), the radiative effects dominate. The climate system here also provides a compensatory mechanism in the ocean that reduces the change in heat transport that would be expected from a change in ocean circulation, in the form of the non-advective heat flux. This is not observed in current

climate models when modelling the slowdown/shutdown of the THC in the Atlantic, where significant regional coolings are observed with no great diffusive heat flux (Houghton et al., 2001). This minimal effect however contrasts with what happens when all forms of ocean heat transport are suppressed and a very large change *is* observed (section 4.1.2). How can this be reconciled with the previously noted insensitivity?

All of the results presented here depend on the sensitivity of the atmospheric response to changes in the distribution of heat and available water at the ocean surface. In the swamp WaterWorld case, the changes in heat distribution brought about by the lack of ocean heat transport are so large that a qualitatively different radiative response from the atmosphere results - there is a general climate change, mediated through the atmosphere. The question is thus one of the strength and sensitivity of the coupling between the different components in specific scenarios - although the atmosphere is the final, direct agent of the change it is not necessarily the initial trigger or basic cause. Given this, more work is required in making sure that the responses of the atmosphere to perturbations in ocean heat fluxes are accurately known and quantified before attempting to make any quantitative predictions as to the scale of the effects of changing the ocean circulation.

5.3.2 Compensation within transport mechanisms

The climate system is traditionally seen as having two dynamic parts: the atmosphere and the ocean, each of which play an active role in distributing heat across the globe. The concept has long existed of compensation between the transports of these two parts (Bjerknes, 1964; Stone, 1978) - if one should be reduced for some reason then the other would increase, and vice versa. This has not been rigorously quantified; there are suggestions of this compensation in observations and it has been shown to hold well in simple models (Stone, 1978). The concept of some self-regulation within the system is not, then, that new. One of the most surprising results of this study is the existence and effect of the non-advective ocean heat transports that occur in the aquaplanet experiments. Non-advective ocean heat fluxes are not thought to play any great part in the current climate, and indeed,

are not noted as being observed to increase when THC change experiments are done in other models. The basin planet experiments show them to have reduced in effect in these scenarios however, with a weaker atmospheric greenhouse forcing than in the aquaplanet case.

A question not addressed by this study is that of the actual nature of this flux. Molecular diffusion would seem to be to weak an agent to carry this much heat, so one must appeal to the eddy fluxes, caused by features that are subgridscale in a model of this resolution and thus rather crudely parametrized. Eddy parametrization in ocean models is an open research topic, and the horizontal diffusive fluxes used in most of the runs cannot be said to provide a faithful representation. That the non-advective flux is also seen in a model employing a more realistic mixing/eddy scheme is encouraging, but this is still far from reality, or even a test in an eddy resolving model. For this question to be answered, more in depth study is required than is possible with a model of this resolution.

The non-advective flux here seems to be dependent on the level of greenhouse forcing the atmosphere provides. Following from the ideas of Pierrehumbert (1996) on the limitations on tropical SSTs, if the air everywhere, not just over the tropics, is largely saturated then there will be no real radiative 'window' through which to lose heat from other areas. The surface temperature will thus be more strictly controlled by the local radiative properties of the atmosphere and the more likely it may be for the direct forcing of the non-advective flux to occur. This can be seen by comparing the two Drake Passage opening cases, where the aquaplanet case with the stronger greenhouse sees both a compensating increase in atmospheric *and* non-advective ocean fluxes in response to the decrease in advective heat transport - for the basin planets the compensation by both the other components is weaker. Although the basin planet temperature change is of the same magnitude as for the aquaplanet case, this is because of a change in the local properties of the atmosphere, not attributable to the change in ocean circulation. This non-advective flux is also not seen in the model's RealWorld simulation, nor does it seem to be present in other's runs where the advected heat transports are changed by, say reducing the strength of the thermohaline circulation in the North Atlantic - all situations with much weaker greenhouses than seen here. There is

clearly a limit to the compensation that can be induced by the stiff greenhouse climate - in the case where the ocean heat transport (of both types) is removed entirely (section 4.1.2) the atmospheric compensation is not nearly adequate to replace the loss and a rather different climate state is achieved.

Another question provoked by the appearance of these fluxes is that of the timescale on which they act. This is important, both for ascertaining the nature of the physical mechanism involved, and also for the possibility of observing them in other systems, either in observations or other climate simulations where suitably long timescales to observe their full evolution and effect may not be available. Preliminary results here suggest that a timescale of around 100-200 years may be suitable for observing their effect, but a more extensive, fully synchronous modelling study is required to investigate the nature of the transitional effects properly.

This study then proposes the possible existence of a heat transport mechanism in the ocean that, under favourable circumstances, can be of equivalent magnitude and importance to that of the advective ocean heat flux. This flux is probably related to the eddy flux in the ocean and is somehow dependent on the strength of the greenhouse forcing present. This may have implications for the dynamics and heat budgets of oceans during the extremely warm periods of geologic history when strong atmospheric greenhouse conditions were known to exist.

5.4 Model Specificity

The scenarios addressed in this study have, in general, not been looked at before in a model of equivalent complexity. Nor was this model particularly designed to study them - what tuning the component models have undergone was designed to reproduce the current climate, and some of the results seem unusual or extreme from what we know of our climate system on more familiar ground. In the general absence of equivalent results to compare them to then, to what extent are the results likely to reflect climatic 'reality', and to what extent may they simply be ascribed to the quirks of one particular model applied to one, limited set of curious circumstances?

The study here has produced global warmth greater than that seen before without any increase in atmospheric CO_2, a robust hemispherically symmetric oceanic overturning system without fixed surface restoring and a non-advective ocean heat transport of significant amplitude. All have however been analysed and a self-consistent picture of the model climates drawn in each case, all fitting into a framework built from known feedbacks and processes in the climate system. To this extent then, the model is 'valid' - there does not seem to be anything occurring that is outside the bounds of normal climate science and the model is fully self-consistent. The model also produces a reasonable current climate which does not feature a runaway greenhouse or symmetric ocean overturning, so the model cannot be said to have any systematic skew away from realistic reproduction and interplay of climate processes.

All of the unusual features seen in the idealised scenarios seem to turn on the increased humidity levels found in the atmosphere in each case, which in turn depend on the model's representation of the hydrological cycle and, given that the RealWorld scenario starts from a sensible representation of this, its sensitivity to changes. An atmosphere model's representation of the hydrological cycle is one of the most complex, poorly approximated parts of any model, an area that, although based on understandings of the physical concepts at work, is so complicated and subgridscale that the parameters are often tuned empirically to give the right response in the desired situation. Given that this tuning has not been done here, indeed could not be done as the sensitivity for an aquaplanet is unknown, to what extent can faith be put in results that depend so strongly on such a factor?

Absolute answers to this question can only be made by an attempt to reproduce them in a more detailed, higher resolution climate model. A step towards them could be made in a systematic sensitivity study of FORTE, something that is being carried out as part of the ongoing development process. But it has been stressed throughout this study that the results found and conclusions drawn are to be purely qualitative, that the aim is to find *possible* behaviours of the climate system. Given that all the features have been explained within a self consistent framework of known climate processes, we conclude that, even if this study has not reproduced the actual climates that would pertain if all the land on earth were covered by sea

to produce the same scenarios, the analysis and conclusions of the processes that would occur are valid and deserving of further investigation with a more quantitative eye.

CHAPTER

SIX

Future Work

The model presented here is new, the scenarios tested are novel and a number of results found are unexpected and unusual, so this project raises many questions that are deserving of further investigation. Any particular climate state generated in a model of GCM complexity contains a wealth of detail and feedbacks and the limited scope of this project has allowed only a few features of those generated here to be looked at. Quite apart from a more detailed exposition of the climates produced here though, there are some further questions that have been provoked by the study.

6.1 The Model

The model development contributed to by this project is still in progress, and other people are using FORTE in a number of arenas for differing purposes - this study is currently the most extensive piece of work that has been completed with FORTE however and suggests two main areas for improvement.

Firstly, although several thousand years of model time were integrated, none of the runs achieved a true equilibrium. This situation is far from ideal, and future studies also looking at theoretical climate simulations would be better served if

the computational efficiency of the model were increased. Without further sacrificing resolution or greatly increasing the periodic coupling interval, this could be achieved through optimisation of the atmosphere code. The kernel of the atmosphere code is rather old and currently cannot take advantage of parallel computing methods (unlike the ocean) and improvements in this area would greatly increase the speed of the model. Some advantage could also be gained through the replacement of the FFTs with more modern, optimised code - a 2 or 3 fold increase in speed would make the model easily capable of 100 years a day on a desktop PC and far more with the use of serious computing resources which would make it a very powerful tool.

Perhaps more importantly with regard to the 'accuracy' of the climates produced by the model is the matter of tuning the model parameters. This is the process of changing the parameters used in the model approximations, in the absence of perfect knowledge of the processes and feedbacks of the real climate, to optimise the state and sensitivity of the simulated climate. When using a coupled model the individual components are usually tuned together to produce the 'best' state, e.g. Jones et al. (2003). As it stands, FORTE's ocean has not been tuned at all, and the atmosphere is in the same state as used in Forster et al. (2000), so is optimised towards standalone running with modern day fixed SSTs - no work at all has yet been done on the coupled system. The results presented here highlight the strong effects of water vapour in the atmosphere on the mean climate state and it may be that the coupled model overestimates the sensitivity of the real climate to this feedback. Whilst this study looks for qualitative possibilities and the processes found here, even if not realistic as to their magnitude or likelihood of occurring in the real climate, are thus valid, a more quantitative study would be well advised to test this and other climate sensitivities before proceeding.

6.2 Heat Transports

The non-advective transport found here in the aquaplanet cases, and its compensating effects, is something not previously noted in climate modelling studies. Whilst this may be a result of the novel nature of the experiments carried out

here, any result obtained with only one model is naturally called into question. It would therefore be a good idea to attempt to reproduce this result in other models by means of a similar study. If nothing else, they deserve to be looked at with a more quantitative eye than used here, and some attempt made to determine the dependency of their strength on other features of the climate, i.e. the greenhouse forcing.

A further series of experiments to investigate the nature and extent of this transport compensation naturally suggests itself. In the coupled WaterWorld we are dealing with both advective and non-advective transports in the ocean, plus the atmospheric transport. For the swamp WaterWorld, the two ocean components are suppressed - here the atmosphere only partly compensates for lack of ocean transport. Useful additions to these would be experiments where each of the transports was suppressed in turn, to see to what extent the others compensate. This would be particularly interesting for the case where each ocean component was suppressed separately - the aquaplanet experiments suggest that the non-advective component matches the changes in the advective one well, but does this carry to the extremes of having no advective transport?

If the existence and importance of the non-advective fluxes is to be accepted, a number of further questions are also raised. What mechanism carries this flux, and what induces it? Assuming that molecular diffusion in the real ocean would be too weak, and that the eddy parametrization (in the form of either the horizontal diffusion specified or the GM flux) is responsible, would real eddies in the ocean system behave in a similar manner? Although robust to a slightly higher resolution and better mixing scheme here, would a model capable of resolving eddies produce the same behaviour? If not, is it purely an artefact of the coarse resolution, and should other models of similar or lesser resolution be discounted for being incapable of correctly simulating an important effect? Also, the timescale on which these fluxes act is important, not only from the point of view of assessing the actual climate states observed following a change in ocean circulation that may trigger effects seen here, but also as an integral part of explaining the mechanism by which they act. The data here, although not suited to this task, suggest that a timescale of a few hundreds of years is appropriate, but further work is nec-

essary to clarify the details of this, requiring a fully synchronous coupled run of several hundred years.

6.3 Climates

The number of scenarios investigated here was of course limited by the timescale of the project. An investigation of the effects of basin geography on ocean circulation and climate could involve an almost infinite number of variations, and 5 scenarios with only one basin is little more than a beginning. The differences between the idealised scenarios and the RealWorld simulation would best be investigated by continuing the series into experiments with two, then three ocean basins, then including the effects of topography, both in the ocean basin and on land to influence the atmospheric flow. The significant changes in regime that must occur between the greenhouse worlds with symmetric MOCs and the more asymmetric modern day climate should be noted and their causes ascertained.

Linked to this concept are the results from the atmosphere-only 'land shapes' experiment (section 4.1.2) where significant effects on the mean climate were observed dependent on the precise location and geometry of the land masses. These features were barely investigated here, yet promise some interesting climate dynamics, especially if done with a reasonable ocean model, unlike the swamp used here.

Also touched on, but not investigated to FORTE's full ability, is the question of the paleoclimates mentioned in the course of this study. Two questions of paleoclimate have been addressed: the effect of the opening of the Drake Passage, and that of the climate and monsoon on Pangea. For reasons of continuity within the study the geographies used throughout were highly idealised and other features of the real scenarios (i.e. CO_2 levels, orbital parameters) left out, but there is no reason that FORTE could not be applied with more realistic parameters to produce more sophisticated paleoclimates. Thus far these and other paleoclimate questions have only been addressed with simpler coupled models or standalone models with non-interactive boundary conditions - a coupled GCM like FORTE could bring a

new perspective on such issues and be used to inform the shorter, more detailed studies often done with higher resolution GCMs.

CHAPTER

SEVEN

Appendix

1. Hardware and Software

Details of Hardware and Software setup

Software

Communication between the models is achieved through the OASIS (Ocean Atmosphere Sea Ice Soil) coupler (Terray et al., 1999), a program designed by the Centre Europeen de Recherche et de Formation Avancée en Calcul Scientifique as a modular set of tools to simplify the process of allowing arbitrary grid-based models to pass data between each other whilst running. To this end it needs to be able to deal with differences between the grids that the models run on, the different units in which they work and the different speeds at which they run. It is designed so that the component programs only need small alterations: it requires only a call to an import routine to provide data for a boundary condition when required and a call to an export routine when data needs to be passed out. Everything else is done in a completely separate program that sits in between the two components and deals with issues like mapping data between the different model grids.

A more basic level of technology is also required to achieve the inter-process communication - a pipeline through which the data can be passed between the running component models. In this implementation this is done through the use of the Parallel Virtual Machine [PVM] system (PVM, 2003), whereby a virtual network is created and the running processes connected onto it as nodes. This allows great flexibility in the platforms on which the model runs, since the communication is done entirely through this abstract layer - different components can be run on physically separate machines as long as they are connected by some form of network and each has a PVM client. This has proved useful in the course of the project as IGCM3 and MOMA are coded to suit different hardware profiles and the greatest efficiency has been achieved through running the ocean on a parallel machine with many, weak nodes and the atmosphere on a powerful, single processor machine.

OASIS also takes care of a number of minor points required to ensure compatibility between the models, e.g. MOMA uses temperatures in degrees centigrade, IGCM3 in Kelvin, so it is necessary to add the conversion constant when passing

temperature between the two models. The two models also arrange their grids differently: MOMA counts from South to North and West to East (starting at the Greenwich meridian) whilst IGCM3 counts from North to South, but in the same sense longitudinally - this is another factor that needs to be accounted for in the interpolation process.

Hardware

Various hardware configurations were used throughout the project, but all of the results presented here have been run with all components on one machine - either a dual 2G Intel (Xeon) Dell running RedHat 7.3 with the Intel Fortran compiler 6/gcc 2.96, a 24 node SGI Origin 2000 with IRIX 6.5 and MIPSpro Compiler 7.3.1.2m or a 12 node SGI Onyx 300 with IRIX 6.5 and MIPSpro Compiler 7.3.1.3m. The Xeon box is a common PC workstation and all required software is free (and freely) available - FORTE can be thus be run at useful speeds without great computational expense unlike other coupled models.

On the Xeon and Onyx 300, with the previously stated periodic coupling ratio of 17/60 months, the model runs at ~50 model years a day. The fully synchronous version completes ~12 model years a day. The Origin 2000 is about a third slower.

BIBLIOGRAPHY

Alexeev, V., 2003. Sensitivity to CO_2 doubling of an atmospheric GCM coupled to an oceanic mixed layer: a linear analysis. Climate Dynamics 20, 775–787.

Anderson, D., Killworth, P., 1977. Spin-up of a stratified ocean with topography. Deep-Sea Research 24, 709–732.

Arakawa, A., 1966. Computational design for long-term numerical integration of the equation of fluid motion: two-dimensional incompressible flow. Part I. Journal of Computational Fluid Dynamics 1 (119-143).

Barron, E., Washington, W., 1984. The role of geographic variables in explaining paleoclimates: results from a Cretaceous climate model sensitivity study. Journal of Geophysical Research 89, 1267–1279.

Barron, E., Washington, W., 1985. Warm cretaceous climates: high atmospheric CO_2 as a plausible mechanism. In: The carbon cycle and atmospheric CO_2: Natural Variations, Archaean to Present. Geophysical Monograph 32. American Geophysical Union, pp. 546–553.

Berner, R., 1990. Atmospheric carbon dioxide levels over Phanerozoic time. Science 249, 1382–1386.

Betts, A., 1986. A new convective adjustment scheme. 1. Observational and theoretical basis. Quarterly Journal of the Royal Meteorological Society 112, 667–691.

Bice, K. L., Barron, E. J., Peterson, W. H., 1998. Reconstruction of realistic early Eocene paleobathymetry and ocean GCM sensitivity to specified basin configuration. In: Tectonic boundary conditions for climate reconstructions. New York OUP, pp. 227–247.

Bice, K. L., Marotzke, J., 2001. Numerical evidence against reversed thermohaline circulation in the warm Paleocene/Eocene ocean. Journal of Geophysical Research 106 (C6), 11529–11542.

Bjerknes, J., 1964. Atlantic air-sea interactions. Advances in Geophysics 10, 1–82.

Bjerknes, J., 1969. Atmospheric teleconnections from the equatorial Pacific. Monthly Weather Review 97, 163–172.

Bjornsson, H., Toggweiler, J., 2001. The climatic influence of Drake Passage. In: The Oceans and Rapid Climate Change: Past, Present and Future. Geophysical Monograph 126. American Geophysical Union, pp. 243–259.

Boville, B., Gent, P., 1998. The NCAR Climate System Model, version one. Journal of Climate 11, 115–1130.

Boyles, J. S., 1993. Sensitivity of dynamical quantities to horizontal resolution for a climate simulation using the ECMWF (cycle 33) model. Journal of Climate 6, 796–815.

Brass, G., Southam, J., Peterson, W., 1982. Warm saline bottom water in the ancient ocean. Nature 296, 620–623.

Bárdossy, G., Aleva, G., 1990. Lateritic Bauxites. Elsevier, Amsterdam.

Broecker, W., Peteet, D., Rind, D., 1985. Does the ocean-atmosphere system have more than one stable mode of operation? Nature 315, 21–26.

Bryan, F., 1986. High-latitude salinity effects and interhemispheric thermohaline circulations. Nature 323, 301–304.

Bryan, K., 1969. A numerical method for the study of the circulation of the world ocean. Journal of Computational Physics 4, 347–376.

Bryden, H., Cunningham, S., 2003. How wind-forcing and air-sea heat exchange determine the meridional temperature gradient and stratification for the Antarctic Circumpolar Current. Journal of Geophysical Research 108 (C8), 31.1–31.9.

Claussen, M., Mysak, L., Weaver, A., Crucifix, M., Fichefet, T., Loutre, M.-F., Weber, S., Alcamo, J., Alexeev, V., Berger, A., Calov, R., Ganapolski, A., Goosse, H., Lohmann, G., Lunkeit, F., Mokhov, I., Petoukhov, V., Stone, P., Wang, Z., 2002. Earth system models of intermediate complexity: closing the gap in the spectrum of climate system models. Climate Dynamics 18, 579–586.

Cox, M. D., 1984. A primitive equation, 3-dimensional model of the ocean. Tech. Rep. 1, Geophysical Fluid Dynamics Laboratory/NOAA, Princeton University.

Cox, M. D., 1989. An idealized model of the world ocean. Part I: The global-scale water masses. Journal of Physical Oceanography 19, 1730–1752.

Crowley, T., North, G., 1991. Paleoclimatology. Oxford University Press, New York.

Douglas, R., Woodruff, F., 1981. Deep sea benthic foraminifera. In: The Sea, 7. Wiley-Interscience, New York.

Egbert, G., Ray, R., 2000. Significant dissipation of tidal energy in the deep ocean inferred from satellite altimeter data. Nature 405, 775–778.

England, M., 1993. Representing the global-scale water masses in ocean general circulation models. Journal of Physical Oceanography 23, 1523–1533.

Enos, P., 1993. The Permian in China. In: Permian of Northern Continents. Springer-Verlag, New York.

Fanning, A. F., Weaver, A. J., 1997a. A horizontal resolution and parameter sensitivity study of heat transport in an idealized coupled climate model. Journal of Climate 10, 2469–2478.

Fanning, A. F., Weaver, A. J., 1997b. On the role of flux adjustments in an idealized coupled climate model. Climate Dynamics 13, 691–701.

Fawcett, P. J., Barron, E. J., 1998. The role of geography and atmospheric CO_2 in long term climate change: Results from model simulations for the late Permian to the present. In: Tectonic boundary conditions for climate reconstructions. New York OUP, pp. 21–36.

Forster, P. d. F., Blackburn, M., Glover, R., Shine, K., 2000. An examination of climate sensitivity for idealised climate change experiments in an intermediate general circulation model. Climate Dynamics 16, 833–849.

Frakes, L., 1979. Climates throughout Geologic Time. Elsevier, New York.

Furevik, T., Bentsen, M., Drange, H., Kindem, I., Kvamstø, N., Sorteberg, A., 2003. Description and evaluation of the Bergen climate model: ARPEGE coupled with MICOM. Climate Dynamics 21, 27–51.

Ganopolski, A., Brovkin, V., 2003. The role of the reorganizations of the global thermohaline circulation in the glacial climate changes. Geophysical Research Abstracts 5.

Gent, P., McWilliams, J., 1990. Isopycnal mixing in ocean circulation models. Journal of Physical Oceanography 20, 150–155.

Gent, P., Willebrand, J., McDougall, T., McWilliams, J., 1995. Parameterizing eddy-induced transports in ocean circulation models. Journal of Physical Oceanography 25, 463–474.

Ghil, M., 1987. Nonlinear phenomena in climate dynamics. In: Irreversible phenomena and dynamical systems analysis in geosciences, ed. Nicolis and Nicolis. Dordrecht: D.Reidel, pp. 313–320.

Gildor, H., Tziperman, E., 2001. A sea ice climate switch mechanism for the 100-kyr glacial cycles. Journal of Geophysical Research 106 (C5), 9117–9133.

Gill, A. E., 1982. Atmosphere-Ocean Dynamics. Academic Press.

Gill, A. E., Bryan, K., 1971. Effects of geometry on the circulation of a three-dimensional southern hemisphere ocean model. Deep-Sea Research I 18, 685–721.

Glennie, K., 1987. Desert sedimentary environments, present and past - a summary. Sedimentary Geology 50, 135–165.

Goloneva, L., 2000. The Maastrichtian (Late Cretaceous) climate in the northern hemisphere. In: Climates: Past and Present. The Geological Society, London, pp. 43–54.

Gordon, C., Cooper, C., Senior, C., Banks, H., Gregory, J., Johns, T., J.F.B., M., Wood, R., 2000. The simulation of SST, sea ice extents and ocean heat transports in a version of the Hadley Centre coupled model without flux adjustments. Climate Dynamics 16, 147–168.

Gregory, J., Mitchell, J., 1997. The climate response to CO_2 of the Hadley Centre coupled AOGCM with and without flux adjustment. Geophysical Research Letters 24 (15), 1943–1946.

Griffies, S. M., Böning, C., Bryan, F. O., Chassignet, E. P., Gerdes, R., Hasumi, H., Hirst, A., Treguier, A.-M., Webb, D., 2000. Developments in ocean climate modelling. Ocean Modelling 2, 123–192.

Hadley, G., 1735. Concerning the cause of the general trade-winds. Philosophical Transactions of the Royal Society, London 39, 58–62.

Halley, E., 1686. An Historical Account of the Trade Winds and Monsoons, observable in the Seas between and near the Tropicks, with an attempt to assign the Phisical cause of the said Winds. Philosophical Transactions of the Royal Society, London 16, 153–168.

Haug, G., Tiedemann, R., 1998. Effects of the formation of the Isthmus of Panama on Atlantic Ocean thermohaline circulation. Nature 393, 673–676.

Hays, J. D., Imbrie, J., Shackelton, N. J., 1976. Variations in the Earth's orbit: Pacemaker of the ice ages. Science 194, 1121–1132.

Heinrich, H., 1988. Origin and consequences of cyclic ice rafting in the northeast Atlantic Ocean during the past 130,000 years. Quaternary Research 29, 143–152.

Held, I., Hou, A., 1980. Nonlinear axial symmetric circulations in a nearly inviscid atmosphere. Journal of Atmospheric Science 37, 515–533.

Hellerman, S., Rosenstein, M., 1983. Normal monthly wind stress over the world ocean with error estimates. Journal of Physical Oceanography 13, 1093–1104.

Henderson-Sellers, A., Robinson, P., 1986. Contemporary climatology. Longman.

Higgins, P., Vellinga, M., Mastrandrea, M., Schneider, S., 2003. Responses and feedbacks to abrupt climate change: The biosphere's role in the coupled earth system. Geophysical Research Abstracts 5.

Hirschi, J., Baehr, J., Marotzke, J., Stark, J., Cunningham, S., Beismann, J.-O., 2003. A monitoring design for the Atlantic meridional overturning circulation. Geophysical Research Letters 30 (7), 66.1–66.4.

Hoffman, P., Kaufman, A., Halverson, G., Schrag, D., 1998. A Neoproterozoic snowball earth. Science 281, 1342–1346.

Hoskins, B., Simmons, A., 1975. A multi-layer spectral model and the semi-implicit method. Quarterly Journal of the Royal Meteorological Society 101, 637–655.

Houghton, J., Ding, Y., Griggs, D., Noguer, M., Van der Linden, P., Dai, X., Maskell, K., Johnson, C., 2001. Climate Change 2001: the scientific basis. Contribution of Working Group I to the Third Assessment Report of the Intergovernmental Panel on Climate Change. Cambridge University Press for the Intergovernmental Panel on Climate Change, 2001.

Hughen, K., Overpeck, J., Lehman, S., Kashgarian, M., Southon, J., Peterson, L., Alley, R., Sigman, D., 1998. Deglacial changes in ocean circulation from an extended radiocarbon calibration. Nature 390, 65–68.

Johnson, S., Clausen, H., Dansgaard, W., Fuhrer, K., Gundestrup, N., Hammer, C., Iversen, P., Jouzel, J., Stauffer, B., Stauffer, B., 1992. Irregular glacial interstadials recorded in a new Greenland ice core. Nature 359, 311–313.

Jones, C., Cox, P., Gregory, J., Murphy, J., Sexton, D., Thorpe, R., Valdes, P., 2003. Objective optimisation of the FAMOUS GCM. Tech. rep., Hadley Centre, Met Office.

Kennett, J., 1977. Cenozoic evolution of Antarctic glaciation, the circum-Antarctic ocean, and their impact on global paleoceanography. Journal of Geophysical Research 82, 3843–3860.

Killworth, P. D., 1983. Deep convection in the world ocean. Reviews of Geophysics and Space Physics 21 (1), 1–26.

Kim, S., Flato, G., Boerm, G., 2003. A coupled climate model simulation of the Last Glacial Maximum, part 2: approach to equilibrium. Climate Dynamics 20, 635–661.

Klinger, B. A., 2000. Acceleration of general circulation model convergence by exponential extrapolation. Ocean Modelling 2, 61–72.

Klinger, B. A., Marshall, J., Send, U., 1996. Representation of convective plumes by vertical adjustment. Journal of Geophysical Research 101, 18175–18182.

Kutzbach, J., Gallimore, R., 1989. Pangaean climates: Megamonsoons of the megacontinent. Journal of Geophysical Research 94 (D3), 3341–3357.

Kutzbach, J., Guetter, P., 1990. Simulated circulation of an idealized ocean for Pangaean time. Paleoceanography 5 (3), 299–317.

Lawver, L., Gahagan, L., 1998. Opening of Drake Passage and its impact on Cenozoic ocean circulation. In: Conditions for Climate Reconstructions. Oxford University Press, pp. 212–223.

Ledwell, J., Montgomery, E., Polzin, K., St.Laurent, L., Schmitt, R., Toole, J., 2000. Evidence for enhanced mixing over rough topography in the abyssal ocean. Nature 403, 179–182.

Levitus, 1982. Climatological atlas of the world ocean. NOAA Prof. Paper 13. US Gov't Printing Office.

Levitus, 1998. World Ocean Atlas 1998. National Oceanographic Data Center.

Lynch-Stieglitz, J., Curry, W., Slowey, N., 1999. Weaker Gulf Stream in the Florida Straits during the Last Glacial Maximum. Nature 402, 644–648.

Maier-Reimer, E., Mikolajewicz, U., Crowley, T., 1990. Ocean general circulation experiments with an open Central American Isthmus. Paleoceanography 5, 349–366.

Manabe, S., Bryan, K., 1969. Climate calculations with a combined ocean-atmosphere model. Journal of Atmospheric Sciences 26, 786–789.

Manabe, S., Stouffer, R., 1988. Two stable equilibria of a coupled ocean-atmosphere model. Journal of Climate 1, 841–866.

Manabe, S., Stouffer, R., 1993. Century-scale effects of increased atmospheric CO_2 on the ocean-atmosphere system. Nature 364, 215–218.

Manabe, S., Terpstra, T., 1974. The effects of mountains on the general circulation of the atmosphere as identified by numerical experiments. Journal of Atmospheric Science 31, 3–42.

Marotzke, J., 1991. Influence of convective adjustment on the stability of the thermohaline circulation. Journal of Physical Oceanography 21, 903–907.

Marotzke, J., 1997. Boundary mixing and the dynamics of three-dimensional thermohaline circulations. Journal of Physical Oceanography 27 (8), 1713–1728.

Marotzke, J., Klinger, B. A., 2000. The dynamics of equatorially asymmetric thermohaline circulations. Journal of Physical Oceanography 30, 955–970.

Marotzke, J., Stone, P. H., 1995. Atmospheric transports, the thermohaline circulation and flux adjustments in a simple coupled model. Journal of Physical Oceanography 25, 1350–1364.

Marotzke, J., Willebrand, J., 1991. Multiple equilibria of the global thermohaline circulation. Journal of Physical Oceanography 21, 1372–1385.

Marsh, R., Edwards, N., Shepherd, J., 2002. Development of a fast coupled climate model (C-GOLDSTEIN) for earth system science. Tech. Rep. 83, Southampton Oceanography Centre.

Mesinger, F., Arakawa, A., 1976. Numerical methods used in atmospheric models. vol I. JOC, GARP publication series no. 17, C.P. no. 5, CH-1211. Tech. rep., World Meteorological Organization.

Mikolajewicz, U., Maier-Reimer, E., 1993. Effect of Drake and Panamanian gateways on the circulation of an ocean model. Paleoceanography 8 (4), 409–426.

Milankovitch, M., 1941. Kanon der Erdbestrahlung und seine Anwendung auf das Eiszeitproblem. Akad. R. Serbe 133, 1–633.

Molteni, F., 2003. Atmospheric simulations using a GCM with simplified physical parametrizations. I: Model climatology and variability in multi-decadal experiments. Climate Dynamics 20, 175–191.

Morcrette, J., 1990. Impact of changes to the radiative transfer parametrisations plus optical cloud properties in the ECMWF model. Monthly Weather Review 118, 847–873.

Murdock, T., Weaver, A., Fanning, A., 1997. Paleoclimatic response of the closing of the Isthmus of Panama in a coupled ocean-atmosphere model. Geophysical Research Letters 24 (3), 253–256.

NCAR, 2000. Rep: NCAR/TN-423+STR. http://www.cgd.ucar.edu/csm/models/ocn-ncom.

Neale, R., Hoskins, B., 2000. A standard test for AGCMs including their physical parametrizations. II: Results for the Met. Office model. Atmospheric Science Letters 1, 108–114.

Nof, D., Van Gorder, S., 2003. Did an open Panama Isthmus correspond to an invasion of Pacific water into the Atlantic. Journal of Physical Oceanography 33, 1324–1336.

Nong, G. T., Najjar, R. G., Seidov, D., Peterson, W. H., 2000. Simulation of ocean temperature change due to the opening of Drake Passage. Geophysical Research Letters 27 (17), 2689–2692.

Opsteegh, J., Haarsma, R., Selten, F., Kattenberg, A., 1998. ECBILT: a dynamic alternative to mixed boundary conditions in ocean models. Tellus 50A, 348–367.

Orszag, S., 1970. Transform method for calculation of vector coupled sums: application to the spectral form of the vorticity equation. Journal of Atmospheric Science 27, 890–895.

Pacanowski, R., Dixon, K., Rosati, A., 1990. The GFDL modular ocean model users guide: version 1.0. Tech. Rep. 2, Geophysical Fluid Dynamics Laboratory/NOAA, Princeton University.

Parrish, J., 1982. Upwelling and petroleum source beds, with reference to the Paleozoic. American Association of Petroleum Geologists Bulletin 66, 750–774.

Parrish, J., Spicer, R., 1988. Late Cretaceous terrestrial vegetation: A near-polar temperature curve. Geology 16, 22–25.

Peixoto, J., Oort, A., 1992. Physics of Climate. American Institute of Physics, New York.

Petit, J. R., Jouzel, J., Raynaud, D., Barkov, N. I., Barnola, J.-M., Basile, I., Bender, M., Chappellaz, J., Davis, M., Delaygue, G., Delmotte, M., Kotlyakov, V. M., LeGrand, M., Lipenkov, V. Y., Lorius, C., Pépin, L., Ritz, C., Stievenard, E. S. . M., 1999. Climate and atmospheric history of the past 420,000 years from the Vostok ice core, Antarctica. Nature 399, 429–436.

Philander, S., 1990. El Nino, La Nina, and the Southern Oscillation. Academic Press.

Philander, S., Gu, D., Halpern, D., Lambert, G., Lau, N.-C., Li, T., Pacanowski, R., 1996. Why the ITCZ is mostly north of the equator. Journal of Climate 9, 2958–2972.

Phillips, N., 1956. The general circulation of the atmosphere: A numerical experiment. Quarterly Journal of the Royal Meteorological Society 82 (352), 123–164.

Pierrehumbert, R., 1996. Some remarks on mechanisms for the regulation of tropical sea surface temperature. In: Clouds, Chemistry and Climate: Nato ASI Series 35. Springer, Berlin.

Poulsen, C. J., Barron, E. J., Johnson, C. C., Fawcett, P., 1999. Links between major climatic factors and regional oceanic circulation in the mid-Cretaceous. In: Special Paper 332. Geological Society of America, pp. 73–89.

PVM, 2003. http://www.csm.ornl.gov/pvm/pvm_home.html.

Ramanathan, V., Collins, W., 1991. Thermodynamic regulation of ocean warming by cirrus clouds deduced from observations of the 1987 El Nino. Nature 351, 27–32.

Raynaud, D., Jouzel, J., Barnola, J., Chappellaz, J., Delmas, R., Lorius, C., 1993. The ice record of greenhouse gases. Science 259, 926–934.

Robinson, P., 1973. Palaeoclimatology and continental drift. In: Implications of Continental Drift to the Earth Sciences, I. Academic Press, London, pp. 449–476.

Rooth, C., 1982. Hydrology and ocean circulation. Progress in Oceanography 11, 131–149.

Rumford, 1798. The propagation of heat in fluids. In: The Complete Works of Count Rumford, Volume 1. 1870 American Academy of Sciences, Boston, pp. 237–400.

Sakai, K., Peltier, W., 1997. Dansgaard-Oeschger oscillations in a coupled atmosphere-ocean climate model. Journal of Climate 10, 949–970.

Sausen, R., Barthel, K., Hasselmann, K., 1998. Coupled ocean-atmosphere models with flux correction. Climate Dynamics 2, 145–163.

Sausen, R., Voss, R., 1996. Techniques for asynchronous and periodically synchronous coupling of atmosphere and ocean models. Climate Dynamics 12, 313–323.

Schmitz, W., 1996. On the world ocean circulation: volumes I and II. Tech. Rep. WHOI-96-08, Woods Hole Oceanographic Institution.

Scotese, C., 2001. Atlas of Earth History, Volume 1, Paleogeography. PALEOMAP Project, Arlington, Texas.

Scotese, C., 2002. http://www.scotese.com, (PALEOMAP website).

Sellwood, B., Valdes, P., Price, G., 2000. Geological evaluation of multiple general circulation model simulations of Late Jurassic palaeoclimate. Paleogeography, Palaeoclimatology, Palaeoecology 156, 147–160.

Semtner, A., 1974. A general circulation model for the world ocean. Tech. Rep. 9, Department of Meteorology, University of California.

Shackleton, N., Kennett, J., 1975. Paleotemperature history of the Cenozoic and the initiation of Antarctic glaciation: Oxygen and carbon isotope analysis in DSDP sites 277, 279 and 281. In: Initial Report of Deep-Sea Drilling Project, vol. 29. U.S. Govt. Printing Office, Washington D.C., pp. 743–755.

Slingo, J., 1987. The development and verification of a cloud prediction scheme for the ECMWF model. Quarterly Journal of the Royal Meteorological Society 113, 899–927.

Stevens, G., Clayton, R., 1971. Oxygen isotope studies on Jurassic and Cretaceous belemnites from New Zealand and their biogeographic significance. New Zealand Journal of Geology and Geophysics 14, 829–897.

Stocker, T. F., Wright, D. G., Mysak, L. A., 1992. A zonally averaged, coupled ocean-atmosphere model for paleoclimate studies. Journal of Climate 5, 773–797.

Stommel, H., 1961. Thermohaline convection with two stable regimes of flow. Tellus 13, 224–230.

Stone, P. H., 1978. Constraints on dynamical transports of energy on a spherical planet. Dynamics of Atmospheres and Oceans 2, 123–139.

Takahashi, K., Azami, A., Takashi, A., Hirofumi, S., Tetsuya, S., 2003. Developing coupled ocean-atmosphere global climate model for the Earth Simulator and its computation/physical validation. NEC Research and Development 44 (1), 109–114.

Tansley, C., Marshall, D., 2001. Flow past a cylinder of a beta-plane, with application to Gulf Stream separation and the Antarctic circumpolar current. Journal of Physical Oceanography 31 (11), 3274–3283.

Taylor, Hammer., K. C. C. U., Alley, R. B., Clausen, H. B., Dahl-Jensen, D., Gow, A. J., Gundestrup, N. S., Kipfstuhl, J., Moore, J. C., Waddington, E. D., 1993. Electrical conductivity measurements from the GISP2 and GRIP Greenland ice cores. Nature 366, 549–552.

Terray, L., Valcke, S., Piacentini, A., 1999. OASIS 2.3 user's guide. Tech. Rep. TR/CGMC/99-37, CERFACS, Toulouse.

Trenberth, K. E., Caron, J. M., 2001. Estimates of meridional atmosphere and ocean heat transports. Journal of Climate 14, 3433–3442.

Tsonis, A., 1989. Chaos and unpredictability of weather. Weather 44 (6), 258–263.

Valdes, P., Blackburn, M., 1989. An atlas of initial UGAMP climate modelling. Tech. rep., UGAMP, Dept. of Meteorology, University of Reading.

Valdes, P., Sellwood, B., 1992. A paleoclimate model for the Kimmeridgian. Paleogeography, Palaeoclimatology, Palaeoecology 95, 47–72.

Voss, R., Sausen, R., Cubasch, U., 1998. Periodically synchronously coupled integrations with the atmosphere-ocean general circulation model ECHAM3/LSG. Climate Dynamics 14, 249–266.

Wallace, J., Gutzler, D., 1981. Teleconnections in the geopotential height field during the northern hemisphere winter. Monthly Weather Review 109, 784–812.

Warren, B. A., 1981. Deep circulation of the world ocean. In: Evolution of physical oceanography: scientific surveys in honor of Henry Stommel. MIT Press, Cambridge, M.A., pp. 6–41.

Weaver, A. J., Bitz, C., Fanning, A., Holland, M., 1999. Thermohaline circulation: high-latitude phenomena and the difference between the Pacific and Atlantic. Annual Review of Earth and Planetary Sciences 27, 231–285.

Weaver, A. J., Marotzke, J., Cummins, P. F., Sarachik, E., 1993. Stability and variability of the thermohaline circulation. Journal of Physical Oceanography 23, 39–60.

Webb, D., 1996. An ocean model code for array processor computers. Computers and Geosciences 22 (5), 569–578.

Webb, D., 1998. The first main run of the OCCAM global ocean model. Tech. Rep. 34, Southampton Oceanography Centre.

Webb, D., deCuevas, B., Richmond, C., 1998. Improved advection schemes for ocean models. Journal of Atmospheric and Oceanic Technology 15, 1171–1187.

Wells, N., 1997. The Atmosphere and ocean: a physical introduction. 2nd ed. John Wiley, Chichester.

Zhang, S., Lin, C. A., Greatbatch, R. J., 1995. A decadal oscillation due to the coupling between an ocean circulation model and a thermodynamic sea-ice model. Journal of Marine Research 53, 79–106.